Carbohydrate and lipid metabolism in insulin resistant states and the development of in vivo magnetic resonance spectroscopic techniques for the analysis of gluconeogenesis and glycogen synthesis

Changani, Kishore Kumar

CARBOHYDRATE AND LIPID METABOLISM IN INSULIN RESISTANT STATES AND THE DEVELOPMENT OF *IN VIVO* MAGNETIC RESONANCE SPECTROSCOPIC TECHNIQUES FOR THE ANALYSIS OF GLUCONEOGENESIS AND GLYCOGEN SYNTHESIS.

by Kishore Kumar Changani, B.Sc.

A thesis submitted for the degree of Doctor of Philosophy

in the University of London.

1995

The Royal London Hospital Medical College.

To my parents with all my love.

Acknowledgements

I am indebted to my supervisor, Dr Richard A. Iles for his patient understanding and his continual support and guidance throughout this thesis and also to Professor R.D. Cohen and Professor G. Vinson for giving me the opportunity to work in their departments. I would like to thank Dr. Sugden for allowing me to work in her laboratory.

I would also like to thank Dr. Steve C.R. Williams who provided me with enthusiasm for NMR and for his many contributions to the project. I would also like to pay gratitude to Dr Jimmy D. Bell and Dr Maria M. Barnard for useful help and advise and to Miss G. Hansen and Miss K. Masewyk for support in the form of part-time employment.

A special "thank you" to Dr Shamus Burns for help, understanding and, beyond the duty, support. Also Dr Tom Going for his "constructive" involvement and helpful advise.

Finally, none of this would have been possible without the understanding of my parents, Dr and Mrs P. D. Changani, my sisters and my loving and very patient wife, Jennifer.

ABSTRACT

This thesis will provide new information on carbohydrate and lipid metabolic control in various related physiological states both *in vitro* and *in vivo* in the rat model. Pregnancy is one such state which elicits many complex changes both physiologically and metabolically, one major consequence of which is the development of insulin resistance/glucose intolerance by the mother. The aim was to evaluate the mother's capacity to utilise glucose during the various stages of pregnancy. For the first time, an unrestrained un-anaesthetised rat model was used to produce indices of glucose utilisation (GUI) in a wide range of tissue types ranging from non-working postural muscles to continually contracting muscles like the heart. In the various fed conditions investigated, significant reductions in the GUI of up to 80% were seen during late pregnancy in some tissues. A method of feeding was also applied to the pregnant model producing results contrary to normal pregnant glucose utilisation values *ie.* increasing the GUI up to 90% of normal pregnancy values in some tissues. Lipogenic rates in five major tissue sites were concurrently investigated which showed increases of between 2.2 and 4 fold during late pregnancy compared with virgin controls. Analysis of glycogen levels and an attempt to probe the pyruvate dehydrogenase activities of the heart and diaphragm in the various physiological states are also discussed.

To obtain further insight into glycogen synthesis/non-oxidative disposal of glucose in the liver, a less invasive approach was then followed to explore, by non-invasive techniques, the extent to which insulin resistant states, like pregnancy, can be

explained by *in vivo* hepatic glucose metabolic studies. For this, carbon-13 magnetic resonance spectroscopy (MRS) was employed to determine the fate of 1-^{13}C glucose in the liver of rats in the same physiological states as those studied in the above methodology. Bolus infusions of ^{13}C-glucose were administered into the hepatic portal vein of the rats under investigation. The incorporation or degradation of the glucose was followed in real time by observing rapid proton-decoupled carbon spectra. From this methodology, continuous real time glucose utilisation rates together with glycogen synthesis rates were measured. ^{13}C incorporation into the glycogen macromolecule was seen to be negligible in 20 day pregnant *ad libitum* fed rats however in routine meal fed (RMF - allowed free access to food for 2h per 24h day) 20 day pregnant rats, incorporation reached a level 2.3 fold higher than the former. Maximal increases of ^{13}C incorporation were shown by the 10 day pregnant RMF rats which attained levels 2.4 fold higher than the 20 day pregnant RMF group. Results indicate an enhancement of the direct route for glycogen deposition during RMF regimes in pregnancy.

A consequence to the above MRS study led an investigation into gluconeogenic control in the rat model. Gluconeogenesis is a major metabolic pathway which may be perturbed in insulin resistant states like non-insulin dependent diabetes mellitus. In this study ^{31}P MRS was employed as a tool to look at the relative changes *in vivo* of the hepatic phosphorus spectrum. This study involved external manipulation of hepatic gluconeogenesis by the infusion of alanine. Large increases in the phosphomonoester region of the phosphorous spectrum were seen both *in vivo* and *in vitro* which was secondary to increases in 3-phosphoglycerate. The inorganic

phosphates also increased dramatically together with concomitant declines in ATP both of which recovered to pre-infusion values. This study shows many promising features which could be applied to clinical studies in humans.

CONTENTS

		Page
1:	**Introduction**	
1.1.	Physiolological and metabolic changes during pregnancy.	26
1.2.	Hormonal changes during pregnancy.	26
	1.2.1. Steroid hormones of gestation.	27
	1.2.2. Polypeptide hormones of gestation.	27
	1.2.3. Synopsis of the metabolic effects of specific hormones during pregnancy.	28
	1.2.4. Hormonal effects on maternal dietary intake during pregnancy.	29
1.3.	Maternal blood flow.	30
	1.3.1. Distribution and regulation of maternal blood flow during pregnancy.	30
	1.3.2. Effects of starvation on blood flow during pregnancy.	31
	1.3.3. Cardiac output and blood volume during pregnancy.	32
1.4.	Energy demands imposed on the heart during pregnancy.	33
1.5.	Conceptus nutritional requirements.	34
	1.5.1. Substrate supply to the foetus(es).	34
	1.5.1.1. Amino acids.	35
	1.5.1.2. Lipids.	36
	1.5.1.3. Glucose.	36
1.6.	Background to fuel selection.	37

		Page
1.6.1.	Carbohydrate management of the liver.	37
1.6.2.	Blood glucose homeostasis and fuel selection. during the fed-starved transition.	40
1.6.3.	The conservation and regulation of carbohydrate.	41
1.6.4.	The effects of meal feeding on hepatic fuel deposition.	42
1.7.	Glycaemic control during pregnancy.	43
1.8.	Maternal insulin resistance during pregnancy.	46
1.9.	Purpose of this study.	50
2:	**Methods**	
2.1.	Formation of cannulae.	53
2.1.1.	Tubing and equipment required.	53
2.1.2.	Method of formation.	54
2.2.	Method for atrial cannulation.	55
2.3.	Glucose utilisation measurement in various rat tissues.	59
2.3.1.	Introduction.	59
2.3.2.	Protocol for *in vivo* experiment.	61
2.3.2.1.	Animal preparation and its nutritional status.	61
2.3.3.	Protocol for *in vitro* tissue extraction.	64
2.3.3.1.	Methods.	64
2.3.3.2.	Calculation of glucose utilisation index (G.U.I.).	65
2.4.	Blood glucose determination for G.U.I. calculation.	66
2.4.1.	Reaction scheme.	66

Page

2.5. Plasma glucose determination. 67

2.5.1. Reaction scheme. 68

2.6. Method of pyruvate, acetoacetate & 3-hydroxybutyrate determinations. 68

2.6.1. Pyruvate determination. 69

2.6.2. Acetoacetate and 3-hydroxybutyrate determination. 69

2.6.3. Reaction Schemes. 70

2.7. Measurement of *in vivo* lipogenic rates in the liver and adipose tissue sites. 71

2.7.1. Methods. 71

2.7.1.1. *In vivo* experiment and tissue removal. 71

2.7.1.2. *In vitro* extraction of tissues. 72

2.7.1.3. Extraction procedure for total lipids. 73

2.7.1.4. Extraction procedure to obtain separate cholesterol and fatty acid synthesis values. 73

2.7.1.5. Method of calculation. 75

2.8. Preparation of arylamine acetyltransferase (AAT). 76

2.8.1. Method. 76

2.9. Measurement of pyruvate dehydrogenase activity (active form). 77

2.9.1. Introduction. 77

2.9.1.1. Reaction scheme. 77

2.9.1.2. Control of the pyruvate dehydrogenase complex. 78

2.9.2. Methods. 80

2.9.2.1. Chemicals. 80

	Page
2.9.2.2. Solutions.	81
2.9.2.3. Method of extraction	81
2.9.3. Active form pyruvate dehydrogenase activity assay.	82
2.9.3.1. Solutions	82
2.9.3.2. Assay Method	83
2.9.4. Calculations for pyruvate dehydrogenase activity.	83
2.10. Determination of citrate synthase [EC 4.1.3.7] activity.	85
2.10.1. Reaction Scheme.	86
2.11. Method for hepatic glycogen quantitation.	87
2.11.1. Glycogen extraction protocol.	87
2.11.2. Glycogen digestion protocol.	88
2.11.3. Reaction scheme.	88
2.11.4. Calculation of hepatic glycogen.	89
2.12. Statistics.	89
3: RESULTS	
3.1. Rat weight, liver weight, heart weight and chow intake during the period of gestation.	90
3.2.1. Effects of pregnancy on the glucose utilisation capacity of various tissues during the immediate fed period.	93
3.2.2. Effects of pregnancy on the glucose utilisation capacity of various tissues during the post-absorptive fed period.	95
3.2.3. Hepatic glycogen, lipid fuels, ketone bodies and insulin	

		Page
	concentrations during late pregnancy.	101
	3.2.4. Discussion.	103
3.3.	Effects of pregnancy on the lipogenic rates of the liver and white adipose tissue sites.	106
	3.3.1. Liver.	106
	3.3.2. Adipose tissues.	107
3.4.	Effects of routine meal feeding during pregnancy on GUI.	113
	Results and discussions.	113
	3.4.1. Effects of 10 day meal fed pregnant rats on GUI values during the absorptive phase.	113
	3.4.2. Effects of 10 day meal fed pregnant rats on GUI values during the post-absorptive phase.	116
	3.4.3. Effect of administering controlled food amounts on the GUI values of 10 day meal fed 19 day pregnant rats.	118
	3.4.4. Effect of 10 day meal feeding pregnant rats on GUI values in absorptive-post absorptive states in various adipose tissue sites.	119
3.5.	General discussion.	128
3.6.	PDH activities and other aspects of pregnancy.	131
4:	**INTRODUCTION - Nuclear magnetic resonance spectroscopy**	
4.1.	Brief history.	135
4.2.	Basic principles of nuclear magnetic resonance spectroscopy.	137

		Page
4.3.	The r.f. coil.	148
4.4.	Advantages and disadvantages of NMR.	150
4.5.	Previous *in vivo* studies using ^{13}C and ^{31}P nuclei.	152
	4.5.1. ^{13}C-Nuclei.	152
	4.5.2. ^{31}P-nuclei.	158
4.6.	Human studies using ^{13}C and ^{31}P NMR.	162
5:	**^{13}C-glucose metabolic studies during pregnancy.**	
5.1.	Pilot study to assess the incorporation of ^{13}C-glucose into the hepatic glycogen moiety using NMR.	165
	5.1.1. Introduction.	165
	5.1.2. Methods.	167
	5.1.2.1. Development of a proton-decoupled carbon NMR probe for *in vivo* purposes.	167
	5.1.2.2. General animal preparation and cannulation procedure for *in vivo* NMR study.	170
	5.1.2.2.1. Animal feeding regimes.	170
	5.1.2.2.2. Removal of blood sample via the inferior jugular vein.	170
	5.1.2.2.3. Cannulation of hepatic portal vein.	171
	5.1.2.3. *In vivo* proton-decoupled carbon spectroscopic protocol.	172

Page

5.1.2.4. Interpretation and quantitation of *in vivo* carbon spectra. 176

5.1.2.5. Method for aqueous extraction of liver for *in vitro* ^{13}C-N.M.R. analysis. 176

5.1.2.5.1 Extraction procedure. 176

5.1.2.5.2. Preparation of freeze-dried sample for high resolution N.M.R. analysis. 177

5.1.2.6. Method for lipid extraction of liver for *in vitro* ^{13}C-N.M.R. analysis. 181

5.1.2.6.1 Extraction procedure. 181

5.1.2.6.2 Preparation of lipid extract for high resolution N.M.R analysis. 181

5.1.2.7. Statistics. 182

5.1.3. Results and discussions. 182

5.2. Assessment of NMR protocol for *in vivo* hepatic metabolic studies. 192

5.3. *In vivo* hepatic glycogen synthesis rates during late gestation in the rat. 193

5.3.1. Introduction. 193

5.3.2. Methods. 194

5.3.2.1. Animal feeding regimes. 194

5.3.3. Results. 195

5.3.3.1. ^{13}C-glucose incorporation into the glycogen macromolecule during late pregnancy. 195

Page

5.3.3.2. ^{13}C-glucose incorporation into the glycogen macromolecule during early pregnancy. 197

5.3.4. Discussion. 204

6: Studies of hepatic gluconeogenesis using ^{31}P-NMR.

6.1.1. Introduction. 209

6.1.2. Method of *in vivo* determination of gluconeogenesis by ^{31}P NMR. 211

6.1.2.1. Animals. 211

6.1.2.2. Cannulation of the jugular vein. 212

6.1.2.3. Spectroscopy methodology. 212

6.1.3. Method for *in vitro* extraction of liver for phosphorus NMR analysis. 213

6.1.3.1. Animal experimentation. 213

6.2. Method of liver metabolite extraction. 214

6.2.1. Extraction and lyophilisation. 214

6.2.2. Preparation of sample for NMR analysis. 215

6.3. Isolated perfused liver experiments. 216

6.3.1. Perfusion apparatus. 216

6.3.2. Preparation of the perfusate. 218

6.3.3. Cannulation procedure of the isolated perfused liver. 219

6.3.3.1. Preparation of perfusion circuit. 219

6.3.3.2. Cannulation. 220

		Page
6.4.	Quantification of ^{31}P liver spectra.	223
6.5.	Statistics.	227
6.6.	Results.	228
	6.6.1. Changes in hepatic phosphomonoesters during alanine infusion in the rat.	228
	6.6.2. Changes in hepatic phosphodiesters during alanine infusion in the rat.	239
	6.6.3. Changes in hepatic inorganic phosphate during alanine infusion in the rat.	240
	6.6.4. Changes in hepatic ATP during alanine infusion in the rat.	248
	6.6.5. Assessment of overall hepatic metabolism following bolus infusions of alanine.	258
6.7.	Discussion.	263
6.8.	Future work.	272
	Publications arising from thesis.	275
	References.	277

List of Tables **Page**

Table 1. Placental polypeptide hormones of pregnancy. 27

Table 2. Tissues investigated for GUI measurements. 63

Table 3. Tissues investigated for lipogenic activity. 72

Table 4. Dilutions used for citrate synthase activity. 86

Table 5. Changes in rat weights and food intakes during the course of gestation in the Wistar rat. 91

Table 6. Changes in heart and liver weights during the course of gestation in the Wistar rat. 92

Table 7. Muscle GUI values during the course of gestation in the absorptive phase. 97

Table 8. Muscle GUI values during the course of gestation during the post-absorptive state. 98

		Page
Table 8a.	Hepatic glycogen, lipid fuels, ketone bodies and insulin concentrations during pregnancy in the absorptive state.	102
Table 9.	Changes in hepatic cholesterol, fatty acid and total lipid synthesis rates during the course of pregnancy.	109
Table 10.	Changes in cholesterol, fatty acid and total lipid synthesis rates in white adipose tissue sites during the course of pregnancy.	110
Table 11.	Muscle GUI values for 10 day meal fed 19 day pregnant rats and control 22h starved 2h refed rats during the absorptive state.	122
Table 12.	Muscle GUI values for 10 day meal fed 19 day pregnant rats and control 22h starved 2h refed rats during the post absorptive phase.	123
Table 13.	Effect of administering controlled food amounts on the GUI values of 10 day meal fed 19 day pregnant rats.	124

		Page
Table 14.	Effects of 10 day meal feeding 19 day pregnant rats on the GUI values of different white adipose tissue sites.	125
Table 15.	NMR properties of biologically important nuclei.	139
Table 16.	Important considerations for acquiring NMR spectra.	140
Table 16a.	Chemical shifts of metabolically important carbon compounds.	175
Table 17.	Comparison of ^{13}C-glycogen deposition between pre-meal and post-meal 4 week routinely meal fed virgin rats.	191
Table 18.	Comparison of ^{13}C-glucose incorporation into hepatic glycogen between control *ad libitum*, 20 day pregnant refed, 20 day pregnant *ad libitum* and 20 day pregnant RMF groups during the absorptive state.	198
Table 19.	Comparison of ^{13}C-glucose incorporation into hepatic glycogen between 10 day pregnant *ad libitum* and 10 day pregnant RMF rats & 20 day *ad libitum* pregnant & 20 day pregnant RMF rats during the absorptive state.	201

		Page
Table 20.	Glucose concentrations pre and post ^{13}C-glucose infusion in all groups studied.	203
Table 21.	Preparation of stock Krebs-Henseleit buffer.	219
Table 22.	Summary of gluconeogenic experiments.	223
Table 23.	Changes in hepatic phosphomonoesters during alanine infusions.	233
Table 24.	Changes in hepatic inorganic phosphate during alanine infusions.	242
Table 25.	Changes in hepatic beta ATP levels during alanine infusions.	250
Table 26.	Changes in hepatic gamma ATP during alanine infusions.	251
Table 27.	Changes in hepatic alpha ATP during alanine infusions.	252
Table 28.	Assessment of overall hepatic metabolite changes over a 70 min period post alanine infusion.	259

		Page
Table 29.	Assessment of overall hepatic metabolite changes over a 70 min period post alanine and glucagon infusion.	259
Table 30.	*In vitro* analysis of liver extracts from rats infused with alanine ± glucagon.	260

List of figures **Page**

Figure 1. Important hepatic metabolic reactions of carbohydrates, fatty acids and amino acids. 39

Figure 2. Cannula "former" and "borer". 57

Figure 3. Diagram of cannula. 58

Figure 4. GUI values during pregnancy during the absorptive and post-absorptive states. 99

Figure 5. GUI values of cardiothoracic muscles during pregnancy during the absorptive and post absorptive states. 100

Figure 6. Rat liver lipogenic rates during various stages of gestation. 111

Figure 7. Rat white adipose tissue lipogenic rates during various stages of gestation. 112

Figure 8. GUI values for virgin, 20 day pregnant *ad libitum* and 20 day pregnant RMF in working and non-working tissue types. 126

		Page
Figure 9.	GUI values for virgin, pregnant *ad libitum* and pregnant RMF in cardiothoracic muscles.	127
Figure 10.	GUI values for 22 h starved 2 h refed control, control pregnant and 10 day RMF pregnant rats in cardiothoracic muscles.	127a
Figure 11.	Precession of nuclei about the *z* axis setting up a net magnetisation $\mathbf{M_z}$.	142
Figure 12.	Tilting of magnetisation towards the *x'y'* plane following the $\mathbf{B_1}$ pulse.	143
Figure 13.	Free induction decay - FID.	147
Figure 14.	NADPH derivation from the oxidation of ethanol.	156
Figure 15.	Proton decoupled carbon surface coil.	169
Figure 16.	SISCO system 4.7 T wide bore magnet and cradle.	174
Figure 16a.	Typical *in vivo* ^{13}C spectra.	178

		Page
Figure 17.	Base-line subtracted spectra.	179
Figure 17a.	Comparison of carbon spectra obtained from the commercial and "home-made" surface coils.	180
Figure 18.	Sequential carbon spectra following 1-^{13}C glucose infusion.	187
Figure 19.	Graph showing relative hepatic glycogen synthesis and glucose disposal in 4 week meal fed rats.	188
Figure 20.	High resolution proton decoupled carbon spectra of liver aqueous extracts of 4 week RMF rats pre and post meal.	189
Figure 21.	High resolution proton decoupled carbon spectra of liver lipid extracts of 4 week RMF rats pre and post meal.	190
Figure 22.	Hepatic glycogen synthesis in *ad libitum* virgin and 20 day pregnant rats and RMF 20 day pregnant rats.	199
Figure 23.	Hepatic glucose disposal in *ad libitum* 20 day pregnant and virgin control and RMF 20 day pregnant rats.	200

		Page
Figure 24.	Hepatic glycogen synthesis in RMF and *ad libitum* rats on days 10 and 20 of gestation.	202
Figure 25.	Perfusion box setup.	222
Figure 25a.	Method of ^{31}P hepatic quantitation.	226
Figure 26.	Typical *in vivo* rat liver ^{31}P spectra.	232
Figure 27.	Changes in PME_{PL} - saline, glucagon.	234
Figure 28.	Changes in PME_{PL} - 2.8 mM alanine ± glucagon.	235
Figure 29.	Changes in PME_{PL} - 2.8, 5.6 mM alanine.	236
Figure 30.	Changes in PME_{PL} - 5.6 mM alanine ± glucagon.	237
Figure 31.	Changes in PME_{PL} - 2.8, 5.6 mM alanine + glucagon.	238
Figure 32.	Changes in Pi_{PL} - saline, glucagon.	243
Figure 33.	Changes in Pi_{PL} - 2.8 mM alanine ± glucagon.	244

		Page
Figure 34.	Changes in Pi_{PL} - 2.8, 5.6 mM alanine.	245
Figure 35.	Changes in Pi_{PL} - 5.6 mM alanine ± glucagon.	246
Figure 36.	Changes in Pi_{PL} - 2.8, 5.6 mM alanine + glucagon.	247
Figure 37.	Changes in ßATP$_{PL}$ - saline, glucagon.	253
Figure 38.	Changes in ßATP$_{PL}$ - 2.8 mM alanine ± glucagon.	254
Figure 39.	Changes in ßATP$_{PL}$ - 2.8, 5.6 mM alanine.	255
Figure 40.	Changes in ßATP$_{PL}$ - 5.6 mM alanine ± glucagon.	256
Figure 41.	Changes in ßATP$_{PL}$ - 2.8, 5.6 mM alanine + glucagon.	257
Figure 42.	*In vitro* analysis of liver using high resolution NMR.	261
Figure 43.	*In vitro* analysis of liver using high resolution NMR-*expansion*	262
Figure 44.	Reactions of the urea cycle.	264
Figure 45.	Gluconeogenic pathway of alanine.	274

CHAPTER 1.

1.1. Physiological and metabolic changes during pregnancy.

Pregnancy has been characterised as producing a varied array of physiological and metabolic effects to both the mother and developing conceptus (foetus(es) and placenta(s). Pregnancy resembles an almost symbiotic partnership between the mother and foetus(es) in which any factors imposed onto the mother, whether they be environmental or metabolic, may threaten foetal development. Most of the changes brought about during pregnancy are hormonal, originating from both the mothers endocrine system and the placenta, which plays an ever increasing role as gestation progresses. The changes to be discussed are essential for the continuous well being of the conceptus, ensuring its correct development, as well as the mothers well being.

1.2. Hormonal changes during pregnancy.

The normal development of pregnancy is dependent on the secretion of specific steroid and polypeptide hormones. These hormones increase in circulation at the same rate as foetal growth (Tulchinsky and Ryan, 1980). Most of these hormones originate from the placenta (Everett and MacDonald, 1979; Tulchinsky and Ryan, 1980) and influence a wide range of maternal metabolism.

1.2.1. Steroid hormones of gestation.

Steroid and sterol precursors from both maternal and foetal blood are converted to progesterone and oestrogens (oestradiol, oestrone and oestriol). More specifically, progesterone is synthesised from maternal cholesterol; oestradiol and oestrone from maternal and foetal dehydroepiandrosterone sulphate, and oestriol from foetal 16 α-hydroxydehydroepiandrosterone sulphate (Diezfalusy, 1969). Placental steroid production does not begin until week 7-8 of gestation in humans, therefore the initial supply of progesterone and oestrogen are met by the maternal corpus luteum.

1.2.2. Polypeptide hormones of gestation.

The principle polypeptide hormones synthesised by the placenta include the human chorionic gonadotropin (hCG) and the growth hormone-like human chorionic somatomammotropin (hCS) [placental lactogen (hPL)], a full list is shown in *Table 1*. These hormones can be detected in the maternal blood system 5-10 days post conception in humans.

Table 1. Placental polypeptide hormones of pregnancy.

Human chorionic gonadotropin (glycopolypeptide, 39 000 MW)
Human chorionic somatomammotropin (single chain polypeptide, 22 308)
Human chorionic corticotropin and ß-endorphin
Human chorionic thyrotropin
Human chorionic follicle stimulating hormone
Human uterotropic placental hormone

1.2.3. Synopsis of the metabolic effects of specific hormones during pregnancy.

The physiological role of a given hormone is difficult to assess since considerable interactions occur. The effects of progesterone on maternal metabolism include increased tubular reabsorption of sodium (Davey *et al.*, 1961; Gray *et al.*, 1964), an increase in respiration and an increased sensitivity of arterial smooth muscle cells to angiotensin II, preventing hypertension otherwise associated with elevated levels of this compound (Everett *et al.*, 1978). It is thought that progesterone may also play a significant role in stimulating triglyceride uptake by maternal adipose tissue sites. However there is a degree of controversy depending on the animal model used. A study on pre-menopausal women, who have elevated progesterone levels, showed increases in plasma triglyceride removal (Kissebah, 1973), however only small increases were seen in late pregnant rats (Kim and Kalkhoff, 1975). Oestrogens are thought to play an important role in lipid , protein and vitamin metabolism. Human studies have shown that administration of progesterone and oestrogen alone, in starved individuals, produced no net effect on circulating glucose, alanine and ketone body concentrations. However when both hormones are administered, states of ketonaemia, triglyceridaemia and hypoalaninaemia together with the elevation in free fatty acid circulation (see above) are seen, but plasma glucose levels remain constant (Morrow *et al.*, 1981). It is likely that these hormones have an ever increasing collaborative role in eliciting the above effects during pregnancy and consequently reducing maternal insulin sensitivity, despite hyperinsulinaemia through increased pancreatic islet secretion.

Human chorionic somatomammotropin is the major hormone responsible for elevated free fatty acids (Samman *et al.*, 1968), in the maternal blood, and a contributory factor to the insulin resistance seen in late pregnancy (see *section 1.8.*). Finally, human chorionic gonadotropin is also thought to have a minor role in lipid mobilisation, but also is thought to act as an immunosuppressive agent thus preventing blastocyte rejection (Younger *et al.*, 1969).

1.2.4. Hormonal effects on maternal dietary intake during pregnancy.

The exponential growth of the conceptus places an increasing nutritional demand on the mother, reflected in the increased maternal food intake, during the course of gestation in the rat, *see Table 5*. This increase in maternal nutrient consumption is controlled by a number of interacting physiological and metabolic factors. Progesterone and oestrogen have both been implicated in changes in the dietary intake (Hervey and Hervey, 1967). In this study progesterone was administered to virgin rats resulting in increased food consumption. The opposite was seen when oestradiol was administered to rats, which can act as an opiate receptor antagonist (Morley *et al.*, 1984), by decreasing the response to ketocyclazocine, a kappa agonist which also stimulates feeding (Mclaughlin *et al.*, 1983). Another important factor is the gradual increase in the conceptus mass which naturally implies a greater nutrient supply for the foetus(es) as well as for the mother. The physical consequence of an increased conceptus weight results in an extra nutrient requirement for day to day mobility.

1.3. Maternal blood flow.

1.3.1. Distribution and regulation of maternal blood flow during pregnancy.

Placento-foetal development invokes an increase in nutritional and respiratory demands on the mother. These demands are met by the expansion of the blood volume to supply the extra mobilized metabolites and oxidisable substrates together with the increased oxygen quotient required by the rapid metabolism of the foetus(es). Any disruptions in supply to the conceptus can cause developmental abnormalities. Therefore maternal blood flow undergoes dramatic changes to cope with the extra demands associated with gestation. The changes seen in blood volume represent increases in blood cell mass as well as plasma volume. Increase in blood cell mass, representing 30% in man (Pritchard, 1965), is thought to be influenced by a variety of hormones which include progesterone, placental lactogen, and oestrogen (Jepson, 1968), together with erythropoietin, a specific hormone for erythrocyte production. Plasma volume expansion involves greater fluid retention, controlled by increased sodium reabsorption and influenced by aldosterone (Ehrlich, 1971), as well as an increase in the circulating protein pool which involves movement of interstitial albumin into the vascular system, rather than synthesising new albumin (Hönger, 1968).

Blood flow changes have been investigated and have shown a variety of responses, these include an increased blood flow to the uterus of 25-fold in the average sized woman (Assali *et al.*, 1960) as the development of the placenta and foetus demand

an increased transfer rate of vital catabolic products, oxygen and foetal waste. The rat uterine system requires blood flow not to just one conceptus but an average of 12 implying an even greater bulk flow of blood, and hence the importance of this model in pregnant studies. Studies conducted on pregnant rats, where uterine blood flows were restricted by uterine artery ligation or embolism of the uterine vasculature, resulted in retarded growth in both the placenta and foetus (Wigglesworth, 1964). Increases in blood flow of up to 75% (Tindall, 1975) and 50% (Sims and Krantz, 1958) in the maternal liver and kidneys respectively, reflect the increases in metabolite processing by the mother, to control substrate and waste product levels of both mother and offspring, *see section 1.3.*. Two other areas of blood flow increase include the vascular system of the skin (Hytten and Leitch, 1971) and the mammary glands. The mammary glands during the latter stages of gestation require a continual supply of substrates for maternal milk production, reflected in the high enzyme activities of lipoprotein lipase [EC 3.1.1.34] and 3-hydroxybutyrate dehydrogenase [EC 1.1.1.30], during lactation (Crabtree and Newsholme, 1972). Various human studies on skin vascularity have shown increases in the feet and hands while the forearm and leg remain constant.

1.3.2. Effects of starvation on blood flow during pregnancy.

During prolonged starvation periods fat mobilisation (Tyson *et al.*, 1971), glycogenolysis and gluconeogenesis are enhanced (Freinkel, 1972; Felig *et al.*, 1972), under the control of catecholamine, glucagon and placental lactogen release.

Concurrently, there are distinct changes in blood flow to various regions of the mother. In a study on sheep there was a significant reduction in blood flow to the uterine system of 25% (Morris *et al.*, 1980). Reductions were also seen in the skin and mammary glands. However blood flow to the liver increased. These changes are thought to be due to concentration fluctuations of prostaglandins (Wallenburg, 1981), oestrogen (Meschia, 1975), angiotensin II (Ferris *et al.*, 1972) and catecholamines (Barton *et al.*, 1974). During the fasted state the vasoconstrictive hormones such as the catecholamines, angiotensin II and oestrogen are elevated, thus reducing blood flow to the uterus. Under normal nutritional conditions, naturally occurring prostaglandins are thought to interact with the other vasoactive compounds resulting in the net increase in vascularity.

1.3.3. Cardiac output and blood volume during pregnancy.

There are two significant implications of elevated blood flow to the various organs during pregnancy, firstly a substantial increase in circulating blood volume and secondly, an increased cardiac output. The increase in cardiac output results from an initial increase in stroke volume, reflected in a small degree of hypertrophy, *see section 3.1.*, followed by a more gradual increase in heart rate nearer term (Hytten and Leitch, 1971). Cardiac output increases occur more rapidly during the second and third trimester with a term output 40% higher than pre-gestation in pregnant ewes, compared with non-pregnant values (Metcalfe *et al.* 1966). From this value it was estimated that 24% of the increase represented the extra flow for the provisions

of the uterine system (Clapp, 1978) and hence cardiac output increases were primarily due to the expansion in flow through this "organ". Therefore, cardiac output during pregnancy is more a function of stroke volume rather than time.

1.4. Energy demands imposed onto to heart during pregnancy

The heart is a continually contracting muscle, producing a sufficient pressure to pump blood around the body. During pregnancy, the blood capacity of the vascular system is greatly increased, which places more strain on the heart to perform at its optimal capacity under the ever changing physiological and functional aspects of pregnancy. This extra strain on the heart must be met by the utilisation of additional oxidisable substrates to produce the required ATP levels associated with this extra demand. During a normal fed state the heart is an aerobically respiring organ obtaining its energy requirement largely from glucose and lactate, but in states of exercise or starvation, the heart utilises an increasing amount of lipid derived fuels for its contractile activity. The heart, therefore has the advantage of having the capacity to utilise a variety of different fuels such as glucose, ketone bodies, lactate and amino acids depending on nutritional status. Experiments have shown for example, that perfusing the heart with high concentrations of fatty acids and ketone bodies (breakdown products from long chain fatty acids in the liver), as would be the situation during a period of starvation, can cause a suppression in glycolytic activity of the heart and hence, increase ß-oxidation of fatty acids to ketone bodies and probably more importantly, the oxidation of free ketone bodies to acetyl CoA (Randle

et al., 1964), *see figure 1.*. Utilisation of circulating ketone bodies probably prevails over the utilisation of fatty acids for two reasons. Firstly, before fatty acids can be oxidised by the heart, they need to be transported in a non-toxic form and so are associated with albumin. Association with this protein will decrease the relative amounts of free unbound fatty acids, and hence diffusion rates into the cell will be very much reduced. Secondly, oxidising the long chain fatty acids in the liver, rather than in the peripheral tissues, produces ketone bodies which are readily soluble in the blood and easily transported across plasma membranes. With this in mind, ketone bodies can play a very important role during starvation states when glucose levels are relatively low. Due to their ease of extracellular and intracellular transport, ketone bodies can act in a buffering capacity to provide an alternative source of energy for the heart.

1.5. Conceptus nutritional requirements.

1.5.1. Substrate supply to the foetus(es).

Any disruption in placental function may produce adverse affects on the development of the young and in this respect the placenta is better equipped to sustain disruptions to normal metabolism than the foetus. All nutrients required by the foetus must pass the synciotrophoblast and cytotrophoblast, before entering the foetal blood-stream. This is achieved by a number of transport mechanisms namely, simple and facilitated diffusion, active transport and endocytosis. Water supply to the foetus(es) however,

is dependent on the osmolarity and hydrostatic differences between mother and foetus. Carbohydrates are transported to the foetus by facilitated diffusion via stereospecific carriers with a high K_m for maternal glucose (Leturque *et al.*, 1987).

Requirements of the conceptus mass increase exponentially as gestation progresses and so development is totally dependent on the mothers ability to provide the substrates required for foetal oxidative metabolism, storage compounds and new molecular synthesis at the same level. Most of the nutrient requirements depend on the rates of placental transfer and the ability of the nutrient to pass across the maternal-foetal blood membrane via various transport processes. During the second half of gestation some nutrients can be obtained from the amniotic fluid via swallowing, however, this route is negligible in comparison to the more direct route.

1.5.1.1. Amino acids.

The foetus has a very high dependence on the 10 essential amino acids for protein synthesis and catabolic processes. Studies of foetal lambs indicate that 50% of maternally derived amino acids are retained by the foetus (Rattray *et al.*, 1974; McDonald *et al.*, 1979) and the rest catabolised to urea, ammonia, glutamate production and oxidation (Gresham *et al.*, 1972; Holzman *et al.*, 1977; Lemons and Schreiner, 1983; Krishnaumurti and Kitts, 1982). The neutral and basic amino acids traverse the placenta by a concentration dependent active transport system (Holzman *et al.*, 1979).

1.5.1.2. Lipids.

Lipids are thought to be a minor metabolic fuel for the foetus (Battaglia and Meschia, 1978) but uptake is high, depending on maternal dietary intake and the rate differences in placental transfer seen in various species. Lipid uptake is prevalent during the second half of gestation and accelerated near term [human] (Ziegel *et al.*, 1976) and is primarily for accumulation as a *post partum* fuel reserve. Lipids can also be synthesised by the foetal liver and adipose tissue sites from 2 and 3 carbon glucose metabolic products and amino acids. Free fatty acids and cholesterol transfer easily across the placenta, whereas triglycerides and phospholipids must be metabolised by the placenta before entering the foetal blood circulation (Noble and Shand, 1981).

1.5.1.3. Glucose.

Amino acids and lipids are both essential requirements but it seems glucose is by far the most important metabolite, see *section 1.8.*. In humans, glucose-oxygen quotient values suggest that 80% of the daily energy requirement of a near term foetus is provided by glucose (Morris *et al.*, 1975). This transcribes to a total of approximately 40 g/day (Rosso and Lederman, 1984) of glucose required by the foetus for the demands on energy and glycogen, lipid, glycoprotein and mucopolysaccharide synthesis. In the normal adult woman, total glucose turnover is approximately 200 g/day (Kalhan *et al.*, 1979). During normoglycaemic conditions

in the rat, the conceptus uses glucose as its primary fuel substrate. However, during periods of starvation and hence hypoglycaemia, ketone bodies can be utilised as precursors for energy generation and lipid synthesis (Robinson & Williamson, 1980; Edmond, 1974; Leturque *et al.*, 1987). Ketone bodies have been shown to pass easily across the placental barrier in rats and humans, depending on maternal concentrations (Girard *et al.*, 1977; Kim & Felig, 1972). This is a very important consideration since both humans and animals are easily susceptible to ketosis during pregnancy (Felig & Lynch, 1970; Scow *et al.*, 1964; Girard *et al.*, 1977); Miodovnik *et al.*, 1982).

1.6. Background to fuel selection

1.6.1. Carbohydrate management of the liver.

The liver has an enormously varied role as an organ of storage, supply and detoxification of blood. Without the organ, life would last for only 6 hours due to severe hypoglycaemia and the accumulation of toxic metabolites within the blood. Its role in the homeostatic control of blood glucose levels during adverse physiological conditions such as starvation, diabetes mellitus and insulin resistance during pregnancy, is by far the most important aspect and is one which this thesis has concentrated on. During periods of feeding, carbohydrates are transported to the liver for accumulation to glycogen. As blood glucose levels fall following feeding, the liver will break down glycogen to glucose, to be released into the blood supply

as free glucose. Normoglycaemic conditions are maintained by glycogenolysis during short term starvation, however during periods of prolonged starvation (>24h), glycogen stores become depleted thus stimulating gluconeogenesis from protein derived amino acids together with increased fat mobilisation. The important hepatic pathways of gluconeogenesis, glycogen synthesis, glycogenolysis, lipogenesis and lipolysis are outlined below (*see figure 1.*).

Figure 1.

Important hepatic metabolic reactions of carbohydrates, fatty acids and amino acids.

P = *phosphate.*

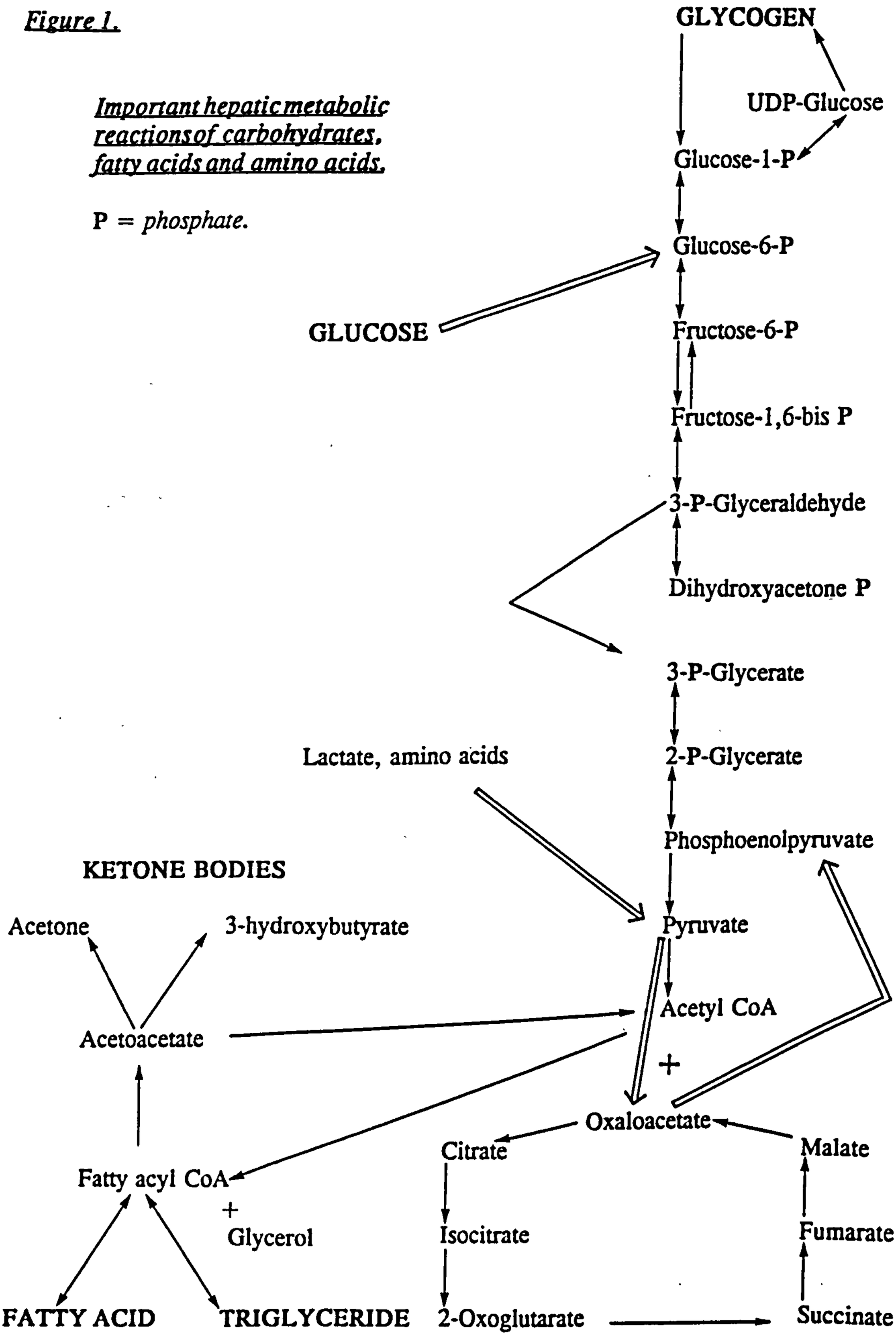

1.6.2. Blood glucose homeostasis and fuel selection during the fed-starved transition.

The nutritional and physiological states of the animal depict the contribution of glucose, free fatty acids and ketone bodies to the respiratory fuel selection of the major tissues. The liver has a unique role of storing and processing these subunits from triacylglycerol (producing subunits of fatty acids and ketone bodies) and glycogen (producing glucose subunits, a process also prevalent in muscle where glucose-1-phosphate subunits are produced). During a fasting period, glycogen will be broken down in both the liver and muscle to maintain blood glucose levels. However, glycogen stores in both rat and man are largely depleted after a 24 h starvation period. Triacylglycerols, which produce five times more energy than glycogen, gram per gram, are then relied on to a greater extent. Unfortunately, not all cells can survive solely on fat derivatives but require a constant supply of glucose at a level exceeding 2.2 mmol/l. Such cells include erythrocytes, those of the renal medulla, lens and some from the small intestine, all of which do not possess enzyme(s) required for ß-oxidation. The brain and some cells of the central nervous system could be categorised as also being glucose dependent. However, these cells do have the capacity to adapt to utilising high concentrations of ketone bodies (N.B. free fatty acids cannot pass across the haemato-encephalic barrier). In order to supply glucose to cells dependent on glycolysis amino acids from protein degradation, are transported to the liver (*see figure 1.*) for gluconeogenesis. Gluconeogenesis is thought to play an very important role during short term starvation, IDDM, glycogen storage diseases, NIDDM and other insulin resistant states such as pregnancy, as well

as being a mechanism for supplying glucose for glycogen synthesis. Gluconeogenic pre-cursors include glycerol, lactate, pyruvate and amino acids (notably alanine), (*see chapter 6.* for further discussion on the control and mechanism of this pathway). In order to conserve glucose reserves, regulatory mechanisms at enzymatic levels exist which switch fuel selection predominantly towards fat utilisation. After an overnight fast in humans in comparison with the fed state, on an average Western diet, the contribution of fat to the fuel requirement increases from 33% to 70% with a concomitant decrease in carbohydrate selection from 50% to 12%. This mechanism, known as the glucose-fatty acid cycle protects against accelerated hypoglycaemia and depletion of protein reserves. The glucose-fatty acid cycle is hormonally independent, relying solely on the competition of the relative concentrations of glucose and free fatty acids. However, it is the consequence of hormone action.

1.6.3. <u>The conservation and regulation of carbohydrate.</u>

During a period of starvation the insulin/glucagon ratio is decreased, this promotes glycogenolysis in liver and muscle together with increased lipolysis from adipose tissue sites, producing glycerol and non esterified fatty acids (NEFA) which competitively inhibit glucose utilisation by the muscles (especially the oxidative working muscles). The hypoinsulinaemic state directly "de-stimulates" glucose uptake and oxidative phosphorylation by skeletal muscle, and the elevated glucagon levels elevate the intrahepatic concentration of cyclic AMP, hence promoting glycogenolysis and gluconeogenesis (due to increased transport of amino acids to the liver) in the

liver. The control of complete oxidation of carbohydrate is tightly controlled by one particular enzyme, the pyruvate dehydrogenase complex (PDH), as flux mediated by this enzyme represents an irreversible loss of carbon as carbohydrate for which there is no known mammalian system for re-synthesis. The PDH complex is inhibited by the increased activity of PDH kinase, which phosphorylates the complex, due to the elevated mitochondrial levels of acetyl CoA/CoA, NADH/NAD^+ ratios (Kerbey *et al.*, 1977) (from ß-oxidation of fatty acids) and cyclic AMP levels. Increases in the citrate pool, due to ß-oxidation, have a de-activating allosteric effect on the 6-phosphofructo-1-kinase [EC. 2.7.1.11] (together with the indirect action of glucagon via cyclic AMP) activity reducing fructose 1,6 bisphosphate concentrations and causing a build up of fructose-6-phosphate and glucose-6-phosphate which further inhibit uptake of circulating glucose.

1.6.4. <u>The effects of meal feeding on hepatic fuel deposition.</u>

The metabolic adaptations acquired upon placing rats on strict feeding regimes, where food is available for a few hours in a day ("meal-feeding"), was first shown by Dickerson *et al.* (1943) and Tepperman and Tepperman (1958). These groups noticed increased lipogenic rates in liver slices of meal fed rats, compared with *ad libitum* fed rats, when incubated with ^{14}C-labelled acetate or glucose. Pallardo and Williamson (1989) compared glycogen, fatty acid and cholesterol synthesis rates in *ad libitum* and routinely meal fed (RMF) rats and showed 6-fold higher total lipid (fatty acids and cholesterol) synthesis rates upon refeeding in the RMF group. Glycogen synthesis

rates in the two groups however, were comparable, with slight increases seen 90 min after the start of refeeding in the RMF group. In general, lipid synthesis was shown to be greatly enhanced at all time intervals following re-feeding and more importantly the lipogenic response time to re-feeding was significantly reduced. Since the rate of glycogen synthesis was similar in the two groups, carbohydrate flux in the RMF group must be greatly enhanced. One explanation could be that glycogen is repleted directly from glucose units rather than through the indirect route of gluconeogenesis (*see section 5.3.4.*), ie both glycolysis and direct glycogen synthesis could be operating at near maximal rates. However, a similar study by Holness and Sugden (1989), failed to show the same levels of glycogen synthesis within the two groups following 60 mins after refeeding. Hepatic PDH activity was also measured during re-feeding, showing 14-fold increases 60 min into re-feeding compared with *ad libitum* rats. PDH activity continued to remain higher after 2 h of refeeding. These results suggest increased glycolysis and therefore carbon loss to supply the acetyl CoA requirements for lipogenesis. Unfortunately this study did not measure lipogenic rates to confirm the findings of reduced glycogenesis and increased PDH activity.

1.7. Glycaemic control during pregnancy.

Pregnancy constitutes a very important nutritional stress upon the mother where very strict control of substrate oxidation has to be employed so as to protect both the mother and foetus(es). During pregnancy plasma glucose decreases to hypoglycaemic levels during the post absorptive state (4-6 hours after the last meal) (Scow *et al.*,

1964; Knopp *et al.*, 1973; Herrera *et al.*, 1969). This decrease in plasma glucose levels can be looked upon in two different ways; firstly, it could be the direct result of the haemodilution effect caused by the expansion in blood volume (Kalhan *et al.*, 1979). Secondly, it could be the consequence of the developing foetus placing an increased glucose demand on the mother who cannot accelerate glucose production at the levels required. (Spellacy, 1975; Adam and Felig, 1978). This glucose decline becomes more interesting when you bring in two other facts of pregnancy. Firstly, during the course of gestation glucose turnover increases at the same rate as the growth of the conceptus but total turnover per kg body weight remains the same (Leturque *et al.*, 1981; Ogata *et al.*, 1980). This implies that hypoglycaemia is not a result of the haemodilution effect unless blood volume increases disproportionately to the increase in body size. The second, is that the mother's tissues develop a degree of insulin resistance, (Leturque *et al.*, 1984; Leturque *et al.*, 1986; Hauguel *et al.*, 1987) therefore, decreasing their capacity to utilise glucose. So despite an increased turnover of circulating glucose, in parallel with the growth of the conceptus, and a reduced maternal glucose utilisation, blood glucose levels still decrease. This then raises two questions, to what degree are the mothers' tissues insensitive to the insulin action and do the developing foetus(es) constitute a major drain on the maternal glucose pool (see *chapter 3.*)?

Thus far a very general insight into the metabolic control of the mother during pregnancy has been given but the events are far more intricate as the variables are considered. Glucose metabolism is very closely controlled by one hormone in particular, insulin. Insulin is a relatively small polypeptide produced by the ß-cells

of the islets of Langerhans in the pancreas. This hormone has far reaching effects on the metabolism of various fuel substrates depending on the nutritional status of the subject. Its actions include the control of glucose metabolism, in the liver and muscle; lipid synthesis rates in the liver and adipose tissue sites together with protein breakdown, and various aspects of protein metabolism. Its regulatory action of control is at the enzymatic level where a particular regulatory enzyme in a particular metabolic process is targeted. The most important of these enzymes include pyruvate dehydrogenase, glycogen synthase, acetyl-CoA carboxylase, phosphorylase kinase, 3-hydroxy-3-methylglutaryl-CoA (HMG) reductase and triacylglycerol lipase. Pyruvate dehydrogenase, a multi-holoenzyme (consisting of 3 different polypeptide chains; E1, pyruvate decarboxylase; E2, lipoate acetyltransferase; E3 lipoamide dehydrogenase) catalysis the irreversible conversion of the 3-carbon pyruvate metabolite to the 2-carbon acetyl CoA. Its regulation controls the relative rates of glycolysis and hence, the rates of complete oxidative phosphorylation of carbohydrate substrates. It is important to note that maternal insulin cannot pass across the placenta to the foetus therefore it cannot influence foetal glucose utilisation which is accomplished by foetal insulin. However it can be bound to the placenta and even degraded in both human (Freinkel and Goodner, 1960) and rat placentas (Goodner and Freinkel, 1959). Another important feature is the production of acetyl CoA resulting in a carbon loss, a non-recoverable state. Following this conversion gluconeogenesis cannot be performed. However, lipogenesis can be activated, since an accumulation of acetyl CoA, a precursor for lipid synthesis, will activate the acetyl CoA carboxylase enzyme in the adipose tissue sites under the correct metabolic state, controlled by insulin. Glycogen synthase and HMG CoA reductase, like pyruvate

dehydrogenase and acetyl CoA carboxylase, both increase in activity as insulin activities increase due to a high carbohydrate input. Phosphorylase kinase and triacylglycerol lipase both decrease in activity in the presence of high insulin concentrations, resulting in an elevation in glycogen and triacylglycerol. Hormonal regulation of these key regulatory enzymes determines the type of substrates oxidized in various nutritional states.

1.8. Maternal insulin resistance during pregnancy.

As previously mentioned, pregnancy exerts a state of insulin resistance on the mother. The extent and progression of this resistance has never been fully explained in the animal model, due to experimental restrictions, but such models have shed some light on this phenomena. Early studies by Knopp *et al.* (1970) showed that large doses of exogenous insulin did not increase glucose utilisation in late pregnant rats whereas, increases were seen in virgin rats suggesting a decreased response by maternal tissues to hyperinsulinaemic states. Further studies in humans and rats demonstrated *in vivo* insulin resistance by various tissues (Burt, 1956; Kalkoff *et al.*, 1964; Costrini and Kalkhoff, 1971; Leturque *et al.*, 1980). Leturque *et al.* (1984a), showed, by using euglycaemic-hyperinsulinaemic clamp techniques, that insulin insensitivity involves tissues which utilise glucose as well as those which produce it. This study implied a wide ranging tissue type sensitivity including skeletal muscle, adipose tissue sites and the liver. However depending on the technique used, opposing views on tissue sensitivity have been reported. A study by Rushakoff & Kalkhoff (1981) reported

decreased rates of insulin stimulated glucose uptake by perfused hind-limb in starved pregnant rats compared with starved virgin hind-limb. However, a similar study by Leturque *et al.*, (1981a) using *isolated* rat soleus muscle showed no insulin stimulation of [U-^{14}C]glucose uptake and utilisation. Studies on *isolated* adipose tissue (Leake & Burt, 1969; Knopp *et al.*, 1970) reported the same situation where no differences were seen in insulin stimulated [U-^{14}C]glucose utilisation by the tissue in late pregnant and virgin rats. These studies suggested that pregnancy did not induce insulin resistance in these particular tissues. It has been suggested, that from the studies on isolated soleus muscle (Leturque *et al.*, 1981), isolated adipocytes (Leturque *et al.*, 1984) and isolated hepatocytes (Davidson, 1984), insulin resistance shown *in vivo* but absent *in vitro* could be accounted for by a loss of circulating factors inducing insulin resistance under normal gestational metabolism. During pregnancy hormones such as progesterone (Sutter-Dub *et al.*, 1973) and placental lactogen (Shiu *et al.*, 1973) are at an elevated level together with lipid fractions *ie* triacylglycerol and non-esterified fatty acids (Scow *et al.*, 1964; Knopp *et al.*, 1973). Elevation of any one of these compounds is known to counteract the action of insulin (Kalkhoff *et al.*, 1978) and therefore can be regarded as a contributory factor toward maternal insulin resistance.

Insulin insensitivity by the various tissues during late pregnancy places the mother under a false state of "starvation" due to the reduced amount of glucose it can now utilise. This must therefore imply greater utilisation of other oxidisable substrates such as ketone bodies from fatty acid degradation in the liver but also from free fatty acids and amino acids. The nutritionally related metabolic changes of pregnancy are thought to be a mechanism by which the mother can accommodate sufficient

substrates for the exponential growth of the developing conceptus. By imposing onto itself a decreased capacity for glucose utilisation, the mother allows the foetus(es) to take advantage of the extra circulating glucose. If this is the case, glucose must be a preferred fuel substrate for foetal growth, possibly due to its ease of transport in the mother's blood, as well as across the synciotrophoblast and cytotrophoblast into the foetal blood. Alternatively, the enzyme systems for complete oxidative phosphorylation in the conceptus are better developed compared with systems requiring other substrates for the production of energy releasing phosphate rich compounds. Circulating glucose in the mothers extracellular pool is, therefore, indirectly diverted away from the mothers intracellular metabolic systems by the progressive insulin resistance developed by the various tissue types. Pregnancy therefore produces a situation similar to a starved state by decreasing the ability of the mother to use the otherwise abundant glucose. The decrease in maternal glucose utilisation is essential for the well being of foetal growth and development and can be seen to be vitally required when the rates of glucose utilisation in the conceptus is measured. A study by Leturque *et al.* (1986) set out to measure glucose utilisation rates of the conceptus and found that in a rat of 10 foetuses and 10 placentas the rate of glucose utilisation was 23% of the total maternal rate. These rates of utilisation are dependent on maternal and foetal glucose requirements, the K_m of the carrier, foetal insulin levels [the foetal placenta is capable of secreting insulin at a very early stage of development (Girard *et al.*, 1974)] and, during the early stages of gestation, maternal plasma glucose levels. Insulin sensitivity of the placenta is a matter of controversy but present knowledge indicates that in normoglycaemic conditions the insulin receptors of the placenta (Posner, 1974) are influenced by maternal insulin

levels. However, when blood glucose levels decrease, placental uptake is not compromised by exogenous insulin (Testar *et al.*, 1985). Other studies involving different animal species have shown similar utilisation rates ranging of 30% and 36% in the sheep (Hay *et al.*, 1983) and the rabbit (Gilbert *et al.*, 1984), respectively. These studies enhances the idea that glucose is in fact a very important fuel requirement for the conceptus especially during the later stages of pregnancy.

Decreased utilisation of glucose by maternal tissues reflects the increased circulation of ketone bodies cholesterol, triglycerides, free fatty acids, phospholipids and different lipoprotein fractions in the blood, producing a hypertriglyceridaemic state. Increases in both the very low density lipoprotein fractions (VLDL) and the high density lipoproteins (HDLP) fraction have been seen during the course of pregnancy (Knopp *et al.*, 1986; Fåhraeus *et al.*, 1985; Warth *et al.*, 1975). Elevation in the HDLP fraction is primarily due to the increase in the high density lipoprotein$_2$ ($HDL_{2)}$ subfraction as well as the HDL_3 which are metabolised as an energy source for both mother and foetus as well as important for mammary milk production. These lipoprotein changes seen during gestation are not influenced by factors such as diabetes mellitus, hypercholesterolaemia, diet, obesity and body weight (McMurry *et al.*, 1981; Warth and Knopp, 1977; Green, 1966) but thought to be controlled by the increases in progesterone and oestrogen. Increases in the plasma phospholipid fractions of sphingomyelin, lecithin and phosphatidylethanolamine have all been reported. However, lysolecithin plasma levels have shown marked decreases (Svanborg and Vikrot, 1965). By far the greatest increase in mobilisation is shown by the triglycerides which increase by 4.4 fold in normal pregnant individuals

(Svanborg and Vikrot, 1965).

These two observations imply a gradual move of maternal tissues from carbohydrate to lipid utilisation.

1.9. Purpose of this study.

Starvation in any physiological condition results in a degree of hypoglycaemia and an elevation in blood ketone body concentration (Felig and Lynch 1970). Blood glucose levels must be maintained above 2.2 mmol/l to adequately supply the brain with this essential oxidisable fuel substrate and hence starvation can be regarded as a life-threatening situation. Normoglycaemic conditions are maintained by degradation of hepatic glycogen stores under short term starvation. However during prolonged starvation, glycogen stores become depleted stimulating gluconeogenesis from protein derived amino acids together with increased fat mobilisation. During pregnancy glycaemic control is compromised. The mother must maintain sufficient control of glucose levels to provide her own needs together with the demands imposed by the foetus(es). As a consequence, maternal tissues tolerate prolonged periods of hypoglycaemia through maternal insulin resistance. This study set out to investigate the extent and progression of insulin resistance/glucose intolerance of various rat skeletal muscles as well as the heart, diaphragm and adipose tissue sites during the immediate absorptive and post absorptive phases. The studies discussed above have concentrated on only a very few muscle types and have not shown the comparison of

glucose uptake and phosphorylation by the various muscle types. Previous studies have concentrated on hind-limb muscles and a few adipose tissue sites but have not looked closely at the differences between oxidative and non-oxidative muscles and more importantly no studies have looked at the changes in the glucose utilisation capacity of the heart during the latter stages of pregnancy. The heart is by far the most important organ for consideration by virtue of its continual requirement for oxidisable fuels to maintain the high ATP levels required to sustain an ever increasing demand. For this simple reason glucose utilisation rates of the heart were measured during three stages of gestation along with the diaphragm, again a tissue with an obligatory high fuel requirement.

If maternal nutritional supply is limited over prolonged periods during gestation, foetal development can suffer depending on the timing and extent of the food restriction. As restriction increases from day 1 of gestation net maternal and foetal weights decrease (Berg, 1965), resulting in infant mortality rates and disproportionate foetal development. Glucose utilisation rates were therefore assessed for pregnant rats placed on routine meal feeding regimes. This was to provide a potentially very interesting observation which could have further clinical applications.

A major aim of this investigation was to perform the measurements of glucose utilisation on rats which were not under the influence of anaesthesia. Various studies previously mentioned have measured glucose utilization rates in different tissues in both the pregnant and non-pregnant states however, most of these studies have involved anaesthesia. The use of anaesthesia (sodium pentobarbitol) for glucose

utilization experiments has been shown to suppress uptake and phosphorylation by the diaphragm and soleus muscles (Penicaud *et al.*, 1987). Therefore, in this study the glucose utilization rates in various tissues were investigated in un-restrained rats without the use of anaesthesia during the experiment. The method employed required the catheterisation and surgical implantation of a specially designed cannula to the jugular vein of the rat. The procedure was performed so as to give no discomfort to the rat following surgery. The cannula was secured by various ties and channelled under the skin so as to emerge between the ears. This ensured no discomfort allowing un-hindered movement by the rat, as well as preventing the dislodgement of the cannula, see *sections 2.1.& 2.2.*. The rat provided an excellent model for pregnancy for a number of reasons. Firstly, the biochemical and physiological development of the foetus and placenta have similarities to human. Secondly, there is a wealth of biochemical knowledge already associated with rat metabolism which can be related to human. Thirdly, the rat shows similar eating habits during pregnancy to humans, where food is consumed erratically during the active hours. The two major differences between human and rat pregnancies are firstly the time scale involved for gestation where the rat can give birth within 21 days of conception compared with 9 months in humans. Secondly, the rat give birth to approximately 12 off-spring, however humans give birth to on average just one. Both these differences imply the rat must regulate metabolic and physiological changes during pregnancy quicker to cope with extra nutrient requirements over a shorter space of time for a greater number of off-spring. Apart from these two differences the development of the foetus and placenta in the two models are very similar and so a good understanding of human pregnancy can be gleaned from rat studies.

CHAPTER 2.

METHODS.

2.1. Formation of cannulae (*see figure 3*).

2.1.1. Tubing and equipment required.

A = 20mm Portex pp10 non-sterile polyethylene tubing = "U-bend" [ID 0.28mm, OD 0.61mm].

B = 120mm Portex pp50 non-sterile polyethylene tubing = "Mainstem" [ID 0.58mm, OD 0.96mm].

C = 10mm Portex pp100 non-sterile polyethylene tubing = "Half dumbell" [ID 0.86mm, OD 1.52mm].

D = 50mm Portex pp160 non-sterile polyethylene tubing = "Reinforced tubing" [ID 1.14mm, OD 1.57mm].

E = 10mm PE60 (Becton Dickinson Intramedic) non-sterile polyethylene tubing = "Dumbell" [ID 0.81mm, OD 1.37mm].

F = 35mm Silastic (Dow Corning vivosil) elastic tubing [ID 0.12mm, OD 0.25mm].

2.1.2. Method of formation.

The "cannulae former" (*Figure 2.*) was placed through tubing ***B***. Onto the thin piece of wire (ID 0.27 mm) attached to the "former", tubing ***A*** was placed and pushed onto tubing ***B***, over-lapping by 3-5 mm. Using a soldering iron, this area was gently heated to fuse the tubes together by squeezing the molten plastic between finger and thumb. Approximately 10-15 mm below this area tubing ***B*** was gently heated and pushed from opposite directions so as to crimp the tubing. Tubing ***C*** was made into a "half dumbell" by allowing one end to be heated so that the tubing melted back upon itself, thus forming the dumbell shape. This tubings' internal diameter was increased by the use of a heated rod of diameter 1.1mm. Tube ***C*** was slid over the non fused end of ***B*** by 30 mm. Using a 2.0 mm diameter rod, tube ***D*** was enlarged at one end and then slid over tube ***C*** so as to make a tight seal. By starting at the dumbell end the tubings were heated until they went transparent and then fused by pressing and rolling with finger and thumb. This was repeated gradually all the way down to the end of tubing ***D***, making sure that the different plastic tubings had melted completely and evenly over the "former". The "former" was removed and the fused tubings cleanly cut with a razor. Another piece of wire, covered with silicone fluid (Dow Corning 200/5CS), was inserted into tubing ***A*** and tube ***F*** slid firstly onto the wire and then onto tube ***A*** by approximately 4 mm. This was not heated as the seal is quite adequate. A dumbell was constructed with ***E*** in the same way as with tube ***C*** except this time both ends are treated. The dumbell was placed over the junction of ***A*** and ***F***. A "U-bend" was produced by bending tube ***A*** around a nail set in a board, the tubing was then placed into boiling water for 5 seconds and then into cold

water for 5 seconds. The cannulae were tested for leaks by injecting distilled water from a syringe through the reinforced end of the cannula while obstructing the passage at the silastic end.

2.2. Method for atrial cannulation.

N.B. All cannulations were carried out 5-7 days prior to the actual experiment, so as to allow sufficient time for recovery from the surgery. The meal fed group were cannulated in the same way. However, surgery was performed on either day 12 or 13 of gestation at 16:00 so as not to interfere with their meal feeding regime.

Age-matched female albino Wistar rats maintained at 18-20 °C and constant humidity were housed on a 12h light/12h dark cycle. Rats were allowed free access to a standard chow diet (except the meal fed group) consisting of 52% carbohydrate, 15% protein, 3% fat and 30% non-digestible residue. The RMF group were housed in a reverse light/dark room [light off 10:00/light on 22:00] and allowed free access to chow for 2 h per 24h day (between 10:00 and 12:00) from day 9 of pregnancy. The rat was anaesthetised with an intramuscular injection of Hypnorm™ (1.0 ml/kg Janssen Pharmaceuticals Ltd., Grove, Oxford.) [fentanyl citrate (0.315 mg/ml) and fluanisone (10 mg/ml)] followed by an intraperitoneal injection of Diazepam ([5 mg/ml] Phoenix Pharmaceuticals Ltd.] (1.0ml/kg). This type of anaesthesia takes effect within 5-10 minutes and lasts for approximately 1 hour. The anaesthetised rat was placed on a heating blanket maintained at 37°C and secured by its feet with masking tape. The skin was cut just below the thoracic cavity to a point parallel to

the left fore-limb, the inner body cavity wall was then carefully cut and the inferior jugular vein exposed by carefully pulling away surrounding tissue with curved forceps. The jugular vein was gripped with curved forceps and a small hole made with a blue needle (23G 0.6x30 mm). A cannula, which was filled with saline (0.9% NaCl w/v) and attached via an extension tubing (tube ***B*** *see section 2.1.1.*) to a 1 ml syringe also containing saline, was carefully inserted into the vein until all the silastic tubing had entered into the jugular vein and hence, the right atrium of the heart. A length of cotton (*ca.* 20 cm) was tied around the middle of the dumbbell, *see section 2.1.1.*, so as to leave two ends of cotton which are used for anchoring the cannula. Each end of the cotton was secured into muscle just below the area of cannulation. It was important to ensure that the cotton showed no slack to prevent the tubing from easing its way out of the vein. Another length of cotton was tied around the crimped area of the cannula and secured around muscle. The "U-bend" was positioned inside the thoracic cavity; this procedure requires the use of forceps to clear away tissue to producing room to position the "U-bend". The skin cavity was sutured (Ethicon thread) from the thoracic cavity downwards, leaving one stitch short to allow the "the borer" *see figure 2.*, to be inserted between the skin and body cavity. The "borer" was pushed under the left fore-limb and then directed towards the back of the head. At a point between the ears the "borer" was forced through the skin, hence producing a hole. With the "borer" in position the cannula was disconnected from tube ***B*** and re-attached to the end of the "borer". The "borer" was gently pulled out through the opening between the ears to allow the emergence of the cannula through this opening. The cannula was reconnected to the syringe extension and tested for blood withdrawal. The small exposed area at the chest was then sutured.

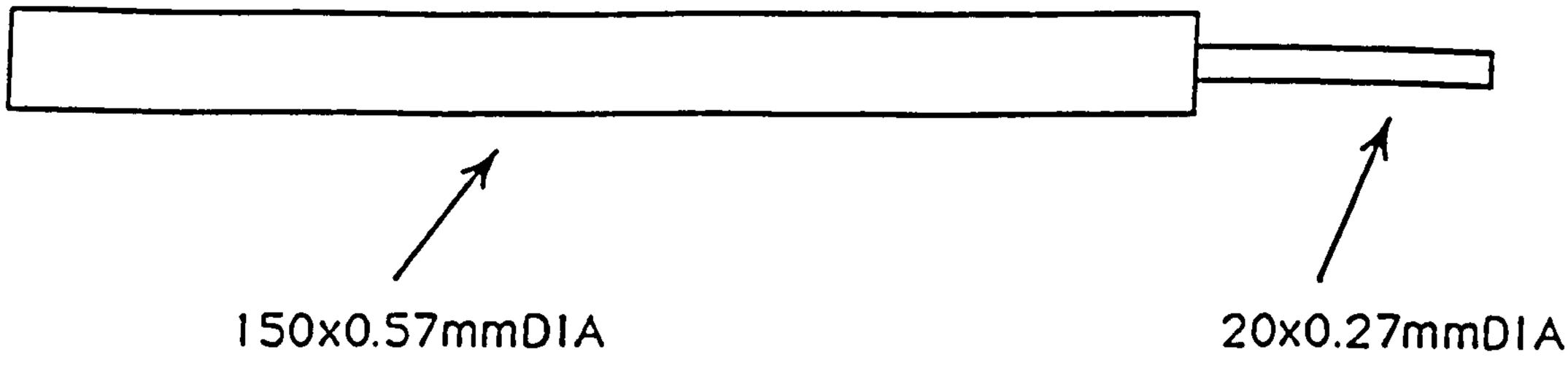

a) "Former"

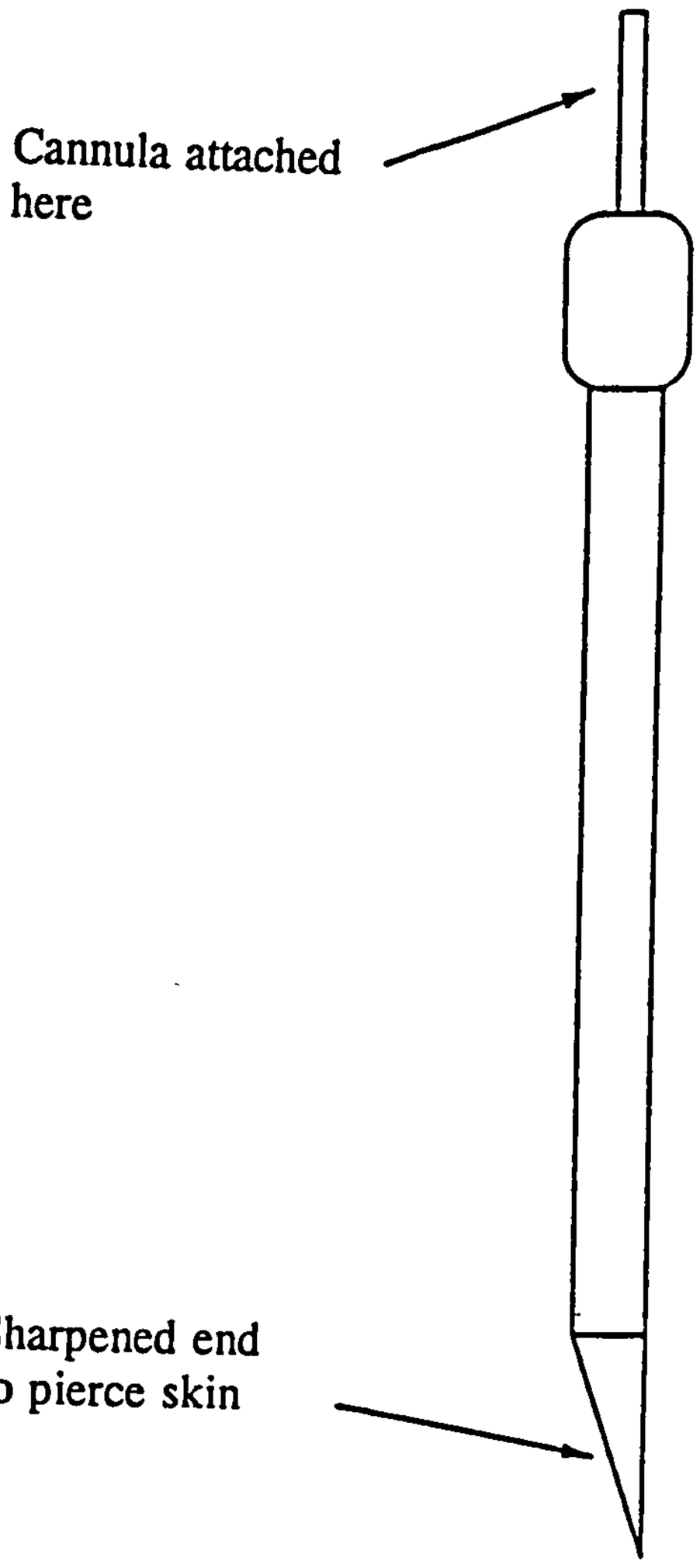

b) "Borer"

Total length = 200mr
Maximum width = 3r

Figure 2. Cannula "former" and "borer".

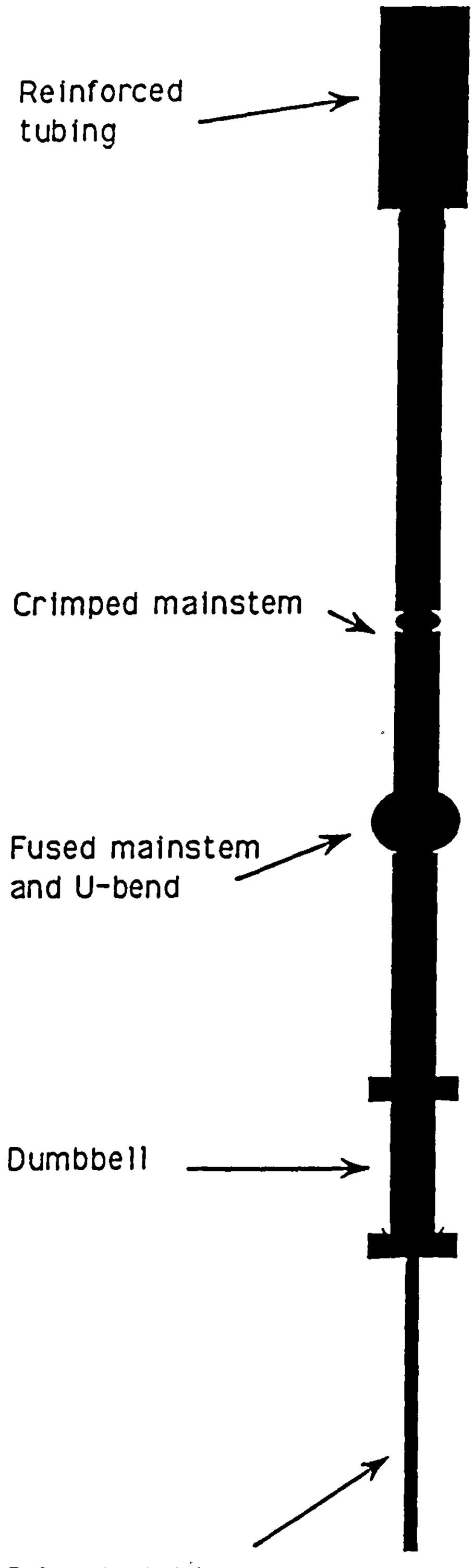

Figure 3. Diagram of cannula.

Total length = 100 - 120mm

The half dumbbell (*see section 2.1.2.*) was located under the skin and a small incision made so as to expose it. Two sutures were placed in front and behind the half dumbell so as to secure the cannula at this point. The incision was sutured and the cannula tested for blood withdrawal. A blue needle was cut from its base and both ends sealed, this was then placed into the end of the cannula to prevent blood escaping and/or air entering the cannula.

The rat was placed back into the cage on top of a layer of tissue and the cage placed on top of a heating blanket until recovery from the anaesthesia.

2.3. Glucose utilisation measurement in various rat tissues.

2.3.1. Introduction.

The method of glucose utilization is based on the method by Sokoloff *et al.* (1977) who measured glucose utilization rates in the brain by using the kinetic and metabolic properties of 2-deoxyglucose. This carbohydrate has been shown to behave in a similar fashion on contact with cell tissue as glucose. Uptake and phosphorylation of this compound, which represents the glucose utilization index, shows little discrimination compared with glucose and hence is a useful substrate when labelled either as 2-deoxy[^{14}C]glucose or 2-deoxy[^{3}H]glucose. The principles behind using 2-deoxyglucose lies in the fact that it is transported by the same carrier as glucose

(Kipnis and Cori, 1959; Olefsky, 1975; Rennie *et al.*,1983) and that phosphorylation is by hexokinase. There is, however, one important difference from glucose ie when it has been phosphorylated to 2-deoxyglucose-6-phosphate, metabolism goes no further. If concentrations of glucose-6-phosphatase (Lackner *et al.*, 1984) are negligible, then the 2-deoxglucose-6-phosphate will be trapped within the tissue and its relative quantity measured after tissue digestion and scintillation counting. An index of glucose utilization can only be determined if the relative amounts of phosphorylated 2-deoxyglucose and the un-phosphorylated form can be differentiated, since simple uptake through carriers in the plasma membrane are no measurement of utilization. After the 2-deoxyglucose has been phosphorylated then the utilization of glucose by the particular tissue can be assessed. A method of separation of 2-deoxyglucose from 2-deoxyglucose-6-phosphate is by using the properties of perchloric acid and $Ba(OH)_2/ZnSO_4$ (Somogyi, 1945). The perchloric acid will not precipitate out either form of 2-deoxyglucose whereas the 'Somogyi reagent' ($BaSO_4/Zn(OH)_2$ will only precipitate out the 2-deoxyglucose-6-phosphate. By counting the amount of radioactivity in both fractions the relative amount of 2-deoxyglucose-6-phosphate can be measured. Glucose utilization indices for various tissues can thus be quantified from the relative conversion rates of 2-deoxy [^{3}H] glucose to the metabolically stable 2-deoxy [^{3}H] 6-phosphate with respect to the integral of labelled 2-deoxyglucose removal from the blood. An important consideration which has to be assessed before using this technique, is the relative discrimination between the two forms of glucose. Previous work on the discrimination between 2-deoxyglucose and glucose in various tissues have indicated that pregnancy shows no detrimental influence to the preference of tissues to the two

forms of glucose. Another important consideration is the relative amount of 2-deoxyglucose-6-phosphate hydrolysis by the various tissues under investigation. If these concentrations are quite high then the conversion of 2-deoxyglucose-6-phosphate back to 2-deoxyglucose will produce a significant mis-representation of the glucose utilisation rates. Studies have shown that skeletal muscles, adipose tissue (Ferré *et al.*, 1985) and the diaphragm (Kipnis and Cori 1959) all have very low concentrations of glucose-6-phosphatase, hence, conversion back to 2-deoxyglucose can be thought of as being negligible. This does still put restrictions on looking at certain tissues like the liver and kidney, as both these organs have high glucose-6-phosphatase levels.

2.3.2. Protocol for *in vivo* experiment.

2.3.2.1. Animal preparation and its nutritional status.

All experiments in the absorptive fed state (*ie* maximal gut carbohydrate availability) were started immediately after the light was turned on, post-absorptive fed state (*ie* gut carbohydrate availabilty depleted) experiments were started 4 h after the last meal. Atrially cannulated rats included a control *ad libitum*, 22h starved 2h refed control; 10, 15 and 20 day *ad libitum* pregnant groups (term = 21 days) and a 20 day pregnant RMF group, *see section 2.2* for RMF method. GUI measurements were carried out for both the absorptive and post absorptive states.

Eight syringes were filled with 0.9% saline and blue Sabre needles attached, making sure that all air bubbles were removed (these were used for flushing the cannula of blood and initiating the removal of blood). Eight more syringes were also required

but remained empty (these were used for the removal of the blood sample). A syringe filled with saline (0.9% NaCl) and attached to tube ***B*** (40 cm) was attached to the cannula of the rat. Prior to administration of labelled glucose, 100 μl of blood was withdrawn from the cannula by withdrawing saline from the cannula until blood reached the syringe. At this point the saline filled syringe was removed and an empty syringe attached in its place. The sample was placed into a labelled Eppendorf tube, containing one drop of Heparin (Multiparin; 5000 units/ml). The tube was shaken and 50 μl carefully pipetted into 2.51% zinc sulphate (w/v) [$ZnSO_4.7H_2O$ (250 μl)], this was then shaken and 2.63% barium hydroxide (w/v) [$Ba(OH)_2$ (250 μl) - this was prepared fresh each week as barium carbonate is formed in the presence of CO_2] added, shaken and placed on ice. As soon as the blood sample was removed it is flushed with 500 μl of heparinised saline [0.9% NaCl (w/v) + Heparin (5000 units/ml) 60 μl/100 ml] . The experiment was initiated by the injection of 200 μl of 2-deoxy [^{3}H] glucose (30μl) [1mCi/ml stock (Amersham Ltd.) diluted to 0.15 mCi/ml]. The stop clock was started immediately after the cannula was flushed with 500 μl of heparinised saline.

At time points 1, 3, 5, 10, 20, 40 and 60 minutes, 100 μl blood samples were taken and processed as above. At 60 minutes, approximately 1ml of blood was withdrawn, 50μl being processed as before, and a further 250 μl pipetted into 1 ml of 10% perchloric acid (w/v) for deproteinisation and hence, metabolite determination *see sections 2.5., 2.6., 2.7.*). The experiment was terminated by an over-dose infusion of sodium pentobarbital through the cannula. Cardiac arrest occurs almost instantly post-infusion allowing immediate removal of the tissues shown in *table 2.* Tissue

removal does not have to be too rapid since the amounts of circulating 2-deoxy [^{3}H] glucose after 60 minutes are relatively low and so continued uptake by tissues is small. Each tissue was immediately freeze-clamped in liquid nitrogen and wrapped in labelled aluminium foil. These frozen tissues can be stored at -196°C but are extracted within one week.

After processing of all blood samples, the supernatant was recovered after centrifugation at full speed on a Hettich Rapid/K centrifuge for 5 minutes at 4°C.

Table 2. **Tissues investigated for GUI measurements.**

Muscles and tissues.	**Adipose tissues.**
Gastrocnemius	Parametrial white adipose tissue
Soleus	Mesenteric white adipose tissue
Tibialis anterior	Perirenal white adipose tissue
Extensor digitorum longus	Intrascapular white adipose tissue
Adductor longus	Subcutaneous white adipose tissue
Diaphragm	Brown adipose tissue
Heart	
Placenta (x3)	
Foetus (x3)	

2.3.3. Protocol for *in vitro* tissue extraction.

2.3.3.1. Methods.

This procedure is used to extract the relative amounts of 2-deoxy [^{3}H] glucose and 2-deoxy [^{3}H] glucose-6-phosphate from the tissues freeze clamped and to produce an integral of glucose disappearance from the blood.

Excised tissue was weighed (100-150 mg) and placed into a 5 ml Alpha tube containing 0.5 ml of 1.0M NaOH. The samples were placed in a heating block set at 60°C and incubated for 45 minutes (or until all tissue had been dispersed) with occasional shaking to disperse surface digested tissue. The placentas and foetuses were treated slightly different in that 3 of each were weighed and placed into tubes containing 1 ml and 10 ml NaOH, respectively. Following digestion, tissues were neutralised with 1M HCl, at this stage the samples are stable and can be stored at -20°C.

Two sets of Eppendorf tubes were prepared for each of the tissues, one set contained 1ml of 10% perchloric acid (w/v), and the other 0.5 ml of 2.51% $ZnSO_4.7H_2O$ (w/v) plus 30 μl of universal indicator. Into each set of tubes 200 μl of sample was placed. Into the $ZnSO_4.7H_2O$ tubes, 0.5 ml of 2.63% $Ba(OH)_2$ (w/v) was added to form a precipitate with sulphate which conjugates with 2-deoxy [^{3}H] glucose-6-phosphate and hence removes it from solution. All samples were mixed and centrifuged at 4°C for

8 minutes at full speed in a Hettich Mikro Rapid/K centrifuge. If the barium sulphate precipitated tubes were too acidic or alkaline, then they were neutralised with either NaOH or HCl (adjustment of the pH was usually not required). The supernatants were immediately transferred into another set of tubes following centrifugation. At this stage the samples were either stored at -20°C or counted for tritium.

Sample radioactivity was measured as disintegrations per minute (D.P.M.) by pipetting 800 μl of the supernatants into plastic scintillation vials followed by 10ml of scintillation fluid (Optiphase "HiSafe"; Pharmacia Ltd.) added. The samples were shaken and counted for 3 minutes in a Pharmacia Wallac 1410 scintillation counter.

The de-proteinised blood sample supernatants (100 μl) were counted for 2-deoxy [^{3}H] glucose activity, and their glucose concentrations determined by a glucose oxidase method, *see section 2.4.*.

2.3.3.2. Calculation of glucose utilisation index (G.U.I.).

The counts from each blood sample together with their respective glucose concentration were combined to give a value of D.P.M./ng glucose. This value was plotted against time and the integral of the curve calculated. The integral represented the rate of glucose disappearance in the whole of the body and hence was the comparative value required when looking at specific tissues.

For each of the tissues, the two sets of counts were subtracted from one another to give a value of 2-deoxy [^{3}H] glucose-6-phosphate. This value was then divided by the tissue weight (in mg.) counted and then divided by the integral.

G.U.I. = (2-deoxyglucose-6-phosphate/wt. tissue sample)/ Integral (2-deoxyglucose uptake of body mass).

G.U.I. = (dpm/mg tissue)/(dpm.min/ng glucose).

2.4. Blood glucose determination for G.U.I. calculation.

A glucose oxidase kit was used (Boehringer Mannheim Gmbh Diagnostica, cat. number 124 028) based on the conversion of glucose to gluconate and hence, the production of hydrogen peroxide which oxidises a coloured complex to produce an absorbance change.

2.4.1. Reaction scheme.

glucose + O_2 + H_2O ------*GOD*------► gluconate + H_2O_2

H_2O_2 + ABTS ------*POD*------► coloured complex + H_2O

GOD = glucose oxidase ≥ 10 U/ml

POD = peroxidase ≥ 0.8 U/ml

ABTS = di-ammonium 2,2'-azino-bis(3-ethylbenzothiazoline-6-sulphonate) 1.0 mg/ml.

Into 0.6 ml of the buffer (containing enzymes and coloured reagent) 50 μl of sample was added and incubated at room temperature for 45 minutes. A blank was set up, containing 50 μl of distilled water (dd.H_2O), together with two sets of glucose standards [50 μl standard (0.505 mmol/l) and 25 μl standard plus 25 μl dd.H_2O]. After incubation of all samples for 45 minutes at room temperature, the optical densities were recorded on a PU 8610 spectrophotometer set at 610 nm. Plasma glucose concentrations were calculated on the basis of the standard O.D. readings.

2.5. Plasma glucose determination

Plasma glucose determination was via phosphorylation of glucose by hexokinase [2.7.1.1] followed by the non-equilibrium reaction by glucose-6-phosphate dehydrogenase [1.1.1.49] reducing the $NADP^+$ to NADPH, detected at 340 nm.

Plasma samples must be neutralised using NaOH. The glucose assay buffer was prepared fresh each day from 20 mg ATP (Boehringer 127 523), 17 mg $NADP^+$ (Boehringer 128 058) and 250 μl glucose-6-phosphate dehydrogenase mixed with 50 ml of buffer containing 57.8 mmol/l Tris (Tris[hydroxymethyl]aminomethane Sigma

T 6791), 10.7 mmol/l magnesium chloride (Sigma M 8266) at pH 8.1. Control, blank and standards (1 mmol/l glucose solution) were set up together with sample cuvettes (0.8 ml buffer + 0.1 ml sample). Absorbance at 340 nm was measured prior to and post addition of hexokinase. Incubation period at room temperature was 45 mins..

2.5.1. Reaction scheme:

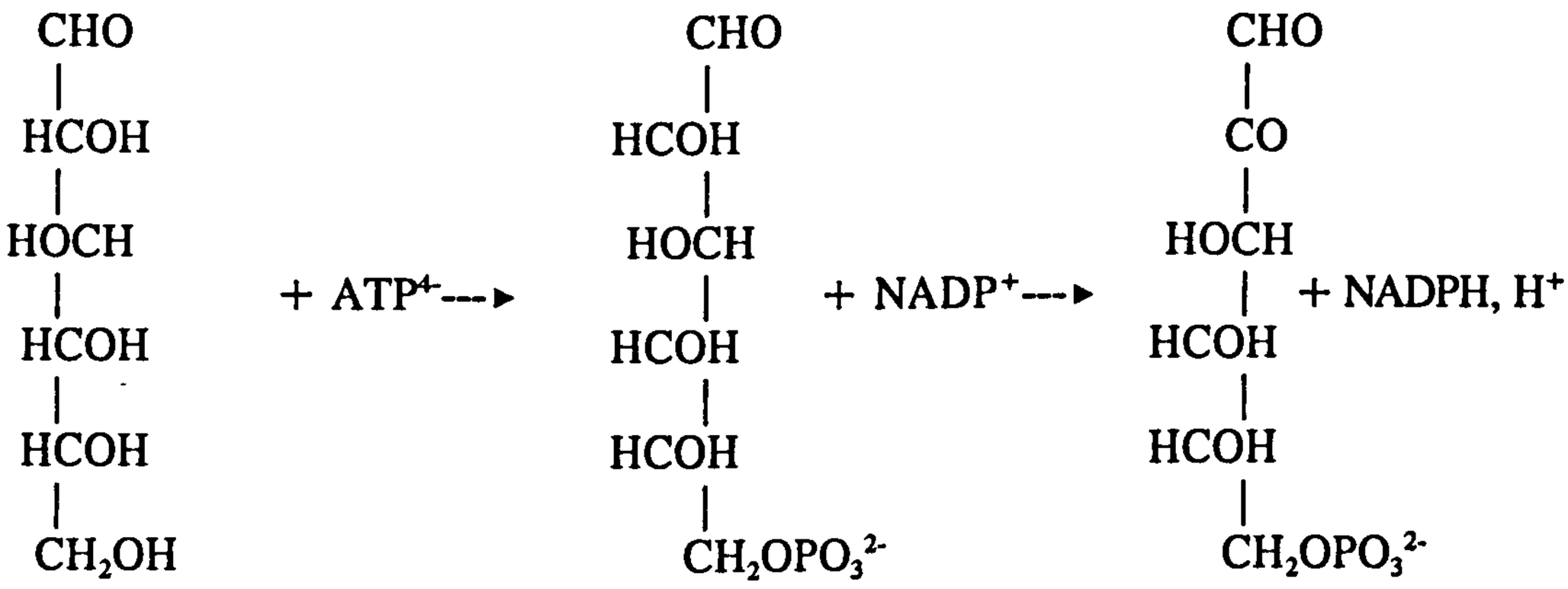

Glucose | Glucose-6-phosphate | 6-phosphogluconolactone

2.6. Method of blood pyruvate, acetoacetate & 3-hydroxybutyrate determination

Blood samples were de-proteinised with 10% perchloric acid, *see section 2.3.2.1.*. The PCA extract was then neutralised with KOH, recording the weight of the sample before and after neutralisation to obtain the dilution factor. Results of pyruvate determinations not shown.

2.6.1. Pyruvate determination.

Sample cuvettes were set up containing 0.3 ml of phosphate/NADH buffer (this contained 5 mg NADH + 20 ml potassium phosphate buffer (0.1 M, pH 7.0)), 0.2 ml ddH_2O and 0.1 ml of sample. Blank readings were recorded at 340 nm on a PU 8610 spectrophotometer after referencing to a blank. Lactate dehydrogenase [EC 1.1.1.27] (10 μl) was added and the samples incubated at room temperature for 5 minutes. Absorbance readings were taken and repeated every 5 minutes until the readings remained stable. From the dilution factors of the samples and the extinction coefficient of NADH (ϵ_{340nm} = 6.23 x 10^3 $M^{-1}cm^{-1}$) the concentration of the samples could be evaluated. Results not shown however method required for acetoacetate determination.

2.6.2. Acetoacetate & 3-Hydroxybutyrate determination (Ketone bodies).

For acetoacetate determination the same cuvette samples as above were used and 10 μl 3-hydroxybutyrate dehydrogenase [EC 1.1.1.30] (Boehringer Mannheim 737 054, 2.5 mg/ml) was added and incubated for 30 minutes at room temperature. Absorbance readings were repeated until the optical density remained constant.

For 3-hydroxybutyrate determinations a stock solution of 5 ml hydrazine hydrate (Sigma H-0883), 7 ml of Tris buffer (1 mmol/l) and 125 mg of EDTA (disodium salt)

was made up to 100 ml with distilled water at pH 8.5 and stored at 4°C. A 20 ml aliquot of this buffer was mixed with 20 mg NAD^+ and 0.3 ml pipetted into 3 ml cuvettes. Control and blank cuvettes were set up with the addition of 0.3 ml of distilled water whereas, sample cuvettes contained 0.2 ml sample and 0.1 ml distilled water. Cuvettes were mixed and optical densities recorded at 340 nm. Hydroxybutyrate dehydrogenase (10 μl; 2.5mg/ml Boehringer 737 054) was added to all cuvettes, except the blank, and optical density readings taken following an incubation period of 45 min..

2.6.3. <u>Reaction Schemes.</u>

I

$$2H^+ + CH_3COCOO^- + 2NADH \dashrightarrow CH_3CH(OH)COO^- + 2NAD^+$$

Pyruvate — Lactate

II

$$2H^+ + CH_3COCH_2COO^- + 2NADH \dashrightarrow CH_3CH(OH)CH_2COO^- + 2NAD^+$$

Acetoacetate — 3-hydroxybutyrate

I - *lactate dehydrogenase.*

II - *3-hydroxybutyrate dehydrogenase.*

2.7. Measurement of *in vivo* lipogenic rates in the liver and adipose tissue sites.

2.7.1. Methods.

2.7.1.1. In vivo experiment and tissue removal.

The rat was injected intraperitoneally with 4 mCi of tritiated water (^3H_2O in 0.9% saline- 10 mCi/ml Amersham Ltd.) and the rats' drinking water removed. The exact time of administration was recorded. After a period of approximately 55 minutes, the rat was anaesthetised with sodium pentobarbital (Sigma P 3761; 60 mg/ml/kg body weight). The body cavity and wall were cut to reveal the gut which was displaced to one side. A blood sample was removed (*ca.* 1.0 ml) from the aorta using a syringe and blue Sabre needle by inserting the needle in the artery via a fat deposit above the kidney area. The blood sample was placed into a heparinised Eppendorf tube and placed on ice. The tissues (see *table 3.*) were excised and freeze-clamped in liquid nitrogen as quickly as possible. As much of each of the tissues was removed to provide adequate sample size for processing. Tissues could be stored at -20°C at this stage.

The blood sample was centrifuged in a Hettich Mikro Rapid/K centrifuge at full speed for 5 minutes at 4°C. The plasma was carefully transferred, with a glass pasteur pipette, into another tube. A volume of plasma was diluted ten times and 10 μl of this counted, in triplicate, for tritium in a Pharmacia Wallac 1410 scintillation counter after the addition of scintillation fluid (Optiphase "HiSafe"; Pharmacia Ltd.). This

gives the total activity of tritiated water in 1 μl of plasma.

Table 3. **Tissues investigated for lipogenic activity.**

(i) Liver.

(ii) Parametrial white adipose tissue.

(iii) Mesenteric white adipose tissue.

(iv) Perirenal white adipose tissue.

(v) Subcutaneous white adipose tissue.

2.7.1.2. In vitro extraction of tissues.

Tissues were weighed (200-500 mg) [two samples of liver were weighed out for cholesterol and fatty acid determination], placed into 25 ml boiling tubes containing 3 ml of 30% potassium hydroxide (KOH w/v). The tubes were incubated for 10 minutes in a DriBlock (Techne, Cambridge Ltd.) set at 80°C to digest the tissue. The tubes were cooled and 3 ml of absolute ethanol (95% v/v) added followed by a further incubation of 3 hours at 80°C to saponify the fatty acids and cholesterol. The tubes were occasionally shaken to aid the saponification process.

2.7.1.3. Extraction procedure for total lipids.

Distilled water (3 ml) was added to dilute the ethanol and increase the volume of the acqueous layer. To obtain total fatty acid and cholesterol synthesis rates the samples were immediately acidified with 6M sulphuric acid and the lipids extracted by the following method. The solution was shaken with light petroleum ether [b.p. 40-60°C AnalaR grade], vented and the top organic layer recovered after separation of the two layers. This was repeated three times in total with the extracts being pooled together in the same tube [N.B. for each of the extractions 10 ml, 8 ml and 6 ml of ether was used, respectively.].

2.7.1.4. Extraction procedure to obtain separate cholesterol and fatty acid synthesis values.

In the case of the liver, where separate values for cholesterol and fatty acids were obtained, one of the liver samples was extracted for cholesterol first followed by the fatty acids. In this situation the solution was shaken with light petroleum ether [b.p. 40-60°C AnalaR grade], vented and the top organic layer recovered after separation of the two layers. This was repeated three times in total with the extracts being pooled together in the same tube [N.B. for each of the extractions 10 ml, 8 ml and 6 ml of ether was used, respectively.]. Following cholesterol extraction, the solution was acidified as above and re-extracted for fatty acids by following the same above

procedure.

All extracts were washed three times with d.H_2O (5 ml) to remove any tritiated water and aqueous components that may persist. The aqueous layer was removed by aspiration and the petroleum ether extracts poured into pre-weighed scintillation vials. The extracts were dried down in a fume cupboard (1-2 days). The vials were re-weighed to give the dry weight of the lipid extracted from the tissue and 10ml of scintillation fluid (Optiphase "HiSafe"; Pharmacia Ltd.) added. After extensive shaking the extracts were counted in a Pharmacia Wallac 1410 scintillation counter.

2.7.1.5. Method of calculation.

Assuming: 1 g H_2O ≡ 1 g plasma ≡ 1 ml plasma

Then: x dpm in 1 μl plasma = x dpm/1 mg H_2O .....1)

Each molecule of H_2O has 1 atom of ^3H

1 μg atom ^3H = 18 μg H_2O = 0.018 mg ^3H_2O

Therefore, 1/0.018 μg atom ^3H = 1 mg H_2O .....2)

Substitute 2) in 1),

$$\frac{x \text{ dpm}}{1/0.018\mu\text{g atom } ^3H} = x \text{ dpm. } 0.018/\mu\text{g atom } ^3H.$$

$$\frac{\text{Counts in tissue}}{\text{Counts in plasma x } 0.018} \times \frac{1}{\text{wet wt.}} \times \frac{1}{\text{time}} = \mu\text{g atom } ^3H/h/g.$$

$$\equiv \mu\text{mol}H_2O\,(^3H+^1H)/h/g$$

N.B. It must be noted that plasma will contain appreciable amounts of protein which has not been taken into consideration for the purposes of the calculation. It has also been assumed that the plasma specific activity of ^3H, following instant mixing with the blood, is equivalent to the total tissue water specific activity for ^3H.

2.8. Preparation of arylamine acetyltransferase (AAT).

2.8.1. Introduction.

2.8.2. Method.

Pigeon liver acetone powder (10 g) [Sigma L-8376] was placed in a conical flask and 100 ml of cold distilled water added. The contents were homogenised at high speed (Polytron Tissue Homogeniser; large probe; position 6) for 3 minutes on ice. The homogenate was distributed into high density polyethylene centrifuge tubes and centrifuged at 13 000 rpm for 15 minutes at 4°C in a MSE Europa 24M Centrifuge. The supernatants (*ca.* 70 ml) were pooled into a 250 ml conical flask and placed on ice, the ice being further cooled with the addition of ammonium chloride (BDH 27149). Into the gently stirring flask, cold acetone (40ml) [AnalaR grade] was slowly dripped from a separating funnel to precipitate protein out of solution. The supernatant was transferred into polypropylene centrifuge tubes and carefully balanced. The tubes were centrifuged for 15 minutes at 13 000 rpm and at -10°C. The supernatants were pooled and re-extracted and centrifuged, as above, but with 25 ml of cold acetone and an operating temperature of the centrifuge at -20°C. Following centrifugation, the pellet was kept and the supernatant extracted for the final time with the dropwise addition of 50 ml of cold acetone. The solution was centrifuged as above at -20°C.

The pellet from the last spin was retained and re-suspended in as small a volume as

possible of 10 mmol/l potassium phosphate buffer [dipotassium phosphate titrated with potassium dihydrogen phosphate obtaining pH 7.0]. The pellet from the third centrifugation was also resuspended in the phosphate buffer. The two sets of pooled pellets were transferred to 1 ml Eppendorf tubes and spun at half speed in a Hettich Mikro Rapid/K centrifuge at 4°C for 2 minutes. The supernatants were carefully recovered, this contained the arylamine acetyltransferase which was assayed for activity, *see section 2.10.3.*. The AAT was stored in aliquots of 250 μl at -20°C.

2.9. Measurement of pyruvate dehydrogenase activity (active form).

2.9.1. Introduction.

The complex consists of three enzymes which catalyse the conversion of pyruvate to Acetyl CoA during aerobic respiration on the inner mitochondrial membrane. The three enzymes are pyruvate dehydrogenase, dihydrolipoamide acetyltransferase and dihydrolipoamide reductase which collectively carry out the following reaction.

2.9.1.1. Reaction scheme.

$$\text{Pyruvate} + \text{CoA} + \text{NAD}^+ \dashrightarrow \text{Acetyl CoA} + \text{NADH} + \text{CO}_2$$

For this reaction to reach completion other factors are needed in conjunction with

three enzymes, these are: thiamine pyrophosphate (TPP), lipoic acid coenzyme A, $FADH_2$ and NAD^+. The pyruvate dehydrogenase (or pyruvate decarboxylase) converts the pyruvate to hydroxyethylthiamine pyrophosphate and the dihydrolipoamide acetyltransferase then transfers a two carbon component from the thiamine pyrophosphate and to CoA to form acetyl CoA. The dihydrolipoamide reductase then oxidises the reduced form of lipoic acid to form $FADH_2$ followed by NADH.

2.9.1.2. Control of the pyruvate dehydrogenase complex.

Control of this enzyme system relies on the phosphorylation state of the complex. Phosphorylation of PDH is catalysed by pyruvate dehydrogenase kinase (PDH kinase) and this form of the enzyme is inactive. De-phosphorylating the PDH complex with pyruvate dehydrogenase phosphatase activates the complex so that pyruvate conversion to acetyl CoA can be carried out. The relative amounts of active and inactive quantities of the PDH complex determine the relative activity of that particular tissue under investigation. Control of the two regulatory enzymes which phosphorylate and dephosphorylate the PDH complex is dependent on several factors, the most important of which are the ratios of ATP/ADP, acetyl CoA/CoA, NAD^+/NADH and Ca^{2+} levels. For example, if there is a relatively high concentration of acetyl CoA or ATP around, then the PDH kinase would be activated to switch the PDH complex off, whereas, with high concentrations of NAD^+ or Ca^{2+} the opposite occurs. Due to the very delicate balance between activation and

inactivation of the PDH complex, it is very difficult to get an accurate measurement for tissue activity unless tissues are assayed on the same day of extraction.

The method of assaying the activity of the PDH complex relies on the transfer of acyl groups onto a coloured compound called aminophenylazobenzene sulphonic acid (AABS). Acyl groups, produced by the pyruvate dehydrogenase complex, are transferred to the AABS via -SH groups of cysteine residues. This reaction is catalysed by the enzyme arylamine acetyltransferase which involves the formation of an acylthioenzyme:-

$$E\text{-}SH + CH_3COS\text{-}CoA \dashrightarrow E\text{-}SH.CH_3COS\text{-}CoA \dashrightarrow E\text{-}S\text{-}COCH_3 + CoA$$

$$E\text{-}S\text{-}COCH_3 + RNH_2 \dashrightarrow E\text{-}SH + RNHCOCH_3.$$

Where RNH_2 = AABS.

The pyruvate dehydrogenase complex, discussed in *section 2.10.1.*, is very easily inactivated once metabolic conditions are drastically altered. Due to this, it is vitally important that, when the tissues were extracted, they were done so as quickly as possible. It is impossible to assay every tissue as in the glucose utilization experiment due to the rapidity of PDH inactivity and therefore, only a couple of tissues can be used per rat which must be removed before any other tissue.

2.9.2. Methods.

2.9.2.1. Chemicals.

1.0 mmol/l KH_2PO_4 (stored at 4°C).
1.0 mmol/l K_2HPO_4 (stored at 4°C).
0.2 mmol/l EDTA-K^+ {Add dropwise 30% KOH to dissolve the salt at its correct pH} stored at 4°C.
0.2 mmol/l EGTA-K^+ {Add dropwise 30% KOH to dissolve the salt at its correct pH} stored at 4°C.
1.0 mmol/l Tris Buffer pH 8.0.
0.1 mmol/l $MgCl_2$.
Dithiothreitol (DTT) (Boehringer 708 992).
Pyruvate (Boehringer 128 147).
Tosyl-Lysine-Chloromethyl Ketone (TLCK) (Sigma t-7254).
Leupeptin 5 mg/ml (Sigma l-2884).
Benzamidine (Aldrich B200-4).
Triton X 100 (25%).
p-(p-aminophenylazo) benzene sulphonic acid (AABS) (1mg/50ml d.H_2O; stored at 4°C).
Mercaptoethanol.
NAD^+.
Co-enzyme A (Sigma C-3144).
Cocarboxylase [Thiamine Pyrophosphate Chloride (TPP) (Sigma C-8754).
Arylamine acetyltransferase (AAT) (Extracted from Pigeon Liver Acetone Powder and stored at -20°C

2.9.2.2. Solutions.

PDH Assay buffer A:

50ml 1.0M KH_2PO_4 (50mM).

50ml 1.0M K_2HPO_4 (50mM).

25ml 0.2M EDTA (5mM).

50ml 0.2M EGTA (10mM).

Extraction Buffer B:

17.5ml PDH Assay Buffer A

30.7mg DTT (2mM)

11.1mg TLCK (0.3mM)

100ul 5mg/ml Leupeptin (10μM)

15.7mg Benzamidine (1mM)

110mg Pyruvate (0.1mM)

pH 7.5 and made up to 100ml

Extraction Buffer C:

Identical to B except, 20 ml of 25% "Triton X-100" was added.

2.9.2.3. Method of extraction

In order to obtain maximal enzyme activity rates, the tissue was removed from the rat and immediately freeze-clamped in liquid nitrogen. Pyruvate dehydrogenase activity was assayed on the same day as excision, with the tissues stored in liquid nitrogen until required.

Extraction buffers B and C were made up fresh each day and kept on ice.

Approximately 100-200 mg of tissue was weighed into a liquid nitrogen cooled scintillation vial and ice-cold extraction buffer B added (0.5 ml/100 mg tissue). The tissue was homogenised using a Polytron Tissue Homogeniser (PT 10 probe; position 3 for 5-10 seconds) to disperse and increase the surface area of tissue. Ice-cold extraction buffer C was added (0.5 ml/100 mg) to the homogenate and homogenised for a further 1-2 seconds to solubilise the cell membranes. The homogenate was transferred into an Eppendorf tube with a pin-hole in the lid, and then frozen in liquid nitrogen. The mitochondrial membranes were then disrupted by a process of freeze-thawing the homogenate three times, ie frozen in liquid nitrogen followed by a gradual thaw at 30°C in a water bath. Insoluble material was removed by centrifugation at full speed in an Eppendorf 5415 C centrifuge for 30 seconds. The fibrous pellet and the supernatant was re-frozen in liquid nitrogen until required for the assay.

2.9.3. Active form pyruvate dehydrogenase activity assay.

2.9.3.1. Solutions

Assay buffer A.

100 ml Tris buffer pH 8.0 (1.0M)
10 ml magnesium chloride (0.1M)
2.5 ml EDTA-K^+ (0.2M)

Made up to 1 litre and pH=7.8.

Assay buffer B.

50 ml Assay buffer A
1 ml AABS
15 μl Mercaptoethanol
Equilibrated at 30°C

NCT solution

30.7 mg NAD^+
10 mg Co-enzyme A
48 mg TPP
Dissolved in 1 ml dd.H_2O
Made fresh each week.

Assay buffer C

0.75 ml Assay buffer B
7.5 μl NCT solution
7.5 μl 100mM Pyruvate
5.0 μl AAT

2.9.3.2. Assay Method

Micro-cuvettes containing assay buffer C were mixed by inversion and placed in a Philips PU 8610 spectrophotometer set at 460 nm and containing a cell temperature controller, set at 30°C. A PM 8521 chart recorder was set at a rate of 1 cm/min. The absorbance change produced by this blank should be relatively negligible, however in the case of a non-steady state, caused by trace acetate contamination, the reaction mixture was allowed to equilibrate until a steady base-line was achieved. The sample was thawed at 30°C and 20-100 μl (*ie.* smaller volumes for tissues with greater PDH activity, like the heart) swiftly added to the reaction cuvette, inverted twice and placed into the spectrophotometer cell temperature controller. The rate of absorbance decrease at 460 nm was recorded on the chart recorder with a suitable full scale deflection.

2.9.4. Calculations for pyruvate dehydrogenase activity.

The trace obtained from the chart recorder gave the relative rate of pyruvate

dehydrogenase activity and hence, the gradient of the trace represented OD change (mm) / time (cm).

This value was multiplied by the below factor, giving the enzyme activity in terms of mUnits/ml.

$$\text{Multiplying factor} = \frac{\text{fsd x assay volume x } 10^3}{\text{pw x } \Sigma_{460} \text{ x sv}}$$

Where:

fsd = full scale deflection of chart recorder (OD)

assay buffer = total volume of reaction mixture (μl)

pw = chart recorder width

Σ_{460} = Extinction coefficient of AABS [6.5 $M^{-1}cm^{-1}$]

sv = sample volume

By knowing the weight of the sample and the volume of extraction buffers used, the concentration of tissue assayed can be calculated and combined with the above value to produce a value in terms of mUnits/gm wet weight.

The value obtained from the above calculation was specific to each individual tissue extracted since different tissues have differing amounts of the PDH complex in their mitochondria. Therefore, the only way to quantify the relative amount of PDH complexes was to compare the activities with a tissue constant. For this purpose the

citrate synthase activity was calculated from the tissue samples. The relative number of citrate synthase molecules compared to PDH complex macromolecules is fairly constant in different tissues. The PDH activity rate is therefore divided by the respective citrate activity. This produces an activity of the pyruvate dehydrogenase complex activity termed as a function of citrate synthase activity.

2.10. Determination of citrate synthase [EC 4.1.3.7] activity

Samples prepared for the pyruvate dehydrogenase assay in *section 2.10.2.* were used for this assay. Citrate synthase, unlike pyruvate dehydrogenase is relatively stable and can therefore be stored at -20°C until required.

Samples were defrosted and diluted as in *table 4.*

Micro-cuvettes were set up as below:

1.5 ml 100 mM Tris buffer, pH 8.0

20 μl 10 mM *DTNB

30 μl 10 mM Acetyl CoA

20 μl diluted sample

*DTNB = 5, 5 -Dithio-bis(2-nitrobenzoic acid) [a sensitive sulphydryl reagent; Sigma D 8130].

A total of five blank readings were taken in a PU 8610 spectrophotometer at 412 nm

to produce an average. Citrate production was initiated by the addition of 20 μl of 75 mM oxaloacetate. The samples were immediately shaken and placed back into the spectrometer. Five readings were taken sequentially to obtain an average rate. Activity rates were expressed in terms of Units/ml.

2.10.1. Reaction Scheme.

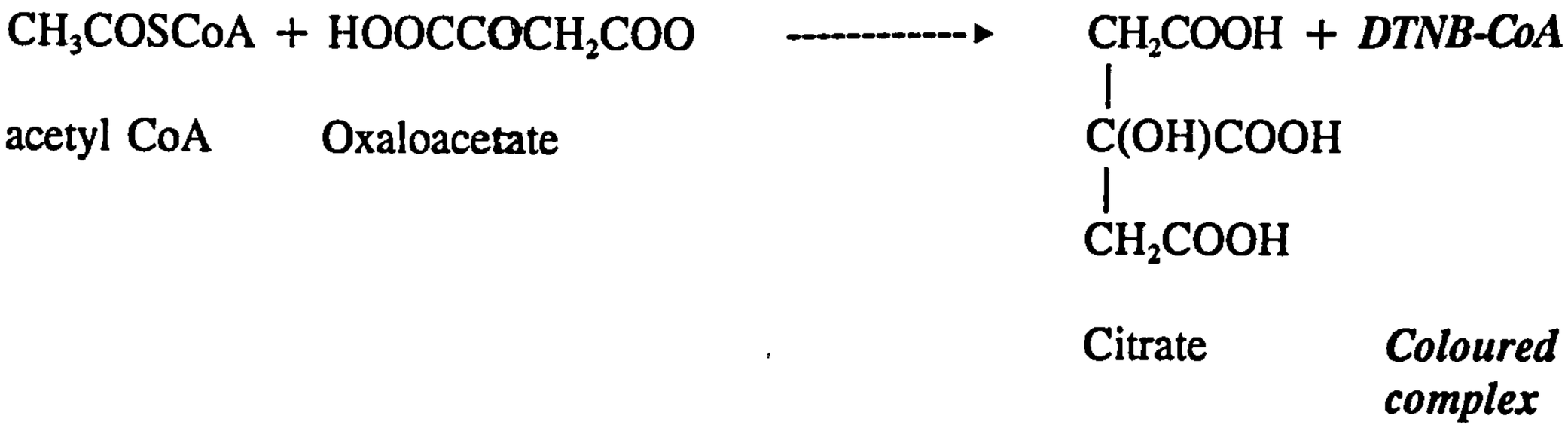

Table 4. **Dilutions used for citrate synthase activity.**

TISSUE	SAMPLE VOLUME	100mM TRIS VOL. pH 8.0.
Heart, Brown adipose tissue.	20 μl	480 μl
Diaphragm.	20 μl	180 μl
Liver, Gastrocnemius, Soleus, Tibialis anterior, Extensor digitorum longus.	20 μl	80 μl
Adductor longus.	50 μl	50 μl

2.11. Method for hepatic glycogen quantitation.

2.11.1. Glycogen extraction protocol.

Approximately 50-100 mg. of frozen liver was weighed into a pre- "liquid nitrogen cooled" glass scintillation vial. The liver was homogenised with 0.03 mmol/l HCl (5 ml) for 5-10 seconds with a Polytron PT10 Tissue Homogeniser [large probe; position 5). The homogenate (0.5 ml) was transferred to a 10 ml centrifuge tube and 0.03 mmol/l HCl added. At this stage 3 triplicate standards were made up:-

x3	**(a)**	1.0 ml 0.03M HCl.
x3	**(b)**	0.5 ml glycogen stock solution (Sigma G-8876) [0.3 mg/ml 0.03M HCl] + 0.5 ml, 0.03M HCl.
x3	**(c)**	1.0 ml glycogen stock.

All samples and standards were placed into a water bath at 100°C for 5 min. The tubes were removed and 0.1 ml of 1 mmol/l NaOH added. After mixing, the tubes were returned to the water bath for a further 10 min. The tubes were allowed to cool down and 0.1 ml of 1.5 mmol/l acetic acid pipetted into the samples, the samples were mixed thoroughly and 2 ml of 0.1 mmol/l acetate buffer added [4.1g sodium acetate + 2.86 ml glacial acetic acid made up to 1 litre; pH 4.7 and stored at 4°C]. After mixing, the samples were centrifuged in a MSE Mistral 3L at 5000 rpm for 5 mins. at 4°C. Supernatants (0.5 ml) were collected into labelled Eppendorf tubes ready for glycogen digestion with amyloglucosidase.

2.11.2. Glycogen digestion protocol.

A solution containing amylo-1,6-glucosidase was freshly made with the following components:-

20 mg Bovine serum albumin (Sigma A 6003)

10 mg Amylo-1,6-glucosidase (Boehringer Mannheim Gmbh. 208 469)

10 ml Tris [Tris(hydroxymethyl)aminomethane (Sigma T 6791)

buffer (20 mmol/l ; pH 7.5 stored at 4°C)

To both samples and standards a 0.1 ml aliquot of amylo-1,6-glucosidase solution was added and mixed by gentle inversion. The samples were incubated at room temperature for 2h.

2.11.3. Reaction scheme:

Amylo-1,6-glucosidase catalyses the release of glucose subunits between branches of glucose chains in the glycogen macromolecule. The α-1,6 linkage is broken down releasing approximately 7% of the total glucose subunits. Therefore use of this enzyme does not constitute the complete release of all glucose subunits but the value obtained is a measure of total glucose on the assumption that glycogen molecules closely resemble one another. Released glucose was measured by the hexokinase/glucose-6-phosphate dehydrogenase method, *section 2.5.*.

2.11.4. Calculation of glycogen.

Glycogen was calculated from the relative amount of glucose released by the debranching enzyme. From the optical densities of the glycogen standards the weight of glycogen (mg) per gram of tissue assayed was calculated.

$$\text{Total liver weight assayed} = \frac{\text{Dry wet weight of sample}}{384}$$

$$\text{Total glycogen content following digestion} = \frac{OD_{sample}}{OD_{standard}} \times [\text{standard}].$$

Where OD = optical density
[] = concentration assayed.

2.12. Statistics.

Statistical significance of differences between means was assessed by Student's unpaired t test. All results are given as means ± SEM for n=6 rats unless otherwise stated.

CHAPTER 3.

RESULTS.

3.1. Rat weight, liver weight, heart weight and chow intake during the period of gestation.

From the results shown in *table 5* it can be seen that rat weights increase steadily during pregnancy. Up to day 10 of pregnancy the increase is almost linear, after which the rate of increase is more exponential. Just prior to giving birth, the mother gains almost 50% more weight within a space of just 3 weeks, reflecting the extent of the physiological change brought about during pregnancy. To cope with the extra foetal demand chow intakes are also shown to increase substantially compared with the virgin condition. On day 20 of pregnancy, chow consumption increases to approximately 33 g. Chow intake represented a net increase of 84% during late gestation as against day 3 of gestation, this far exceeds the net rat weight increase implying enhanced metabolic growth systems being promoted in the conceptus. From a diurnal food consumption study it was revealed that approximately 30% of the total daily food intake was consumed during the final 3 h of the dark phase just prior to sampling. Approximately 80% of total food intake was consumed in the 12 h dark phase, independent of pregnancy.

Table 5.

Changes in rat weights and food intakes during the course of gestation in the Wistar rat.

Day	Rat Weight ± SEM (g).	Daily Food Intake ± SEM (g).
2	215.42 ± 5.91 (13)	--
3	227.20 ± 4.85 (16)	18.33 ± 2.04 (7)
4	231.48 ± 6.57* (12)	21.23 ± 1.37 (8)
5	229.48 ± 4.26* (23)	19.50 ± 2.11 (8)
6	232.79 ± 3.45** (38)	21.55 ± 1.68 (16)
7	240.19 ± 4.65*** (39)	22.69 ± 0.81 (25)
8	233.74 ± 3.58*** (32)	22.78 ± 0.63# (22)
9	238.85 ± 3.10*** (32)	23.73 ± 1.14# (22)
10	240.15 ± 3.86*** (33)	24.22 ± 1.09## (19)
11	253.30 ± 5.62**** (30)	23.99 ± 1.35## (16)
12	256.23 ± 4.50**** (41)	25.37 ± 0.77### (18)
13	262.83 ± 3.55**** (54)	26.03 ± 1.15### (27)
14	264.59 ± 3.02**** (47)	27.80 ± 0.96#### (33)
15	268.95 ± 3.92*** (37)	28.88 ± 1.32#### (21)
16	278.73 ± 4.58**** (32)	27.79 ± 1.30#### (19)
17	290.93 ± 5.08**** (27)	30.49 ± 0.92#### (19)
18	289.67 ± 6.29**** (28)	28.18 ± 1.54#### (17)
19	300.22 ± 8.48**** (19)	31.24 ± 2.30#### (10)
20	319.35 ± 11.70**** (10)	33.80 ± 1.96#### (10)

Numbers in brackets represent the number of rats in each group. Statistical significance between the means of age-matched virgin rats for increases in rat weight are represented by *P<0.1; **P<0.2; ***P<0.01; ****P<0.001. Significant differences between food intakes during gestation compared with age-matched virgin rats are represented by #P<0.05; ##P<0.02; ###P<0.01; ####P<0.001.

In *chapter 1*, organ weights were said to increase during pregnancy as the demands on them also increased. From *table 6.*, liver weights increased by 45% and the heart by a modest 8% at 20 days. The hearts weight increase was relatively small and not really apparent until approximately day 15 of pregnancy, this being the period of enhanced foetal growth. This was not expected, especially with the very substantial increase in the uterine system and the liver, both implying a greater blood flow requirement.

Table 6. **Changes in heart and liver weights during the course of gestation in the Wistar rat.**

	Heart wt. (g)	Liver wt. (g)
Virgin	0.778 ± 0.028 (12)	10.21 ± 0.36 (13)
10 days	0.754 ± 0.038 (6)	12.58 ± 0.82$^{\#}$ (4)
15 days	0.828 ± 0.024 (11)	13.70 ± 0.82$^{\#\#}$ (7)
20 days	0.842 ± 0.024* (6)	14.82 ± 0.33$^{\#\#\#}$ (5)

Statistically significant differences to the virgin weights are represented by $^{*}P<0.1$; $^{\#}P<0.02$; $^{\#\#}P<0.01$; $^{\#\#\#}P<0.001$. Numbers in brackets represent the sample size.

3.2.1. Effects of pregnancy on the glucose utilisation capacity of various tissues during the immediate fed period (absorptive state).

From *table 7* it can be seen that as gestation progresses the relative degree of hypoglycaemia increases. At 10 days of gestation glucose concentrations were already significantly reduced from virgin values *ie.* 5.81 ± 0.23 to 5.00 ± 0.18 mmol/l ($P<0.05$). By days 15 and 20 of gestation blood glucose levels were 3.68 ± 0.18 mmol/l and 3.37 ± 0.10 mmol/l ($P<0.001$), respectively. These values represent decreases of 37% and 42%, respectively.

From the results in *table 7 and figures 4 & 5* significant effects of pregnancy can begin to be seen in most tissues (except the soleus) as early as day 10 of gestation. As pregnancy progresses to days 15 and 20 the effects are very apparent, with the greatest changes shown by the normally high glucose utilising tissues of the heart, diaphragm and soleus muscles. The skeletal muscles can be grouped into two, the first being the working oxidative muscles (soleus and adductor longus) and the second, the non-working muscles (tibialis anterior (TA) and extensor digitorum longus (EDL). Both sets of tissues show their most significant declines during the latter part of the gestation period with the non-working muscles showing the greatest degree of suppression in GUI. On day 15 of pregnancy the glucose utilisation rates of the non-working muscles were reduced by 51-61%, whereas the working muscles reduced by 27-37%. By day 20 of gestation the working muscles showed reductions of 58%. However, the non-working muscles decline even further by 76% and 80%, in the TA and EDL, respectively.

The reductions shown in the various tissues can be seen to be progressive through the course of pregnancy. The stage of pregnancy therefore, depicts the relative degree to which the tissues reduce their capacity to utilise glucose as their preferred fuel substrate. As pregnancy progresses so does the decline in glucose uptake and phosphorylation by the tissues. The heart and diaphragm both expend large amounts of energy due to their constant rhythmic contractions and hence are expensive utilisers of the maternal free circulating glucose pool. Significant reductions in GUI values of 34% were seen on day 10 of pregnancy in both heart and diaphragm. As gestation progressed to 15 days the suppression increased to 46% in the heart, however no further reduction in GUI was observed in the diaphragm. The greatest suppression was shown on day 20 of pregnancy where the heart reduced to a value of 160.0 ± 35.6 nmol/min/g which is 51% lower than the 15 day value and 74% lower than the control virgin value. The diaphragm showed a reduction from the 10 day pregnant and virgin values of 59% and 73%, respectively. The most significant decrease in glucose utilisation by these two tissues were seen between 15 and 20 days which coincides with the most rapid developmental stage of the conceptus, shown by the rat weight increase (*table 5.*), which during this period increased by almost 30%.

3.2.2. Effects of pregnancy on the glucose utilisation capacity of various tissues during the post-absorptive fed period.

Blood glucose concentrations show a marked difference to the corresponding values in the immediate absorptive state, compare *table 7 and table 8.* Glucose concentrations in non-pregnant rats reduce from 5.81 ± 0.23 mmol/l to 4.68 ± 0.13 mmol/l in the post absorptive state. Unlike the absorptive state significant reductions in glucose concentrations during pregnancy are not seen until day 15. The value obtained on this day of gestation is 14% ($P<0.01$) lower than the non-pregnant values however, in the absorptive state the value is 37% ($P<0.001$) lower than the corresponding non-pregnant value *ie.* 3.68 ± 0.18 mmol/l. By day 20 of pregnancy glucose concentrations reduce to 3.37 ± 0.38 mmol/l which is similar to the corresponding absorptive state.

From the results in *table 8 and figures 4 & 5* it can be seen that performing glucose utilisation measurements 4 hours after the light is switched on shows a reduction in the tissues' ability to utilise glucose in the virgin rat. This is expected since during the light phase the rat would be resting and hence, in a state of starvation, reducing the tissues' need to utilise glucose. The GUI values for the different stages of gestation show the same pattern of suppression as in the absorptive state but values are slightly lower due to the post-absorptive nutritional status. The greatest suppression of glucose uptake and phosphorylation is once again shown on day 20 of gestation. The heart and diaphragm show a decline of 74% and 51%, respectively, from the virgin post-absorptive state which is similar to values obtained for the

absorptive 20 day pregnant state. This would imply that the limit of glucose utilisation suppression has been reached. Despite this suppression in GUI during the latter stage of gestation there was no significant suppression during the early stages of gestation although values were lower. The two working muscles (soleus and adductor longus) showed reductions of 40% and 78%, respectively, on day 20 of gestation these values are greater than the corresponding absorptive values. Non-working muscles on day 20 of gestation showed a similar suppression as the absorptive state of 38% in the tibialis anterior and 18% in the EDL. On day 10 of gestation, values were similar to the virgin post-absorptive values; however, by day 15 of gestation they had fallen by 38% and 18% in the tibialis anterior and EDL, respectively.

Table 7. *Muscle GUI values during the course of gestation in the absorptive phase.*

Tissue	Virgin	10 days	15 days	20 days
	GUI (nmol glucose/min per g of tissue)			
Heart	611.1 ± 64.4	401.7 ± 66.1*	327.8 ± 59.4**	160.0 ± 35.6***
Diaphragm	358.3 ± 40.6	235.0 ± 32.2*	250.0 ± 36.7*	97.2 ± 25.0***
Soleus	327.2 ± 26.7	253.9 ± 31.1	240.0 ± 17.8*	134.4 ± 16.7***
Adductor Longus	282.8 ± 31.7	201.1 ± 21.1*	178.3 ± 19.4*	120.0 ± 22.2**
Tibialis Anterior	86.7 ± 14.4	41.1 ± 6.1*	33.9 ± 10.0*	21.1 ± 4.4**
EDL	64.4 ± 12.8	31.7 ± 7.8*	31.7 ± 11.1*	12.8 ± 1.1**
Glucose [mmol/l]	5.81 ± 0.23	5.00 ± 0.18*	3.68 ± 0.18***	3.37 ± 0.10***

Statistically significant effects of pregnancy compared with the control virgin condition are represented by *P<0.05; **P<0.01; ***P<0.001. n=6 for all groups. Abbreviation: EDL, Extensor digitorum longus.

Table 8. *Muscle GUI values during the course of gestation during the post-absorptive state.*

	GUI (nmol glucose/min per g of tissue)			
Tissue	**Virgin**	**10 days**	**15 days**	**20 days**
Heart	477.2 ± 68.9	432.8 ± 51.6	330.0 ± 41.7	123.3 ± 10.0***
Diaphragm	175.0 ± 20.0	233.3 ± 38.9	156.7 ± 31.1	83.9 ± 30.0*
Soleus	115.6 ± 17.2	150.0 ± 26.1	68.3 ± 9.4*	69.4 ± 12.2*
Adductor Longus	96.1 ± 14.4	98.3 ± 27.8	51.1 ± 6.1*	26.1 ± 3.3***
Tibialis Anterior	27.7 ± 3.9	35.6 ± 10.0	17.2 ± 2.8*	11.1 ± 2.8**
EDL	18.3 ± 0.6	23.9 ± 4.4	15.0 ± 12.2*	8.9 ± 1.7***
Glucose [mmol/l]	4.68 ± 0.13	4.69 ± 0.19	4.03 ± 0.14**	3.37 ± 0.38**

Statistically significant effects of pregnancy compared with the control virgin condition are represented by *P<0.05; **P<0.01; ***P<0.001. n=6 for all groups. Abbreviation: EDL, Extensor digitorum longus.

GUI Values During Pregnancy During The Absorptive & Post-Absorptive States.

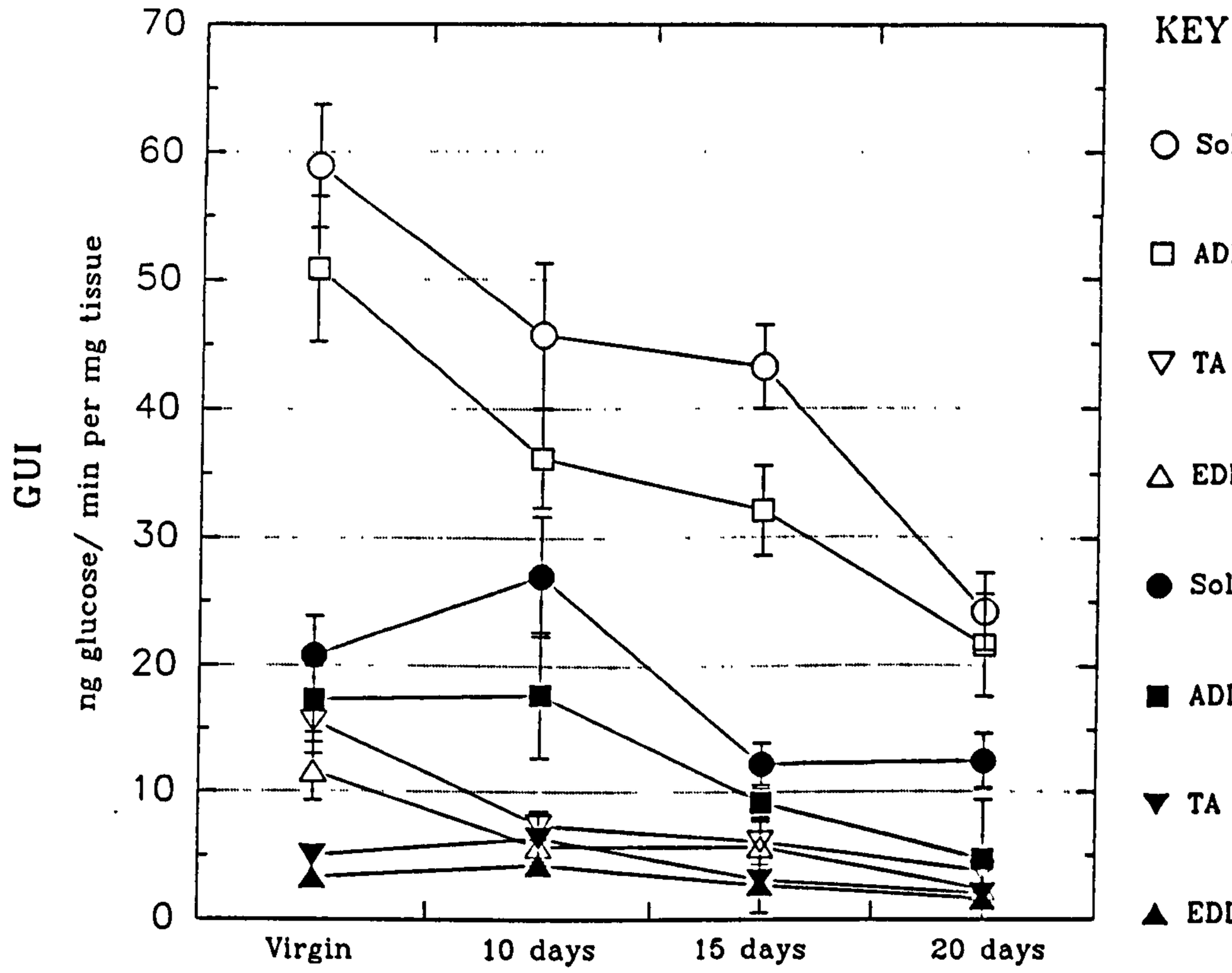

Figure 4.

GUI Values During Pregnancy During The
Absorptive & Post-Absorptive States.

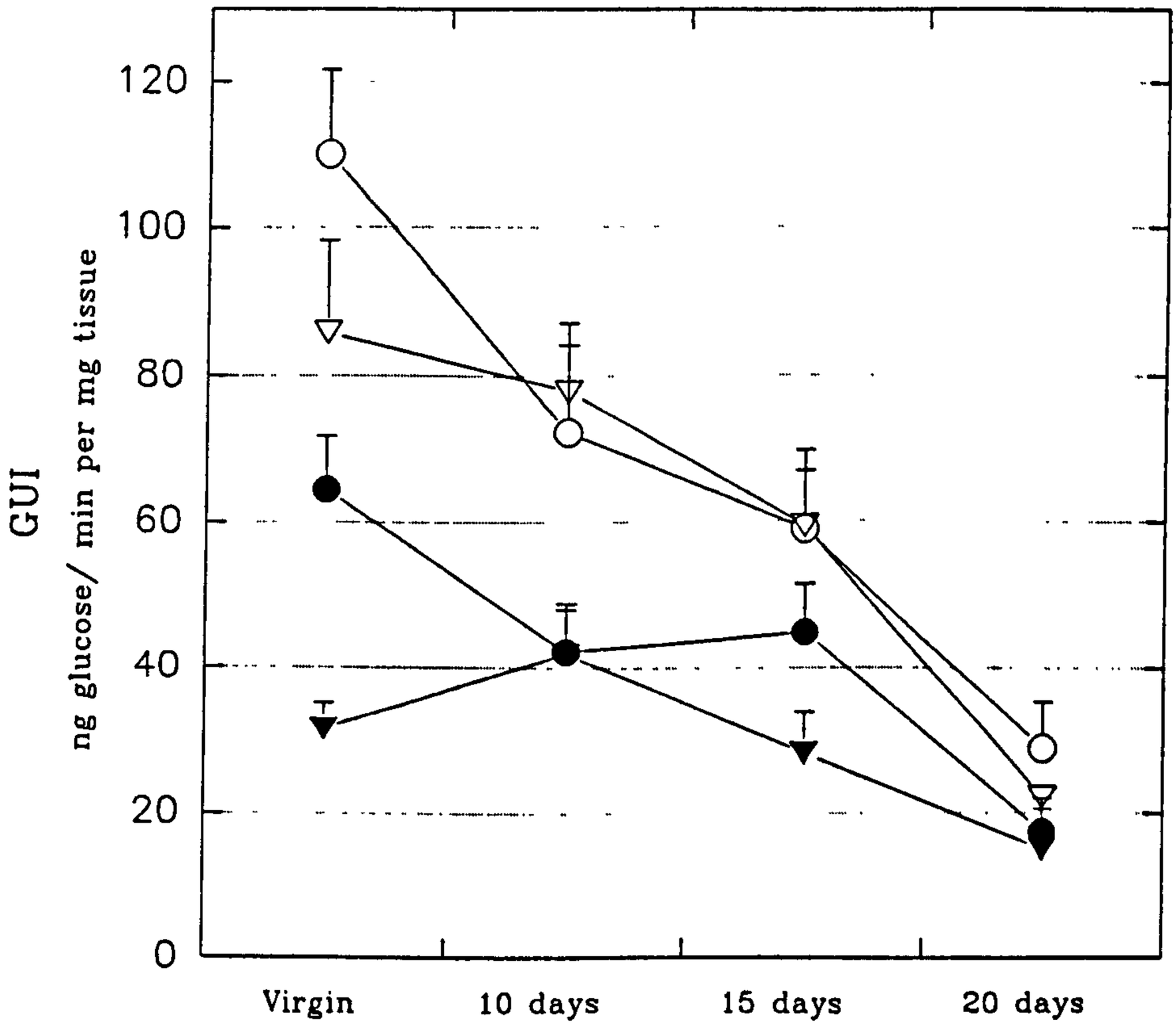

Figure 5.

3.2.3. Hepatic glycogen, lipid fuels, ketone bodies and insulin concentrations during pregnancy in the absorptive state.

From *table 9* it can be seen that despite increased food intakes, free access to food and measurements being made in the absorptive state, significant increases in total ketone bodies and non-esterified fatty acids (NEFA) occur. Largest increases of 480% and 135% were seen in ketone body and NEFA plasma concentrations, respectively. Triacylglycerols also increased but to a lesser degree. The large increases in ketone body and NEFA concentrations were only seen on day 20 of gestation, this is despite the increase in blood plasma vascularity, *see section 1.3.3.*. Hepatic glycogen levels indicate that the progression of pregnancy does not affect levels. However, on day 20 of gestation slightly lower glycogen levels of 58.8 $\pm$ 4.5 mg/g compared with 72.6 $\pm$ 8.2 mg/g in the non-pregnant group were seen The insulin concentration decreased from 26.2 $\pm$ 2.2 μ-units/ml to 14.1 $\pm$ 3.1 μ-units/ml by day 20 of gestation, a reduction of 46% which is comparable to the plasma glucose reduction of 42% in the absorptive state. This implies that the insulin response by the mother is unaffected during gestation.

Table 8a. ***Hepatic glycogen, lipid fuels, ketone bodies and insulin concentrations during pregnancy in the absorptive state.***

Day of pregnancy	Glycogen mg/g	NEFA mmol/l	Total ketone bodies. mmol/l	Triacylglycerols mmol/l	Insulin μ-units/ml
0	72.6 ± 8.2	0.34 ± 0.08	0.12 ± 0.04	1.45 ± 0.23	26.2 ± 2.2
10	65.7 ± 9.9	0.22 ± 0.01	0.23 ± 0.08	--	--
15	73.3 ± 5.7	0.27 ± 0.06	0.15 ± 0.05	--	--
20	58.8 ± 4.5	0.80 ± 0.12*	0.70 ± 0.15*	1.7 ± 0.19	14.1 ± 3.1*

All concentrations, except for glycogen, were from plasma measurements (n=6). Glycogen values represent the mg of glycogen per gram wet weight of liver assayed by amyloglucosidase digestion. Significant differences to virgin values are represented by *$P<0.01$.

Discussion.

A study by Leturque *et al.* (1986) showed no difference in glucose utilisation rates by the diaphragm and soleus muscles of anaesthetised rats in the post absorptive state. In a later study by Pénicaud *et al.* (1987) the effect of anaesthesia on glucose utilisation was shown. Pentobarbital anaesthesia has the effect of reducing the capacity for tissues to utilise glucose hence, under-estimating *in vivo* glucose utilisation. In the above study the rats were unrestrained and conscious and showed clear suppression in glucose utilisation rates by the various muscle types investigated. This study has shown the extent of glucose intolerance by the various skeletal muscles irrespective of their fibre composition. It is apparent that the extent of suppression of glucose utilisation is dependent on the duration of gestation and the nutritional status of the rat. The GUI capacity of the various muscles were maximally reduced on day 20 of gestation, however in the immediate absorptive state significant reductions were observed 10 days into pregnancy. Greatest suppressions in GUI were shown by the heart which by 20 days of gestation, in both the absorptive and post-absorptive states, were significantly reduced to values normally seen in 24 h starved virgin rats (Holness and Sugden, 1990). Non-working muscles and oxidative working muscles all showed vast reductions in glucose uptake and phosphorylation during the latter stages of pregnancy in the rat. It is interesting to note that even when carbohydrate is readily available, as in the absorptive state, GUI values were at levels resembling virgin post-absorptive values, except the heart and diaphragm which resembled higher degrees of starvation.

This study shows the extent by which maternal blood glucose is diverted away from the mothers' intracellular metabolic pool, presumably for use by the developing foetus(es). All the muscle fibre types investigated showed significant degrees of suppression in their capacity to utilise glucose. The post-absorptive study demonstrated the accelerated response to food withdrawal during pregnancy. Once again the response to food withdrawal by the various tissues was highly dependent on the duration of gestation, the greatest suppressions shown by the 20 day pregnant groups. In general the GUI values by all the working and non-working muscles showed a decrease in their ability to utilise glucose in the post-absorptive state compared with the corresponding absorptive state. This was not true for the heart which had GUI values which were very similar in both nutritional states. This is despite the free availability of glucose in the immediate absorptive state and would suggest that as gestation progresses the heart has the greatest susceptibility to the imposed glucose intolerance. The heart, even during the absorptive state, must be using other oxidisable substrates such as ketone bodies and lipids to meet its demands. The fact that there was no difference between the two nutritional states at any of the three time points during pregnancy seems to imply that the heart has been "targeted" as an expensive glucose drain. The control virgin GUI values indicate this point. Fortunately the heart has the capacity to utilise other oxidisable substrates depending on the physiological condition imposed, *see section 1.4.*

Despite the relatively high glucose concentration in the post-absorptive state, which is very comparable to the absorptive 20 day pregnant state, the mother is restrained from utilising glucose. Reducing the capability of the mother to utilise the circulating

glucose imposes a large energy deficit which has to be met by other fuels such as lipids and ketone bodies both of which are shown to increase substantially, *see table 8a*. Both these fuels can substitute for carbohydrate substrates especially in the oxidative tissues and the brain. Considering the extent of suppression of glucose utilisation by the various tissues it may be expected that concentrations of NEFA and ketone bodies would steadily increase during gestation to compensate for the reduced maternal glucose utilisation. However, from *table 8a* it is clear that plasma concentrations of these substrates are not seen to increase until day 20 of gestation in the post absorptive state. A possible explanation could be the increased utilisation of these fuels, especially by the heart. This would have the net effect of decreasing the plasma concentrations which would otherwise be seen to increase *ie.* increased utilisation of these fuels is directly met by increased mobilisation therefore, producing no net effect on concentrations. It must be noted that NEFA plasma concentrations are seen to decrease slightly during the first two trimesters of pregnancy which could reflect the increased utilisation of this fuel.

An important observation was the decrease in insulin levels in late pregnant rats. A reduction in insulin would imply reduced glucose utilisation by the mother. Hence, it could be thought that the glucose intolerance is not secondary to insulin resistance but to other factors such as a reduction in numbers of tissue or pancreas glucose receptors *etc.* A study by Leturque *et al.* (1984) showed, using a euglycaemic hyperinsulinaemic clamp on anaesthetised pregnant rats, that pregnancy does constitute an insulin resistant state. It was shown that insulin concentrations causing half maximal utilisation of glucose in virgin rats was 200 μU/ml and in 19 day

pregnant rats was 500 μU/ml. However, in this same study insulin levels during pregnancy were shown to be slightly higher compared with age-matched virgin rats. This contradicts the changes seen in this study where insulin levels reflect the degree of glycaemia of the rats, anaesthesia could therefore be influencing insulin secretion. However, studies on pregnant women have shown steady increases in the levels of plasma insulin during gestation (Freinkel, 1980). Insulin resistance must therefore be assessed by euglycaemic hyperinsulinaemic clamp studies on unrestrained unanaesthetised rats to resolve this discrepancy.

3.3. Effects of pregnancy on the lipogenic rates of the liver and white adipose tissue sites.

3.3.1. Liver.

Glucose uptake and phosphorylation by the various muscle types has been shown to be greatly suppressed as gestation progresses. Fuel demands of the mother however, still must be met. The most likely oxidative substrate candidates are the lipid derived fuels such as FFAs and ketone bodies. These are supplied by the liver following triglyceride oxidation. *Tables 9 & 10 and Figures 6 & 7* show the lipogenic rates during the course of pregnancy in the liver and five different adipose tissue sites. The liver shows an exponential increase in its lipogenic activity. This increase however, is mainly due to the contribution of newly synthesised fatty acids rather than cholesterol. Cholesterol synthesis rates remain relatively constant throughout

pregnancy. However, there is a slight increase but its significance is difficult to assess, as this increase could be the result of increased hormone production. Total lipid synthesis rates increase by 190% towards the end of gestation which again reflects the similar increase in fatty acid synthesis. The increased fatty acid synthesis will have two benefits for the "fuel" starved mother. Firstly, the fatty acids can be exported out of the liver packaged with apolipoprotein to be used as fuel in peripheral tissues or stored in adipose tissue. Secondly, in the fasting periods the liver will breakdown fatty acids to release ketone bodies into the maternal blood. Ketone bodies, as previously discussed, are far more easily transported both inter and intracellularly compared with either FFA or lipoprotein fractions.

3.3.2. Adipose tissues.

The various adipose tissue sites show a similar lipogenic response to pregnancy as the liver. Significant changes can be seen from day 15 onwards in all the adipose tissue sites investigated. By day 20, the parametrial and perirenal white adipose tissues increased to a value 180% higher than virgin fed controls, the mesenteric increased by 125% and the subcutaneous to a greatly enhanced level which was 305% higher than the non-pregnant condition. The response by the adipose tissue sites to gestation reinforces the idea that the mother has the potential to use lipid derived fuel substrates when utilisation of glucose is suppressed. Lipids play a significant role in supplying the mother with oxidisable substrates allowing the developing foetus(es) to utilise what seems to be the preferred substrate, glucose. The rates of lipid synthesis in both

the liver and adipose tissue sites can be seen to increase exponentially towards term, this directly coincides with the growth pattern of the foetus(es) which show their greatest development in the latter stages of gestation.

Table 9.

Changes in hepatic fatty acid, cholesterol and total lipid synthesis rates during the course of pregnancy.

Liver Lipogenic Rates μmol $H_2O(^3H+^1H)$ incorporated / h / g liver.

	Virgin n=7	10 days pregnant n=4	15 days pregnant n=8	20 days pregnant n=8
Fatty acids	10.16 ± 1.41	14.15 ± 1.82	14.04 ± 4.51	35.47 ± 5.81***
Cholesterol	2.95 ± 0.46	2.41 ± 0.32	4.06 ± 0.77	4.54 ± 0.32*
Total lipid	13.40 ± 1.72	15.79 ± 1.80	24.96 ± 2.67**	39.22 ± 6.08**

Statistically significant differences between virgin and pregnant rats are represented by *P<0.02; **P<0.01; ***P<0.001.

Table 10.

Changes in total lipid synthesis rates in white adipose tissue sites during the course of pregnancy.

White Adipose Tissue Lipogenic Rates μmol H_20 ($^3H+^1H$) incorporated / h / g.

	Virgin (n=7)	10 days pregnant (n=4)	15 days pregnant (n=8)	20 days pregnant (n=8)
Parametrial	1.80 ± 0.64	1.71 ± 0.62	3.08 ± 0.83	5.07 ± 1.76*
Mesenteric	3.16 ± 0.68	3.48 ± 0.69	4.56 ± 1.12*	7.09 ± 1.72***
Perirenal	2.84 ± 0.61	3.03 ± 0.63	5.06 ± 1.52	7.91 ± 3.01
Subcutaneous	3.45 ± 0.67	2.88 ± 0.60	8.36 ± 1.91**	13.96 ± 2.58****
Interscapular	5.28 ± 1.59	3.00 ± 0.70	8.32 ± 1.49	13.02 ± 3.87*

Statistically significant differences between pregnancy and control virgin rats are represented by *P<0.1; **P<0.05; ***P<0.02; ****P<0.01.

Rat Liver Lipogenic Rates During Various Stages Of Gestation.

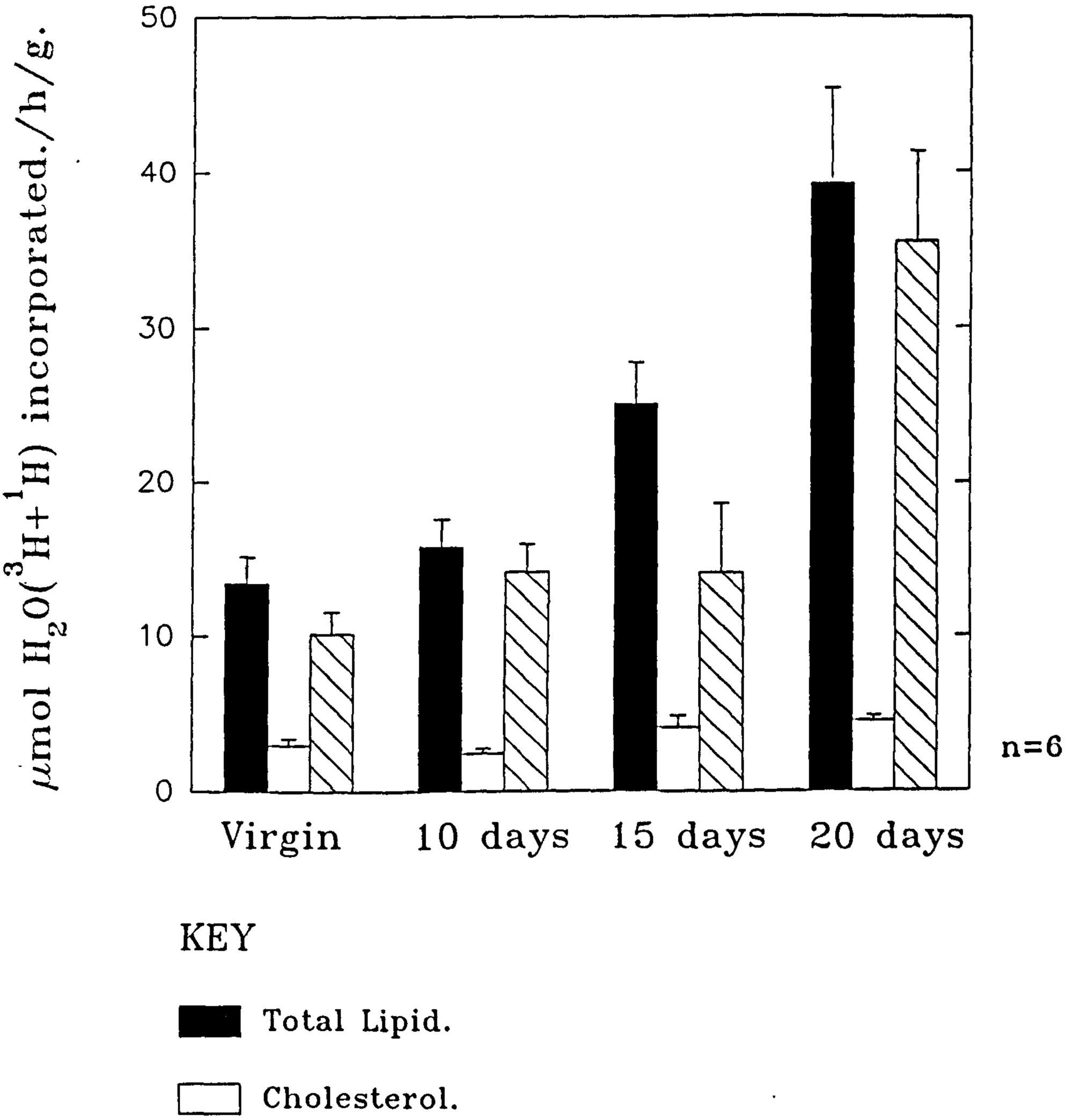

Figure 6.

Rat White Adipose Tissue Lipogenic Rates During Various Stages Of Gestation.

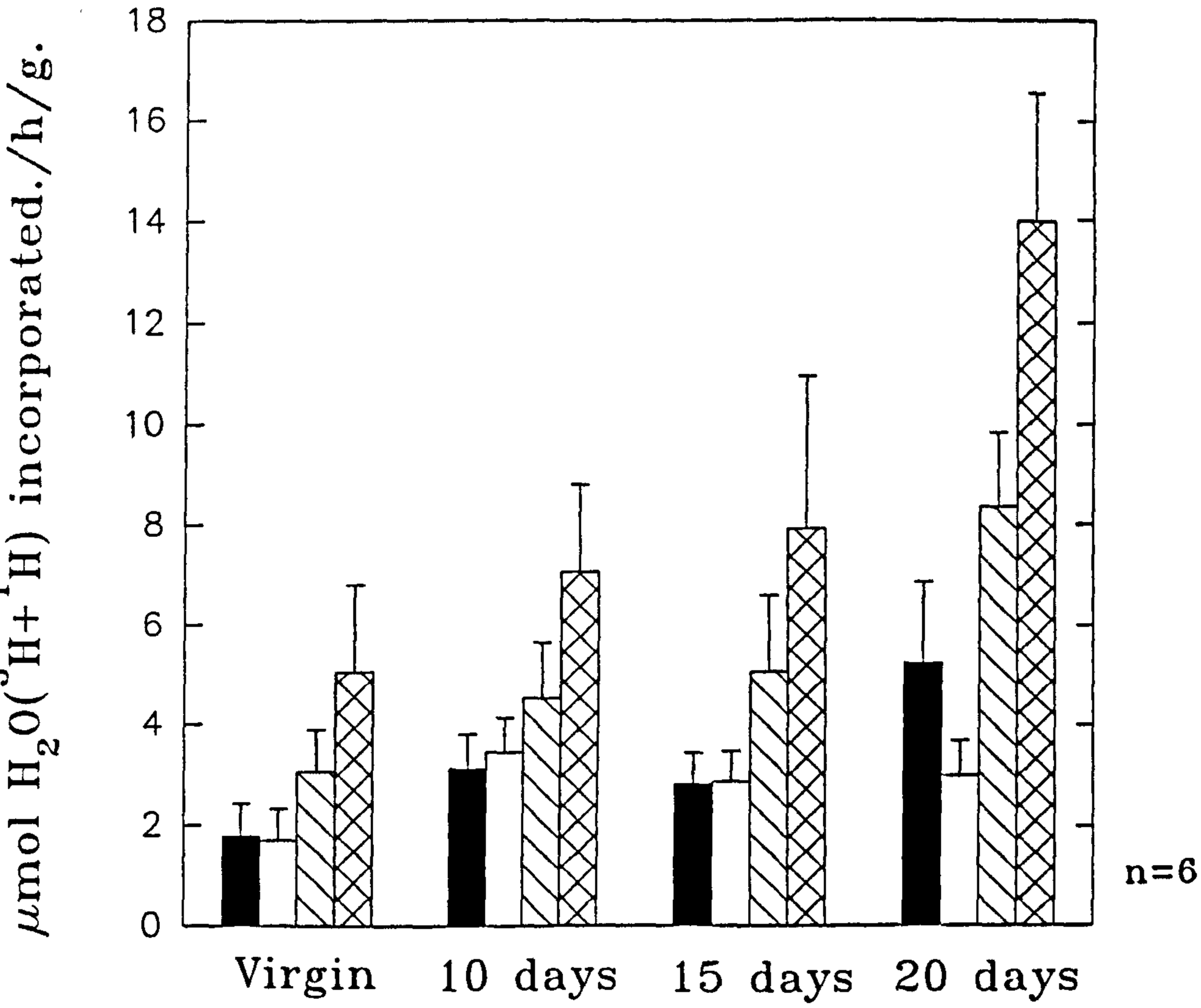

Figure 7.

3.4. Effects of routine meal feeding during pregnancy on GUI. Results and discussions.

3.4.1. Effects of 10 day meal fed pregnant rats on GUI values during the absorptive phase.

From the information obtained in this current study glucose uptake and phosphorylation, by the otherwise glucose intolerant tissues during pregnancy, have been "re-stimulated". Direct comparison of pregnant meal fed rats and control virgin 22h starved 2h refed rats (*table 11 and figure 8, 9 & 10*) shows increases in glucose utilization indices (GUI) of 54% and 97% in soleus and adductor longus (ADL), respectively, showing the effect of conditioning the animal over a period of meal feeding. The non-working muscles namely the gastrocnemius, tibialis anterior and EDL show a different variation; with the posterior hind-limb muscles gastrocnemius and EDL showing increases of 225% and 40%, whereas the TA shows a modest decline of 21%. The two cardiothoracic muscles investigated showed opposing changes with the diaphragm increasing its utilization of 2 deoxyglucose by 91%, whereas, the heart remains low at 156.7 nmol glucose.$min^{-1}.g^{-1}$ which is half the control value but exactly the same as fed pregnant control rats.

The greatest effect which meal feeding has on pregnancy can be seen when the GUI results are compared with normal fed 20 day pregnant rats. The previous study (*section 3.2.*) showed a very substantial suppression of glucose uptake and phosphorylation by both the working and non-working muscles with the most

significant reductions by the two cardiothoracic muscles. This type of decline was seen for all other skeletal muscles investigated and is thought to be the result of the glucose insensitivity brought about by the insulin resistant state induced by pregnancy onto tissues (Hauguel *et al.*, 1987; Leturque *et al.*, 1980). However, from the RMF study it can be seen that meal feeding has actually enhanced glucose uptake and phosphorylation in the tissues investigated, except the heart. On comparison with fed virgin rats it can be seen that the GUI values for the pregnant meal fed rats have increased to almost normal fed values, except in the heart. Meal feeding these otherwise glucose intolerant rats has increased the capacity for all tissues (except heart) to utilize C_6 substrates. Pallardo and Williamson (1989) observed increased lipogenic rates within the liver of meal fed rats: however glycogenic rates were similar to control *ad libitum* chow fed rats. The former observation was reinforced by Holness and Sugden (1989) showing hepatic pyruvate dehydrogenase activities 4-fold higher in a meal fed group when compared with rats fed *ad libitum*. Due to the inability of skeletal muscle to perform lipogenesis it is reasonable to assume that the bulk of this glucose is taken up and assimilated as glycogen, especially in the non-working muscles, or passed to the pyruvate dehydrogenase complex for complete oxidation to replenish energy stores after the 22h starvation period.

Glucose utilization of the heart however, remains at surprisingly low levels when compared with the response by the other insulin sensitive tissues during meal feeding. Meal feeding pregnant rats produces a GUI value in the heart of 156.7 ± 29.4 nmol glucose.min^{-1}.g^{-1} which is exactly what would be expected in normal late pregnancy (Holness *et al.*, 1991). The heart, a powerfully contracting muscle, under normal

physiological conditions relies substantially on C_6 substrates to maintain its continuous demand for energy. However, it has the ability to use other oxidisable substrates during states of starvation and differing physiological conditions such as pregnancy. Pregnancy induces a greater demand on the heart to pump a greater volume of blood, up to 40% more, to the ever increasing uterine blood system and other organs such as the liver. This implies a greater utilization of fuel, but as previously shown during late pregnancy does not involve the increased use of glucose. Meal feeding causes no influence on the heart, unlike the other tissues, to once again utilize the glucose. The heart remains a conserved area for the minimisation of glucose utilisation which is vitally required for the conceptus growth during its most rapid developmental stage of the third trimester.

The diaphragm, also a continually contracting muscle, has a glucose utilization requirement of half the value of the heart which makes it a significant glucose drain. The control pregnant GUI value of the diaphragm is 97.2 ± 25.0 nmol glucose.min^{-1}.g^{-1} ,whereas, in the meal fed condition it increases to 306.7 ± 50.6 nmol glucose.min^{-1}.g^{-1}; an increase of 215% and comparable to virgin control values of 358.3 ± 40.6 nmol glucose.min^{-1}.mg^{-1}.

The soleus and adductor longus show increases of 73% and 91% respectively, when compared with control pregnant values. These increased values are almost comparable to virgin controls being approximately 19-29% less. The non-working muscles; gastrocnemius, tibialis anterior and extensor digitorum longus all increase to vastly enhanced levels, equivalent once again to virgin control values. The tibialis

anterior increased 380% and the EDL 800% compared with pregnant controls both of which are very substantial increments. Enhancements of glucose utilization at the levels seen in the non-working muscles compared with working muscles is most probably associated with elevated glycogen synthesis of which the non-working muscles have a greater capacity compared with working muscles (soleus and ADL), a consequence of meal feeding (Pallardo and Williamson 1989). Absorptive state glucose utilization in meal fed pregnant rats is, therefore, producing values which far exceed those seen in pregnant control rats, with the greatest enhancements seen in the two non-working muscles, EDL and TA, and to a lesser extent the two working postural muscles, soleus and ADL. The constantly contracting muscles, as previously discussed, show differing responses; the diaphragm increased to almost fed virgin values with the heart remaining at the greatly suppressed value, normally seen in pregnancy.

3.4.2. Effects of 10 day meal feeding of pregnant rats on the GUI values during the post-absorptive phase.

The enhanced starvation status which late pregnancy induces has been shown in both the absorptive and post-absorptive states (Holness *et al.*, 1991), with the post-absorptive state showing a further reduction from the absorptive pregnant state.

During the post-absorptive phase shown in *table 12*, the meal fed pregnant heart has a value of 296.7 $\pm$ 72.8 nmol glucose.min^{-1}.g^{-1} which is directly comparable to the control value of 317.8 $\pm$ 66.1 nmol glucose.min^{-1}.g^{-1} and a relative increase of 89%

of the absorptive state. From this data it does seem that the heart does have the capability to increase its utilisation of glucose in the meal fed condition, but its responsiveness to the higher glycaemic conditions is obviously not as fast as the other insulin sensitive tissues. The heart is the only tissue to display this response in the post-absorptive state, the other tissues investigated have a varied suppression from the initial fed condition.

The other muscle types investigated showed the expected decrease in GUI values while in the post-absorptive state. The diaphragm is reduced to a value equivalent to the control virgin but 27% higher than the control pregnant value. The two non-working muscles (TA and EDL), show declines of 85% and 86% respectively, from meal fed absorptive levels indicating the accelerated starvation state which pregnancy has on the mother after food withdrawal. Despite this dramatic decrease from the absorptive meal fed values they still remain higher than control pregnant post absorptive values by 45% in the TA and by 84% in the EDL. It is interesting to note that the rate of decrease from the two nutritional states is 3-5 times more in the meal fed pregnant group and yet the GUI values still remain higher than the control pregnant group. The soleus and ADL have very much smaller reductions of 27% and 35% respectively, compared with the absorptive values which reflects in the 145% and 470% relative increases from the control post absorptive pregnant rat.

Meal feeding pregnant rats, as with normal fed pregnant rats, shows the expected decline in glucose utilization from the absorptive to the post-absorptive states due to the developing starved status imposed by carbohydrate removal. However, the

relative rates of suppression in GUI values between the two nutritional states can be seen to be very different in different tissue types. The non-working muscles all decrease to levels which are approximately 85% less than their absorptive values, whereas the working muscles reduce to a rate equivalent to control pregnancy. The non-working muscles show an enhanced starvation pattern, during the fed period these tissues are rapidly assimilating and utilizing the circulating glucose for replenishing the glycogen stores for the subsequent 22h starved period. Once circulating blood glucose levels start to decrease from the fed state glycogen synthesis in these muscles is relatively switched off. The 10 day meal feeding regime seems to be sufficient to cause an enhancement by the non-working muscles to utilize the glucose for glycogen synthesis in preparation for the forthcoming starved period.

3.4.3. Effect of administering controlled food amounts on the GUI values of 10 day meal fed 19 day pregnant rats.

Control 19 day pregnant rats eat approximately 28.7g of chow in a 24h period whereas the same time-mated 10 day meal fed pregnant rat will eat approximately 11.0 g. Despite this substantial reduction in total chow intake the values for glucose utilization as have already been shown are very much greater than in the normal pregnant condition in the two nutritional states mentioned. If the chow allowed is then restricted to the equivalent amount eaten by a 22h starved 2h refed virgin control rat ie approximately 8.2g, representing 73% of the total meal fed intake, a dramatic reduction in the GUI of all the insulin sensitive tissues looked at occurs.

GUI values were therefore measured at 12:00h immediately after the controlled quantity of chow had been given. The response by the tissues to the reduced carbohydrate availability on the GUI was dramatic (*table 13*), showing reductions of approximately 70% in all the tissues. However, in the two non-working muscles, tibialis anterior and EDL, values still remained higher than control pregnant values by 63% and 320%, respectively. The heart was reduced to a value of only 47.8 nmol glucose.min^{-1}.g^{-1}. The fact that the two non-working muscles remained higher than control pregnant rats may suggest that carbohydrate levels at lower concentrations can be utilized at relatively high rates by these tissues and that glycogen synthesis is, therefore, one of the mechanisms enhanced during a sustained period of meal feeding.

3.4.4. Effect of 10 day meal feeding pregnant rats on GUI values in absorptive-post absorptive states in various adipose tissue sites.

The physiological condition imposed by pregnancy has been shown to suppress the use of glucose by the mother (Holness *et al.*, 1991). This condition can be reversed by meal feeding pregnant rats for a relatively short period of time of only 10 days causing enhanced utilization of glucose in most tissues. Since meal feeding is associated with increased lipogenic, glycogenic (Pallardo and Williamson 1989) and pyruvate dehydrogenase activities (Holness and Sugden 1989), the GUI of various adipose tissue sites was investigated in the 10 day meal fed 19 day pregnant rat.

Very few studies have been conducted on glucose utilization by different adipose

tissue sites, especially during pregnancy. It has previously been shown in that during the initial stages of pregnancy fat storage is enhanced, reflecting the increased glucose conversion in adipose tissue sites. As pregnancy reached the third trimester, glucose conversion to maternal fat stores was substantially reduced as the tissues' insulin responsiveness declined (Knopp *et al.*, 1973).

Table 14 shows the glucose utilization values of five different white adipose tissue sites; the parametrial, mesenteric, perirenal, subcutaneous and interscapular. The meal fed pregnant rats show a vast enhancement for the utilization of glucose in the three nutritional conditions imposed on the pregnant rat ie. absorptive meal fed; absorptive meal fed restricted last meal of 8 g and post-absorptive meal fed when compared with respective controls. The greatest enhancement shown is by the perirenal adipose tissue which has a value of 168.3 nmol glucose.min^{-1}.g^{-1} in the absorptive state, this represents an increase of 24 times the value of 22h starved 2h refed virgin controls. The interscapular increases by 7.3 times, the mesenteric and subcutaneous by 4.5 and the parametrial by 3.2 times. The total glucose utilization of these tissues represents a value of 476.7 nmol glucose.min^{-1}.g^{-1}, clearly a major glucose expender. This vast enhancement by the adipose tissues to utilize the circulating glucose must be a consequence of increased lipogenic rates by the tissue cells. As previously discussed meal feeding rats increases hepatic lipogenic rates to substantially higher rates. Pallardo and Williamson (1989) showed increases in the rates of fatty acid synthesis of nearly 10 fold in a meal fed group on refeeding, whereas the control 21h starved 3h refed group showed no significant increase in lipogenic rates. These results suggest that glucose must therefore be a very important

substrate for fatty acid and cholesterol synthesis in the white adipose tissue sites during pregnancy, together with the possible utilization of lactate and amino acids. Previous studies on glucose utilization rates in white adipose tissue sites have shown no real change during pregnancy (Leturque *et al.*, 1986) together with normal insulin sensitivity (Leake *et al.*,1969; Knopp *et al.*,1970). This present study suggests that even during late pregnancy lipid synthesis in these tissues must be greatly increased to produce enough energy reserves for the following 22 hour starvation period to which the rat has become accustomed to.

During the post-absorptive state as with the other peripheral tissues discussed, the glucose utilization still remains much higher than control 22h starved 2h refed rats. The perirenal, once again, remains at the highest value when compared with its control (218% increase) but the mesenteric has the highest index. Restricting the amount of chow allowed by the rat to the control amount of 8 g still produces an enhancement in the utilization by the various adipose sites but the values are greatly suppressed from the *ad libitum* meal fed group. The greatest suppression is found in the mesenteric, this tissue falls to just over half of the control value, this maybe due to it requiring a higher concentration of carbohydrate before lipid synthesis will occur, otherwise due to its close proximity to total carbohydrate intake, lipid synthesis would constantly be switched on.

Table 11. Muscle GUI values for 10 day meal fed pregnant rats and control 22h starved 2h refed rats during the absorptive state.

	GUI (nmol glucose/min per g of tissue)		
Tissue	**Control 22h starved 2h refed**	**19 day preg. 10 day meal fed**	**Control 20 day pregnant *ad lib.***
Heart	291.7 ± 5.0	156.7 ± 29.4**	160.0 ± 35.6
Diaphragm	160.6 ± 16.7	306.7 ± 50.6$^{*\#\#}$	97.2 ± 25.0
Soleus	150.6 ± 12.8	232.2 ± 17.8$^{**\#\#}$	134.4 ± 16.7
Adductor Longus	116.1 ± 14.4	228.9 ± 32.8$^{*\#}$	120.0 ± 22.2
Gastrocnemius	23.3 ± 7.8	76.1 ± 6.1***	---
Tibialis Anterior	129.4 ± 15.0	102.2 ± 12.2$^{\#\#\#}$	21.1 ± 4.4
EDL	82.2 ± 11.6	115.6 ± 11.1$^{\#\#\#}$	12.8 ± 1.1
Glucose [mmol/l]	4.88 ± 0.52	4.99 ± 0.38$^{\#\#}$	3.37 ± 0.1

Details of measurements are given in the Materials and Methods section. Statistically significant effects of meal feeding pregnant rats are given compared to both the control virgin (*) and control pregnant ($^{\#}$) conditions: $^{*/\#}P<0.05$; $^{**/\#\#}P<0.01$; $^{***/\#\#\#}P<0.001$, n=6

n=6 for all groups except 19 day preg., RMF = 5. Abbreviation: EDL, Extensor digitorum longus.

Table 12. Muscle GUI values for 10 day meal fed pregnant rats and control 22h starved 2h refed rats during the post absorptive phase.

GUI (nmol of glucose/min per g tissue)

Tissue	Control 22h starved 2h refed	19 day preg. 10 day meal fed	Control 20 day pregnant *ad lib.*
Heart	317.8 ± 66.1	296.7 ± 72.8$^{\#}$	123.3 ± 10.0
Diaphragm	118.3 ± 35.0	115.6 ± 13.9	83.9 ± 30.0
Soleus	129.4 ± 25.6	170.0 ± 8.3$^{\#\#\#}$	69.4 ± 12.2
Adductor longus	98.9 ± 12.2	148.3 ± 23.9$^{\#\#\#}$	26.1 ± 3.3
Gastrocnemius	17.8 ± 2.8	13.3 ± 3.3	---
Tibialis anterior	35.6 ± 6.7	16.1 ± 1.1*	11.1 ± 2.8
EDL	20.0 ± 2.2	16.1 ± 1.7$^{\#}$	8.9 ± 1.7
Glucose [mmol/l]		3.86 ± 0.29	3.37 ± 0.38

Details of measurements are given in the Materials and Methods section. Statistically significant effects of meal feeding pregnant rats are given compared to both the control virgin (*) and control pregnant ($^{\#}$) conditions: $^{*/\#}P<0.05$; $^{**/\#\#}P<0.01$; $^{***/\#\#\#}P<0.001$, n=6
n=6 for all groups. Abbreviation: EDL, Extensor digitorum longus.

Table 13. Effect of administering controlled food amounts on the GUI values of 10 day meal fed 19 day pregnant rats.

Muscle	GUI (nmol of glucose/min per g tissue) 10 day meal fed 19 day pregnant *ad lib.*	10 day meal fed 19 day pregnant 8g chow
Heart	156.7 ± 29.4	47.8 ± 13.9*
Diaphragm	306.7 ± 75.6	75.6 ± 24.6*
Soleus	232.2 ± 17.8	77.2 ± 10.0***
Adductor longus	228.9 ± 32.8	62.2 ± 12.2**
Gastrocnemius	76.1 ± 6.7	24.4 ± 4.4***
Tibialis anterior	102.2 ± 12.2	34.4 ± 5.6**
EDL	115.6 ± 11.1	53.3 ± 3.3**
Glucose [mmol/l]	4.99 ± 0.38	3.83 ± 0.29*

Rats were meal fed *ad libitum* for 9 days and on the 10th (at 19 days of pregnancy) were allowed the equivalent amount of chow which a 22h starved 2h refed rat would eat; approximately 8.2g. Details of measurements are given in the Materials and Methods section. n=5 for both groups. Statistically significant effects of meal feeding pregnant rats are given: *P<0.05; **P<0.01; ***P<0.001, n=6 for all groups. Abbreviation: EDL, Extensor digitorum longus.

Table 14. Effects of 10 day meal feeding pregnant rats on the GUI values of different white adipose tissue sites.

GUI (nmol of glucose/min per g tissue)

Adipose Tissue	Virgin 22h strve 2h refed.	20 day pregnant RMF	20 day pregnant 8g last meal.	Virgin 22h strve 2h refed, 4h strve.	20 day pregnant RMF, 4h strve.
Parametrial	6.7 ± 0.6	21.7 ± 2.8***	10.0 ± 2.8	6.7 ± 1.1	12.2 ± 2.8#
Mesenteric	27.8 ± 6.7	126.7 ± 23.9**	15.6 ± 8.3	20.6 ± 9.4	38.3 ± 6.7
Perirenal	7.2 ± 1.1	168.3 ± 69.4*	21.1 ± 7.2	5.6 ± 1.7	17.8 ± 6.1#
Subcutaneous	14.4 ± 0.6	63.9 ± 18.3*	35.6 ± 6.7*	8.3 ± 1.1	20.6 ± 7.8
Interscapular	13.3 ± 7.2	96.7 ± 23.9**	42.8 ± 7.8*	7.2 ± 1.1	11.7 ± 2.8

Details of measurements are given in the Materials and Methods section. Statistically significant effects of meal feeding pregnant rats compared with virgin refed rats are represented by *P<0.05; **P<0.01; ***P<0.001; #P<0.1 (between virgin 22h starved 2h refed, 4h starved and the corresponding RMF pregnant group, n=6 for all groups.

GUI Values For Virgin, Pregnant ad libitum & Pregnant RMF In Working & Non-Working Tissue Types During The Absorptive State.

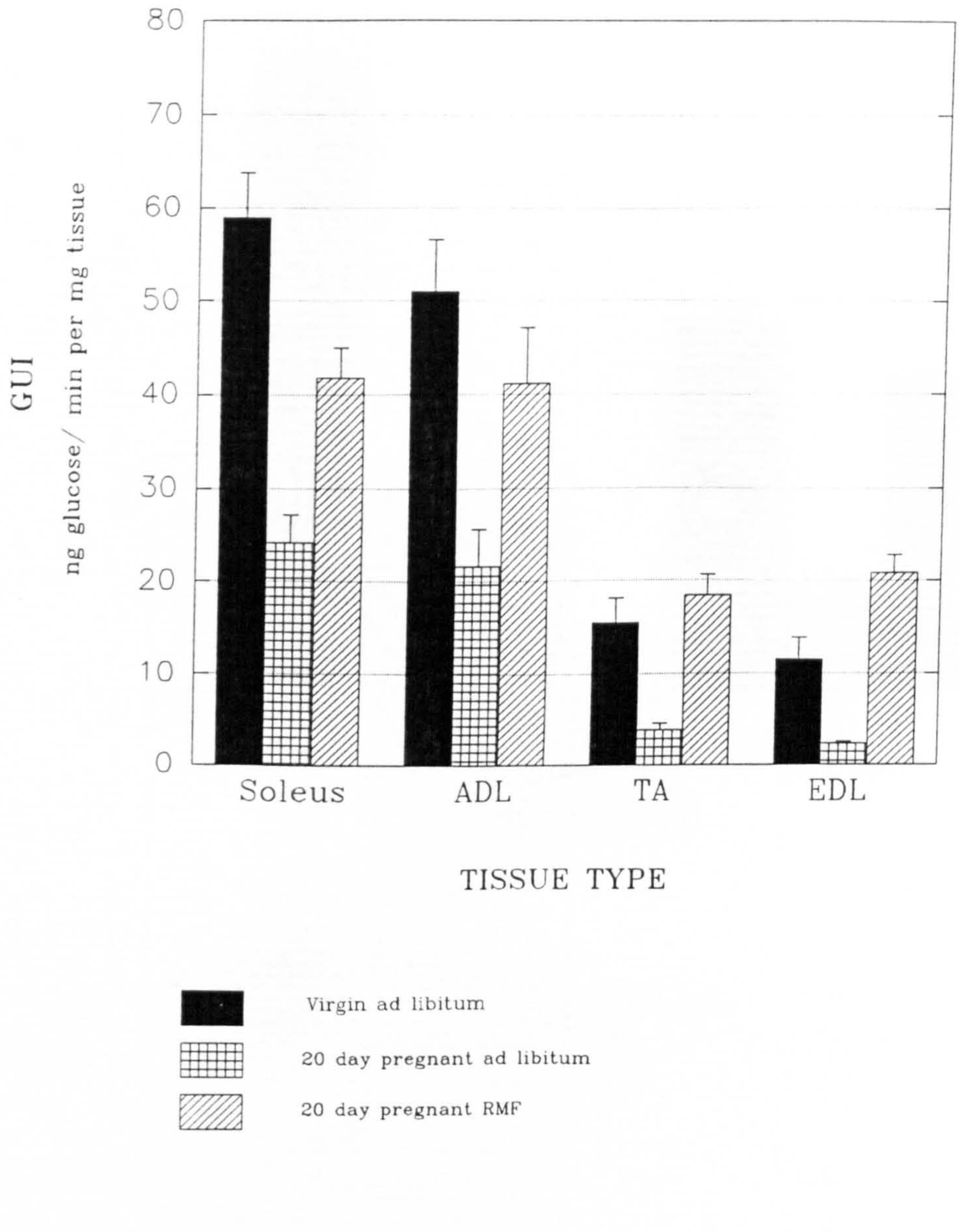

Figure 8.

Absorptive GUI Values For Virgin, Pregnant ad libitum & Pregnant RMF In Cardiothoracic Muscles During the Absorptive State.

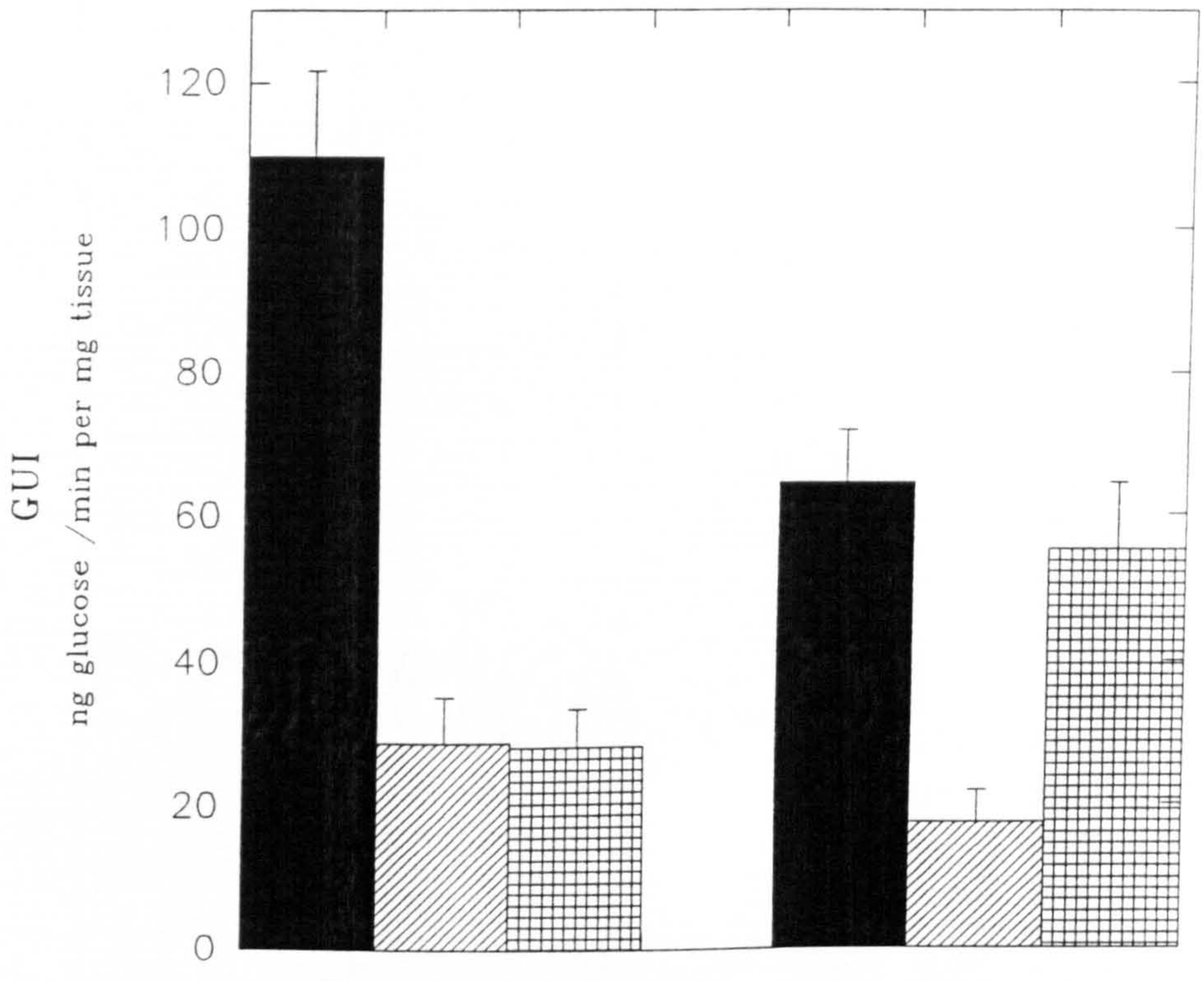

Figure 9.

GUI Values For Control, Control Pregnant & 10 Day RMF Pregnant Rats In The Absorptive State.

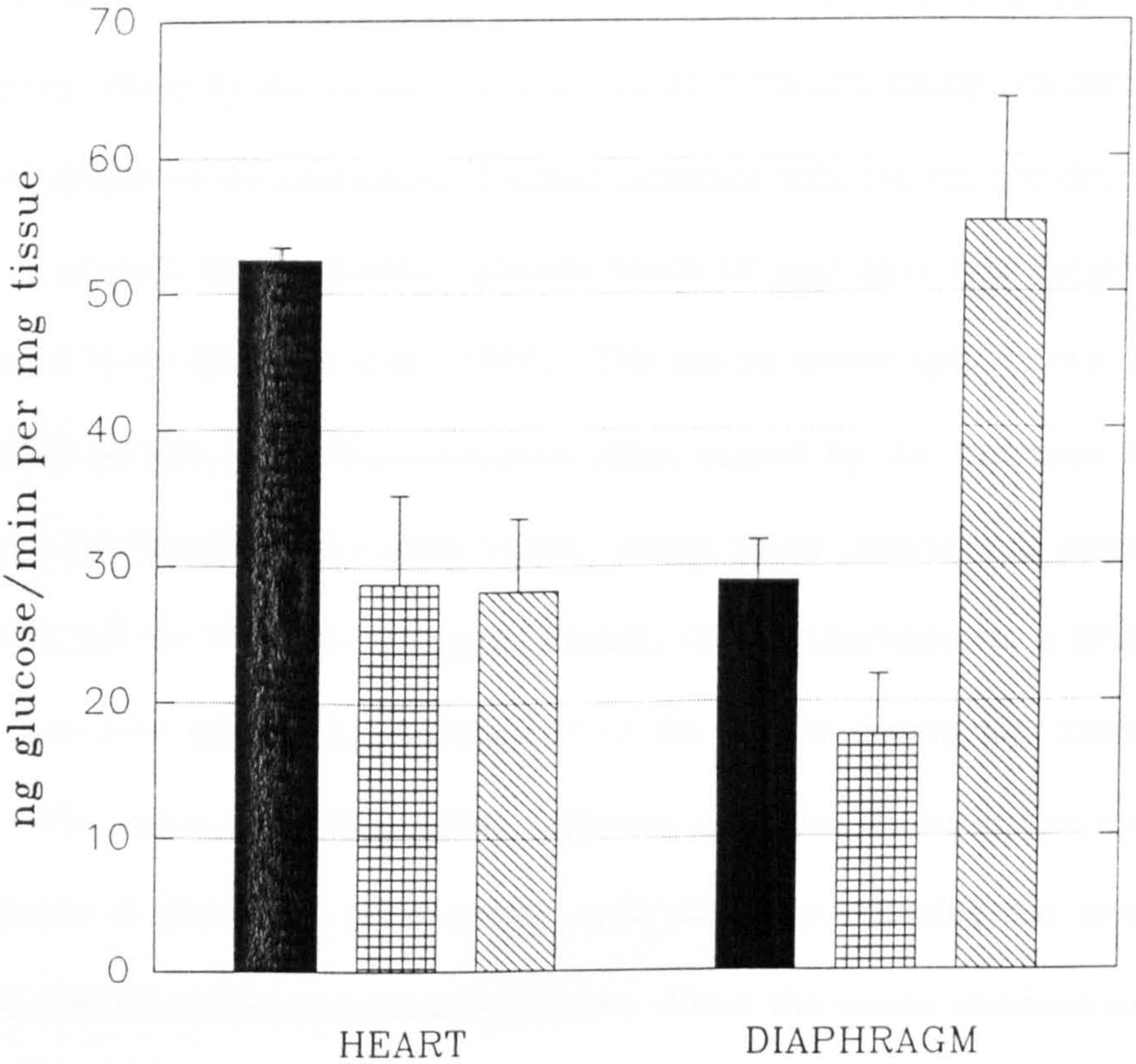

Figure 10.

3.5. General discussion.

The initial studies in this chapter on the effects of pregnancy have demonstrated the glucose sparing ability by the mother, so as to conserve the circulating glucose levels for the development of the conceptus. Despite increased food intakes and decreased utilization of glucose by the mother, glucose levels of near term rats decrease to hypoglycaemic levels (Holness *et al.*, 1991). This can be looked upon in two ways; firstly it could be due to the haemodilution effect caused by the increased blood circulation to the conceptus and other organs, whose blood capacity has increased (Clapp, 1978) like the liver, for example (Tindall, 1975). Alternatively, it could be due to the increased glycaemic requirements of the rapidly developing conceptus (Spellacy, 1975; Adam and Felig, 1978). Glucose utilization by otherwise insulin sensitive tissues is decreased substantially, with the heart showing the greatest reduction in glucose uptake and phosphorylation. From the results obtained in the latter study, the insulin resistant state of late pregnancy has been overcome by placing the rats on a routine meal feeding regime. Tissues which would otherwise have a diminished response to a high carbohydrate challenge show the complete opposite effect, glucose utilization by these tissues is enhanced to levels far exceeding those normally expected during near term pregnancy, resembling values more like control virgin rats. The increases in GUI is despite the substantial reduction in the total chow intake when compared with normal pregnant rats at the same gestational stage. It could be argued that the increase in GUI of the individual tissues is due to the refeeding of the rat as might be expected in a 24 h starved 2 h refed pregnant state. However, a comparable study by Holness and Sugden (1993) reported GUI values

in 24 h starved 2 h refed late pregnant rats of 84.4, 81.1 and 28.3 nmoles/min/g in the EDL, TA and gastrocnemius, respectively. In contrast, this study produced GUI values of 115.6, 102.2, and 76.1 nmol/min/g wet wt. in the RMF late pregnant group in the same tissues, respectively. These values represent increases of 37%, 26% and 169% in the EDL, TA and gastrocnemius muscles. This further implicates the method of meal feeding as producing significant changes in glycaemic control by the otherwise glucose intolerant muscles. During the absorptive phase the two non-working muscles (TA and EDL) show the greatest significant change from control pregnant values, this, no doubt, is due to glycogen being rapidly synthesized. After food removal, during the post-absorptive phase, the non working muscles become greatly suppressed from their original fed values, while the postural working muscles (soleus and ADL) remain significantly enhanced. The various white adipose tissue sites show a similar response to the meal fed conditions with significant increases in glucose utilization in all five sites studied. Meal feeding has produced a concerted response by energy storage tissues to accumulate and utilize as much, as possible, of the free glucose available during the re-feeding state. The food regime has enhanced intracellular storage mechanisms to protect the mother and conceptus for the long fasting period. A large proportion of the circulating glucose must, therefore, be converted to high energy storage compounds such as glycogen and fatty acids.

The heart, however during the routine meal feeding regime, unlike the other tissues investigated, shows very little change in its glucose utilization when compared with normal pregnancy. Glucose utilization indices remained greatly suppressed in the meal fed condition giving values of exactly the same as control pregnant rats. The

heart is a very significant utilizer of glucose and is probably targeted very heavily as a source of glucose conservation during pregnancy. Randle *et al.* (1964) showed that if the heart is being perfused by high concentrations of fatty acids and ketone bodies then the glycolytic rate of the heart will be suppressed. During pregnancy this is in fact the case and could be the special reason for the heart to remain insensitive to a glucose challenge in the meal fed pregnant state.

The heart seems to be a very important regulatory control organ for the glycaemic state of the rest of the body. It has a capacity to utilize other oxidisable substrates more easily, and with the heart being a major energy requiring organ, this allows free glucose to be utilized else where. During pregnancy this is even more important with the welfare of the conceptus being a primary concern. With this in mind, it must be pointed out that during meal feeding since the mothers capacity to utilise glucose has been restored what then is the consequence of the glucose utilisation of the conceptus? Since gestation channels glucose toward the conceptus, is the process of this severe meal feeding affecting normal metabolism of the foetus(es)?

Administration of controlled amounts of food to meal fed pregnant rats was studied to evaluate whether a certain amount of carbohydrate intake is required to promote enhanced glucose utilisation. From *table 13* it can be seen that controlled feeding severely reduces the majority of the tissues glucose utilisation capability. Interestingly, only two tissues, the tibialis anterior and EDL had higher GUI values than control 20 day pregnant rats. All other tissues investigated were oxidative working tissues and had very much suppressed GUI values compared to control 20

day pregnant rats. This may suggest increased glycogen deposition in the non-working muscles rather than glucose oxidation and maybe the key influence of meal feeding during pregnancy. Reductions in GUI values, even in the heart which is severely suppressed during normal pregnancy, may suggest a carbohydrate level is required to trigger enhanced peripheral tissue glucose utilisation as well as the conditioning that meal feeding promotes onto the due to nutrient availability.

The findings in this study have implications for mothers with a high risk of complications of eclampsia and intrauterine deaths during pregnancy caused by abnormal glucose intolerance. These mothers (approximately 1% of all pregnancies) develop gestational diabetes mellitus and up to 24-50% of these mothers develop NIDDM *post partum* (O'Sullivan 1988). The method of routine meal feeding illustrated in this thesis has been conducted at extremes to show the effects during pregnancy. However, on a more clinical line of thought a similar method of controlled food intake could be adopted by mothers at risk of GDM or to those with a history of non-insulin resistant diabetes mellitus. This study does suggest that food intake patterns could be used as a precautionary measure for high risk mothers, however further studies are needed to evaluate the effects on the conceptus as well reducing the severity of controlled feeding shown by this study.

3.5. PDH activities and other aspects of pregnancy.

Activities of PDH were extensively investigated for the heart, diaphragm and liver

during the various stages of gestation. However, despite conducting numerous experiments consistency was not achieved. This was attributed to the a number of reasons. Firstly, the metabolic state which pregnancy exerts upon the mother promotes an "accelerated starvation" state, which has previously been discussed. This makes analysis of the PDH complex extremely difficult on account of its tight control on carbohydrate oxidation. Holness and Sugden (1989) demonstrated the extent of PDH inactivity over a 48 h starvation period and showed dramatic declines of 68% in cardiac PDH activity following 3-4 h of food withdrawal, this was despite hepatic glycogen concentrations being 70% of the fed value. As has been demonstrated, cardiac GUI values in the fed state on day 20 of pregnancy resemble those obtained following a 24 h starvation period in the rat. With this in mind it can be assumed that immediately following food withdrawal, the PDH complex would be in a rapid transition to becoming inactive. The technique for measuring PDH activity would have to be very swift and consistent between the groups. Unfortunately, when experiments were conducted it was assumed that PDH activities remained constant for 3 h following food withdrawal, as is the case in the virgin state (Holness and Sugden, 1989). This obviously is not the situation during pregnancy, where the PDH complex is targeted quicker during periods of short term starvation. Since PDH activity and carbohydrate are tightly linked it must be assumed that during late pregnancy, even in the fed state, PDH activities must reflect a greater degree of starvation compared to the actual nutritional status. The assumption that three hours of starvation during pregnancy does not significantly affect activities of the PDH complex caused the inconsistency within the groups studied. During the period of tissue excision, the PDH complex was already rapidly becoming inactive. The inactivity of the complex

is compounded by the fact that elevations in fatty acids seriously suppresses PDH activity (Randle *et al.*, 1964, Holness *et al.*, 1989). During late pregnancy the circulation of fatty acids and triglycerides are substantially elevated hence contributing to the inactivation of the PDH complex.

A study by Holness and Sugden (1993) investigated the relative changes in PDH activity by fast-twitch muscles during late pregnancy. The tissues studied included the gastrocnemius, tibialis anterior and EDL all of which are non-oxidative and have quite low GUI values in the fed state compared to muscles such as the heart, diaphragm and soleus. It was revealed that during the fed state there was no difference between late pregnant and virgin rats in all three of the tissues investigated. Differences were only noted following a 24 h period of starvation and refeeding, where PDH activities were significantly lower compared with virgin 2 h refed rats, which had already re-established fed PDH values. During starvation of pregnancy non-oxidative tissues rely heavily upon lipid fuel oxidation, following refeeding these substrates still play an important part in the energy requirements of these tissues. Interestingly, fed PDH values were unaffected by late pregnancy, however GUI values were substantially suppressed to 15% (EDL) of virgin fed values, see above. This raises questions concerning carbohydrate control during late pregnancy in non-oxidative muscles. If GUI values decrease and lipid fuel plasma circulation increases during the fed state, PDH activities would be expected to be suppressed, but this was not shown (Holness and Sugden, 1993). If this is the situation, then the glucose intolerance shown by these muscles could be correlated to membrane glucose transport processes. Glucose transport has been observed to be mediated by a

combination of different GLUTs all of which are tissue specific and are not coupled to ATP or H^+ gradients. Despite the close homology of all these proteins they are all independently expressed as specific genes and have varied kinetic capabilities. The role of GLUTs in glucose homeostasis is self-evident, widening the possibilities of understanding physiological states which impose glucose intolerance. Studies on the glucose transporters (GLUTS) (Gould and Holman, 1993) could reveal changes which are relevant to the apparent glucose intolerance shown by skeletal and cardiothoracic muscles. By far the most interesting tissue for investigation would be the heart which undergoes a substantial shift away from glucose utilisation to other forms of oxidative substrates such as ketone bodies and other lipid derived substrates. GLUT 4 and GLUT 1 are the predominant transporters in the heart and it is proposed that either one or both of these transporters are severely depleted as gestation progresses. If the total membrane protein of these glucose transporters are diminished, this would account for some of the glucose intolerance seen during late pregnancy. A study by Kraegen *et al.* (1993) has shown that following 48 h of starvation GLUT 1 levels were severely reduced, implicating an insulin responsive role of the transporter. Glucose intolerance during pregnancy may be attributed to several metabolic factors including hormonal action (*eg.* placental lactogen which is diabetogenic agent) increased lipid circulation, glucose transport systems and insulin responsive aspects of tissues. It is difficult to assess the various contributions of these factors and whether the change in one of the factors is directly related to another and hence is just a direct consequence of the new metabolic state. The trigger mechanism for the glucose intolerance/insulin resistance requires defining.

CHAPTER 4.

Nuclear magnetic resonance spectroscopy

4.1. Brief history

The phenomenon of nuclear magnetic resonance (NMR) was first detected in 1946 independently by Purcell *et al.* and Bloch *et al.*. Since its discovery it has provided a tool primarily for proton detection in the chemical laboratory for the analysis of composition and structure of organic compounds. The first magnets used were extremely large, weighing several tons and consisted of large electromagnets which required very high current to produce the necessary field strength. The power supplied was stored in large oil filled capacitors contained in a vacuum, this made the application of NMR a risky business especially in the event of a breakdown when the capacitors had to be discharged manually. It was not until the late 1950's, when improvements to the design of the magnet and data processing started to develop, that its application could be widened to other nuclei (Lauterbur, 1957; Lauterbur, 1958; Holm, 1957). However, at this early stage in its development only relatively pure compounds in homogenous solutions could be analysed. For its use as a biochemical and clinical tool better magnets were required. The advent of super-conducting magnets in the late 1960's eliminated a lot of the power problems associated with the electromagnets and produced far greater field strengths, a pre-requisite for better

resolution. The principle of the super-conducting magnet relies on the property of certain alloys which exhibit zero resistance at very low temperatures. This allows a closed loop of this alloy wire to absorb electrical current without any heat loss, due to resistance of the wire, which can then remain indefinitely so long as the wire is constantly being cooled at the correct temperature. For this purpose the magnet contains coils consisting of either niobium-titanium or niobium-tin which are immersed in liquid helium (-269°C). Loss of helium is minimised by various vacuum chambers and by cooling with the cheaper cryogen, liquid nitrogen. However, there is always the inevitable loss of these two cryogens and hence, the magnet must be regularly topped up. The magnet is energised by slowly increasing the current from the power supply until the correct field is obtained, the magnet is isolated from the power supply via a special switch thus producing a magnet with constant current and zero potential difference at the required field strength.

Following the advances in the "hardware" of the spectrometer and the advances borne from Fourier transformation NMR (see later), a new era in applications emerged. Spectrometers were no longer just vertical small bore magnets for chemists to insert small sample tubes into, but developed into horizontal wide bore, high field systems capable of producing high resolution images and chemical shift spectra of whole animals and humans. A rapid exploitation into the *in vivo* non-invasive aspect of NMR followed. For the biologist the ability of monitoring metabolic pathways involving several metabolites was an exciting prospect especially in exogenously perturbed systems. The first productive metabolic study of intact cells was reported by Moon and Richards (1973) who showed that by using phosphorus spectroscopy of

red blood cells, 2,3 diphosphoglycerate, inorganic phosphate and the three phosphorus ATP components could be resolved. Furthermore by monitoring the chemical shift difference between the inorganic phosphate and α-ATP resonance, the intracellular pH (pH_i) of the cell could be assigned. Studies then graduated to muscle metabolism where muscle biopsies and single muscle preparations of hind limbs of rats and frogs were placed into the magnet (Hoult *et al.*, 1974; Dawson *et al.*, 1977). As well as phosphorus, carbon was gaining the recognition of being an important nucleus in studies defining metabolic end products (Cohen *et al.*, 1979; Cohen *et al.*, 1979a).

These early experiments provided a foot-hold required for the advancement of NMR application to biological systems. Most recent work has involved a plethora of applications to the heart, liver, muscle, brain and kidney, using a varied array of nuclei (possessing non-zero spin). Nuclear magnetic resonance provides an elegant method for metabolic studies providing information on organs with the minimum of abnormal manipulation. The work in this thesis has utilised the advantages of both carbon and phosphorus NMR for *in vivo* assessment of control of hepatic glucose utilisation, glycogen synthesis and gluconeogenesis.

4.2. Basic principles of nuclear magnetic resonance spectroscopy.

As the name suggests the principle process involves the resonance of specific nuclei whilst in a homogenous and directional magnetic field. Different nuclei resonate at different frequencies (their natural resonances, as in a tuning fork) in a given

magnetic field, hence information on the nuclei in question can usually be gained without the participation of other nuclei, which have their own natural resonance in the same field strength. Nuclear magnetic resonance involves the interaction of electromagnetic radiation with matter which upon perturbation will emit a similar radiation, in the form of a resonance, which can subsequently be detected. It is important to note that only a certain species of nuclei are NMR visible, these include nuclei with an odd mass number and hence, have a half integral spin, and those which have an even mass number but an odd atomic number and hence, have an integral spin. Those nuclei which have an even mass number and an even atomic number have zero spin and are not NMR visible. In the case of biological systems the most relevant nuclei include hydrogen (^{1}H), carbon (^{13}C), phosphorus (^{31}P), sodium (^{23}Na) and nitrogen (^{14}N and ^{15}N). Since the technique is critically dependent on the natural abundance of these isotopes certain nuclei are easier and quicker to detect. From *table 15.* proton and phosphorus nuclei are shown to be amongst the most prevalent naturally occurring isotopes and hence, their extensive use in spectroscopy and imaging.

Table 15. **NMR Properties Of Biologically Important Nuclei.**

Nucleus	Spin quantum number	Resonance frequency at 5T (MHz)	Natural abundance	*Relative sensitivity
^{1}H	1/2	213.0	99.985	100.0
^{13}C	1/2	53.5	1.108	1.6×10^{-2}
^{31}P	1/2	86.2	100.00	6.6
^{23}Na	3/2	56.3	100.00	9.3
^{14}N	1	15.4	99.63	1.0×10^{-1}

*Theoretical NMR sensitivity of nuclei at constant field (5T) relative to that of an equal number of ^{1}H, multiplied by the percentage natural abundance. (Gadian, 1982)

Carbon however, has a natural abundance of only 1.1% but this property can be exploited by developing tracer-like experiments which follow the metabolic consequences of a bolus administration of a ^{13}C-enriched compound in the system. Another important aspect of detection is the relative sensitivity of the isotope which reflects the net magnetisation of the nuclei. From *table 15.* it can be seen that relative to the proton, phosphorus and carbon, have relatively poor sensitivity values and therefore weaker magnetisation. Sensitivity and natural abundance of the nuclei are intrinsic factors which determine the detection ability of NMR with respect to time and signal intensity. To obtain spectra with good signal to noise various factors must be considered, these are outlined in *table 16.*

Table 16. **Important considerations for acquiring NMR spectra.**

1. Absolute sensitivity of nucleus.
2. Abundance of nuclei.
3. Volume of sample.
4. Magnetic field strength of magnet.
5. Homogeneity of static magnetic field.
6. Number of acquisitions ie number of averages making up one spectrum.
7. Longitudinal relaxation time of the nucleus (T_1).
8. The splitting/width of the spectral lines (T_2 influenced) and spin-spin coupling.
9. Pulse sequence used to acquire spectrum.
10. Configuration and size of coil relative to the sample.

The variables in *table 16* must all be addressed to obtain the best spectral resolution and signal to noise ratio, see below.

$$\textit{Signal to Noise Ratio} = \frac{\textit{2.5 x signal height}}{\textit{peak to peak noise}}$$

To completely understand the concepts involved in NMR a thorough knowledge of quantum mechanics is required. Fortunately, to grasp an outline of the theory a simpler model can be applied. This illustrates by classic physical phenomena how

nuclei respond to induced changes during the NMR experiment. When a nucleus is placed in the magnetic field the spin and charge of the nucleus try and prevent orientation around the field and so they precess around the $\mathbf{B}_0$ axis (*Z*-axis), rather like a spinning gyroscope, setting up a net magnetic moment *Mz*. As can be seen in *figure 11* the rotation of the nucleus resembles a cone in shape (as would that of a gyroscope viewed from above) and this is called the Larmor precession and the frequency of the precession, the Larmor frequency. The frequency of the oscillation is dependent on the magnetic field strength, see *equation 1*.

Equation 1.

$$\omega_0 = \gamma.B_0$$

where ω_0 = frequency.

γ = gyromagnetic ratio of nucleus.

B_0 = field strength.

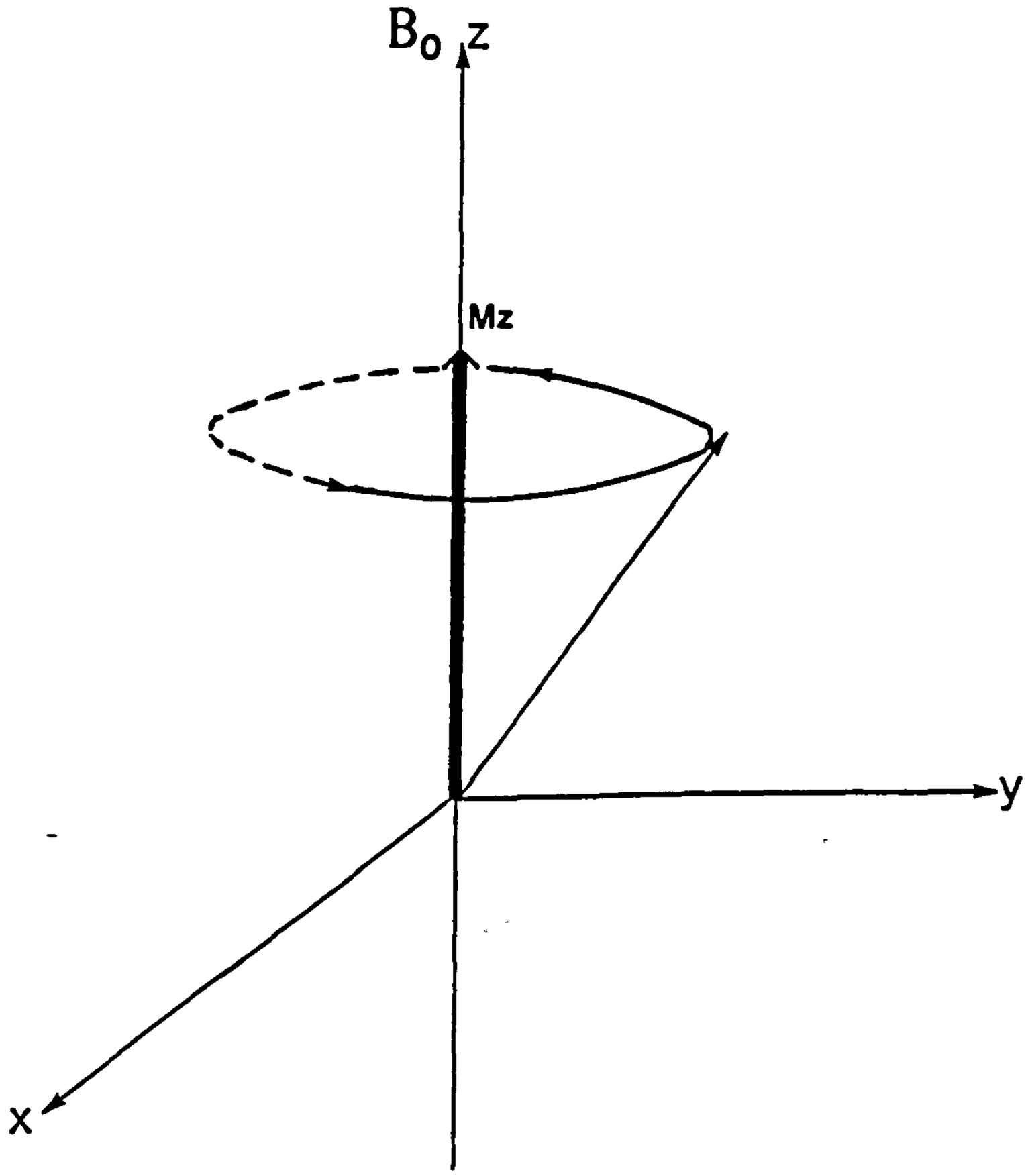

Figure 11. Precession of nuclei about the *z* axis setting up a net magnetisation M_z.

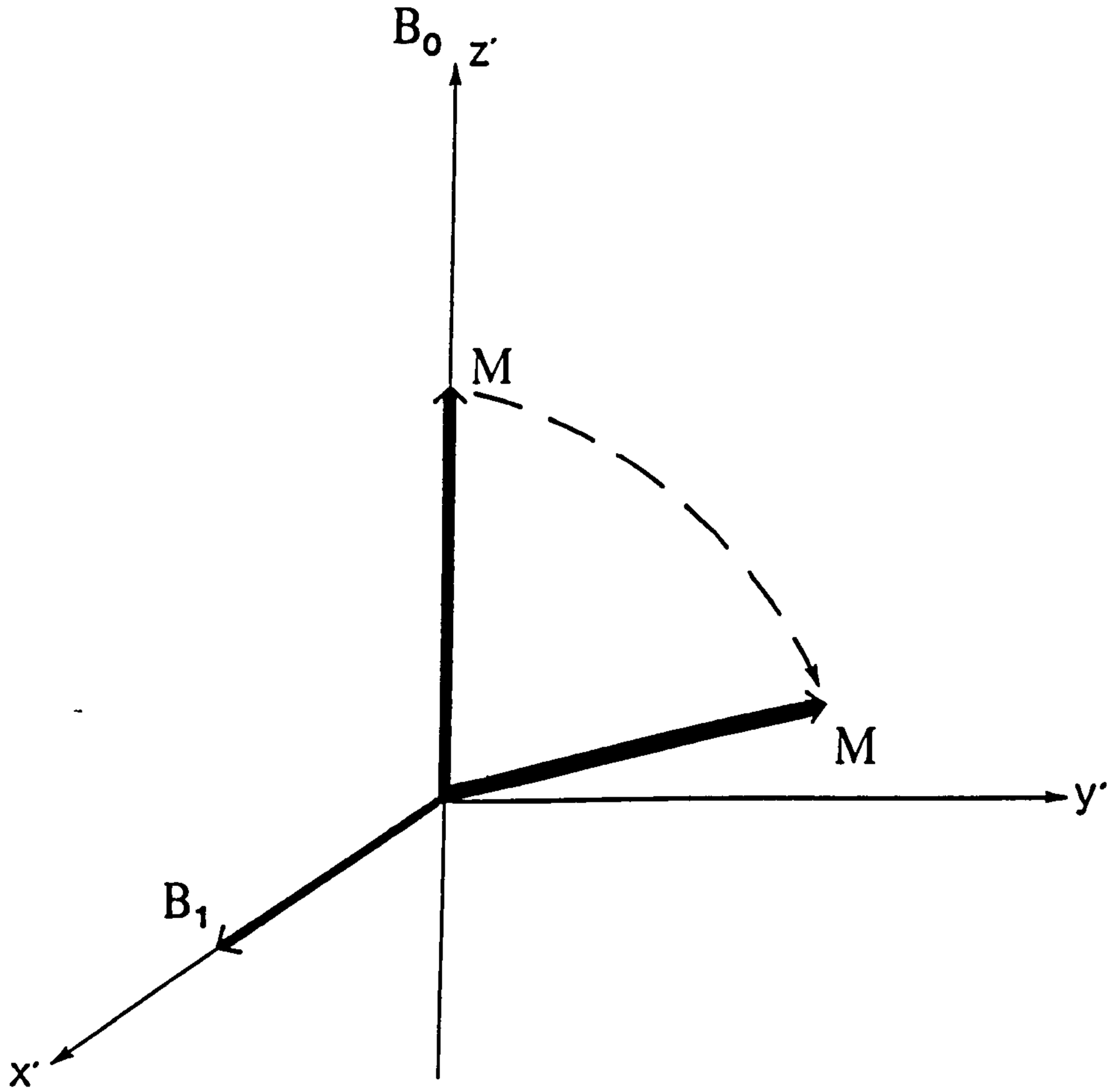

Figure 12. Tilting of magnetisation towards the $x'y'$ plane following the $\mathbf{B_1}$ pulse.

At this point in the discussion the "rotating frame" concept must be introduced in which an orbiting satellites' view of the earth must be imagined. If the satellite is travelling at a velocity which allows the same continuous view of Britain, then the earth will appear stationary and at a fixed angle to the vertical perspective. If this is then applied to the precessing nuclei, in which the observer is rotating at the same Larmor frequency as the nucleus, then the net angle of the nucleus to the *Z*-axis can be visualised as in *figure 11*. Since the sample will contain a population of different spinning nuclei, depending on their chemical environment, phasing and direction of spin (nuclei can spin either clockwise or anti-clockwise), further simplification can be achieved by representing the spinning nuclei as a coherent net magnetic moment (*M*), as in *figure 12*. It must be emphasised however, that the spin population is completely random, there is no coherence in the phasing of the spins and so it is this property which is exploited in NMR. Introduction of another magnetic field ($\mathbf{B_1}$) in the direction of *X'*, as is the case of NMR experiments, causes a perturbation in this net magnetic moment towards the *X'Y'* plane ($M_{X'Y'}$), shown in *figure 12*. The $\mathbf{B_1}$ field is applied perpendicular to the $\mathbf{B_0}$ field and has the same frequency as the Larmor frequency of the nucleus under observation and can therefore be represented on the 'rotating frame' scheme. The $\mathbf{B_1}$ field is provided by a coil placed next to the sample which is pre-tuned to the correct radio frequency (r.f.) (ie the Larmor frequency), it produces two opposing fields of the same frequency, one electric and one magnetic, the latter being important. Typically the r.f. field ($\mathbf{B_1}$) is applied in short pulses (microseconds) and depending on the length of the pulse determines to what extent the angle of magnetisation of the nuclei to the *Z* axis has increased, see *equation 2*.

Equation 2.

$$\Theta = B_1.\gamma.t_p$$

Therefore an r.f. pulse producing a 90° tilt can be expressed as:

Equation 3.

$$\pi/2 = B_1.\gamma.t_p$$

where:

t_p = duration of pulse.

B_1 = r.f. field

Θ = angle tilt with respect to Z

Prior to the r.f. pulse, the spins are randomly phased ie precessing randomly about B_0, then immediately after the pulse the spins become coherently phased, producing a net component of magnetisation ($M_{X'Y'}$) separate from either B_0 or B_1 but rotating about B_0 at a frequency ω_0. This component of magnetisation induces an electromotive force (e.m.f.) in the detecting coil at frequency ω_0, however as $M_{X'Y'}$ decays due to the resonance provided by B_1 being no longer applicable, the spins become randomly phased and eventually produce no net signal due to the loss of spin coherence reflected by $M_{X'Y'}$. The exponential time course associated with this decay in a homogenous static field is called the spin/spin relaxation time (T_2). This parameter is a measure of signal duration or line width produced by the perturbed nuclei and is determined by the interactions of energy transfer by other nuclei. Since no magnet is completely homogenous this value in practice is smaller due to dephasing occurring quicker to that in a perfectly homogenous static field. A second

exponential time constant associated with $M_{X'Y'}$ is the longitudinal (spin-lattice) relaxation time T_1, this determines the rate at which the spinning system returns to the *Z*-axis totally de-phased, producing no induced e.m.f. This parameter determines the duration required between pulses when the nuclei have returned to the resting equilibrium about $\mathbf{B_0}$. As the $M_{X'Y'}$ magnetisation disappears so does the induced e.m.f. producing a signal referred to as a "free induction decay" (FID), see *figure 13.* This oscillating signal contains information about various different species of the nuclei concerned within the sample. Nuclei within a sample will have a variety of chemical environments depending on the type of bonding associated with its neighbour and the type of nuclei it is bonded to. The chemical environment of the nucleus will determine the electron cloud composition surrounding it and hence will slightly *shield* the nucleus (σB) from an applied magnetic field. This gives rise to a local magnetic field to which the applied r.f. field induces an electronic orbital angular momentum producing a small additional field $\delta\mathbf{B}$ such that:

Equation 4.

$$B + \delta B = B(1 - \sigma) \text{.....} \textit{Total local field.}$$

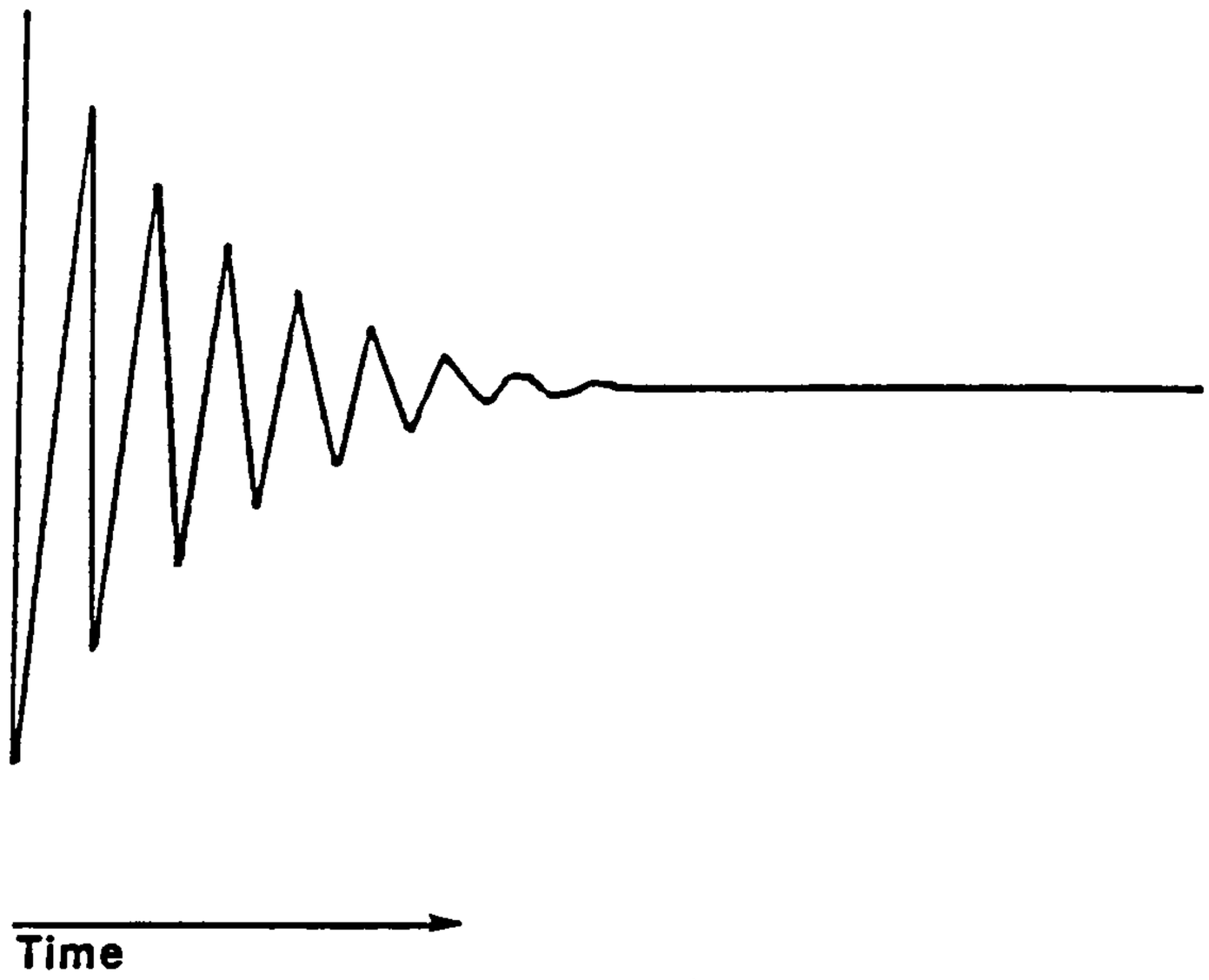

Figure 13. Free induction decay - FID.

It is this shielding effect which will produce a slight variation in the induced e.m.f. to the applied Larmor frequency and hence the precise resonance of the nuclear spins will depend on its particular chemical environment (resulting in variations in both the time and frequency domains). The shielding effect is different for every type of chemical environment within a molecule and so *shielding constants* (σ) for particular nuclear species can be calculated. The slight variation to the Larmor frequency applied produces a different induced frequency called the *chemical shift*. Therefore when a FID is obtained it will contain a multitude of component frequencies

depending on the molecular basis of the sample. To the human eye it would be extremely difficult to differentiate between the frequencies obtained and a more convenient method of interpretation is applied in the form of Fourier transformation (Cooley and Tukey, 1965; Ernst and Anderson, 1966) which employs an algorithm for conversion. This process is computer aided and converts the free induction decay, which is a function of time, into its component frequencies with respect to their relative intensities. The Fourier transformed representation of the FID is measured in parts per million (ppm), this scale does not depend on B_0 as it is dimensionless. This scale allows a universal comparison of spectra obtained from various field strength magnets to be achieved, therefore it can be regarded as a standard normalisation procedure.

4.3. The r.f. coil.

Generation of the r.f. field and the detection of the induced e.m.f. are both usually accomplished using the same coil. In high resolution vertical bore magnets the coil surrounds the sample tube. However, for *in vivo* spectroscopy a wide range of coil designs is implemented. In order to obtain spectra restricted to the tissue or organ of interest, such as the heart and liver coils are designed specifically. Fortunately, probe construction is relatively simple and so the size and shape required can usually fit the experimental protocol. The design, however, must account for the volume of sample to be examined in order to obtain the best sensitivity from the coil. The most frequent type of coil is the *surface coil* which is flat and usually one or two turns

which can be placed directly on the tissue/organ of interest. The major disadvantage, or advantage depending on the experiment, of the surface coil is the inhomogeneous B_1 field which is produced, this however is not the case with either the saddle or solenoid coils. As you move axially away from the coil the B_1 field drops slightly. However the further away you are the greater the drop in field strength which results in the reduction in signal intensity. This produces an array of flip angles, ranging from the r.f. pulse angle down to zero, induced into the sample dependent on the distance from the coil surface, hence surface coils are capable of a limited amount of localisation by choosing correct pulse widths. The degree of localisation will depend on the size of the coil, the r.f. pulse power and the volume of the sample. This introduces an important consideration when using surface coils on multiple tissue systems that the signal produced is solely from the tissue of interest and not from the surrounding tissue which may have different metabolic properties. It is important to note that a B_1 field is induced above and below the coil in an elliptical fashion.

In the studies illustrated in this thesis, two types of surface coils were used, both of which were "home-made". The phosphorus coil consisted of a single turn of insulated wire whereas the carbon coil consisted of one single turn coil and a 2½ turn coil (the former tuned to decouple protons and the latter tuned to ^{13}C) . Depending on the nuclei of concern the coils were developed and tuned to the respective Larmor frequency for the static field strength of the magnet used. Tuning is accomplished by simply applying the correct capacitance across the coil and matching it to 50 Ω.

4.4. Advantages and disadvantages of NMR.

Nuclear magnetic resonance spectroscopy is a relatively new tool for biochemical and medical analysis. Its elegance lies in its non-invasive and non-destructive attributes and is rapidly gaining rightful recognition as its potential is understood. There are many advantages in using this technique, the most important of which is that it allows the analysis of metabolic perturbations in whole body living systems, without the need for elaborate surgery. Conventional metabolic studies usually require many samples to be obtained to provide adequate time courses of the metabolism under question, therefore producing lengthy and laborious studies. With NMR it is possible to follow the time course of perturbed systems of one individual subject over long periods of time. This reduces the number of subjects required considerably and produces a wealth of other synchronous information, not possible with conventional methodologies. In the work presented in this thesis information has been gained on various aspects of hepatic glycaemic control using anaesthetised rats (without the need for laborious chemical assays). (If studied closely enough, information on substrate availability and enzymatic control can be gained.) However, in order to gain maximum sensitivity and less spectral contamination from other surrounding tissues it usually necessary to expose the rat livers directly against the coil itself. This is one disadvantage of NMR in that it lacks sensitivity and anything which can be done to improve this helps in the resolution of the spectra. In this situation NMR is no longer non-invasive but can still be regarded as non-destructive to the organ of interest. Developments in pulse sequences are overcoming this problem producing localisation techniques which allow the study of various organs such as the liver (Cox *et al.*,

1988), brain (Bottomley *et al.*, 1983), heart (Blackledge *et al.*, 1987), kidney (Jue *et al.*, 1987) and muscle (Taylor *et al.*, 1983); Narayana *et al.*, 1988; Pan *et al.*, 1988) from the intact body and hence its application to human metabolism is becoming more prevalent. Unfortunately, there is a trade off in a decreased sensitivity of a nucleus when localisation techniques are applied (due to a smaller volume producing less overall signal whereas, the coil has a bigger volume capability which would produce a greater signal). Since NMR has an inherent lack of sensitivity [ie detection has to be in the millimolar range; >0.2 mmol/l at 100% natural abundance (Cohen *et al.*, 1987b)], localisation exacerbates this which inevitably increases experimental times, a major disadvantage with the technique. When obtaining NMR spectra, considerations must be made for the relaxation times of the metabolites under examination as well as the population of mobile to immobile metabolites since only those which are mobile are detected. The latter consideration is realised *in vitro* where higher concentrations of particular metabolites are seen, suggesting tight binding to divalent metal ions and other macromolecules (Brown *et al.* 1973; Lawson and Veech, 1979) eg. ATP binding to Mg^{+} producing different chemical shifts compared with *in vitro* analysis. The other disadvantages are purely financial, in that the machinery is expensive which reduces its availability and makes machine time a precious commodity. However, the advantages far outweigh the disadvantages in the flexibility and information obtainable using this technique. No other technique has the capability of producing a vast amount of information regarding anatomy and biochemical processes of the intact organ or tissue of interest.

4.5. Previous *in vivo* studies using ^{13}C and ^{31}P nuclei.

4.5.1. ^{13}C-Nuclei.

Carbon has a special role in NMR with regard to biochemical studies. This nucleus is ubiquitous in metabolism and yet ^{13}C, the stable NMR visible isotope, has a very low natural abundance and sensitivity. Experiments can be designed, however, to partly overcome and in some cases take advantage of these properties. As briefly mentioned previously, bolus administration of an enriched source of ^{13}C, such as 1-^{13}C glucose, can give information on end products containing this enrichment, such as 1-^{13}C glycogen. By using specific carbon labelling various pathways can be studied, Placing two ^{13}C nuclei together in a molecule is highly informative since the point of chemical cleavage of these carbons can be verified in a pathway if the ^{13}C-^{13}C coupling disappears. Carbon spectra have a very large chemical shift range of approximately 200 p.p.m. (^{1}H = 10 p.p.m.; ^{31}P = 25 p.p.m.) which enhances the ability to distinguish between structurally similar compounds. Unfortunately carbon is almost always attached to a proton, and depending on the carbon-proton species of a neighbouring carbon-13 (ie -CH_2, -CH_3, -CHO etc.) multiple resonances around the definitive chemical shift will occur; this is due to heteronucleur spin-spin coupling which produces a different shielding effect and hence a variation in the magnetic moment and therefore splitting of the resonance line according to the n+1 rule, where n = number of protons. To overcome this problem the protons are continuously irradiated at the proton Larmor frequencies which makes all proton species the "same" and the carbon spectra can therefore be obtained totally decoupled from the

protons *ie.* proton splittings are eliminated. This process will also increase the peak magnitude and allow different ^{13}C species to be assigned one specific chemical shift, *see table 16a.* Constant irradiation simplifies the spectra obtained but also enhances further the signal intensity by a factor up to 3-fold, caused by the nuclear Overhauser effect (nOe) (Campbell and Dobson, 1979), by altering the relative populations of the ^{13}C spin states. It is therefore important, when obtaining quantitative spectra, that the signal intensities are corrected for nOe effects.

A wide range of applications to cells, tissues, animals and humans has been investigated but in this synopsis ^{13}C relevance to animal hepatic metabolic studies will be discussed.

A study by Alger *et al.* (1981) was one of the first *in vivo* experiments to be carried out exploring the ability of ^{13}C-NMR as a tool for glucose/glycogen metabolism. Several experiments on rats and humans provided carbon spectra prior to and after a bolus intubation of ^{13}C labelled glucose. The hepatic studies on fasted rats showed that the ^{13}C-enriched glucose resonances could be detected 45 min. after administration. Furthermore, 1-^{13}C glycogen could be resolved after 75 min.. The enrichment shown was very small but detectable even at the low field strength of 1.89 T. It suggested that studies could be carried out to further understand this pathway in various physiological states, including diabetic states and that it could be an important tool for characterising nutritional fat deficiencies and abnormalities by examination of the fatty acid resonances, most prevalent in hepatic ^{13}C-NMR. Prior to this study various perfused liver experiments had been carried out (Cohen *et al.*,

1979; Cohen *et al.*, 1980; Cohen and Shulman, 1980; Bailey *et al.*, 1981) together with rat liver cell experiments showing the conversion of 1,3-^{13}C-glycerol to the various α and ß anomers of glucose (Cohen *et al.*, 1979a). Metabolic pathways have been followed by the recognised technique of ^{14}C tracer experiments. These experiments require the quenching of metabolic processes to prevent complications in interpretation followed by laborious tissue extractions. Use of ^{13}C eliminates these problems since various components of metabolic pathways can be monitored *in vivo*. A study by Cohen *et al.* (1981) compared the merits of ^{13}C and ^{14}C and it was concluded that the results from both techniques were highly comparable (experimental errors between the two groups after analysis of specific metabolite labelling ranged from $\pm$2% to $\pm$7%). However, ^{13}C proved to be a more versatile probe of metabolism compared with its ^{14}C counterpart on the simple basis that a wide ranging number of pathways could be measured from the one experiment. The one major disadvantage of ^{13}C metabolic studies is the relatively large quantities of label required to produce sufficient enrichments for NMR detection. A liver perfusion study by Sillerud and Shulman (1983) suggested that all the hepatic glycogen is NMR visible, except particle molecules of 10^7 and 10^8 molecular weight. This was achieved by monitoring real time glycogen synthesis rates after incubation of 30.6 mmol/l 1-^{13}C glucose and hepatic glycogen extraction. By this method, cycling of glucose to the triose phosphates followed by glucose re-formation was seen due to the appearance of 6-^{13}C glucose showing the power of ^{13}C-NMR even at enzymatic levels. A series of experiments by Cohen *et al.* (1987, 1987a and 1987b) set out to determine the effects of diabetes and fasting on carbohydrate metabolism in the perfused rat liver by using 3-^{13}C alanine and 2-^{13}C pyruvate. Measurements of the rate of flux

through the pyruvate kinase enzyme [E.C. 2.7.1.40] were made by comparison of the gluconeogenic rate (which is at non-steady state in these physiological conditions) and the distribution in label caused by pyruvate kinase activity (Cohen *et al.*,1987a). Increases in alanine, aspartate, acetate, lactate and carbamyl aspartate are all indicative of pyruvate kinase flux. In the insulin dependent diabetic model, large increases in the activity of hepatic pyruvate kinase were measured upon administration of 7 nmol/l of insulin which were comparable to values in 24 hour fasted control livers, in the absence of insulin there was no detectable flux through pyruvate kinase. This study shows the application of ^{13}C-NMR as a tool to provide information on the fate of a label by non-destructive means and more importantly in real time. In a sequel to this study Cohen *et al.*, 1987b looked at the metabolism of pyruvate in the Krebs cycle together with the utilisation of pyruvate and ethanol during lipogenesis in the fasting and diabetic perfused rat livers. Estimation of pyruvate entering the Krebs cycle via the pyruvate dehydrogenase complex [E.C. 4.1.1.1., 2.3.1.12, 1.6.4.3.] and pyruvate carboxylase [E.C. 6.4.1.1.] were estimated by monitoring the ^{13}C-enrichments of glutamate after perfusion of ^{13}C-3 alanine [C-2 and C-3 labelling indicate pyruvate carboxylase activity whereas, C-4 labelling indicates PDH activity]. The relative activities of these two enzyme pathways give an indication of the physiological state of the animal since carbohydrates entering the system at the level of pyruvate can either enter the Krebs cycle to be completely oxidised (PDH) or synthesised to fatty acids, or be carboxylated to oxaloacetate for the conversion to phosphoenol pyruvate and therefore, gluconeogenesis. In the study, the relative flux through the two pathways was similar in the fed livers, however in the 24 hour fasted and streptozotocin induced diabetic livers relatively more of the pyruvate entered the

Krebs cycle as oxaloacetate, this correlated with higher rates of gluconeogenesis (Cohen *et al.*, 1987). A further experiment was also carried out to show the application of ^{13}C-NMR to the study of fatty acid synthesis by using 1-^{13}C acetate. It was possible to distinguish the different carbon elongations produced and hence a determination on the flux of lipogenesis could be achieved. It was also interesting to note that ^{13}C labelling from acetyl CoA only occurred with the co-addition of ethanol implying additional reducing equivalent requirement to supplement those produced by the pentose phosphate pathway. Ethanol can be oxidised via three separate pathways in the liver which produces NADH see *figure 14.* The synthesis of one molecule of palmitate requires 14 molecules of NADPH implying ethanol involvement for NADPH production. However, NADPH production is indirectly made from NADH produced by alcohol dehydrogenase via the production of pyruvate by malate dehydrogenase, see *figure 14.*

Figure 14. NADPH derivation from the oxidation of ethanol.

1. $CH_3CH_2OH + NAD^+ \longrightarrow CH_3CHO + \mathbf{NADH} + H^+$

Oxaloacetetate + **NADH** + $H^+ \longleftrightarrow$ malate + NAD^+

Malate + $NADP^+ \longrightarrow$ Pyruvate + **NADPH** + CO_2 + H^+

1.-*alcohol dehydrogenase.*

An *in vivo* study by Kalderon *et al.*, (1987) used ^{13}C-2 acetate to determine the amount of metabolic exchange that may occur with the oxaloacetate pool (concentration too small for ^{13}C-NMR visibility) in synthesising glucose in fasted rat livers. It was concluded that the percentage of labelled carbon in newly synthesised glucose amounted to only 7% of that originating from the oxaloacetate pool and therefore, the metabolic exchange at this level is only 7%. Further to this study Shulman *et al.* (1987) freeze clamped livers from previously conscious rats (24h starved) which had been intraduodenally infused with [1-^{13}C]glucose to determine the route of glycogen synthesis. It was estimated that direct conversion of glucose to glycogen accounted for 34% of the glycogen synthesised whereas, approximately 55% was formed from the indirect route from alanine and lactate. These values were estimated following assumptions regarding the relative dilution that occurs as labelled pyruvate flows through to the oxaloacetate pool taking into account the anaplerotic flux through glutamate and glutamine. However, the dilution may be affected by the physiological state of the animal making this estimation difficult to assess accurately. Further to this study, Shalwitz *et al.* (1989) administered, by intraduodenal infusion, 1-^{13}C glucose and 3-^{13}C alanine to 18 h fasted rats and monitored the relative contributions of the direct and indirect pathways to hepatic glycogen repletion. From *in vivo* data, the direct pathway accounted for approximately 30% of total glycogen formed, however dilution of the label into the oxaloacetate pool was not assessed. Active glycogen synthesis from 3-^{13}C alanine occurred over a longer period of time compared with 1-^{13}C glucose which reflected the lower hepatic levels of 3-^{13}C alanine. However, the rate constant for glycogen synthesis from 3-^{13}C alanine was 3-fold higher than from 1-^{13}C glucose implying a greater efficiency of glycogen synthesis

from the indirect route. It was therefore concluded that the glucose phosphorylating capacity of the liver is limited.

Other typical studies have looked at the metabolic pathways for hepatic ketone body production by using ^{13}C-multilabelled fatty acids (Pahl-Wostl and Seelig, 1986) and the effects of long term feeding of various fats (non-enriched) to the carbonyl and olefinic regions of hepatic carbon spectra in rats (Barnard *et al.*, 1993). As well as the liver, metabolic processes have been investigated for the heart (Sherry *et al.*, 1988; Laughlin *et al.*, 1988; Neurohr *et al.*, 1983; Malloy *et al.*, 1988; Malloy *et al.*, 1990), brain (Cerdan *et al.*, 1990; Kauppinen *et al.*, 1994), brain tumours (Navon *et al.*, 1989; Ross *et al.*, 1988) and kidneys (Jans and Willem, 1989) using a variety of ^{13}C-labelled precursors.

4.5.2. ^{31}P-nuclei.

Surprisingly, there have been relatively few liver metabolic studies using ^{31}P as the nucleus of choice. One of the reasons for this could be the *relatively* poor amount of information obtained from the phosphorus spectrum, compared with carbon and proton spectroscopy. The hepatic phosphorus spectrum consists of broad components of the phosphomonoesters (glycerol 1-phosphate, glucose-6-phosphate, fructose-6-phosphate, AMP, phosphocholine, phosphoethanolamine), phosphodiesters (phosphoenolpyruvate, glycerophosphorylcholine and glycerophosphorylethanolamine), inorganic phosphate (HPO_4^{2-} and $H_2PO_4^-$), γ-ATP (γ-phosphate of MgATP and ß-

phosphate of MgADP), α-ATP (α-phosphates of MgATP and MgATP and NADH) and ß-ATP (ß-phosphate of MgATP). Subtle changes within the broad resonances cannot be distinguished and *in vitro* analysis invariably has to be carried out. Another problem associated with *in vivo* hepatic phosphorus NMR is the co-resonance with the above metabolites and the phospholipid components of plasma membranes, between 30 and -30 ppm. This broad resonance produces a large hump, see *figure 26*, which makes quantitation by integration very difficult and hence, integrals must be obtained after removal of the phospholipid component by r.f. saturation techniques, specialised computer programs or by cutting and weighing each spectrum. As briefly mentioned previously, the problem of NMR visibility of certain metabolites must be considered. A good example of this are the contributions of ATP, ADP and P_i visibility in the ^{31}P-NMR spectrum. From *in vivo* and *in vitro studies* it is widely acknowledged that ATP is almost 100% visible in the *in vivo* spectra, however ADP and P_i are thought to be only partially visible (Iles *et al.*, 1985). The reason for this invisibility could be compartmentation within the mitochondria (representing approximately 15% of hepatocyte volume) or binding to other macromolecules (following *in vitro* extraction techniques these would liberate the residual ADP and P_i). It is interesting to note that the extent of invisibility of ADP within the liver is similar to that found in other tissues like the muscle, brain, kidney or even heart, which has an extremely large quantity of mitochondria. With the assumption that ATP is almost totally visible, phosphorus spectra are quantitatively referenced to the ß-ATP resonance which contains only nucleoside triphosphates due to the resonance of the middle phosphate, *see section 6.1.1.*.

Various groups have used ^{31}P NMR to measure pH in various cell types such as tumour cells (Navon *et al.*, 1977), muscle (Dawson *et al.*,1977), perfused heart (Garlick *et al.*, 1979), kidneys (Sehr *et al.*, 1977) and liver (Iles *et al.*, 1980; Cunningham *et al.*, 1986). Studies involving hepatic ^{31}P NMR have included isolated rat hepatocytes (Cohen *et al.*, 1978), perfused isolated mouse and rat livers (McLaughlin *et al.*, 1979; Salhany *et al.*, 1979; Iles *et al.*, 1980) and liver of the anaesthetised rat (Griffiths *et al.*, 1980). The study by Griffiths *et al.* (1980) overcame some of the initial problems of localisation of the liver by adopting a simple surgical procedure to place a surface coil directly on top of the liver. However Gordon *et al.* (1980) used a process of field profiling and rapid pulsing (topical magnetic resonance TMR) to obtain liver spectra from the intact anaesthetised rat. The technique of field profiling produces a small volume of B_0 homogeneity around the position of interest together with an inhomogeneous B_0 field else where. Since this technique there have been other methods of localisation to obtain liver spectra of humans (Sauter *et al.*, 1987; Segebarth *et al.*, 1987; Bailes *et al.*, 1987; Ross & Barker, 1988a; Dagnelie *et al.*, 1992), *see section 6.1.1.*, which include rapid pulsing techniques which take advantage of the relatively short T_1 times of liver metabolites (thought to be due to the presence of paramagnetic ions in the tissue) compared with the surrounding muscle tissue. It is easy to assess the degree of localisation using ^{31}P since a good protocol will produce spectra which have the phosphocreatine (PCr) resonance absent or very low, characteristic of the liver. The presence of PCr would indicate spectral contamination from underlying muscle. Phosphocreatine is present within muscle where short burst activities (due to muscle contractions) require quick replenishment of ATP concentration prior to reaching a steady state rate of glycolysis.

The liver does not require quick adjustments to ATP levels since its activity is more constantly controlled compared with muscle. However, it must be mentioned that the brain also contains PCr which may be regarded as a protection mechanism since the brain does not carry out any physical activities.

Most hepatic work has been on the isolated perfused liver since this provides a more controlled metabolic environment which can easily be perturbed by exogenous additions to the perfusate medium. Cohen (1987) used this technique to obtain ^{31}P spectra of 24h fasted and diabetic rats over a total perfusion time of 4.6h after the addition of ^{13}C-alanine and ^{13}C-ethanol. This study also showed the existence of two P_i species which were slightly shifted from one another in the phosphorus spectrum, this suggested that cytosolic and mitochondrial P_i could be resolved using NMR due to the slightly different pH of the two compartments. Earlier studies concentrated on the energy status of the liver by following the effects of fructose metabolism (Iles *et al.*, 1980). The effect of fructose perfusion showed the expected increases in the PME region associated with the rapid phosphorylation of fructose to fructose 1-phosphate, together with decreases in ATP, P_i and pH. Pre-fructose ATP levels were never re-established due to the probable degradation of the adenylate pool to uric acid.

4.6. Human studies using ^{13}C and ^{31}P NMR.

The problems associated with *in vivo* NMR spectroscopy, whether it be phosphorus or carbon, are inherent with the technique. In 1983, Canioni *et al.* used TMR (developed by Gordon *et al.*, 1980; Hanley and Gordon, 1981; Gordon *et al.*, 1982), *see section 4.5.2.*, to obtain natural abundance ^{13}C spectra of rat livers by totally non-invasive means. It was concluded that the localisation used was by no means perfect as contributions from adipose tissue sites contaminated the spectral analysis of the liver, however this would not interfere with glycogen monitoring. In humans the liver is much larger and hence contamination is reduced but probe size and design determines spectral resolution (Hoult, 1978).

Carbon has the additional complication of requiring proton decoupling to simplify and enhance sensitivity, however this produces a heating component, due to continuous irradiation. Carbon-13 NMR has a very important role to play in providing answers to hepatic carbohydrate abnormalties found in diseased states such as diabetes mellitus and cirrhosis of the liver. Most human ^{13}C NMR studies have been carried out in the last 5 years of which the bulk of the studies have examined muscle tissue of the arm or leg (Jue *et al.*, 1989 and 1989a; Shulman *et al.*, 1990; Beckmann *et al.*, 1990). These studies have concentrated on direct observation of glycogen repletion through natural abundance or after administration of [1-^{13}C] glucose. The work by Jue *et al.* (1989) compared hepatic glycogen repletion rates in 30 h starved individuals pre and post meal showing repletion rates 3.8 times greater in the post meal state compared with the fasted basal rate. A study by Shulman *et al.* (1990) used hyperglycaemic-

hyperinsulinaemic clamps to compare muscle (gastrocnemius) glycogen synthesis of healthy subjects to those with NIDDM. Glycogen synthesis in the NIDDM subjects was 2.3-fold lower than the healthy subjects implying a suppression of muscle glycogen synthesis in this insulin resistant state. Hepatic gluconeogenesis in healthy subjects and those with NIDDM was investigated by Magnusson *et al.* (1992). This study used an elaborate technique for assessing total glycogenolysis and glucose production of the liver. Following infusion of 6-^{3}H glucose and liver imaging (to calculate its volume), gluconeogenesis in the NIDDM subjects was found to be 60 % greater than control subjects and accounted for 88% of the total glucose production compared with 70% in the normal subjects. It was suggested, therefore, that increased gluconeogenesis accounted for the increase in whole body glucose production in overnight fasted NIDDM subjects. A study by Beckmann *et al.* (1993) administered [1-^{13}C] glucose (99% enrichment) intravenously, but was only able to detect hepatic glycogen formation after prolonged infusion times of 60 minutes. In the same study volunteers were given an oral dose of 99% enriched [1-^{13}C] glucose which was detected in the liver within 20 mins together with the C-1 resonance of glycogen; glucose enrichment of 6.6% allowed detection after 45-60 mins. It was concluded that the glucose uptake and glycogen formation of the liver was similar to more invasive techniques used to measure these metabolites.

One of the first ^{31}P-NMR studies of the human liver was carried out on newly born children which were found to have hepatic neuroblastomas (Maris *et al.*, 1985). A surface coil, with an optimised pulse length for localisation, was employed. Unfortunately, contamination from surrounding tissue was a problem, however

PAGE
MISSING
IN
ORIGINAL

CHAPTER 5

^{13}C-glucose metabolic studies during pregnancy.

5.1. Pilot study to assess the incorporation of ^{13}C-glucose into the hepatic glycogen moiety using NMR.

5.1.1. Introduction.

The purpose of this study was to set up a working NMR protocol which could be applied to the various pregnant conditions investigated in *chapter 2* to determine hepatic glycaemic control. Glucose uptake and utilisation cannot be assessed using the 2-deoxyglucose protocol discussed in *chapter 2* due to high concentrations of glucose-6-phosphatase. Following uptake of 2-deoxyglucose by the liver phosphorylation can occur; however, 2-deoxyglucose-6-phosphate can then be converted back to 2-deoxyglucose by glucose-6-phosphatase. This would under estimate the rates of glucose utilisation by the liver. It is therefore necessary to employ other means for the assessment of hepatic glucose uptake and utilisation such as the application of NMR.

For this pilot study, rats were placed on a 4 week meal feeding regime where food was restricted to two hours per day. As previously discussed (*see section 1.6.4.*), rats which are meal fed show some profound changes associated with carbohydrate and lipid metabolism (Pallardo and Williamson 1989). It was decided to investigate the potential of infusing a bolus quantity of ^{13}C-glucose to observe *in vivo* changes in

α and ß 1-^{13}C glucose levels and ^{13}C-1 incorporation into the glycogen macromolecule. An investigation was thus set up to evaluate the carbohydrate status of the liver of 4 week meal fed rats prior and post feeding following a bolus administration of glucose (Changani *et al.* 1994(a)). High resolution ^{13}C-NMR spectroscopy was also carried out to substantiate the findings of the *in vivo* study. This investigation provided substantial proof on the method of glycogen repletion *in vivo* of meal fed rats.

Initially, a bolus of 1.39 mmol/kg (250 mg/kg) was injected intraperitoneally, however very little ^{13}C-glucose signal was obtained from the exposed liver. It was thought that the amount of infused glucose was too low to disturb the metabolic pool of the whole rat, due to the dilution effect caused by haemodilution. This left the choice of either considerably increasing the glucose administration, hence placing the rat under a new metabolic condition (effectively placing all rat models closer to the same nutritional status), or infusing the bolus 1-^{13}C glucose closer into the liver. The second option was decided upon since the bolus amount used could be quantified as equivalent to an average human subject eating a small bar of chocolate. This would not have the effect of grossly altering the metabolic status of the subject and hence, different physiological conditions could be more closely compared.

5.1.2. Methods.

5.1.2.1. Development of a proton-decoupled carbon NMR coil for *in vivo* purposes.

Initial experimentation with a commercially available proton decoupled carbon probe made it apparent that a custom built probe was required. The commercial probe consisted of two sets of coils, the carbon tuned coil positioned within the proton tuned coil, encapsulated with thick poly-tetrafluoroethylene. Unfortunately, the encasement extended from the coils to the capacitors producing a very bulky product making central positioning of the coils onto the organ difficult to assess. In order to try and obtain the best possible localisation of the organ it was necessary to push the probe as far into the chest area as possible, this had the consequence of exerting undue pressures on the diaphragm and liver which inevitably led to either respiratory or circulatory hinderance to the rat. An additional problem due to the encasement was the vertical distance between the coils and the surface of the organ, this resulted in even poorer sensitivity of the coil to carbon-13.

A new coil was therefore designed to be smaller than the commercial coil to allow un-hindered positioning on top of the liver. The coil was based on the commercial one so that it could be attached to the same tuning and matching rods, however both the proton and carbon coils were reduced in diameter by one fifth, *see figure 15*. [The coils were produced from teflon covered silver base wire of 1.3 mm diameter.] This resulted in a proton single turn coil diameter of 3.2 cm and a carbon 3½ turn

diameter of 1.6 cm with the distance between the two coils of 0.8 cm. The resultant coil was not encapsulated which reduced the total diameter of the coil area by over 1 cm compared with the commercial coil. Reduction of the proton and carbon coils meant a change in the capacitance required to tune the coils to 200 MHz and 50 MHz, respectively, this was achieved by trial and error, after working out the rough capacitance required, by using an oscilloscope with a frequency spike generator.

The coil allowed the easy positioning of the carbon coil directly on top of the liver without the need to exert any unnecessary pressures. The spectra obtained were far more detailed, picking up vital resonances between 50 and 100 ppm, *see figure 17a*, contamination from other tissues could be avoided due to the easy manipulation of the liver and coil within the abdominal cavity. The one problem resulting from not encapsulating the capacitors was a gradual dephasing and diminishing of the signal due to sequestration of blood around the capacitors, which essentially de-tuned the carbon coil. This problem was resolved by covering the whole probe with cling-film and placing a 4 mm plate of silicone rubber [Poly dimethyl siloxane (Dow Corning Ltd.)] between the capacitors and the rat body. Justification for the development of the smaller coil came from the higher resolution spectra obtained as well as a survival rate of nearly 90%, opposed to 60% using the commercial probe.

Figure 15. Proton decoupled carbon surface coil

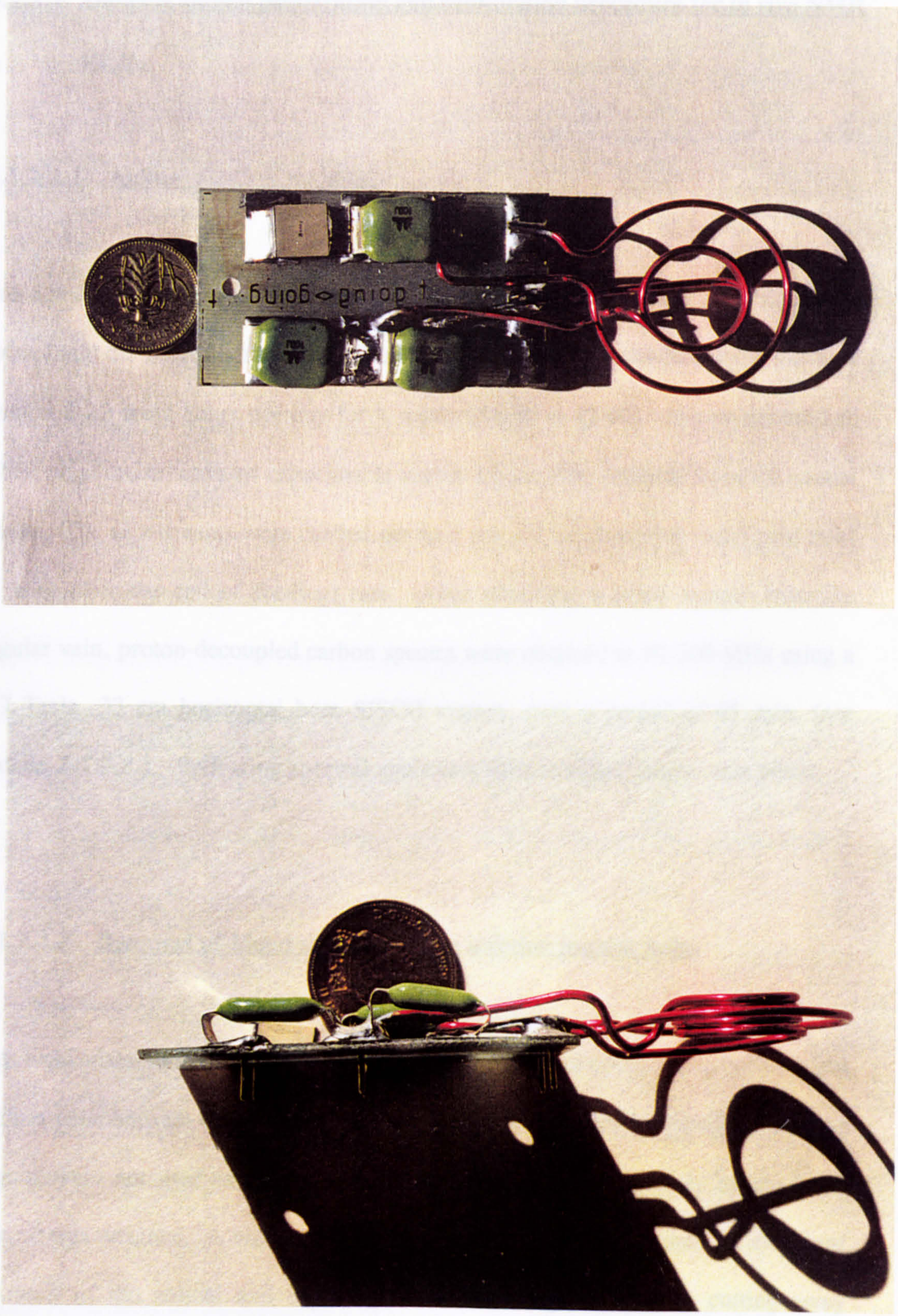

5.1.2.2. General animal preparation and cannulation procedure for *in vivo* NMR study.

5.1.2.2.1. Animal feeding regimes.

Ten age matched female Wistar rats (185-200g) were housed in a reverse light/dark room [light off 10:00/light on 22:00] and allowed access to a standard chow diet (*see section 2.2.*) for 2 hours per day for 4 weeks [10:00 to 12:00]. Due to animal and NMR preparation times all experiments started 1 hour after removal from the animal house. The experiments were carried out on 5 pre (23 hour starved) and 5 post meal (1 hour after the end of feeding) rats. After obtaining a blood sample from the jugular vein, proton-decoupled carbon spectra were obtained at 50.309 MHz using a 4.7 Tesla, 33 cm horizontal bore SISCO system, over a period of 65 min. (*see section 5.1.2.3.*). Following spectral analysis a further blood sample was taken.

5.1.2.2.2. Removal of blood sample via the inferior jugular vein.

Rats were anaesthetised using an intraperitoneal injection of 60mg/ml/kg body weight sodium pentobarbital dissolved in distilled water. Commercial equivalents such as Sagatal were not used as they contain ethanol which is utilised solely by the liver. The rat was weighed. A blood sample was removed by making a small incision near the neck of the animal and exposing the inferior jugular vein by cutting away surrounding tissue. A 1ml syringe with a blue needle (23G, 0.6x30mm) was inserted

through a fat pad and then into the vein. Approximately 350μl of blood was removed and transferred into a heparinised Eppendorf. The blood (250μl) was then deproteinised in 10% perchloric acid (v/v) (1.0ml) and stored at -70°C for future blood glucose determinations. See *section 2.3.2.1.* for blood preparation and *section 2.5.* for glucose assays.

5.1.2.2.3. <u>Cannulation of hepatic portal vein.</u>

A transverse abdominal incision was made extending laterally so as to expose as much liver as possible, without hinderance. The coronary ligament was carefully cut with round nosed scissors, to prevent damage to the diaphragm. The triangular ligament was cut to allow greater accessibility of the liver when positioning the proton-carbon probe. The cannula used was a straight version to that described in *section 2.1.* ie. no "U-bend" was introduced into tube *A* and tube *F* was cut to 20-25mm depending on the rat size.

The small intestine and stomach were pushed to one side exposing the hepatic portal vein. Cotton was tied around the dumbbell of the cannula *see section 2.1.2.* and one end threaded through a curved surgical needle. The cotton was threaded under the hepatic portal vein through the surrounding fat deposits. The hepatic portal vein was held gently with rounded forceps distal to the liver, slight pressure was applied to reduce blood flow to the liver and a hole made into the vein with bent blue needle (23G 0.6x30mm). The cannula attached to a line containing saline (0.9% NaCl w/v)

was immediately inserted into the hole, it was imperative that as little blood as possible was lost. If done quickly enough blood loss was minimal. The cotton threaded under the vein was then knotted to the free end of the cotton and secured around the dumbell of the cannula.

Successful cannulation was assessed by perfusing 100-200μl of saline, if some of the liver lobes discoloured to a creamy/red appearance, the cannula was correctly inserted. The cannula was then attached to 2 metres of tubing ***B*** *see section 2.1.1.* containing D-^{13}C-1-glucose 75mg [200mg/ml] (MSD Isotopes 6260).

5.1.2.3. *In vivo* proton-decoupled carbon spectroscopic protocol.

The magnet cradle, *see figure 16*, was lined with cotton wool and a hot gel pad, used to prevent heat loss from the rat, placed in the cradle. The cannulated animal was placed on top of the hot gel pad and a dual tuned proton/carbon surface coil (*see section 5.1.2.1.*) positioned directly on to the liver. The probe was covered in cling film to prevent blood coming in contact with both the coils and the capacitors, this would lead to a change in the loading of the capacitors and hence a de-tuning of the probe would occur. The M.R.S. machine used was a 4.7 Tesla, 33cm horizontal bore SISCO system. After tuning the proton and carbon channels, the magnet was shimmed for greatest field homogeneity. Proton-decoupled carbon-13 spectra were acquired at 50.309MHz using a decoupling power of 120w and a decoupling mudulating frequency of 5800Hz. An acquisition time of 0.205 secs., a pulse delay

of 0.1 secs., a pulse width of 70μs and a spectral width of 12kHz were used to produce 25 array elements consisting of 512 averages (*ie.* 1 spectrum = 2.5 mins for accumulation of 512 averages). These parameters did not allow the absolute quantitation of metabolites due to partial saturation effects caused by the very short pulse delay. However, this was not a requirement of the study since sequential spectra were compared to the pre-infusion spectrum which cancelled out the partial saturation effects. After acquiring two base-line carbon spectra, ^{13}C-1 glucose was slowly infused as D-glucose-1-^{13}C [75mg; 20mg/min]. Subsequent to infusion, the spectra were referenced to C-1,ß-glucose at 96.60ppm and C-1 α-1,4 glycogen appearance observed at 100.48ppm, *see table 16a*.

After spectroscopy a final blood sample was removed (300μl) from the inferior vena cava. The blood sample was treated as in *section 2.3.2.1.*. The liver was quickly excised and freeze clamped in liquid nitrogen for future high resolution N.M.R. analysis (*see sections 5.4 and 5.5*) and glycogen quantitation (*see section 2.12.*).

Figure 16. SISCO system 4.7 T wide bore magnet and cradle.

Table 16a.

Chemical shifts of metabolically important carbon compounds.

Compound.	**Chemical Shift (ppm.)**
C-3 Alanine	17.5
C-3 Lactate	20.8
$-CH_2CH_2CO-$	25.6
$-CH=CHCH_2CH=CH-$	26.32
$-CH_2CH_2CH=CH-$	28.0
$-(CH_2)$-fatty acyl	30.1, 30.5
Malate	43.5
Citrate	46.0
3-hydroxybutyrate	47.2
C-2 Alanine	51.9
C-2 Glutamine	55.6
C-2 Glutamate	56.0
C-6 α,ß Glucose, Glycogen	61.4
C-1, C-3 Glycerol (ester)	62.6
C-6 Glycogen ß 1,6	67.9
C-2 Lactate, Glycerol (ester)	69.7
C-4 Glycogen ß 1,6	70.0
C-4 α,ß Glucose	70.3
C-2 Glycogen α 1,4, ß 1,6	72.2
C-3 α Glucose	73.4
C-3 ß 1,6 Glycogen	73.5
C-3 α 1,4 Glycogen	74.0
C-3, C-5 ß Glucose	76.5
C-4 α 1,4 Glycogen	77.7
C-2 ß Glucose	79.9
C-1 α Glucose	92.7
C-1 ß Glucose	96.6
C-1 ß 1,6 Glycogen	99.2
C-1 α 1,4 Glycogen	100.5
$-CH=CH-CH_2-CH=CH-$	128.7
$-CH=CHCH_2CH_2-$	130.4
$-CH_2-CH_2-CO-$	172.4
-CO-O*R*	173.8

Assignments accrued from numerous papers.

5.1.2.4. Interpretation and quantitation of *in vivo* carbon spectra.

Typical proton decoupled carbon spectra of the liver can be seen in *figure 16a.*

Glucose and glycogen quantification from the spectra involved computer aided base-line correction and integration across the glucose resonances at 97.00 - 96.00ppm for ß-glucose; 91.150 -93.50ppm for α-glucose and 98.50 - 103.00ppm for the glycogen resonance, *see figure 16a and 17.* Lipid extraction measurements (*section 3.3.*) have shown that total hepatic lipid concentration remains constant at 67.2 $\pm$ 3.7 mg/g wet weight of liver tissue, therefore, the glycogen signal was expressed as a function of the total -CH_2 and CH_3 integrated areas.

5.1.2.5. Method for aqueous extraction of liver for *in vitro* ^{13}C-N.M.R. analysis.

5.1.2.5.1. Extraction procedure.

Approximately 1 g of frozen liver tissue was ground to a powder in a pestle and mortar (cooled in a bath of liquid nitrogen) while under liquid nitrogen. The ground tissue was transferred to a liquid nitrogen cooled glass scintillation vial and its exact weight measured. The tissue was homogenised for 1-2 min (Int. Lab. Appl. Gmbh; Type X 1020; position 5) in 10% perchloric acid (2 ml/gm tissue) to deproteinise the sample. Once a suspension had been obtained the precipitated protein was centrifuged to a pellet at 5000rpm for 5 min at 4°C in a MSE Mistral 3L centrifuge. The

supernatants can be stored at -70°C at this stage.

Prior to lyophilisation the samples were neutralised at 4°C with solution containing 1.5M potassium hydroxide [KOH]; 0.3M potassium chloride [KCl] and 0.1M sodium phosphate [Na_3PO_4]. The samples were centrifuged at 4°C for 10 mins. at 5000rpm to pellet the perchlorate precipitate. The supernatant was transferred to a pre-weighed tube and freeze-dried for 36h in a freeze dryer (Edwards-Modulyo). The freeze dried extract was weighed and stored at -70°C until required for high resolution N.M.R. analysis.

5.1.2.5.2. <u>Preparation of freeze-dried sample for high resolution N.M.R. analysis.</u>

Deuterium oxide (0.5ml) was added to the sample together with 50μl of 100mM TSP (3-(trimethylsilyl)propionic acid Sigma T 5762). Some perchlorate crystals may persist in which case the sample was spun at 5000rpm for 20 mins. at 4°C. The clear supernatant was transferred to a 5 mm N.M.R tube (Goss Instruments Type 507-HP) and analysed quantitatively on a JEOL GSX500 N.M.R. spectrometer operating at 500MHz and 11.75 Tesla. Proton-decoupled carbon spectra were obtained using an acquisition time of 0.544s a pulse width of 15 μs and a pulse delay of 6s.

TEXT BOUND INTO THE SPINE

Figure 16a. Typical *in vivo* ^{13}C spectra.

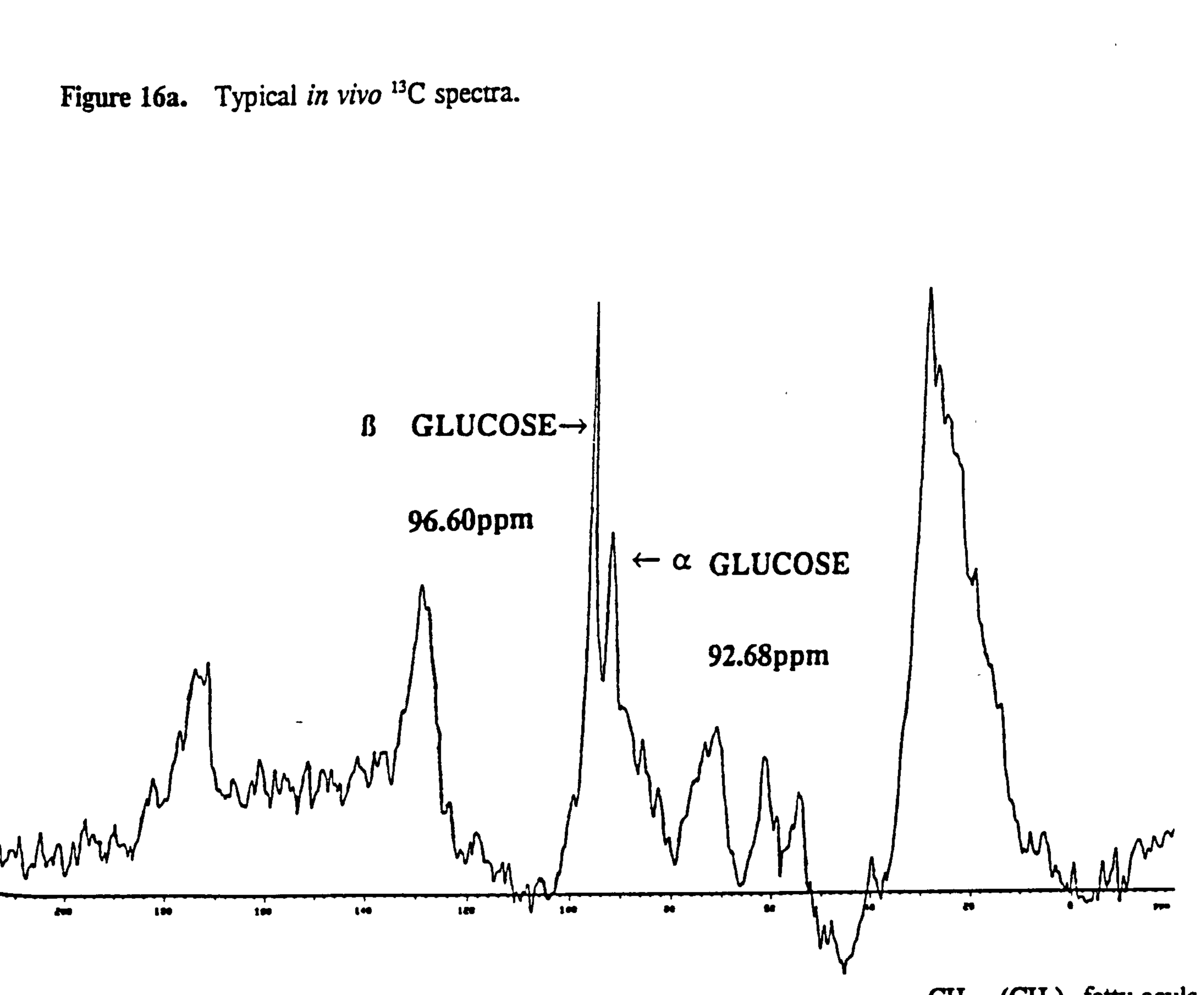

Figure 17. Base-line subtracted spectra.

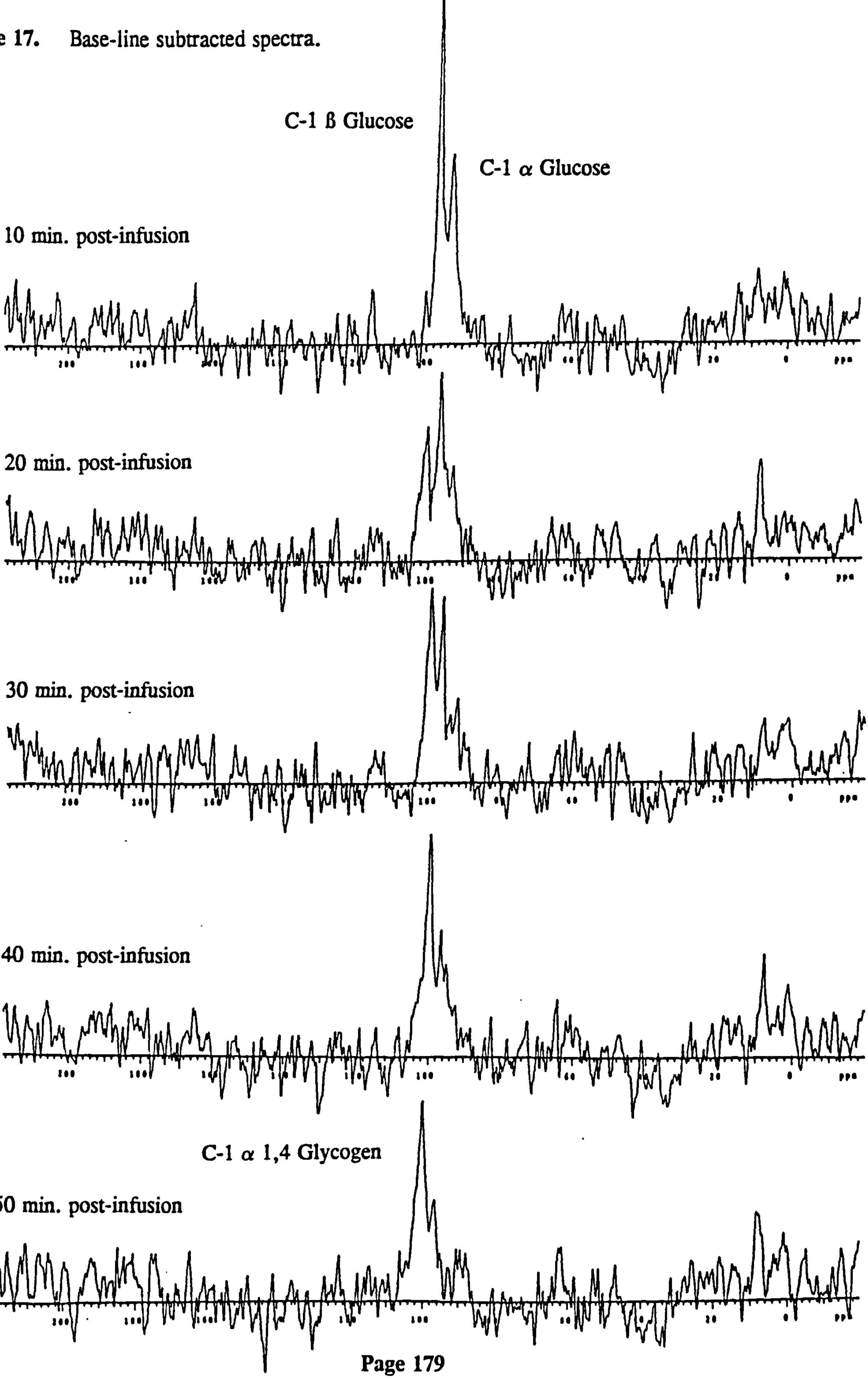

Figure 17a: Comparison of carbon spectra obtained with the

commercial and "home-made" surface coils.

"Home-made probe"

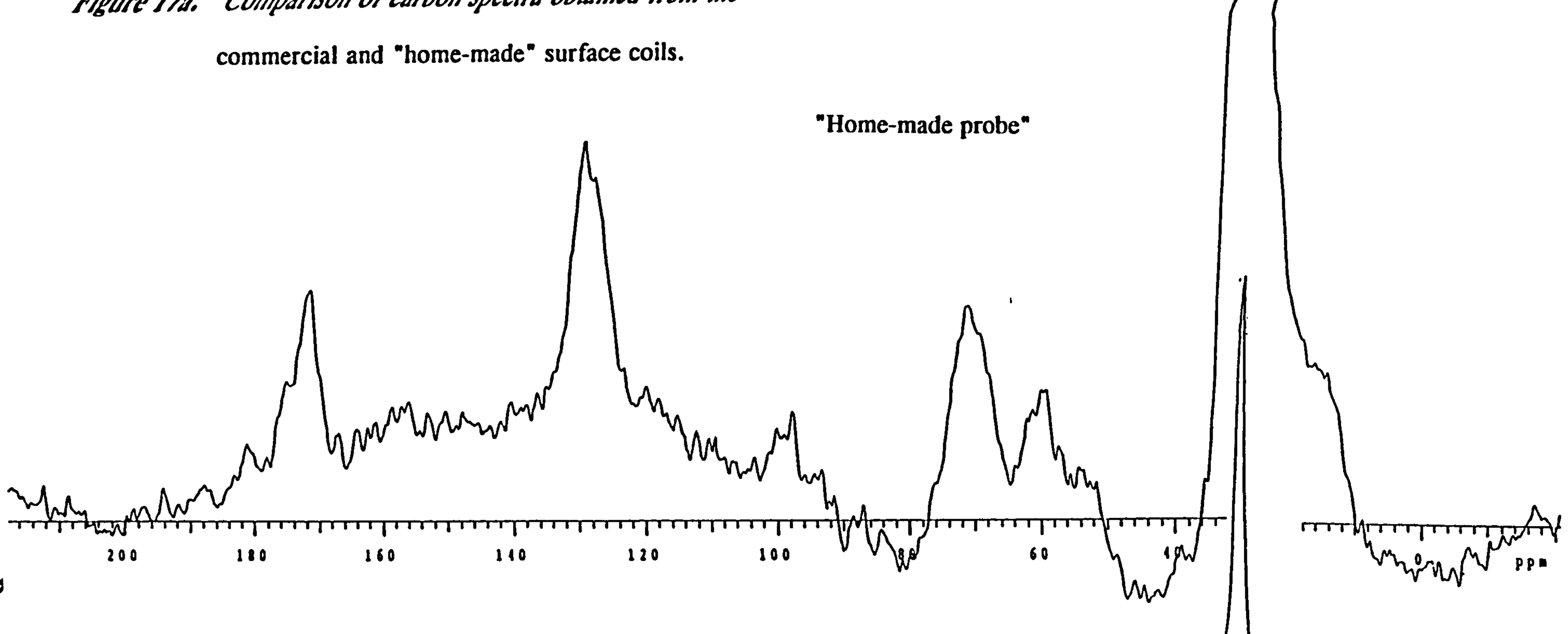

Commercial probe

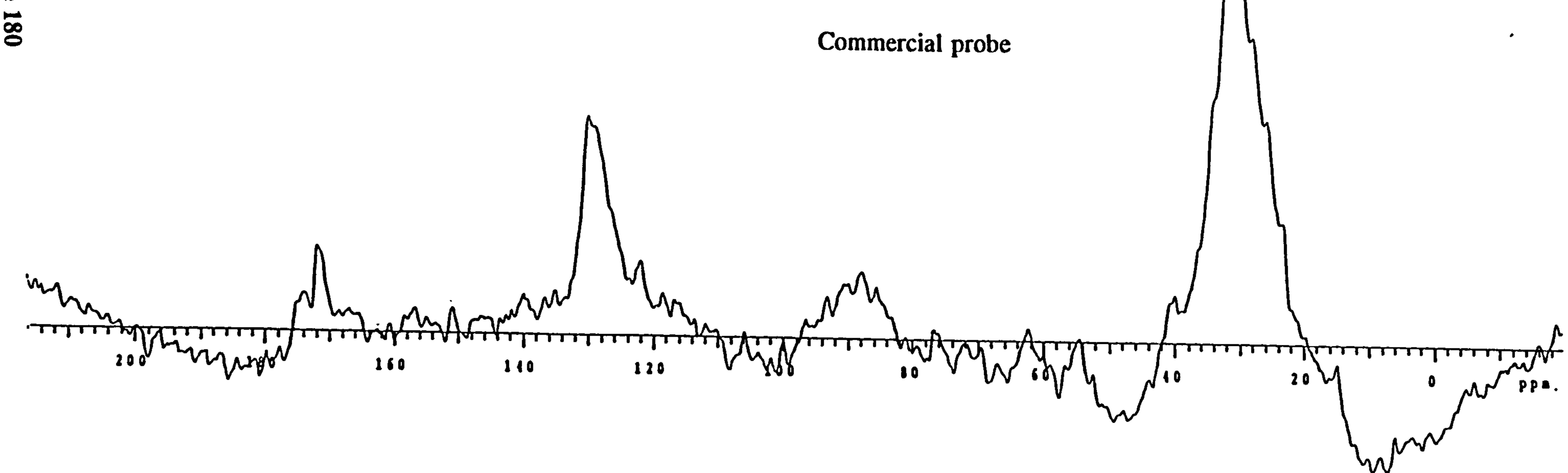

5.1.2.6. Method for lipid extraction of liver for *in vitro* ^{13}C-NMR analysis.

5.1.2.6.1. Extraction procedure.

The frozen liver sample (1 g) was weighed and was crushed under liquid nitrogen in a pestle and mortar. The powdered liver was transferred to a 50 ml boiling tube containing chloroform:methanol [(2:1) 20 ml/1 g tissue] and homogenised briefly using a tissue homogeniser [Inter. Lab. App. Gmbh, Type X 1020; small probe; position 5] to allow greater surface area for lipid extraction. The solution was left shaken every 10 minutes for 1 hour after which the tissue was homogenised thoroughly for 3 - 5 minutes (position 7). Saline (20 ml) was added and tube gently inverted several times, the lipid and aqueous layers were then allowed to settle. The top methanol/saline layer was discarded and the clear, slightly yellow, bottom layer transferred into a pre-weighed scintillation vial to be dried down under a continuous stream of nitrogen (3 - 4 hours). The resultant dry lipid extract was weighed and stored under nitrogen at -70°C.

5.1.2.6.2. Preparation of lipid extract for high resolution NMR analysis.

On the day of NMR analysis the lipid extract was dissolved in 0.6 ml deuterated chloroform together with the addition of tetramethylsilane (Sigma T 3759) as use as a reference and transferred to 5 mm NMR tubes (Goss Instruments Ltd., Type 507-HP). The lipid samples were run on a JEOL GSX 500 N.M.R. spectrometer

operating at 500 MHz and 11.75 Tesla. Proton-decoupled carbon spectra were obtained with an acquisition time of 0.544s a pulse width of 15 μs and a pulse delay of 6s.

5.1.2.7. Statistics.

Statistical significance of differences between means was assessed by Student's unpaired t test. All results are given as means $\pm$ SEM for five rats.

5.1.3. Results and discussion.

It is important to note that the 4 week routine meal fed group had similar food intakes as the *ad libitum* fed rats (*ie.* 17.5 $\pm$ 2.4 g for 4 week meal fed rats and 18.3 $\pm$ 2.0 g for *ad libitum* fed rats over a 24 h period).

Figure 18 shows typical carbon spectra prior to glucose infusion, followed by sequential spectra post infusion. The three main broad components of the hepatic carbon spectra are from fatty acyl chains which include the -CH_2 and -CH_3, between 14 - 35 ppm, the olefinic carbon region, between 125 - 130 ppm, and the carbonyl region between 170 - 185 ppm (all chemical shifts are approximate due to the inherent lack of resolution seen in *in vivo* spectroscopy). The spectra show clearly the appearance at 92.68 and 96.60 ppm of α and ß glucose (ratio of 1:2, respectively) following infusion of ^{13}C-glucose. From *figure 19* and *table 17* it can be seen that

hepatic 1-^{13}C glucose utilisation/assimilation/removal declines at approximately the same rate in both pre and post meal groups with no significance between the two. Plasma glucose concentrations prior to and 60 mins. post 1-^{13}C glucose administration within the two groups were the same, however values were slightly higher in the two groups at 60 mins. post administration. From *figures 19* and *table 17*, ^{13}C-1 glycogen incorporation, seen at 100.48 ppm, increases to a maximum approximately 30 mins post ^{13}C-glucose infusion ($P<0.02$) in the pre-meal group. As early as 10 min post ^{13}C-glucose infusion, there was a significant difference between the two groups ($P<0.05$), with the pre meal group showing enhanced ^{13}C incorporation into glycogen. The rate of incorporation is seen to be considerably faster than rats either fed *ad libitum* or starved for 22 h and refed for 2 h. The post-meal group shows little net incorporation of ^{13}C-glucose into glycogen implying that either maximal glycogen levels had been reached or synthesis was occurring preferentially from the unlabelled pool of 3 carbon precursors. From *in vitro* NMR studies conducted on the livers following *in vivo* analysis (*see diagram 20*), it can be seen that the pre-meal 4 week RMF group show a broad resonance at 100.48 ppm corresponding to the C-1 of glycogen. This resonance was noticeably diminished or absent in all of the post-meal 4 week RMF group, despite normal fed hepatic glycogen levels in this group, see below. This would suggest direct incorporation of ^{13}C-1 glucose into the C-1 of glycogen, since glycogen from naturally abundant ^{13}C-1 glucose (1.1% natural abundance) is very difficult to detect with the spectroscopic parameters used. This is despite the fact that the post-meal group has a glycogen concentration of 63.1 $\pm$ 6.4 mg glycogen/g wet wt.. There were no differences between *in vitro* lipid extracts, in particular there was no enrichment in the glycerol moiety (*see diagram*

21). The signal to noise ratios in the aqueous extracts were consistently poor due to the very low ^{13}C enrichments used for this study.

Upon refeeding 24 h starved *ad libitum* fed rats maximum glycogen levels are not achieved until 6-7 hours after the start of refeeding (Holness *et al.*, 1988). In routine meal fed rats, glycogen levels reach a maximum following 3 h of refeeding, indicating the enhanced capability for the conversion of glucose. A major question arising from glycogen synthesis studies is the relative contribution of C_3 intermediates to the glycogen molecule compared with the direct conversion of glucose to glycogen. The latter method provides a quick method of glycogen repletion however, it is thought that *ad libitum* fed rats undertake both processes with a ratio of 60:40% in favour of the indirect gluconeogenic pathway (Shulman *et al.*, 1985). This line of thought is not conclusive as other studies report glucose as the major glycogenic precursor (Scofield *et al.*, 1985).

Pallardo and Williamson (1989) found that the rates of hepatic glycogen synthesis on re-feeding 10 day meal fed rats were identical to those in rats fed *ad libitum* (approx. 30 μmol of glycosyl units/h per g of liver) however hepatic lipogenic rates were enhanced. It was suggested that in the meal fed group direct conversion of exogenous glucose to glycogen occurred. However, a study by Sugden *et al.* (1993) systematically looked at the glycogen concentrations of 4 week meal fed and virgin rats following refeeding over a 9 h period. It was noted that the meal fed group had a much faster capacity to replenish hepatic glycogen levels compared with control *ad libitum* fed rats. Control rats showed maximal glycogen levels approximately 6-9 h

following refeeding, however, the meal fed group reached maximal values approximately 4 h after food provision. The differences between these two groups can be accounted for by the duration of the meal feeding regimes employed, Pallardo and Williamson studied 10 day meal fed rats whereas, this most recent study looked at long term food restriction (4 week meal feeding). In conjunction with increased glycogen disposal patterns in long term meal fed rats, increased rates of disposal were observed in both 10 day and 4 week meal fed rats which were attributed to increased PDH activities supplying acetyl CoA subunits for lipid synthesis. The results shown in this thesis show high rates of 1-^{13}C glucose incorporation into glycogen C-1 in the meal fed rats when compared to rats fed *ad libitum* (*see section 5.3.3.1.*) and support the view that glucose is directly converted to glycogen in long term meal fed rats. The rates of glycogen repletion shown in *table 17* and *figure 19* compare very favourably with the repletion rates shown by Sugden *et al.* (1993). This study showed a gradual increase in total glycogen to a maximum of 67.8 ± 10.9 mg/g wet wt. within 3 hours following food administration. The study shown here show gradual increases in incorporation of ^{13}C-glucose into the C-1 of glycogen in the pre-meal 4 week RMF group, this incorporation reaches a maximum at 30 min post glucose infusion indicating ^{13}C-glucose units have been "removed" from circulation. From 30 - 60 min. post-infusion no ^{13}C-1 glycogen degradation was seen. The post-meal group, showed no net incorporation of ^{13}C into the C-1 of glycogen. Taking into account that the actual time following food provision is 3 h, due to animal and magnet preparations, it must be assumed that maximum glycogen levels have been reached. From *in vitro* glycogen measurements this was the case, with the post-meal glycogen levels resembling fed values of 63.1 ± 6.4 mg/g wet wt. compared with 8.1

± 2.7 mg/g wet wt. in the pre-meal 4 week RMF group.

One of the earliest studies on meal feeding was conducted on obese mice (Tepperman and Tepperman 1957) in which increased absorption of glucose from the gastro-intestinal tract was noted. This was an interesting observation in light of this present study which suggests that glucose is rapidly assimilated by the liver and directly converted to glycogen. If glycogen repletion was via the indirect gluconeogenic pathway of C_3 substrates (and the glycolysis of glucose followed by carboxylation to oxaloacetate) then a large amount of the label on the C-1 of glucose would be expected to be lost at the level of oxaloacetate and hence loss through intermediates of the Krebs cycle and other anaplerotic pathways associated with this flux. Loss of ^{13}C could also be attributed to the relative pools of dihydroxyacetone and glyceraldehyde 3-phosphate where an equilibrium exists between the two and glycerol phosphate. Of course, the bulk of substrates used via the gluconeogenic pathway would primarily be lactate or amino acids from extra hepatic metabolism, but the above just illustrates the possibility of the futile cycle involving glucose breakdown and subsequent synthesis of glycogen.

This study provides further evidence that glycogen synthesis during long-term food restriction in rats can primarily be accounted for by the direct conversion of glucose subunits. From the study by Pallardo and Williamson (1989), increased lipogenic rates were seen in the meal fed groups and it was suggested that lipogenesis and glycogenesis occur simultaneously albeit with different substrates. It would appear that lipid synthesis is primarily achieved through carboxylation of C_3 precursors.

Figure 18. Sequential carbon spectra following 1-^{13} glucose infusion.

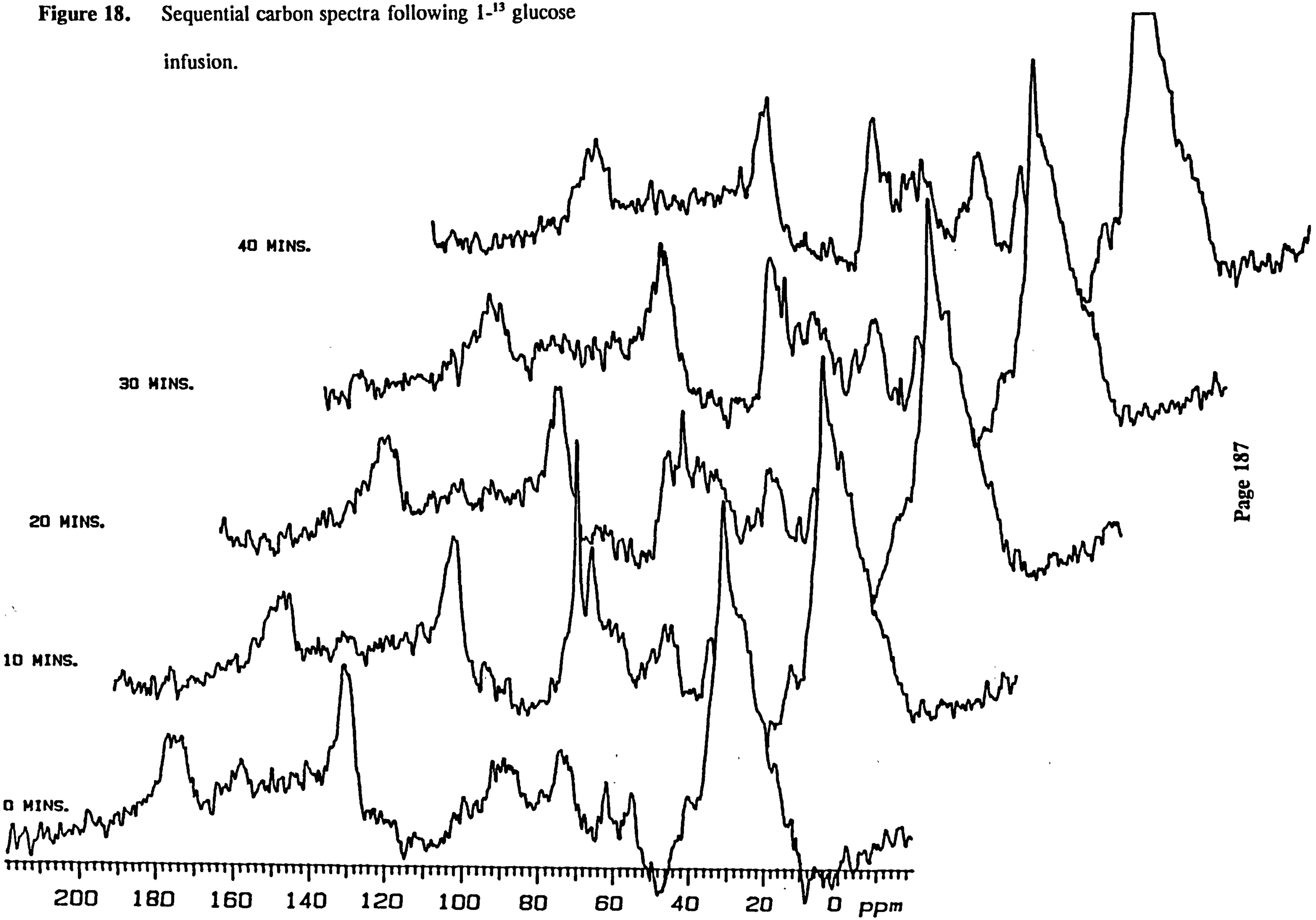

Graph Showing Relative Hepatic Glycogen Synthesis &
Glucose Disposal In 4 Week Meal Fed Rats.

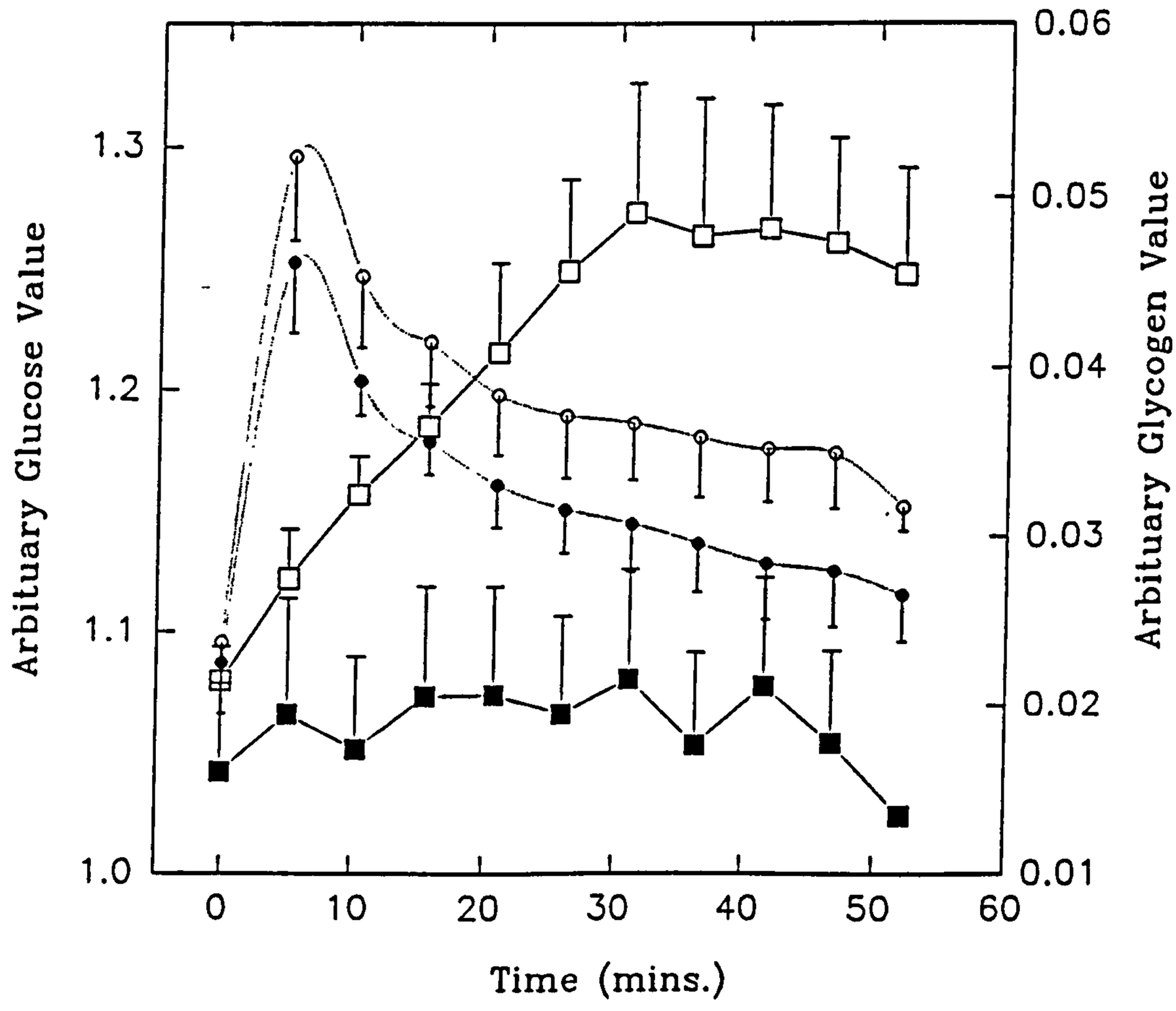

KEY

□ Pre meal 13C–glycogen.
■ Post meal 13C–glycogen.

○ Pre meal 13C–glucose.
● Post meal 13C–glucose.

Figure 19.

Figure 20. High resolution proton decoupled carbon spectra of liver aqueous extracts of 4 week RMF rats pre and post meal.

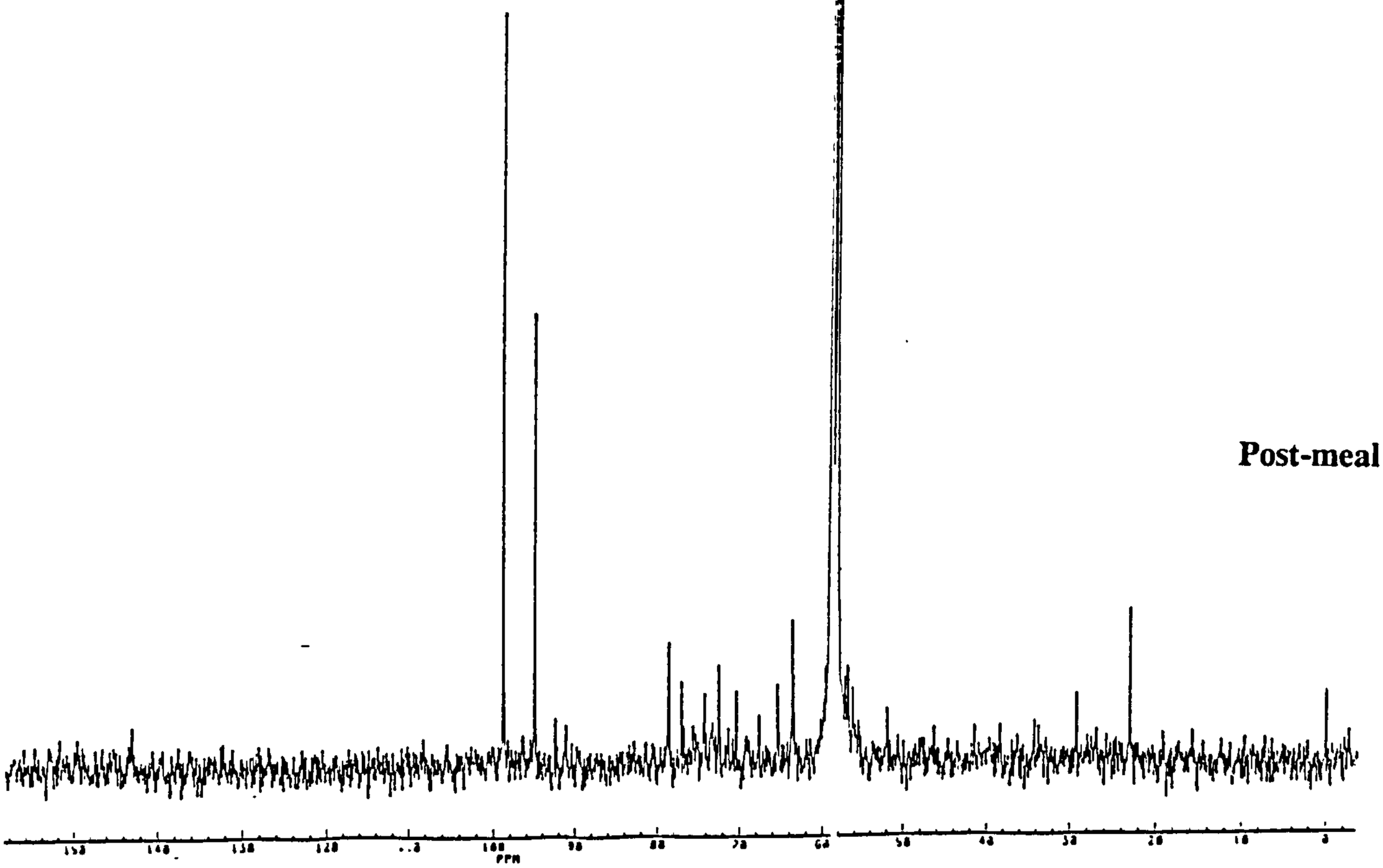

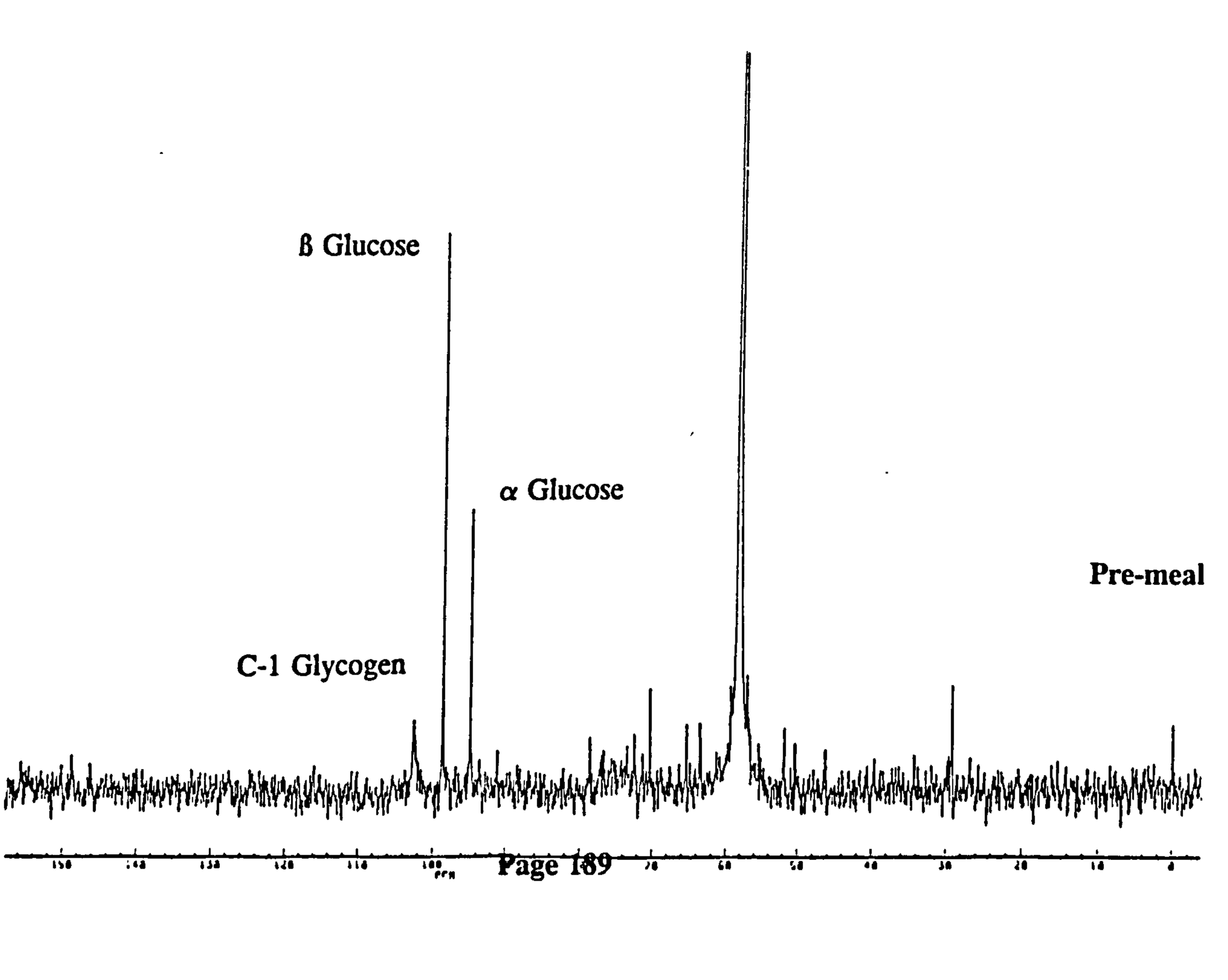

Figure 21. High resolution proton decoupled carbon spectra of liver lipid extracts of 4 week RMF rats pre and post meal.

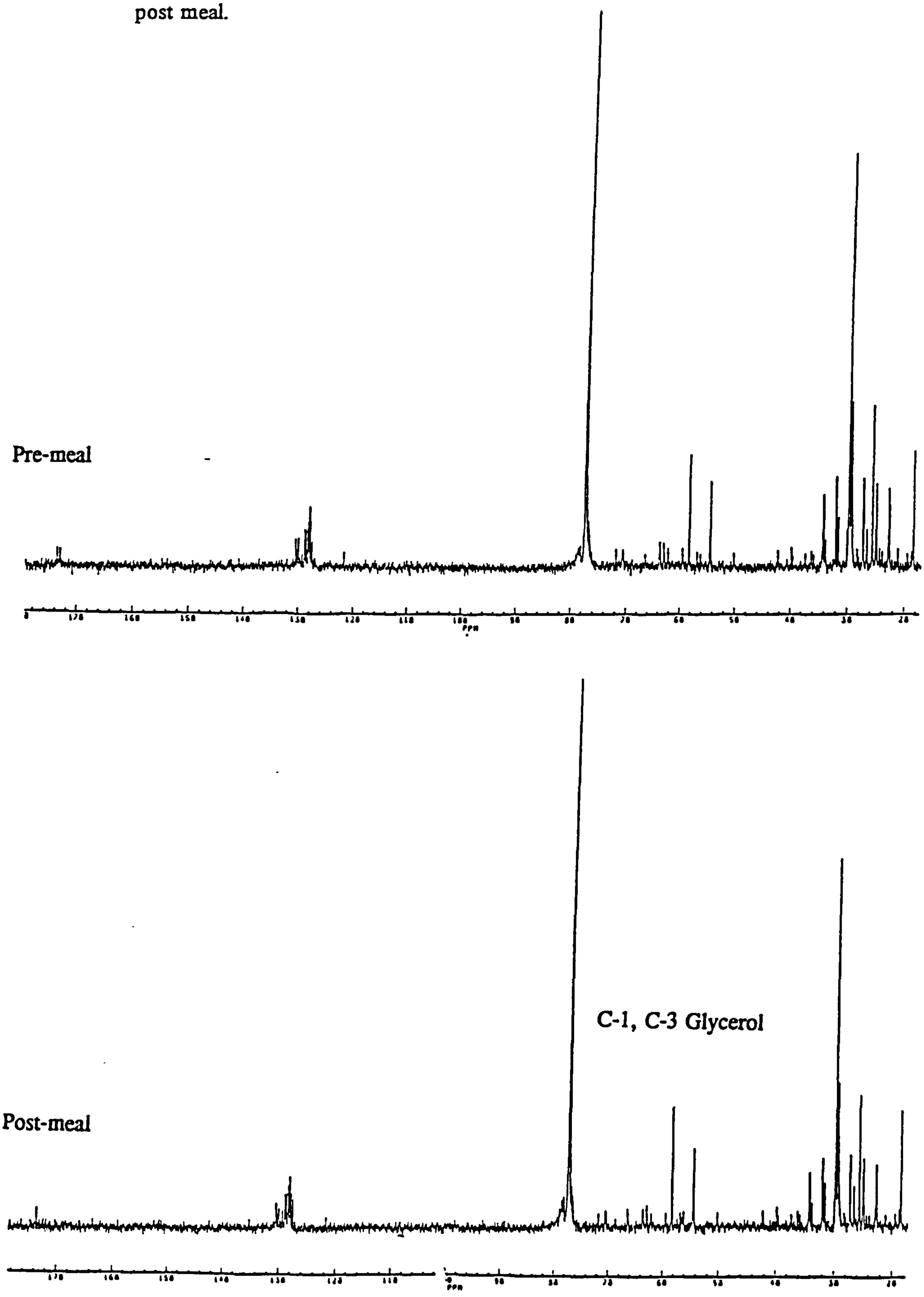

Table 17. **Comparison of ^{13}C-glycogen deposition between pre-meal and post - meal 4 week routinely meal fed rats.**

Time (mins)	Pre-meal n=5	S.E.M.	Post-meal n=5	S.E.M.
0	0.021	0.0020	0.016	0.0053
5.2	0.027	0.0029	0.019	0.0069
10.4	0.032	0.0023	0.017*	0.0055
15.6	0.037	0.0025	0.021*	0.0065
20.8	0.041	0.0053	0.021*	0.0064
26.0	0.046	0.0054	0.019**	0.0058
31.2	0.049	0.0075	0.022*	0.0065
36.4	0.048	0.0080	0.018**	0.0056
41.6	0.048	0.0072	0.021*	0.0065
46.8	0.047	0.0062	0.018***	0.0055
52.1	0.046	0.0062	0.013***	0.0016

Time point 0 mins. represents baseline levels prior to 1-^{13}C glucose infusion. Rat weights for both groups were 216.6 ± 2.6 g. The mean glucose concentrations in pre and post meal jugular vein samples prior to 1-^{13}C glucose administration were 4.560 ± 0.449 mmol/l and 4.569 ± 0.263 mmol/l and 60 mins. after 1-^{13}C glucose administration were 5.184 ± 0.705 mmol/l and 6.146 ± 1.440 mmol/l. Values which were significantly different between pre and post meal are indicated by *$P<0.05$; **$P<0.02$; ***$P<0.001$.

5.2. Assessment of NMR protocol for *in vivo* hepatic metabolic studies.

The results demonstrate the ability of ^{13}C-NMR to monitor both the decay of 1-^{13}C glucose and incorporation into glycogen simultaneously, in real time. In theory it should also be possible to investigate the degree of ^{13}C recycling via 3-carbon intermediates e.g. lactate, and gluconeogenic intermediates, by observing enrichment in the C-6 position of glycogen. However, there is either insufficient resolution and/or signal *in vivo* and *in vitro*. Following this study a new coil, as described in *section 5.1.2.1.*, was built but with the specific requirements of the protocol in mind and used for all subsequent experiments. Although the commercial probe provided the necessary information required for the pregnant study it was by no means perfectly adapted to the physical constraints of the rat model, reflected in the high mortality rates. This was due to the coil being large and bulky which regularly obstructed the movement of the diaphragm as well as placing extreme pressures onto the liver, possibly causing ischaemia and hence hypoxia. It was hoped that with the new coil design these problems would be eliminated and that higher resolution ^{13}C spectrum could be obtained, which could detect fluctuations other than the resonances of C-1 glucose at 92.68 and 96.60 ppm and the C-1 glycogen at 100.48 ppm.

5.3. *In vivo* hepatic glycogen synthesis rates during late gestation in the rat.

5.3.1. Introduction.

As shown in *chapter 2*, glucose intolerance by most tissues is dependent on the progression of pregnancy and the mothers nutritional status; late gestation shows the greatest suppression of uptake and phosphorylation. The insulin resistant state shown during late gestation can apparently be reversed upon placing the rat under a short term course of routine meal feeding, *see section 3.4.*.

Since the liver controls glucose homeostasis, increased knowledge on the pathogenesis of insulin resistant states like pregnancy and non-insulin dependent diabetes mellitus can be gained from hepatic glucose metabolic studies. A study by Davidson (1983) explored the role of the liver during late pregnancy. However, this study used isolated hepatocyte preparations from which no correlation between pregnancy and insulin resistance was observed. A subsequent study by Leturque *et al.* (1985) revealed that isolated peripheral tissues do not exhibit insulin resistance, otherwise shown *in vivo*. It was also suggested that the liver does exhibit a degree of decreased sensitivity to insulin during late gestation, shown by infusing low doses of insulin which did not produce rapid glucose clearance rates as seen in virgin rats. It is imperative therefore, when conducting studies on the insulin resistance of tissues that they are conducted *in vivo*. Measurements of glucose utilisation rates using the methods illustrated in *chapter 2* can not be preformed on the liver due high levels of hepatic glucose-6-phosphatase [EC. 3.1.3.9]. This enzyme catalyses the conversion

of glucose-6-phosphate to glucose and hence phosphorylated 2 deoxyglucose-6-phosphate can be converted back to 2 deoxyglucose producing inaccurate measurements of the GUI. *In vivo* ^{13}C-NMR has therefore been employed to elucidate the liver's glucose utilisation/disposal during pregnancy of rats fed *ad libitum* and those on the strict meal feeding regimes. *In vitro* analysis of freeze clamped liver extracts were assessed using high resolution ^{13}C-NMR spectroscopy, *see section 5.1.2.5. and 5.1.2.6..*

As well as investigating the consequences of late pregnancy on the glycaemic control by the liver, the study was extended to early pregnancy, *ie.* day 10 of gestation. This study was set up primarily to investigate the role of the liver during gestation to equate results to the changes shown in the glucose utilisation capacity of the skeletal and cardiothoracic muscles. A further purpose was to evaluate the possibilities of NMR in a more clinical role for detecting abnormalities in the glucose homeostasis of the liver during disease states.

5.3.2. Methods.

5.3.2.1. Animal feeding regimes.

The methods of cannulation and NMR set up have fully been discussed in *section 5.1.2.*, the following is a synopsis of the animal feeding regimes employed. Four groups of age-matched female albino Wistar rats were time-mated. The RMF group

were housed in a reverse light/dark room [light off 10:00/light on 22:00] and allowed access to chow for 2 h per day from day 9 of pregnancy. The early pregnant group was started on the RMF regime from day 1 of gestation. The *ad libitum* groups had free access to food. Two control groups were studied which were age-matched *ad libitum* virgin controls and 22 h starved; 2 h refed controls. Immediately after the last meal on either day 10 or 20 of pregnancy (term = 21 days), the pregnant rat was anaesthetised with sodium pentobarbital (60 mg/ml/kg). The liver was exposed and the hepatic portal vein cannulated to a line containing D-glucose-1-^{13}C(99atom % ^{13}C) [200mg/ml]. Spectra were obtained as in *section 5.1.2.3.*, the infusion of ^{13}C-1 glucose took place after acquisition of the second base-line spectra over a period of 2 min. during the first time point (5.2 min.).

5.3.3. Results.

5.3.3.1. ^{13}C-glucose incorporation into the glycogen macromolecule during late pregnancy.

From *table 18* and *figure 22* it can be seen that very little incorporation of ^{13}C-glucose into glycogen was detected in 20 day pregnant *ad libitum* and control fed virgin rats, whereas the 20 day pregnant RMF group had a very much enhanced incorporation rate, in an approximately linear fashion. The same incorporation rate was shown in the 20 day pregnant; 22 h starved 2 h re-fed group up to 20 min. post infusion, however no further net increase in incorporation was seen after this. In this group there was reduction in the total net incorporated ^{13}C 20 minutes post ^{13}C-glucose

infusion *ie.* there appears to be no further incorporation into hepatic glycogen indicating a gradual reduction in the ^{13}C-glycogen stores. This would indicate the rapidity by which newly synthesised glycogen can be almost immediately broken down as the rat moves into a post-absorptive nutritional status. During the same time scale the 20 day pregnant RMF group continues to incorporate the administered ^{13}C-glucose into glycogen macromolecules in an unhindered fashion. Approximately 50 min. post infusion the net incorporation is at a level approximately 2.3 times the maximum incorporation levels shown in the 20 day pregnant; 22 h starved 2 h re-fed group. The increase in ^{13}C incorporation slows down 25 min. post infusion, however the increases still continue but in a slower linear fashion. From *figure 23* it can be seen that ^{13}C-glucose levels in the 20 day pregnant *ad libitum* group disappeared very rapidly and by 15 min. post infusion the label had returned to pre-infusion levels. Compared with the virgin rat, label declined at a much slower rate and was at half maximal levels at 15 min.. ^{13}C-glucose levels remained very much higher and for a longer period of time in the 20 day pregnant RMF group. In this group levels of ^{13}C-glucose were equivalent to virgin levels 15 min. post-infusion. However, from this time point onwards the ^{13}C-glucose remained at an elevated level over the virgin condition. By 40 min. post-infusion ^{13}C-glucose resembled pre-infusion levels in the 20 day pregnant *ad libitum* group whereas, in the RMF group the levels remained at of approximately one third of the total infused label. Between 20 and 50 min. post-infusion there was very little decline in the label.

5.3.3.2. ^{13}C-glucose incorporation into the glycogen macromolecule during early pregnancy.

Table 19 and *figure 24* show the relative amounts of ^{13}C incorporation into the C-1 of hepatic glycogen in 10 day pregnant rats compared with late pregnant rats. Food restriction during the first 10 days of gestation produced a large increase in glycogen labelling compared with any other group shown. Compared with the 20 day pregnant rat, restricted in the last 10 days of pregnancy, and the 10 day *ad libitum* group, increases of 2.4 and 4.3 fold were seen, respectively. Maximal increases in the 10 day *ad libitum* group occurred at 25 min. post ^{13}C-glucose infusion after which incorporation declined. However, in the 10 day RMF group glucose incorporation increased linearly for 30 min. post infusion and plateaued out for the period of the experiment (60 - 70 min.).

Table 18. Comparison of ^{13}C-glucose incorporation into hepatic glycogen between control ad libitum, 20 day pregnant refed, 20 day pregnant ad libitum and 20 day pregnant RMF groups.

Time mins.	Control *ad libitum*	20 day preg. 22 h starved 2 h re-fed	20 day preg. *ad libitum*	20 day preg. RMF
0.00	0.000 ± 0.000	0.000 ± 0.000	0.000 ± 0.000	0.000 ± 0.000
5.21	1.090 ± 0.460	0.000 ± 0.000	0.000 ± 0.000	0.274 ± 0.163
10.41	0.533 ± 0.267	0.767 ± 0.626	0.265 ± 0.149	0.433 ± 0.155
15.62	0.740 ± 0.523	1.095 ± 0.568	0.253 ± 0.159	1.436 ± 0.563*
20.82	0.193 ± 0.136^{++}	2.290 ± 1.007	0.354 ± 0.194	2.111 ± 0.531**
26.03	0.830 ± 0.587^{+}	1.883 ± 0.850	0.353 ± 0.171	3.936 ± 1.056**
31.23	0.090 ± 0.064^{+++}	0.958 ± 0.438$^{\#\#\#}$	0.155 ± 0.130	4.167 ± 0.416***
36.44	0.669 ± 0.473^{+++}	1.635 ± 1.335$^{\#}$	0.066 ± 0.049	4.643 ± 0.709***
41.64	0.470 ± 0.332^{+++}	1.572 ± 1.110$^{\#\#}$	0.124 ± 0.111	4.960 ± 0.798***
46.85	---	0.868 ± 0.356$^{\#\#\#}$	0.023 ± 0.020	4.915 ± 0.455***
52.05	---	---	0.074 ± 0.066	5.287 ± 0.312***

Time point 0 mins represents base-line values prior to 1-^{13}C glucose infusion. Values which are significantly different between 20 day pregnant *ad libitum* & 20 day pregnant RMF rats are indicated by $^{*}P<0.1$; $^{**}P<0.01$; $^{***}P<0.001$. Values significantly different between 22 h starved/2 h refed & 20 day pregnant RMF rats are indicated by $^{\#}P<0.1$; $^{\#\#}P<0.05$; $^{\#\#\#}P<0.001$. Values significantly different between *ad libitum* control & 20 day pregnant RMF rats are indicated by $^{+}P<0.05$; $^{++}P<0.01$; $^{+++}P<0.001$. n=6 for all groups. *Abbreviation*:preg-pregnant.

Hepatic Glycogen Synthesis In *ad libitum* Virgin & 20 Day Pregnant Rats, & RMF 20 Day Pregnant Rats.

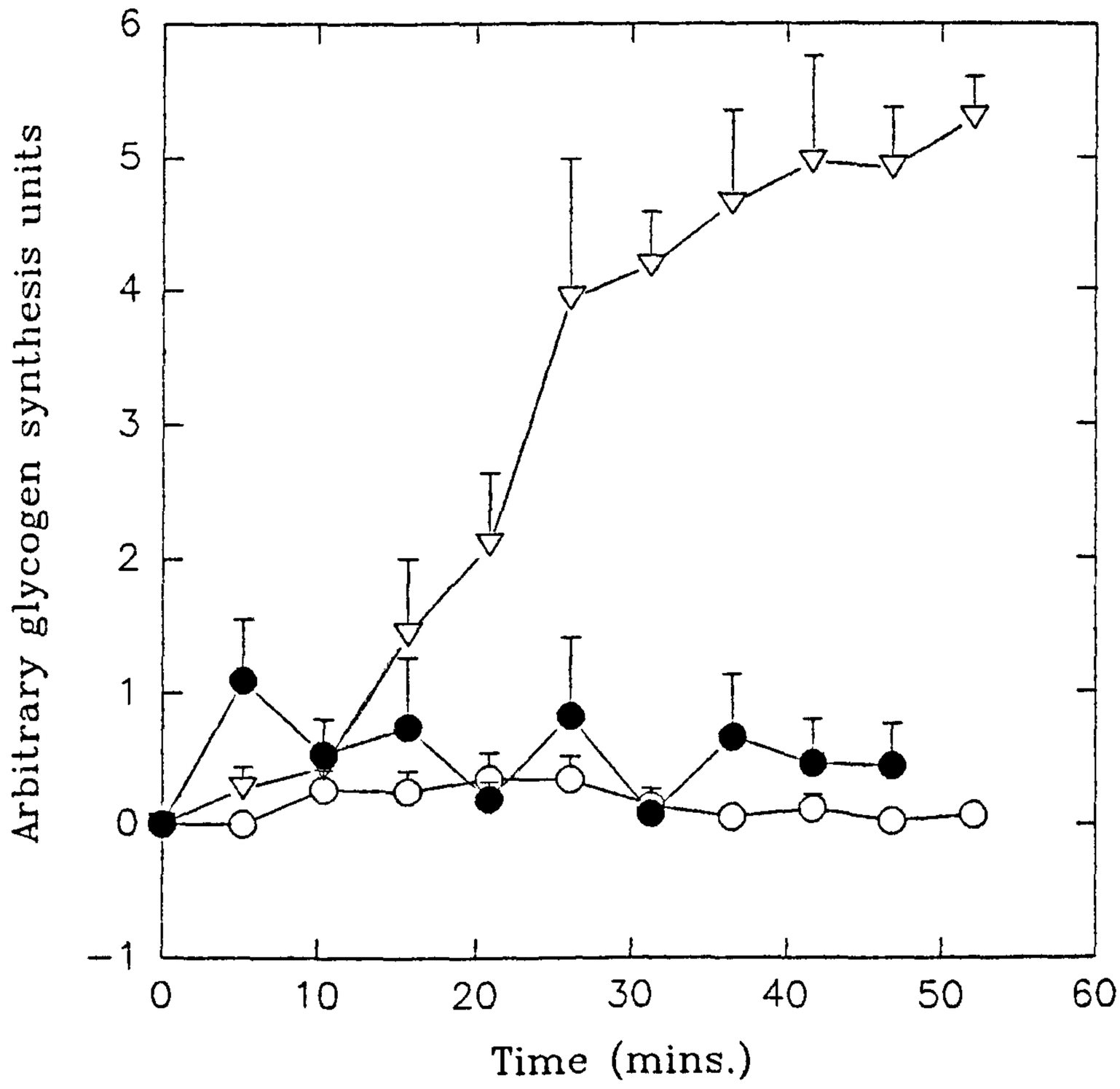

Figure 22.

▽ *RMF, 20 day pregnant.*

○ *ad libitum, 20 day pregnant.*

● *ad libitum virgin.*

Glycogen integral values represent net synthesis after ^{13}C-glucose infusion. All values are normalised to the CH_2 integrated area.

Hepatic Glucose Disposal In *ad libitum* 20d Pregnant & Virgin Control & RMF 20d Pregnant Rats.

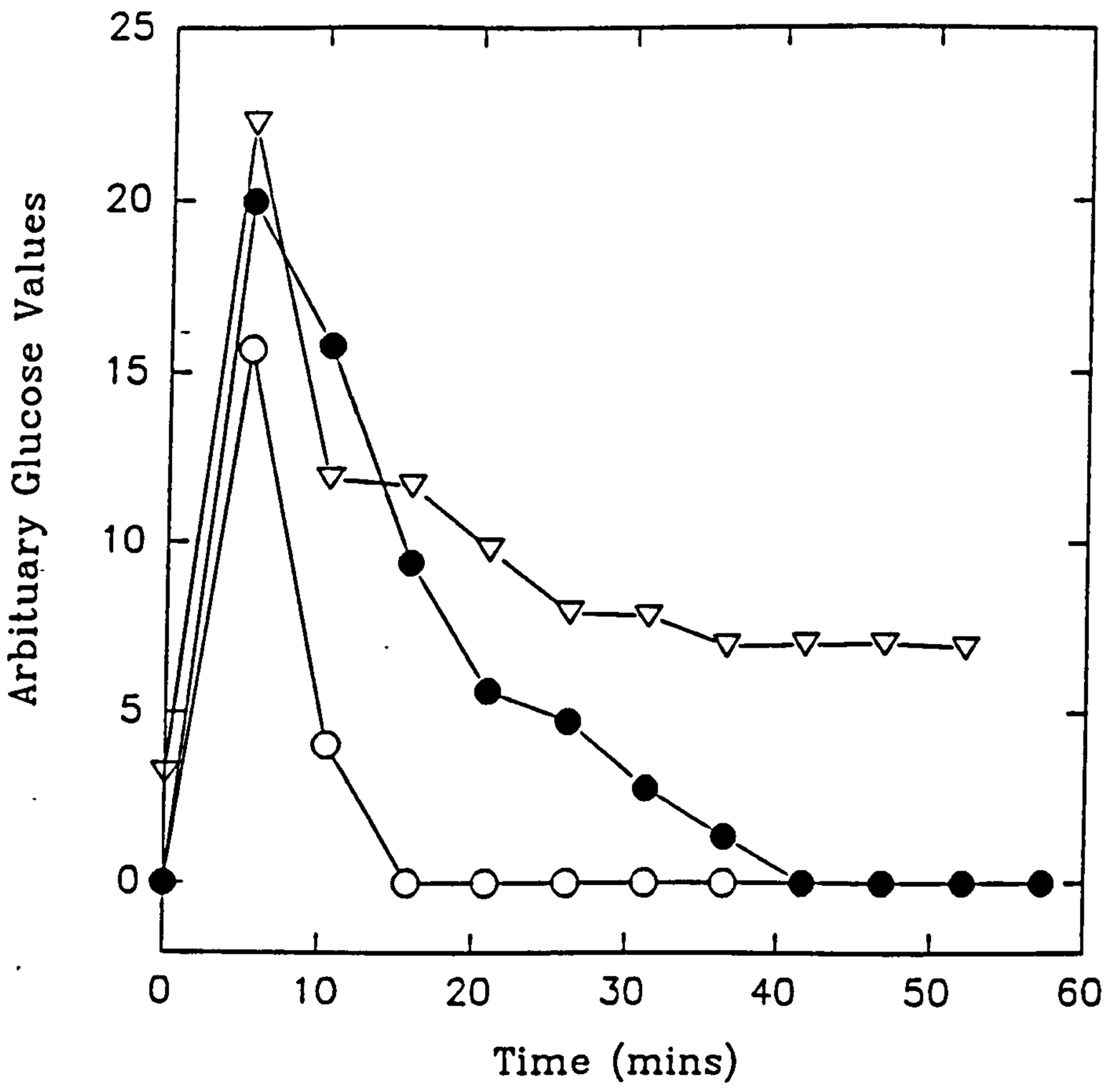

Figure 23.

○ ad libitum, 20 day pregnant; △ RMF, 20 day pregnant; ● ad libitum virgin.
Glucose integral values represent net hepatic ^{13}C infused glucose. All integrals are normalised to the CH_2 integrated area. For clarity the results from one experiment are shown, 4 other experiments showed similar results.

Table 19. Comparison of ^{13}C-glucose incorporation into hepatic glycogen between 10 day preg *ad libitum* and RMF preg rats & 20 day *ad libitum* preg & RMF rats.

Time mins.	20 day preg. *ad libitum.*	20 day preg. RMF.	10 day preg. *ad libitum.*	10 day preg. RMF
0.00	0.000 ± 0.000	0.000 ± 0.000	0.000 ± 0.000	0.346 ± 0.260
5.20	0.000 ± 0.000§	0.274 ± 0.163	0.684 ± 0.259$^{\#\#}$	1.101 ± 0.600
10.41	0.265 ± 0.149§§	0.433 ± 0.155	0.742 ± 0.457	3.960 ± 0.890$^{***\bullet}$
15.61	0.253 ± 0.159§§§	1.436 ± 0.563	1.562 ± 0.456$^{\#\#}$	5.466 ± 0.600$^{******\bullet}$
20.82	0.354 ± 0.194§§§	2.111 ± 0.531	2.148 ± 0.679$^{\#\#}$	7.270 ± 1.350$^{**\bullet\bullet}$
26.03	0.353 ± 0.171§§§	3.936 ± 1.056	3.141 ± 0.585$^{\#\#\#}$	9.194 ± 1.250$^{**\bullet\bullet}$
31.23	0.155 ± 0.130§§§	4.167 ± 0.416	2.113 ± 1.080	10.330 ± 1.500$^{**\bullet\bullet}$
36.43	0.066 ± 0.049§§§	4.643 ± 0.709	1.472 ± 0.840	12.070 ± 1.800$^{**\bullet\bullet}$
41.64	0.124 ± 0.111§§§	4.960 ± 0.798	1.261 ± 0.760	9.870 ± 1.650$^{*\bullet\bullet}$
46.84	0.022 ± 0.020§§§	4.915 ± 0.455	0.819 ± 0.640	12.447 ± 1.82$^{**\bullet\bullet}$
52.05	0.074 ± 0.066§§§	5.287 ± 0.312	1.023 ± 0.487$^{\#}$	13.024 ± 1.70$^{***\bullet\bullet}$
57.26	--	--	0.424 ± 0.236	11.750 ± 2.34$^{\bullet\bullet}$
62.46	--	--	0.185 ± 0.166	11.905 ± 2.40$^{\bullet\bullet}$

Statistically significant differences of means between 10 day pregnant RMF group and 20 day pregnant RMF group are represented by $^{*}P<0.02$; $^{**}P<0.01$; $^{***}P<0.001$. Significance between 10 day pregnant *ad libitum* and 20 day pregnant *ad libitum* are represented by $^{\#}P<0.1$; $^{\#\#}P<0.05$; $^{\#\#\#}P<0.01$. Significance between 20 day pregnant *ad libitum* and 10 day pregnant RMF are represented by $^{\S}P<0.1$; $^{\S\S}P<0.01$; $^{\S\S\S}P<0.001$. Significance between 10 day pregnant *ad libitum* and 10 day RMF are represented by $^{\bullet}P<0.02$; $^{\bullet\bullet}P<0.01$; $^{\bullet\bullet\bullet}P<0.001$. n=6 for all groups.

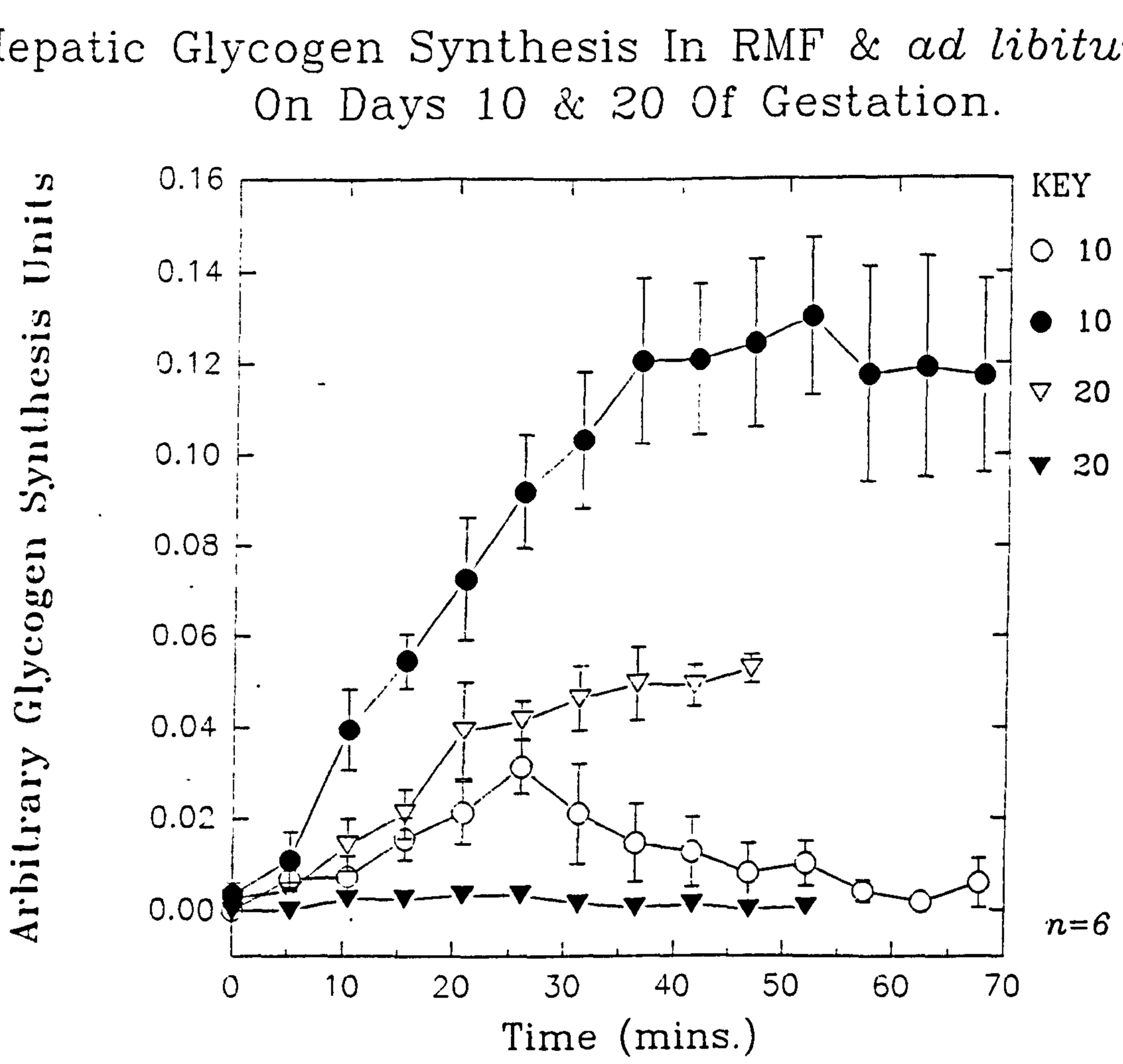
Hepatic Glycogen Synthesis In RMF & ad libitum Rats
On Days 10 & 20 Of Gestation.
Arbitrary Glycogen Synthesis Units
0.16
0.14
0.12
0.10
0.08
0.06
0.04
0.02
0.00
0
10
20
30
40
50
60
70
Time (mins.)
KEY
10 day, ad libitum
10 day, RMF
20 day, RMF
20 day, ad libitum.
n=6

Figure 24.

Table 20.

Plasma glucose concentrations pre and post ^{13}C-glucose infusion in all group studied.

GROUP	Pre ^{13}C-glucose infusion	Post ^{13}C-glucose infusion (60 mins.)
Virgin *ad libitum*.	$5.489 \pm 0.505^{***}$	5.301 ± 0.512
Control 22h stvd 2h refed	$6.200 \pm 0.388^{****}$	6.523 ± 0.899
20 day preg. 22h stvd 2h refed	2.936 ± 0.973^{NS}	$5.587 \pm 0.613^{\#\#}$
20 day preg. *ad libitum*	3.56 ± 0.214	$4.839 \pm 0.505^{\#\#\#}$
20 day preg. RMF	$4.410 \pm 0.232^{**}$	$6.316 \pm 1.070^{\#}$
10 day preg. *ad libitum*	$5.441 \pm 0.161^{****}$	5.387 ± 0.471
10 day preg. RMF	$5.504 \pm 0.765^{**}$	$5.512 \pm 0.844^{\#\#\#}$

Statistically significant differences between means compared with 20 day pregnant *ad libitum* rats pre ^{13}C-glucose infusion are represented by $^{*}P<0.05$; $^{**}P<0.02$; $^{***}P<0.01$; $^{****}P<0.001$. Differences between means of pre and post (60 mins.) ^{13}C-glucose infusion are represented by $^{\#}P<0.1$; $^{\#\#}P<0.05$; $^{\#\#\#}P<0.02$; $^{\#\#\#\#}P<0.01$. n=6 for all groups.

5.3.4. Discussion

This study has been the first to investigate *in vivo* hepatic carbohydrate metabolism using ^{13}C-NMR in the pregnant rat. It has revealed the possibility that carbon spectroscopy can be used as an investigative tool for physiological and pathological conditions which show adaptations to normal glucose metabolism, such as late pregnancy, NIDDM, liver cirrhosis, *etc.*. It is apparent that glycogenesis can occur using one of two pathways, either direct synthesis of glucose subunits to glycogen or, indirectly via C_3 gluconeogenic precursors such as amino acids and lactate (Shulman *et al.*,1985). The relative contributions of these pathways to glycogen repletion may be determined by physiological changes and pathological abnormalities. It is therefore important for studies such as these to be carried out in order to characterise changes seen *in vivo* rather than *in vitro*, since contributory metabolic factors may be lost as a consequence of *in vitro* methodologies. This study was devised to investigate the glucose homeostatic control of the liver in pregnancy and reflect any changes seen to the extensive suppression in glucose uptake and phosphorylation in skeletal and cardiothoracic muscles (*see chapter 3*).

The results show marked changes in hepatic glycogenesis during pregnancy and upon meal feeding pregnant rats. The changes between the groups in ^{13}C-glucose "disappearance" reflect quite closely the degree of incorporation into glycogen. The 20 day pregnant RMF group showed an enhanced degree of ^{13}C incorporation into the glycogen macromolecule together with an apparently greatly reduced dissipation of glucose from the liver. Dissipation of hepatic glucose could be the result of hepatic

oxidation due to glycolysis and the Krebs cycle or via flux through the pentose phosphate pathway (for generation of NADPH, important for fatty acid, cholesterol and steroid synthesis). It could also be due to direct incorporation into glycogen or the simple diversion away to other glucose requiring peripheral tissues. It would appear that during late pregnancy very little of the administered glucose is converted to glycogen. Consequently, it may be diverted away from hepatic vascularity to fuel the development of the foetus(es) rather than requirements of maternal tissue, due to the significant degree of glucose intolerance shown by these tissues, *see chapter 3*. The rapidity in which the glucose dissipates from the liver is remarkably high and it could be argued that this may caused by the haemodilution effect due to increased vascularity and/or a greater glucose turnover rate. However, bolus infusions of glucose were administered in accordance to the rats weight prior to the experiment. The specific activity of the blood was investigated. However, due to the small bolus infusions of 1-^{13}C glucose administered it was impossible to distinguish between the groups. Clearly pregnancy is having an effect on hepatic glucose homeostasis. Glucose absorption/retention by the liver is somehow being compromised during pregnancy, allowing circulating glucose to be channelled towards the foetus(es). It would therefore be useful to evaluate the role of hepatic glucose transport systems and insulin receptors during late gestation. The latter has previously been investigated and was shown to be unaffected by pregnancy (Soman, 1979). The method of glycogen repletion during late pregnancy may be a mechanism of preserving plasma glucose levels for the requirement of the foetus(es). If glycogen is predominantly being repleted by the indirect gluconeogenic pathway this would allow glucose to be diverted away from the liver. It is evident during pregnancy that higher levels of C_3

intermediates are prevalent due to the increased mobilisation of fatty acids (oxidised by peripheral tissues) and ketone bodies together with the consequence of increased glucose utilisation by the foetus generating pyruvate and lactate which can re-enter the maternal blood stream. During pregnancy these intermediates may act to buffer the reduced rates of glycogenesis from glucose. Consistent with the findings in *chapter 3* routine meal feeding late pregnant rats encourages greater glucose absorption by the liver and consequently is diverted to glycogen repletion. Compared with other short-term meal feeding regime studies (Pallardo and Williamson 1989), pregnancy accelerates the adaptation to food availability. The study by Pallardo and Williamson (1989) used 10 day non-pregnant meal fed rats to demonstrate the increase in lipogenic rates of the liver. However, they did not see changes in glycogen repletion rates which is evident during long-term meal feeding regimes, *see section 5.3.4.*. This could be due to the fact that these studies were not designed to evaluate the relative contributions of the direct and indirect method of glycogenesis. Although ^{13}C-glucose incorporation into hepatic glycogen was significantly higher in the 20 day pregnant RMF group it did not compare to the levels of incorporation seen in the 10 day pregnant RMF group. This group showed a greatly enhanced ability to incorporate glucose directly into glycogen, a response which cannot easily be explained. It must be noted however, that in the 10 day pregnant *ad libitum* group, rates of hepatic ^{13}C-glucose incorporation into glycogen were comparable to that found in the 20 day pregnant RMF group. Therefore initially, there are greater levels of direct glycogenesis during early gestation and the effects of routine meal feeding enhance the total level of incorporation into glycogen. As well as significant changes between the two nutritional regimes, early and late gestation also show definite

changes in hepatic glycaemic control when *ad libitum* and RMF groups are compared directly. These changes are despite the fact that plasma glucose concentrations are relatively constant in all groups, except the 20 day pregnant *ad libitum* group, see *table 20.*

It appears from the results in *chapter 3*, and those discussed above, that routine meal feeding dramatically alters maternal glycaemic control during pregnancy. More glucose is being utilised by maternal tissues, including the liver. This raises one important question concerning the nutritional status of the foetus(es). If more glucose is being phosphorylated by skeletal tissues as well as being assimilated as glycogen, does this compromise the development of the foetus(es) with respect to its glucose requirement. Litters from mothers placed on routine meal feeding regimes showed approximately 20% reduction in weights compared with normal pregnant pups immediately following birth. However, these pups grew into normal sized animals with no observable malformations.

This study illustrates the importance that particular feeding regimes have on glucose utilisation by the mother. Benefits could be gained by mothers who have a high risk of developing gestational diabetes or who are diabetic prior to pregnancy. Since pregnancy diverts glucose away from maternal tissues, mothers which already have a degree of tissue insulin resistance may be at greater risk of developing conditions such as eclampsia, which is recognised by acute increases in blood pressure and blood lipids, and the occurrence of intrauterine deaths. Although this study has shown

benefits to the mother in utilising glucose, the extent of the feeding regime is extremely severe. Further studies are required which would extend the periods of feeding to allow correct daily food consumptions to be achieved. If simply altering the frequency of feeding can influence the fate of glucose then this study could be modified to high risk mothers who are diabetic or are prone to acquiring diabetes *post partum*. The acquisition of these conditions could directly be related to the erratic consumption of food during a 24 hour period in the 20 day pregnant rat. Results not tabulated show that during the 3 h periods starting from when the light was switched off [10:00 in reverse light dark room] food consumption was 5.8 $\pm$ 0.6, 7.6 $\pm$ 0.7 and 3.7 $\pm$ 0.7 g at 13:00, 16:00 and 19:00, respectively, and between 19:00 and 10:00 total intake was 11.8 $\pm$ 0.7 g. These results demonstrate that food consumption occurs continually during the 24 h cycle and is not confined to specific feeding patterns. By confining food intake patterns to specified periods alterations in maternal glucose metabolism may provide long term benefits as gestation progresses.

CHAPTER 6.

Studies of hepatic gluconeogenesis using ^{31}P-NMR.

6.1.1. Introduction.

As mentioned in previous sections, gluconeogenesis plays a key role during starvation, maintaining glucose levels supplied to the brain. However, gluconeogenesis may have an aetiological role in certain disease states, such as non-insulin dependent diabetes mellitus (NIDDM). In NIDDM, gluconeogenesis may be a contributory factor to the characteristic post-absorptive hyperglycaemia found in these subjects. It may also be a significant factor during late pregnancy where there is an apparent insulin insensitivity by the mothers' peripheral tissues. Glucose turnover per kg increases during the course of gestation however, hypoglycaemia persists during late gestation. This would imply that any increased plasma glucose levels are for the benefit of the developing foetus(es) preferential to the mothers needs, *see section 1.7.*. Supplying the extra glucose demand required for the conceptus could be achieved by increased glycogenolysis and gluconeogenesis. However, pregnancy induces an accelerated starvation status which would cause accelerated glycogenolysis compared with non-pregnant subjects. This would greatly enhance the need for gluconeogenesis to operate in order to maintain sufficient glucose levels for both mother and conceptus. Unfortunately, the relative contributions of glycogenolysis and gluconeogenesis to any increase in hepatic glucose output is controversial and have not yet been established due to the lack of techniques

for measuring *in vivo* hepatic gluconeogenesis.

Most gluconeogenic studies to date have used conventional radioactive isotopic techniques which employ the ^{14}C labelled precursors of gluconeogenesis (primarily alanine and lactate). The major problem with this lies in the total quantitation of gluconeogenesis since the label could be exchanged with ^{12}C as it is synthesised to oxaloacetate prior to phosphoenolpyruvate production *see figure 1*. This would result in a loss of label via the Krebs cycle and labelling in other intermediates, such as glutamate (a gluconeogenic precursor), which would complicate results. Consoli *et al.* (1989) attempted to overcome the problem of substrate-cycling by dual isotope infusion of [6-^{3}H]-glucose and [2-^{14}C]-acetate. By examining the distribution of ^{14}C within the glucose molecule, the relative contributions of precursors from the Krebs cycle could be assessed since acetate is not a gluconeogenic precursor due to its direct entry into the cycle or biosynthesis into fatty acids and triglycerides. However, since acetate is metabolised primarily by muscle, rather than liver, total quantitation of the Krebs cycle precursors cannot accurately be established (Schumann, *et al.*, 1991).

The important protein-derived precursor, L-alanine, has been shown to increase gluconeogenic rates in the perfused liver of the rat following its conversion to pyruvate (Ross, *et al.*, 1967). The effect of L-alanine infusion has been investigated using *in vivo* hepatic ^{31}P-NMR (Dagnelie *et al.*, 1992). These studies showed maximal increases in the phosphomonoesters, reflected by the increase in 3-phosphoglycerate, and decreases in P_i *ie.* [PME]/[ATP] and [P_i]/[ATP] of 98% and 33% respectively. The study discussed in this thesis used ^{31}P-NMR to look at the

relative changes *in vivo* of the hepatic phosphorus spectrum in the rat as gluconeogenic flux was manipulated by infusion of alanine and glucagon (Changani *et al.*, 1994(b)). The aim was to characterise all the major changes seen in the various components of the phosphorus spectrum to assess the validity of the technique for estimating gluconeogenic rates in disease states. In order to fully interpret changes seen *in vivo*, it was necessary to conduct *in vitro* high resolution ^{31}P NMR spectroscopy on freeze-clamped liver extracts from separate bench experiments which mimicked the *in vivo* protocol. This provided information on the specific changes in metabolites (*eg.* 3PG, sugar phosphates, PEP, ATP, ADP, *etc.*) associated with the broad resonances of the *in vivo* phosphorus spectrum. In addition hepatic glucose output measurements were conducted on *in situ* perfused livers to correlate changes in gluconeogenic intermediates with glucose output. Potentially alanine/^{31}P-NMR could be used clinically as a method of assessing hepatic gluconeogenesis in patients with NIDDM.

6.1.2. Method of *in vivo* determination of gluconeogenesis by ^{31}P NMR.

6.1.2.1. Animals

Male Wistar rats (275-325 gm) were maintained at 20 ± 2°C on a 12 hour light/12 hour dark cycle (light off at 22:00) and fed on a chow diet consisting of 52% carbohydrate, 15% protein, 3% fat and 30% non-digestible residue. Rats were starved for a 12 hour period prior to experimentation. This had the effect of reducing

the hepatic glycogen content by 50% and hence promoting gluconeogenesis when supplied with a three carbon substrate such as lactate, pyruvate or alanine.

6.1.2.2. Cannulation of the jugular vein.

Cannulae were prepared as in *section 2.1.*. Following anaesthesia with sodium pentobarbital (60 mg/ml in dd.H_2O, the inferior jugular vein was cannulated as described in *section 2.1.*, however, the cannula remained external to the body cavity and hence an additional suture was used for anchorage. A midline abdominal incision was made to expose the liver and the coronary ligament severed to drop the liver away from the diaphragm. The cannula was connected to a 5 metre line containing either saline (0.9% NaCl solution) or a 1.099 mol/l stock solution of alanine (T865, The Boots Co. plc. Nottingham, U.K.). The line was attached to an infusion pump set at 0.5 ml/min in order to give a total infusion of either 2.8 mmol/kg alanine ± 250 μg/kg glucagon (HPLC purified Sigma - G 7774) or 5.6 mmol/kg alanine ± 250 μg/kg glucagon or 250 μg/kg glucagon or 1.5 ml of saline.

6.1.2.3. Spectroscopy methodology.

The rat was positioned in a 4.7 Tesla 33 cm diameter horizontal bore SISCO system magnet as previously discussed in *section 5.1.2.3.*. A single turn 1 cm diameter phosphorus tuned coil was used to acquire blocked spectra at 80.984 MHz. After tuning the phosphorus channel, the magnet was shimmed for greatest field

homogeneity. Phosphorus spectra were acquired using an acquisition time of 0.408s, a relaxation time of 5.0 s, a pulse width of 100μs and a spectral width of 8.0 kHz used to produce 20 array elements consisting of 64 averages, over a period of 115 mins.. After acquiring two base-line spectra, the infusion pump was started. Typically the experiment was run for a total of 60 minutes post-infusion. The spectra were referenced to the α-ATP resonance at -7.57 ppm

6.1.3. Method for *in vitro* extraction of liver for phosphorus NMR analysis.

6.1.3.1. Animal experimentation.

The experimental procedure was the same as that described in *section 6.1.2.* the only difference was that the animal was not placed in the magnet. The liver was freeze-clamped *in situ* at 25 minutes post-infusion of either saline, 5.8 mmol/l alanine, 5.8 mmol/l alanine and 250 μg/kg glucagon or 250 μg/kg glucagon. The liver was loosely tied with a length of cotton and held clear of the body cavity, small freeze clamps were pre-cooled in liquid nitrogen and positioned around the liver. As soon as the liver was clamped any connecting tissue around the clamp was quickly cut away and the liver placed in liquid nitrogen. Any tissue not in the clamps was chipped away leaving approximately 3-4 g of tissue in the clamps. This method of freeze-clamping limited the hypoxia of the liver. The tissues were stored in liquid nitrogen until the day of extraction.

6.2. Method of liver metabolite extraction.

6.2.1. Extraction and lyophilisation.

The liver tissue (2 g) was ground to a powder under liquid nitrogen. This was achieved by placing a pestle and mortar, containing liquid nitrogen, into a polystyrene ice-bucket containing a 2 cm depth of liquid nitrogen. The tissue was weighed into a pre-cooled glass scintillation vial and ice-cold 10% perchloric acid (5 ml) [PCA] added to de-proteinize the tissue. The powder was homogenised using a Tissue Homogeniser [Inter. Lab. App. Gmbh, Type X 1020; small probe; position 6), transferred to a plastic tube and centrifuged at 5000 rpm and 4°C for 15 minutes in a MSE Mistral 3L centrifuge. The supernatant was recovered and the pellet re-extracted with 2 ml of PCA. The pellet extract was briefly homogenised and centrifuged as above. The supernatant was pooled with that of the first extraction and neutralised to pH 7.0 - 7.5 using KOH and PCA. The perchlorate suspension was pelleted out at 5000 rpm at 4°C for 15 minutes. The supernatant was frozen at -70°C and lyophilised for 36 hours in a pre-weighed 100 ml beaker covered with perforated "parafilm". The dry weight of the total sample was assessed and then re-frozen until the day of analysis by NMR.

6.2.2. Preparation of sample for NMR analysis.

Total dry weight sample re-suspended in: 0.9 ml distilled water

0.6 ml D_2O

50 μl Phosphocreatine standard (67mM)

EDTA (100mM final concentration)

and neutralised to pH 7.40 - 7.50 using appropriate concentrations of KOH and PCA. Any insoluble material was centrifuged out at full speed in an Eppendorf centrifuge. The addition of EDTA was to chelate any ions which cause broadening of peaks such as Mn, Fe and Mg which is bound to 93-97% of total ATP and hence, shifts the resonance of the ATP molecule. The sample (0.7 ml) was transferred into a high quality NMR tube (Wilmad Glass Company 507-pp).

The sample was run on a Varian 500 MHz 11.7 Tesla machine at 202.315 MHz using the following parameters:

Acquisition time - 0.800 sec
Relaxation delay - 0.100 sec
Pulse width - 13.0 μsec
Spectral width - 10000.0 Hz
Decoupler continuously on
Waltz 16 modulated
Line broadening - 2.0 Hz
No. of averages - *ca.* 2000.

From each group one sample was run overnight with a relaxation delay of 20 s, this allowed quantification of other samples run at shorter relaxation delays which would be partially saturated (Bell *et al*, 1993). This speeded up the process of running numerous samples. The PCr resonance was referenced to 0.00 ppm and the spectrum

analysed using a computer based calculation (NMR1™).

6.3. Isolated perfused liver experiments

6.3.1. Perfusion apparatus

The perfusion set-up was similar to that used by Exton and Park (1967) with the modifications of Cohen *et al* (1973).

The perfusion apparatus consisted primarily of a perspex perfusate oxygenation drum designed to rotate at a fixed 60 revolutions per minute powered by an electric motor (Parvalux Electric Motors Ltd., Bournemouth, Dorset). Three stainless steel pipes contained within a sealed shaft were incorporated horizontally into the centre of the drum via the non-motor driven axle end. These tubes allowed oxygenated removal and deoxygenated perfusate disposal from the drum together with efficient perfusate oxygenation of up to 300 ml. The first tube was angled at 90° so as to draw oxygenated perfusate from the bottom of the drum, the second pipe transmitted venous perfusate back into the drum and the third, allowed access to the humidified gases. The deoxygenated perfusate disposal and oxygenation pipes were long enough to allow the perfusate to be smeared against the motor driven backplate increasing the surface area for oxygenation. A pressure regulated cylinder delivered the gas mixture (95% O_2 / 5% CO_2) into a glass humidifier connected to the respective stainless tube pipe of the rotating drum. Both the humidifier and perfusate drum were contained

within a purpose built perspex box with detachable lid. Perfusate was pumped around the circuit using a variable speed peristaltic pump (Watson Marlow type MHRE 22; Falmouth U.K.) via a silicone rubber tubing [(Portex 800/500/325) OD 8.00 mm ID 5.0 mm], the rest of the circuit was connected with polyethylene tubing [(Portex 800/010/180/800) OD 3.00 mm ID 2.45 mm]. Prior to entering the liver, the perfusate was filtered using 6 cm of transparent polyethylene tubing [(Portex 800/000/450) OD 9.52 mm ID 6.35 mm] containing a 1 cm plug of polymer-wool (Inter-Pet Ltd., Dorking, Surrey, U.K.). Various circuit connections were made using male-male luer connectors (R93, Avon Medicals Ltd., Redditch, Worst., U.K.), two 3-way disposable taps (Vygon, Ecouin, France.) and three types of glass connectors (Chemlab Instruments Ltd., Hornchurch, Essex, London) *ie.* F and h-shaped. From the filter tubing the perfusate entered into a debubbler (F-shaped glass connector) which was also connected to the manometer. The manometer consisted of a manometer chimney (Height 1 m, OD 15.0 mm, ID 13.0 mm) into which perfusate could be fed into the system and a length of polyethylene tubing [(Portex 800/000/180/800 (OD 3.0 mm ID 2.0 mm) the same height as the chimney. The pressure of the perfusion system gave a reading on the manometer as a perfusate level within the chimney, if a blockage occurred this would result in an increase in the height of the perfusate within the manometer providing an important indicator of arterial pressure. From the filter the perfusate entered into the 'h' shaped glass connector via the straight arm and exited from the curved end before entering the liver. The other straight end was capped with a rubber septum into which a needle thermocouple was inserted, this gave a digital temperature reading. The temperature of the perfusate was controlled by a fan-heater, electronically controlled to stabilise

the temperature at 37°C. To maintain the humidity of the box, to prevent drying out of the liver, swabs dipped in distilled water were placed within perfusion box. Incorporated into the tubing system were two 3-way taps, these allowed sampling at the venous end together with the quick adaption to a non-recirculatory system. One of the taps was immediate to the venous end and the other connected to the same peristaltic pump as above. It received pre-warmed perfusate (25°C) from a reservoir channelling it to the perfusate drum or could receive venous perfusate for re-oxygenation by the drum. By turning the taps simultaneously perfusate was either allowed to recirculate for oxygenation in the drum via the two taps or be discarded as waste via tap *a* (*figure 25*)

Figure 25 represents the complete plumbing of the perfusate system.

6.3.2. Preparation of the perfusate.

The perfusate used was a Krebs-Henseleit bicarbonate buffer (Krebs and Henseleit, 1932). This was made up in a concentrated format, *see table 21.* and autoclaved in aliquots of 80 ml in brown bottles. On the day of the experiment each aliquot was made up to 1000 ml after the addition of sodium hydrogen carbonate. The pH was adjusted to 7.4 - 7.5 if required.

Table 21. **Preparation of stock Krebs-Henseleit buffer.**

Chemical.	gm/l.	For 1 l prep.
NaCl	174.5	40 ml
KH_2PO_4	16.4	10 ml
$MgSO_4.7H_2O$	29.6	10 ml
KCl	35.7	10 ml
$CaCl_2.2H_2O$	27.0	9.4 ml

Sodium hydrogen bicarbonate was added on to the day of perfusion [2.1 g/l].

6.3.3. Cannulation procedure of the isolated perfused liver.

6.3.3.1. Preparation of perfusion circuit.

The perfusion circuit was washed thoroughly for 15 minutes with distilled water by placing the system in a non-recirculatory mode *see figure 25*. Following this, Krebs-Henseleit bicarbonate buffer was washed through the system. A volume of 300 ml was pumped directly from the perfusate reservoir into the circuit and allowed to equilibrate at 37°C while constantly being pumped in a circulatory fashion to allow adequate oxygenation by the humidified gases (95% 0_2:5% CO_2). It was imperative that time was taken to ensure no air bubbles remained in the arterial flow.

6.3.3.2. Cannulation.

The animals used were male Wistar rats (275-325 gm) maintained at 20°C ± 2 on a 12 hour light/12 hour dark cycle and fed on a standard chow diet consisting of 52% carbohydrate, 15% protein, 3% fat and 30% non-digestible residue. Rats were starved for a 12-20 hour period prior to experimentation, this has the effect of reducing the hepatic glycogen content, hence promoting gluconeogenesis and glycogen synthesis when supplied with the correct substrate.

The rat was anaesthetised with sodium pentobarbital (60 mg/ml/kg in distilled water) and its limbs taped to the perspex tray. A transverse abdominal incision was made exposing the liver and guts. The hepatic portal vein (HPV) was located and two loose sutures placed 1 cm apart, another loose suture was placed above the right renal vein of the inferior vena cava (IVC). Approximately 100 units of heparin was injected into the IVC just above the renal vein, via a fat pad, this would reduce the risk of blood clotting during the cannulation procedure. The peristaltic pump was turned off and the venous return line blocked by turning tap *c* (*figure 25*) in the appropriate direction, the circuit was then broken and two cannulae fixed into position, the HPV cannula was placed bevel up and the IVC cannula bevel down. The lower HPV suture was tightened and the peristaltic pump started at a very slow flow rate. Using the tied suture the vein was raised and a cut made using a pair of micro surgical scissors and the cannula eased approximately 5 mm into the vein. The cannula was tightly secured using the top suture and the IVC immediately severed below the IVC suture to prevent pressure build up in the liver by allowing a route for

perfusate afflux. The peristaltic pump was increased to the optimum rate according to 10 ml/100g rat weight. The liver was now being artificially perfused and hence was isolated from the rat. Ischaemia and anoxia of the liver was kept to a minimum by performing the above cannulation procedure within 30 seconds. The chest cavity was completely opened to expose the heart; the venous cannula was inserted directly into the right atrium of the heart and pushed down 1 cm into the IVC. Tap *c* (*figure 25*) was turned to allow venous flow and the IVC tied resulting in a completely closed system where the venous return was routed back into the oxygenation drum. A good preparation was indicated by an even brown colouration, any blotches in colouration suggested uneven perfusion.

The perfusion box lid was placed in position and the system allowed to equilibrate for 15 - 20 minutes after which a venous sample (4 ml) was added to 10% perchloric acid (1 ml) and stored at -70°C for future glucose analysis, see *section 2.5.*. Addition of alanine and glucagon was via the gas line followed by immediately turning taps *a* and *b* (*figure 25*) to allow the perfusate reservoir to drain into the oxygenating drum and the venous return to go to waste or be sampled. The perfusate reservoir was warmed to 25°C and contained the correct concentration of l-alanine (T 865, 10% solution, The Boots Co., plc., Nottingham, U.K.) and/or glucagon prior to cannulation. Samples were taken every 10 minutes after the introduction of the substrates for a total of 60 minutes, at the same time the flow rates were also measured. Concentrations of alanine and glucagon used are shown in *Table 22.*

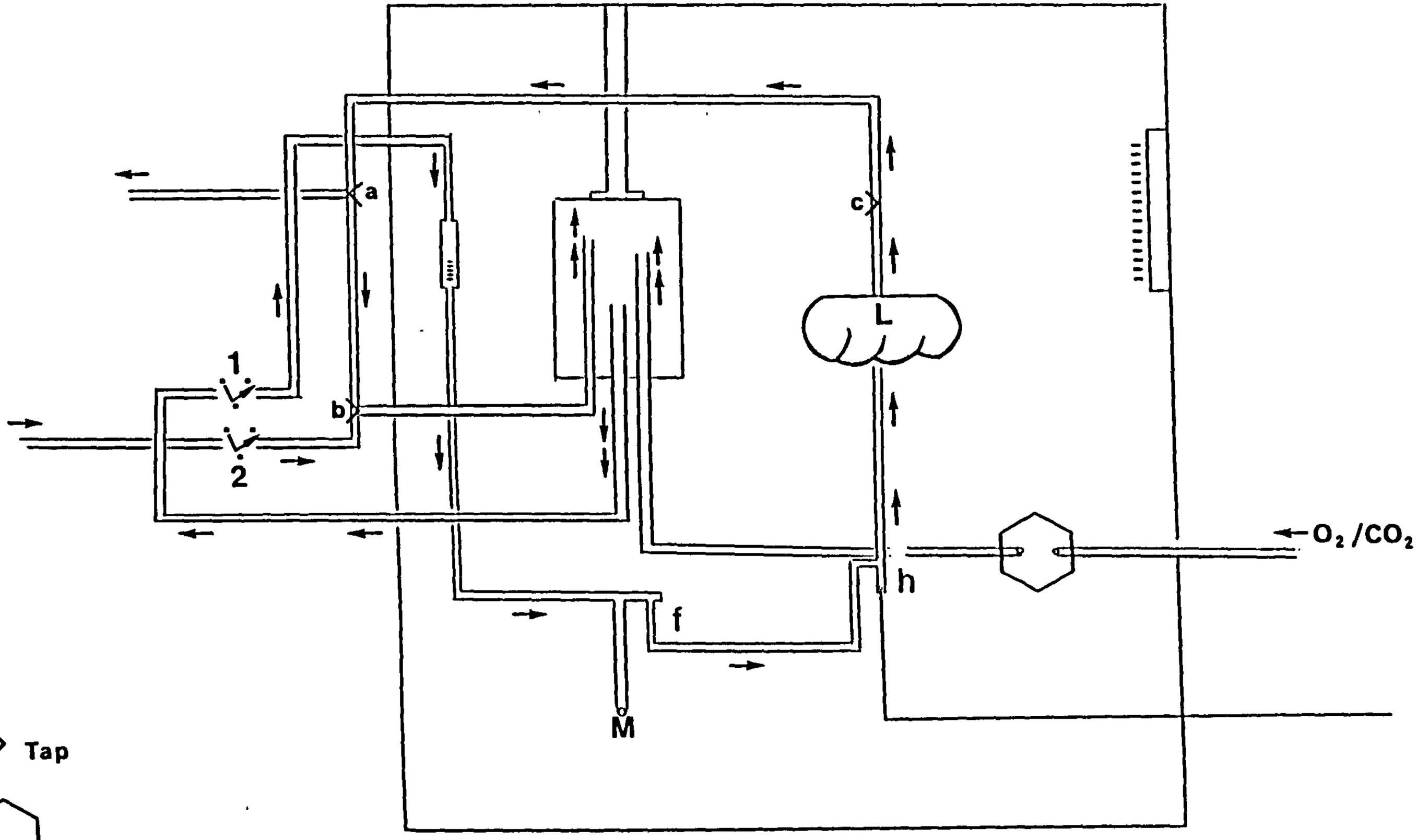

> Tap

Humidifier

Pump

M Manometer

L Liver

Figure 25. Perfusion box setup.

Table 22. **Summary of gluconeogenic experiments.**

1.	2.8 mmol/l L-Alanine [1.122M stock solution]
2.	5.6 mmol/l L-Alanine
3.	5.6 mmol/l L-Alanine + 250 μg Glucagon [200 μg/ml]
4.	250 μg Glucagon.
5.	Saline

6.4. Quantification of ^{31}P liver spectra.

The analysis of the phosphorus spectra obtained from these studies proved to be the most difficult aspect of the project. However, a method was decided upon which gave consistently precise results and described the obvious changes observed by eye. As briefly mentioned in *section 4.5.2.*, the broad co-resonance of phospholipid components of plasma membranes, and slowly mobile proteins, produces a large "hump" between 30 and -30 ppm, coinciding with the metabolites of interest. This makes absolute integration of the resonant peaks far more difficult since a method must be devised to eliminate the contribution of the hump to the metabolite of interest. Several computer programs exist which are supposedly capable of removing the phospholipid hump, hence producing a flat base-line from which integration of the metabolites can be achieved. This was the initial method of choice for processing the huge amount of data shown in this chapter. Unfortunately, the program used

(NMR1™) did not consistently remove the same phospholipid component from each spectra and invariably removed large areas associated with the PME and ß-ATP regions. This was very evident when significant changes were being seen in these two components. Furthermore, all 700 spectra had to be manually phased since the auto-phasing feature of the program was inconsistent. As a result the calculated changes showed no correlation in the pre-infusion values between the groups and did not depict the observed changes; in fact the graphs were very random scatter diagrams with unacceptably large standard errors. The problems associated with the quantitation of the spectra obtained are at present being critically analysed. However, a rigorous solution is not achievable in the time scale for completion of this thesis.

In order to assess the changes in the groups studied a new method was employed which gave relative values of change rather than absolute changes of the metabolites. The method involved obtaining the peak heights of the five observed metabolites measured from the spectral baseline, as illustrated in *fig. 25a* (PME, P_i, gamma ATP, alpha ATP and beta ATP) together with the sum of these peak heights. The component peak heights were divided by the sum of all the peak heights (total phosphorus peak height). The total phosphorus peak height within one experiment was found not to change and hence was regarded as a good standard to be employed for all experiments, allowing direct comparisons to be made for the relative changes in peak heights of the metabolites. All values are therefore expressed relative to the total phosphorus peak height and showed extremely high degrees of precision within the groups. The relative peak height changes are expressed with a component of phospholipid hence changes in PME are represented as PME_{PL}, the same is true for

Pi and ATP (*ie*. Pi_{PL} and ATP_{PL}) It must however be emphasised that the percentage changes quoted are *not* representative of the absolute metabolite changes due to the substantial contribution of the phospholipid hump to each of the metabolites. Depending on the position of the metabolite a different peak height will be observed even though, for argument sake, the heights without the phospholipid hump contribution may be the same. From *diagram 25a* it can be seen that any metabolite near -15 ppm will always have a lower relative peak height to those at around 0 ppm due to the shape of the hump. It must also be noted that the total phosphorus line height is not a true representation of the total phosphorus signal since different metabolite resonances will have different line widths and a narrow peak will contribute more to the total phosphorus signal compared with a broader peak of equal area. All calculations are therefore based on the measurements shown in *Figure 25a* where each metabolite is represented by the following equation:

$$\textbf{Peak height ratio} = \frac{(A + PL)}{Pi_{(total)}}$$

where:

A = metabolite peak height

PL = phospholipid height at frequency of ***A***

$\mathbf{Pi_{(total)}}$ = sum of all ***A*** heights including **PL** contribution.

Figure 25a Method of ^{31}P hepatic quantitation.

A = Metabolite peak height.

PL = Phospholipid peak height

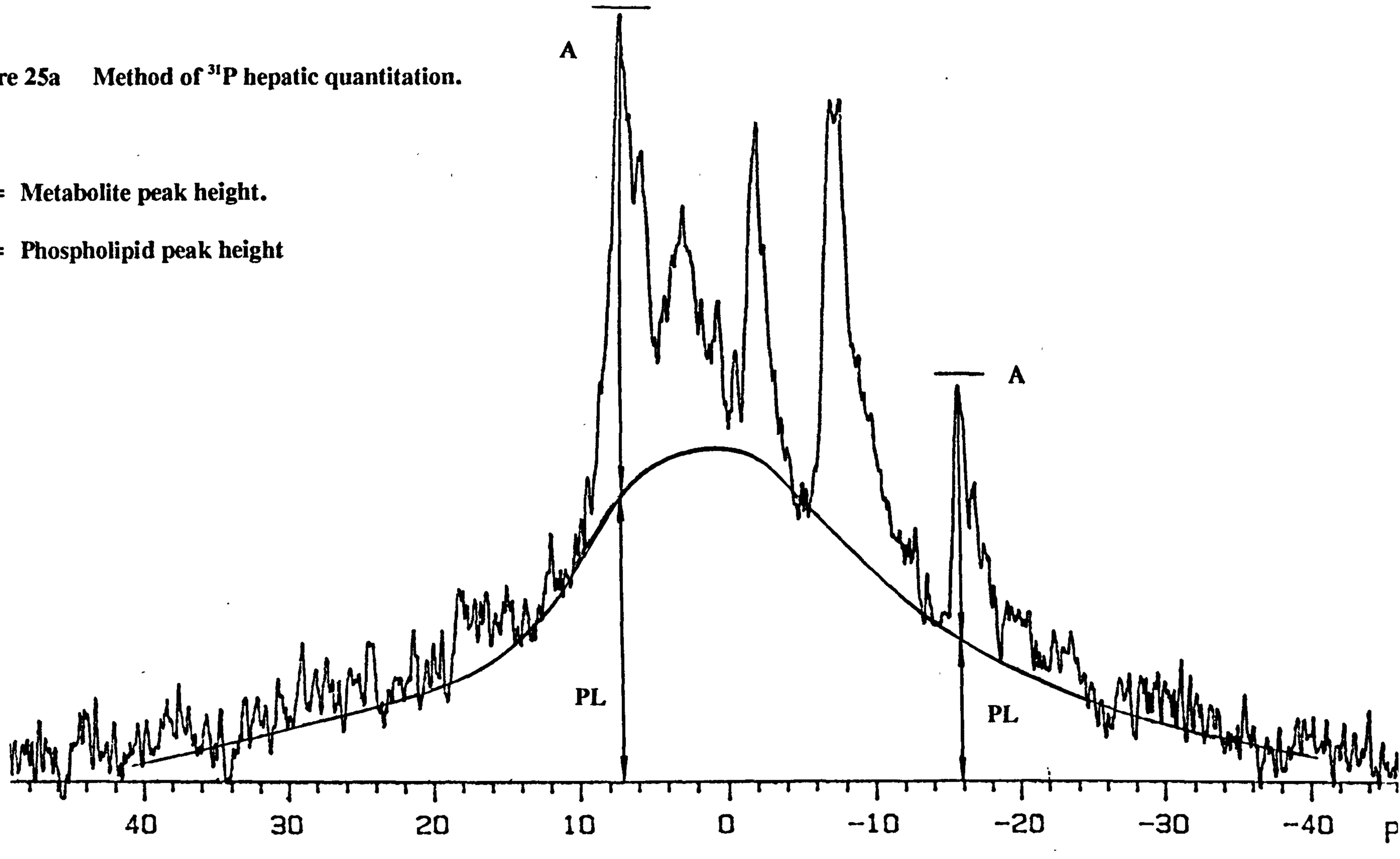

N.B. The curve drawn beneath the spectrum is a *representation* of the phospholipid component and is not meant to be an accurate depiction of the actual shape of the phospholipid "hump". For calculation purposes all metabolite heights (*A* + PL) were added to give the value of $Pi_{(total)}$. The above spectrum shows a resolved contribution from the PDE which was not characteristic of all spectra.

It has also been assumed that the phospholipid component does not change during the course of the experiment. This assumption would be made even if absolute integrals could be obtained and bearing in mind the relatively short time period of the experiments, this seems a relatively valid assumption since it is unlikely that phospholipid and protein components would significantly alter. Verification of this was achieved by obtaining the integral of the total spectrum after applying a line broadening component of 1000 Hz, this resulted in no net change in the integral over the period of the experiment in all of the groups.

A study by Cox *et al.* (1992) used similar methods to quantify the changes seen in patients with liver disease, from spectra with a rolling base-line. Two methods were employed, the first removed a base-line component by joining straight lines between the extremities of the line-width which made up the metabolite resonance then integrating the remaining area. The second was to integrate everything under the metabolite resonance including the base-line contribution, this was thought to give an over-estimation of changes whereas, the first method produced an under-estimation. Therefore an average of the two different base-line measurements was calculated. Measurements were standardised with the ß-ATP resonance which was assumed to remain constant.

6.5. Statistics.

Statistical significance differences between means was assessed by Student's paired t test. All results are given as means $\pm$ SEM for n=6 rats unless otherwise stated.

6.6. Results.

The tables accompanying these results represent the actual mean figures obtained in the various infusion groups. Statistically significant differences are between the pre-infusion (time = 0 in tables/time = -5.77 min on graphs) mean value and the corresponding post-infusion (infusion during second time = 0 in tables/ time = 0 on graphs) mean value, within the group. From *tables 23* to *27*, there were no significant differences in the pre-infusion values between each of the six groups studied, this eliminated the need to assess the relative changes within each group. This fact verified the accuracy in depicting the results on the basis of total phosphorus relativity, since pre-infusion ratios in any of the groups should be similar for the particular resonance considered, due to animals being age-matched and metabolically equivalent. Typical *in vivo* spectral changes are shown in *figure 26*. Differences can quite clearly be seen prior to and following infusion of 5.6 mmol/kg alanine in the PME, P_i and the three resonances of ATP.

6.6.1. Changes in hepatic phosphomonoesters plus underlying phospholipid during alanine infusion in the rat.

Specific values have been tabulated in *table 23* and comparisons have been made in *figures 27 - 31*. From *figure 27* it is shown that saline has no net effect on the peak height ratio of PME_{PL}, however, infusion of glucagon alone does produce a slight increase in PME_{PL}, which becomes significant approximately 30 min post-infusion ($P<0.05$). This slight increase is due to the stimulative effect of glucagon

on gluconeogenesis, such that amino acids (especially alanine and glutamine), lactate and glycerol, primarily from extrahepatic tissues, are converted to glucose. The rate of increase in PME_{PL}, representing gluconeogenic intermediates, is relatively slow probably due to one or two factors. The first is the physiological condition of the rat, which had undergone 12 h of starvation, this would be insufficient to deplete all the hepatic glycogen stores and hence, blood glucose levels can be maintained *via* glycogenolysis. This may suggest that glucagon secretion is secondary to the initiation of gluconeogenesis. Secondly, the rate of gluconeogenesis will depend, amongst other factors, on substrate supply reflecting the degree of starvation.

Figure 28 represents the comparison between infusing 2.8 mmol/kg alanine with or without glucagon. The graph shows a net increase in the PME_{PL} level within these two groups. On first inspection it appears that the group with added glucagon remains relatively low until 20 min post-infusion, after which an enhanced increase over and above the group infused with 2.8 mmol/kg alanine occurs. Infusion of alanine alone appears to have an almost immediate effect, seen within the first 5 min after infusion. *Figure 28* shows quite clearly the net effect of alanine infusion, with glucagon administration producing the greater effects. However, the data must be looked at in more detail with the standard errors in mind. Taking this into consideration, no significance was seen in the 2.8 mmol/kg alanine infused group until 40 min post-infusion, where a transient increase was observed ($P<0.05$) after which, pre-infusion values were reinstated. Upon infusion of 2.8 mmol/kg alanine plus glucagon, increases were seen at approximately 30 min, with maximal increases of 13.1% at 40 min post infusion ($P<0.02$). Following this, the PME_{PL} decreased

back to pre-infusion levels by 50 min, presumably due to the absence of further substrate for hepatic gluconeogenesis.

Increasing the alanine bolus dose to 5.6 mmol/kg produced a greater change in the PME_{PL} region of the phosphorus spectrum compared with the above infusions. Significant increases to the pre-infusion status were seen approximately 10 min after administration of alanine of 6.8% ($P<0.02$), this increased further to a maximum of 20.8% ($P<0.01$) at 35 min, with a maximal significance at 30 min ($P<0.001$). Compared with infusion of 2.8 mmol/kg alanine, where maximal increases were seen at 40 min, these results represent a further increase of 12.7% ($P<0.02$). Comparison of the two groups suggest that maximal increases occur at approximately the same time point after infusion, with the 5.6 mmol/kg group producing the highest increases of PME_{PL} at 35 min, as opposed to 40 min in the 2.8 mmol/kg group. From *figure 29* significance between the two groups can be better appreciated. The two groups seem to follow the same upward trend up to 10 min post-infusion, after which the 5.6 mmol/kg group dramatically increases to a maximum at approximately 35 min, at which point no further increases are achieved. However, the net maximal increase remained high until approximately 50-60 min. At this time point, the PME_{PL} level declines at a fairly rapid rate towards the pre-infusion value. If glucagon is included with the bolus of 5.6 mmol/kg alanine, fairly similar results are obtained, *see figure 30.* As with infusing alanine on its own, the rate of increase in PME_{PL}, with the added glucagon, seems to occur at the same rate; both plots can be seen to follow the same linear gradient as one another. One of the main differences between the two groups appears to be the enhancement of the PME_{PL} level, even at 75 min post-

infusion. Whereas, the alanine group shows a decline in PME_{PL} levels at 50 min, the glucagon group shows a far more gradual decline towards the pre-infusion values, starting at 55 min. Compared with pre-infusion values, PME_{PL} levels remain at a significantly high level even 75 min post infusion (+18.7%, $P<0.001$). Ignoring the time point at 63.45 min, which does not follow the plateau trend of the graph and undoubtedly is spurious, the maximal increases in the PME_{PL} region are found at 30 min post-infusion and remain at this level for a further 30 min, after which a slow decline is observed. The maximal value is 25.6% higher than pre-infusion values ($P<0.001$) but this is not significantly higher than the 5.6 mmol/kg group. In general there was a reduced recovery rate of PME_{PL} levels compared with the group without glucagon.

Figure 26. Typical *in vivo* rat liver ^{31}P spectra.

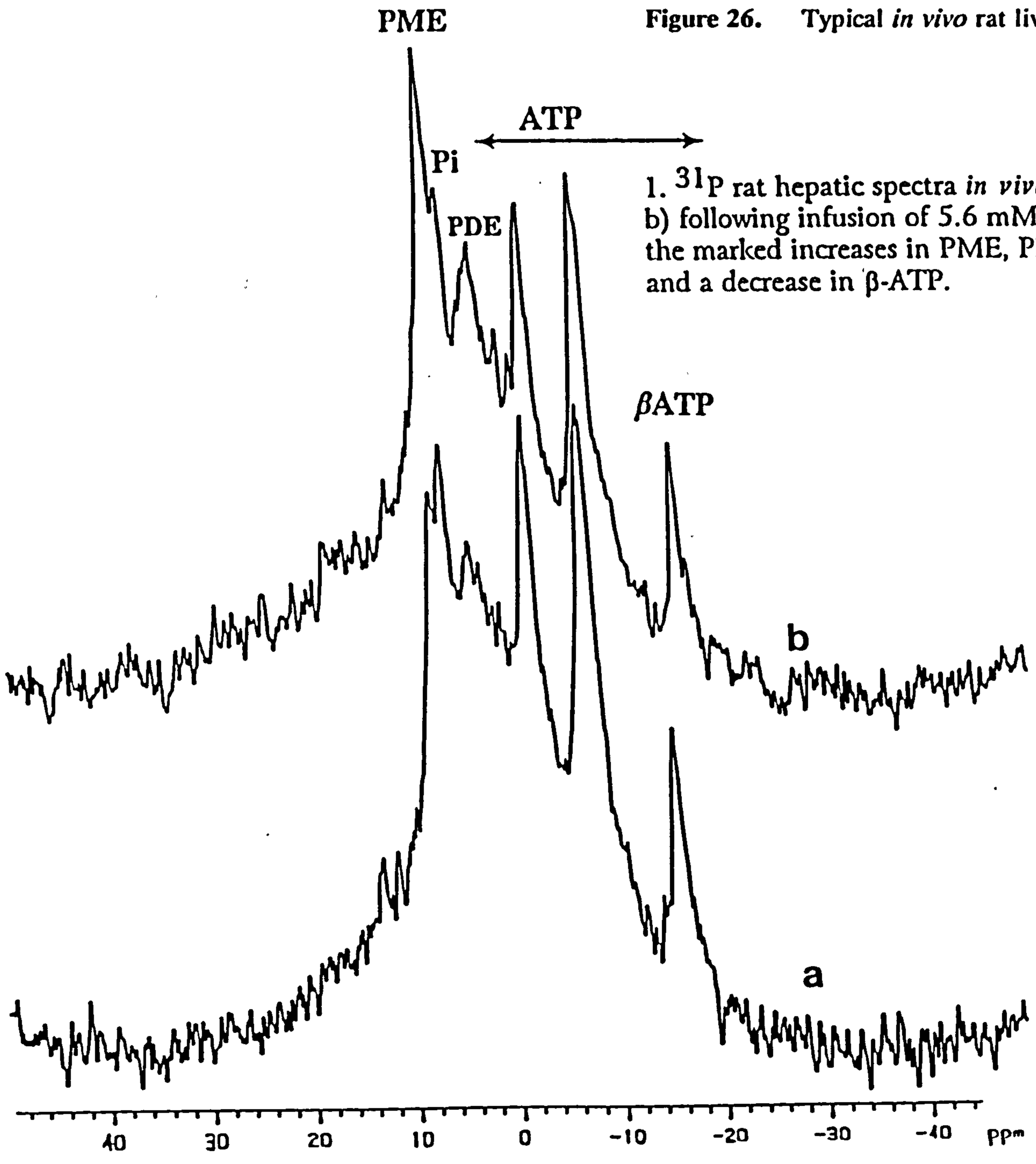

1. ^{31}P rat hepatic spectra *in vivo* : a) prior to and b) following infusion of 5.6 mM/kg alanine. Note the marked increases in PME, Pi and PDE resonances, and a decrease in β-ATP.

Table 23. ***Changes in hepatic phosphomonoesters plus underlying phospholipid during alanine infusions.***

Time (mins.)	Saline n=6	Glucagon n=5	2.8 mmol/kg Ala n=6	2.8mmol/kg Ala + Gln n=5	5.6mmol/kg Ala n=6	5.6mM Ala + Gln n=6
0.00	17.34 ± 0.55	17.33 ± 0.19	17.02 ± 0.32	16 .83 ± 0.48	16.81 ± 0.36	16.39 ± 0.35
0.00	17.02 ± 0.58	17.49 ± 0.11	16.61 ± 0.35	16.80 ± 0.52	17.11 ± 0.32	16.35 ± 0.45
5.77	17.01 ± 0.58	17.55 ± 0.14	17.47 ± 0.32	17.03 ± 0.57	17.54 ± 0.22	17.27 ± 0.50
11.54	16.74 ± 0.68	17.20 ± 0.29	17.77 ± 0.29	16.92 ± 0.42	17.96 ± 0.16$^{\#\#\#}$	17.23 ± 0.41
17.31	17.18 ± 0.56	17.64 ± 0.16	17.65 ± 0.23	17.45 ± 0.25	18.10 ± 0.15$^{\#\#\#\#}$	17.79 ± 0.57$^{\#}$
23.07	16.83 ± 0.68	17.89 ± 0.32	17.63 ± 0.15	17.84 ± 0.35	19.71 ± 0.65$^{\#\#\#\#}$	18.39 ± 0.52$^{\#\#\#\#}$
28.84	16.79 ± 0.71	17.99 ± 0.25$^{\#\#}$	17.49 ± 0.32	18.19 ± 0.42$^{\#}$	19.27 ± 0.27$^{\#\#\#\#\#}$	20.24 ± 0.98$^{\#\#\#\#}$
34.61	16.74 ± 0.67	18.08 ± 0.26$^{\#\#}$	17.89 ± 0.23$^{\#}$	18.86 ± 0.61$^{\#\#}$	20.30 ± 0.89$^{\#\#\#\#}$	19.79 ± 0.48$^{\#\#\#\#\#}$
40.3	17.04 ± 0.56	17.76 ± 0.28	18.01 ± 0.24$^{\#\#}$	19.03 ± 0.55$^{\#\#\#}$	19.48 ± 0.33$^{\#\#\#\#\#}$	20.28 ± 0.68$^{\#\#\#\#\#}$
46.15	17.04 ± 0.56	17.66 ± 0.28	17.85 ± 0.42	18.72 ± 0.76$^{\#}$	20.15 ± 0.85$^{\#\#\#\#}$	20.59 ± 0.89$^{\#\#\#\#}$
51.92	16.95 ± 0.62	18.03 ± 0.18$^{\#\#}$	18.06 ± 0.35$^{\#}$	18.52 ± 1.04	19.77 ± 0.84$^{\#\#\#\#}$	20.58 ± 0.84$^{\#\#\#\#\#}$
57.69	17.14 ± 0.51	17.71 ± 0.16	17.89 ± 0.48	18.35 ± 1.07	19.69 ± 0.82$^{\#\#\#\#}$	20.00 ± 0.79$^{\#\#\#\#}$
63.45	17.11 ± 0.70	17.93 ± 0.29	17.53 ± 0.57	18.20 ± 1.35	19.14 ± 0.81$^{\#\#}$	21.20 ± 0.51$^{\#\#\#\#\#}$
69.22	17.30 ± 0.59	17.80 ± 0.27	17.56 ± 0.43	18.28 ± 1.23	18.16 ± 0.34$^{\#\#}$	19.33 ± 0.60$^{\#\#\#\#}$
74.99				18.52 ± 1.21	18.35 ± 0.45$^{\#}$	19.46 ± 0.62$^{\#\#\#\#}$

Statistically significant differences to pre-infusion levels are indicated by $^{\#}P<0.1$; $^{\#\#}P<0.05$; $^{\#\#\#}P<0.02$; $^{\#\#\#\#}P<0.01$; $^{\#\#\#\#\#}P<0.001$. Infused during third time point. All values are arbitrary units relative to total ^{31}P signal. Abbreviations: Ala = alanine; Gln = 75 μg Glucagon.

Changes in PME plus underlying phospholipid.

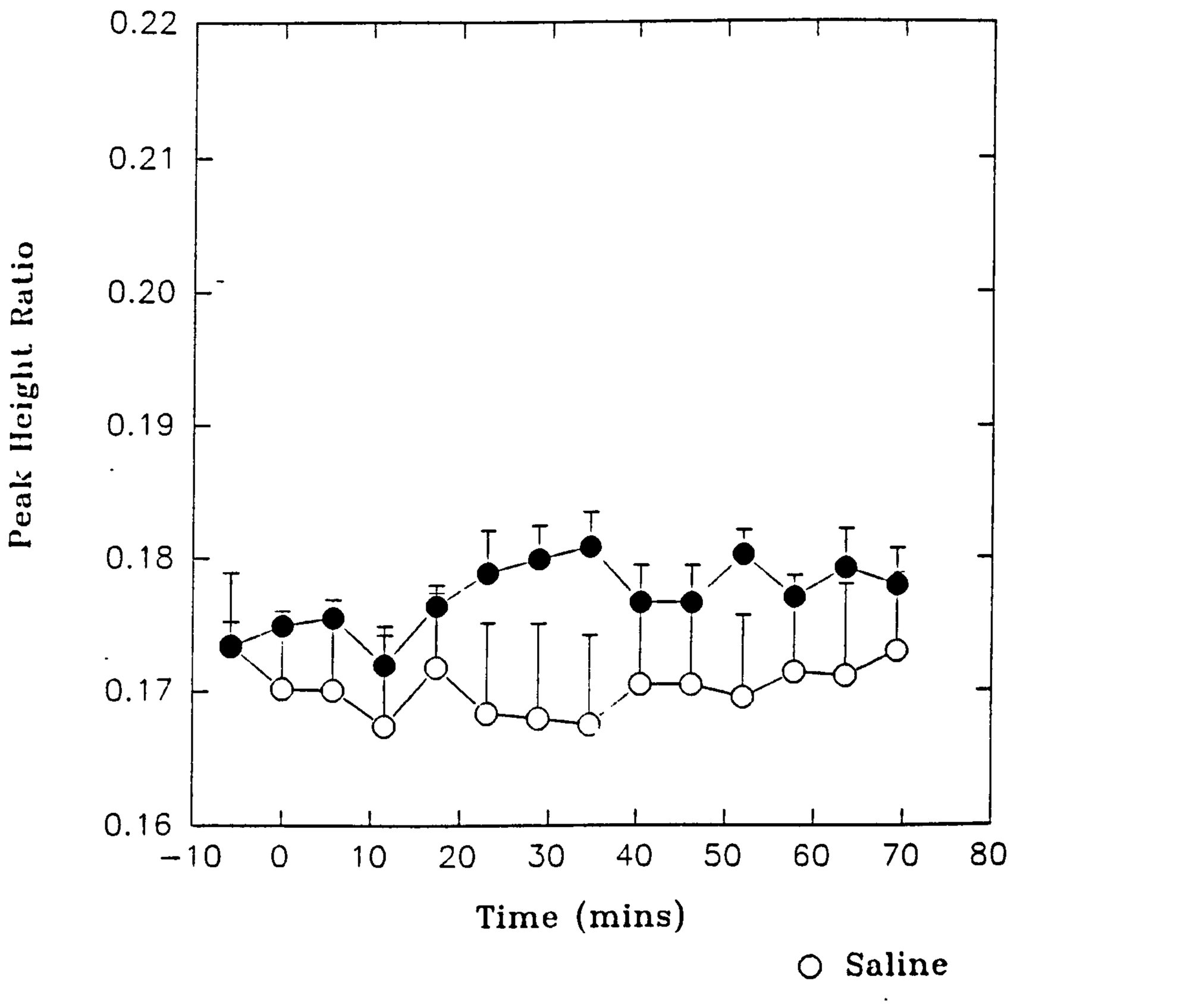

Figure 27.

Changes in PME plus underlying phospholipid.

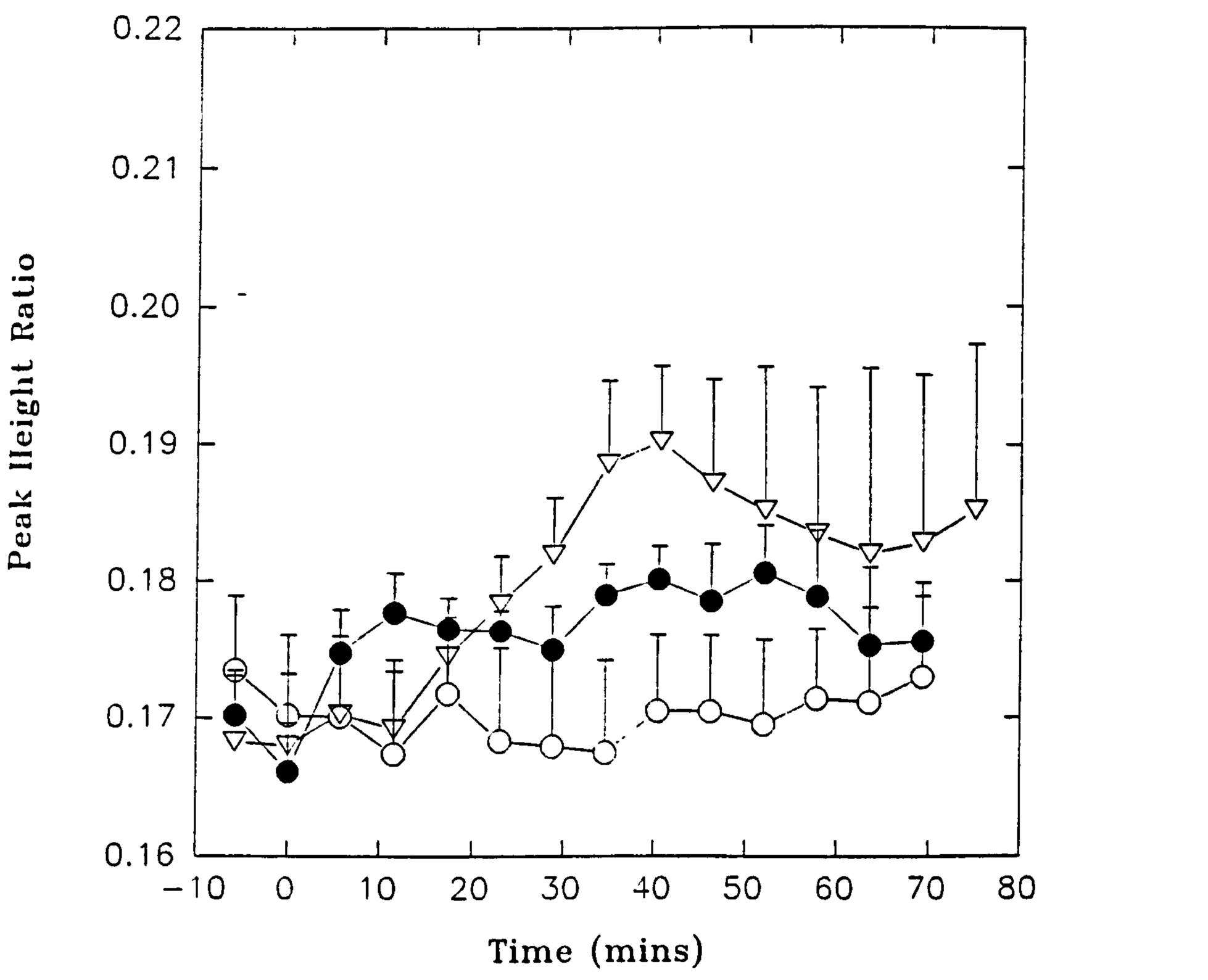

Figure 28.

Changes in PME plus underlying phospholipid.

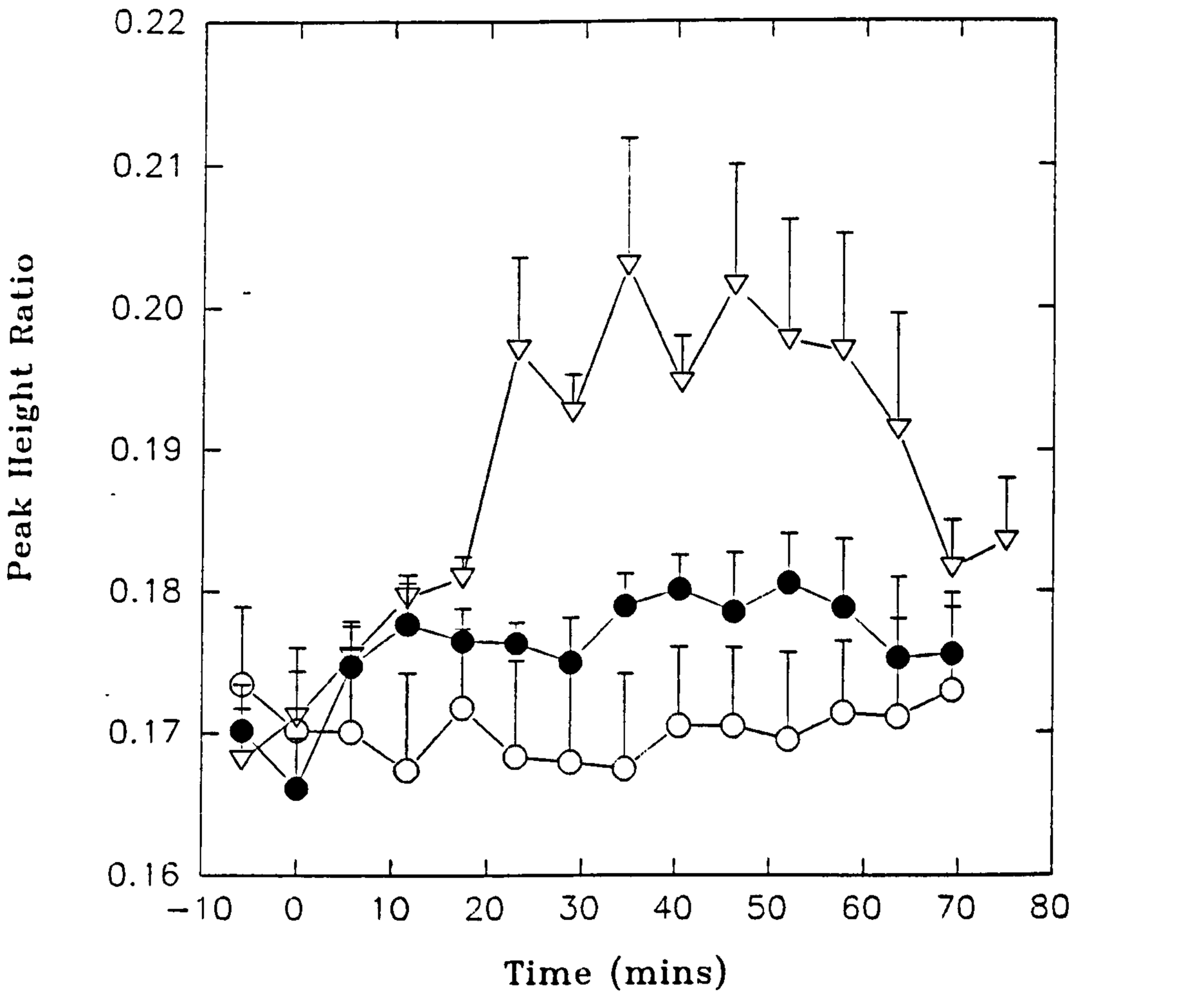

Figure 29.

Changes in PME plus underlying phospholipid.

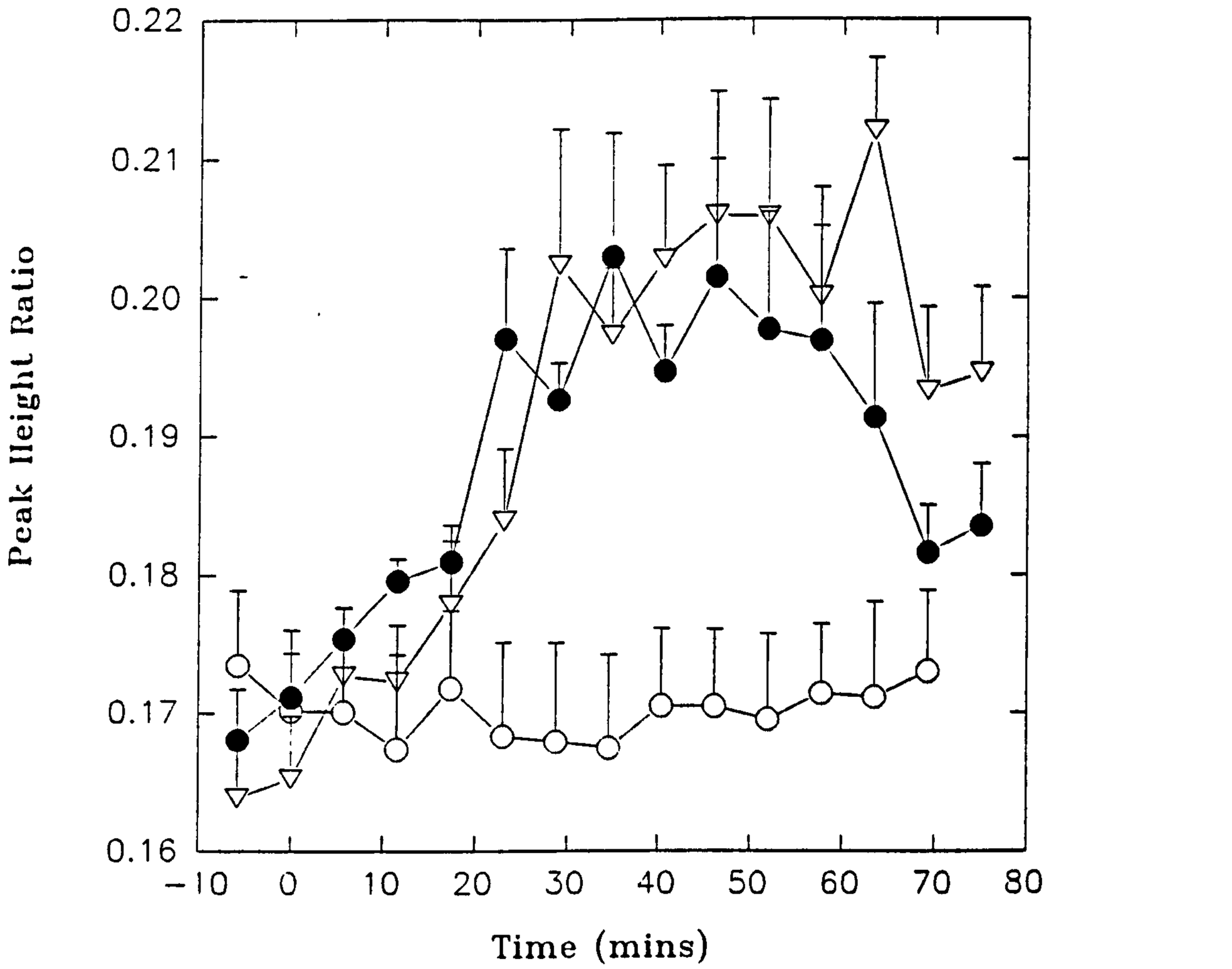

Figure 30.

Changes in PME plus underlying phospholipid.

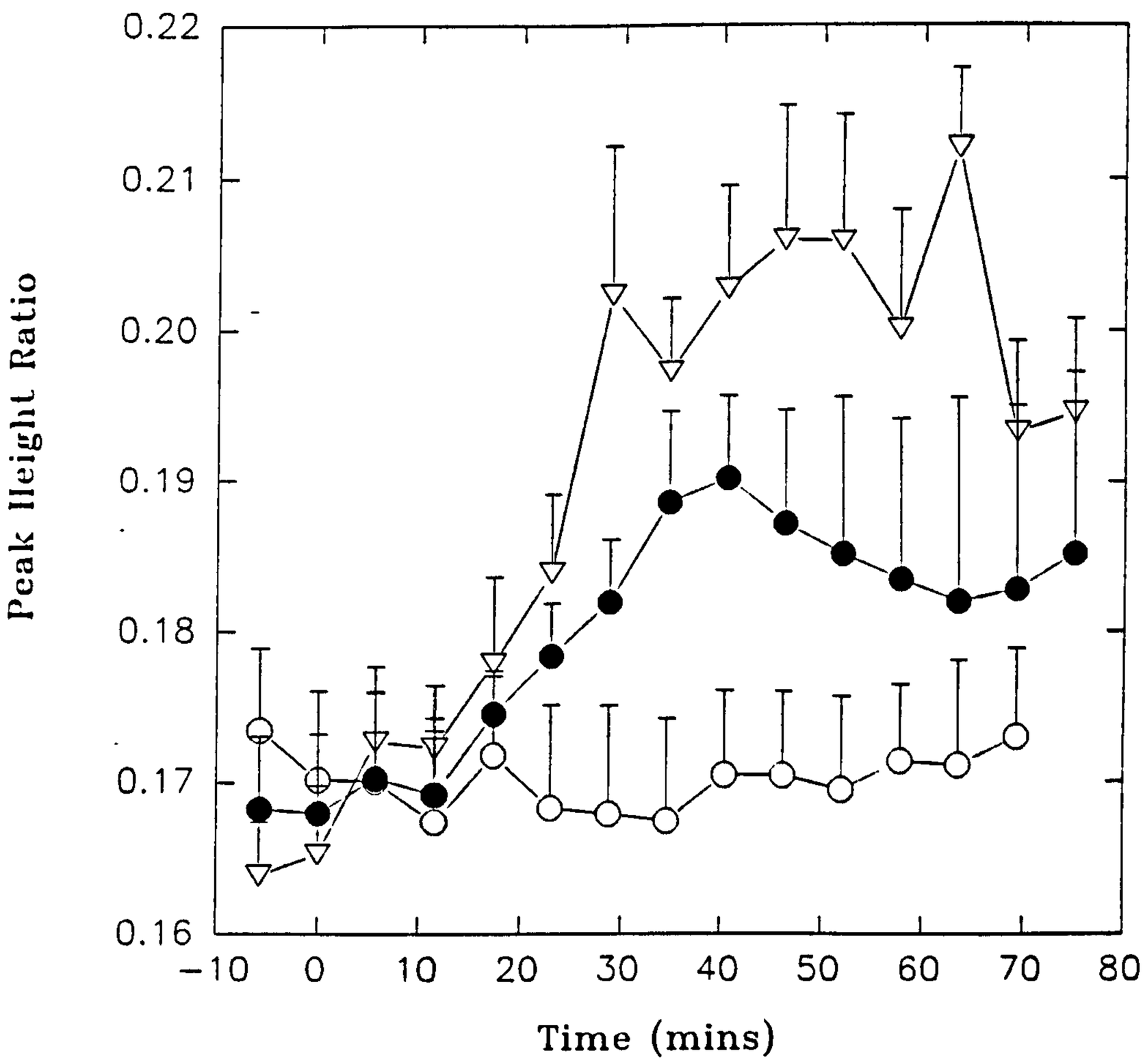

Figure 31.

○ Saline

● 2.8mmol/kg Ala
+250μg/kg Glucagon

▽ 5.6mmol/kg Ala
+250μg/kg Glucagon

6.6.2. Changes in hepatic phosphodiesters during alanine infusion in the rat.

Assigning the phosphodiester resonance proved to be very difficult due to the apparent variability of the chemical shift. This is to be expected for several reasons the first being the contribution of phosphoenolpyruvate, glycerophosphorylcholine (GPC) and glycerophosphorylethanolamine (GPE) occurring at around the same chemical shift, the chemical shift difference being approximately 1.5 ppm. However, more importantly is the positioning and intensity of the PDE region with respect to the *in vivo* liver spectra. As is discussed in *section 6.1.1.*, the contribution of membrane phospholipids to the phosphorus spectrum is extremely large, extending over 50 ppm. This phosphorus component produces a very broad hump which can be visualised by applying an exponential multiplication corresponding to a line broadening of 1000 Hz. This hump by virtue of its size, seems to interfere with the PDE region, varying its intensity quite dramatically, as well as producing contributions from mobile phospholipids at the lower field strength. This is not a problem *in vitro* as the phospholipid components are removed with the deproteinised phase during extraction procedures and field strengths are higher. Another possibility for the lack of specificity of the PDE resonance could be due to the relative long relaxation times of GPC and GPE (>4s), causing a certain degree of saturation, however I do not feel that this was the major contributor to the problems of assessing the PDE region *in vivo*.

6.6.3. Changes in hepatic P_i plus underlying phospholipid during alanine infusion in the rat.

Specific values have been tabulated in *table 24* and comparisons have been made in *figures 32 - 36*. *Figure 32* shows the effects of infusing either saline or glucagon, these results suggest, together with the values in *table 24*, that no substantial changes occur in hepatic inorganic phosphate$_{PL}$ (Pi_{PL}) From the graph there may be a slight increase in Pi_{PL} levels approximately 25 min post glucagon infusion, which corresponds to the slight increase seen in the PME_{PL} region. At 40 min post-infusion, the Pi_{PL} level drops back down to its initial level, this again corresponds to the response by the PME_{PL}. There was no significance between the values attained and the pre-infusion values.

During the first 10 minutes of infusion with alanine at 2.8 mmol/kg, a reduction in Pi_{PL} was observed, after which, levels increased by 4% ($P<0.02$) before returning to pre-infusion values, *see figure 33* and *table 24*. After 60 minutes Pi_{PL} levels returned to pre-infusion levels. A similar response was seen in the group with added glucagon, where the P_i increased by a maximal 8.8% at 25 min post-infusion. After 60 minutes the Pi_{PL} had returned to pre-infusion levels.

From *figure 34*, it can be seen that increasing the alanine dose to 5.6 mmol/kg, once again, showed an initial decrease in Pi_{PL} levels in the first 10 min which became significantly reduced by 5% ($P<0.02$). This was followed by a linear increase in levels, to a maximum of 14.1% above pre-infusion levels, at 35 min. At this point

a plateau was reached until approximately 55 min post-infusion, where the Pi_{PL} returned to normal levels. When glucagon was infused together with the 5.6 mmol/kg alanine an identical response was achieved with the same linear increases until approximately 30 min post-infusion, at this point the Pi_{PL} continued to rise to a level 28.8% ($P<0.01$) higher than the pre-infusion Pi_{PL} level at 40 minutes. At this point the 5.6 mmol/kg plus glucagon group was at a level 19.4% ($P<0.1$) higher than the corresponding time point without glucagon administration. Adding glucagon to the higher alanine concentration prevented hepatic Pi_{PL} from returning to its original steady state. From *figure 35* it can be seen that the Pi_{PL} begins to return to its pre-infusion levels at approximately 65 min, but even after a period of 75 min levels remain 16% above the pre-infusion value. Whereas the 5.6 mmol/kg group returned to its steady state at 65 min, the glucagon administered group remained 27.4% higher ($P<0.02$). If these results are compared to the equivalent changes in the PME_{PL}, *see figure 30*, it should be noted that the rate at which the PME_{PL} declined after infusion was similar in groups infused with 5.6 mmol/kg alanine ± glucagon appeared to be relatively slow and comparable to the observations seen in the Pi_{PL} of the glucagon added group. The inferences of these results are discussed in *section 6.4.*, however it is important to note that glucagon at high concentrations of alanine does seem to promote long lasting Pi_{PL} effects, possibly due to phosphorus cascading following membrane protein stimulation.

Table 24. *Changes in hepatic P_i plus underlying phospholipid during alanine infusions.*

Time (mins.)	Saline n=6	Glucagon n=5	2.8 mmol/kg Ala n=6	2.8mmol/kg Ala + Gln n=5	5.6mmol/kg Ala n=6	5.6mmol/kg Ala + Gln n=6
0.00	16.80 ± 0.14	18.29 ± 0.46	17.63 ± 0.20	18.89 ± 0.35	17.89 ± 0.28	17.60 ± 0.41
0.00	17.08 ± 0.21	17.89 ± 0.49	17.44 ± 0.12	18.56 ± 0.39	18.09 ± 0.30	17.52 ± 0.32
5.77	16.76 ± 0.14	17.65 ± 0.42	16.95 ± 0.35	18.01 ± 0.42	16.88 ± 0.32$^{\#\#}$	17.07 ± 0.24
11.54	16.68 ± 0.18	17.91 ± 0.22	16.78 ± 0.20	18.73 ± 0.13	16.97 ± 0.14$^{\#\#\#}$	17.37 ± 0.31
17.31	17.04 ± 0.71	18.85 ± 0.36	17.46 ± 0.38	19.09 ± 0.42	17.58 ± 0.49	17.93 ± 0.36
23.07	17.16 ± 0.17	19.18 ± 0.55	17.80 ± 0.48	20.02 ± 0.71	19.37 ± 1.49	18.37 ± 0.41
28.84	16.93 ± 0.29	18.95 ± 0.49	18.22 ± 0.34	20.55 ± 1.02	19.73 ± 1.23	20.23 ± 1.00$^{\#\#}$
34.61	17.28 ± 0.18	18.95 ± 0.42	18.18 ± 0.41	19.39 ± 0.64	20.41 ± 2.20	21.11 ± 1.20$^{\#\#\#}$
40.38	16.93 ± 0.39	18.53 ± 0.47	18.32 ± 0.15$^{\#\#\#}$	20.17 ± 0.58	18.99 ± 0.95	22.67 ± 1.40$^{\#\#\#\#}$
46.15	16.78 ± 0.24	18.31 ± 0.45	18.12 ± 0.29	18.87 ± 0.12	19.80 ± 1.31	21.96 ± 1.17$^{\#\#\#\#}$
51.92	17.30 ± 0.19	18.39 ± 0.51	18.00 ± 0.41	19.48 ± 0.28	19.34 ± 1.37	21.95 ± 1.34$^{\#\#\#\#}$
57.69	16.96 ± 0.12	17.95 ± 0.46	18.41 ± 0.38$^{\#}$	19.16 ± 0.18	19.42 ± 1.05	21.30 ± 1.27$^{\#\#\#}$
63.45	16.73 ± 0.27	17.60 ± 0.54	17.89 ± 0.28	19.03 ± 0.19	17.73 ± 0.47	22.42 ± 1.60$^{\#\#\#}$
69.22	16.66 ± 0.14	17.79 ± 0.30	17.41 ± 0.44	19.61 ± 0.44	17.91 ± 0.31	21.37 ± 1.60$^{\#\#}$
74.99				18.22 ± 0.18	18.43 ± 0.62	20.42 ± 1.10

Statistically significant differences to pre-infusion levels are indicated by $^{\#}P<0.1$; $^{\#\#}P<0.05$; $^{\#\#\#}P<0.02$; $^{\#\#\#\#}P<0.01$. Infused during third time point. All values are arbitrary units relative to total ^{31}P signal. Abbreviations: Ala = alanine; Gln = 75 μg Glucagon.

Changes in Pi plus underlying phospholipid.

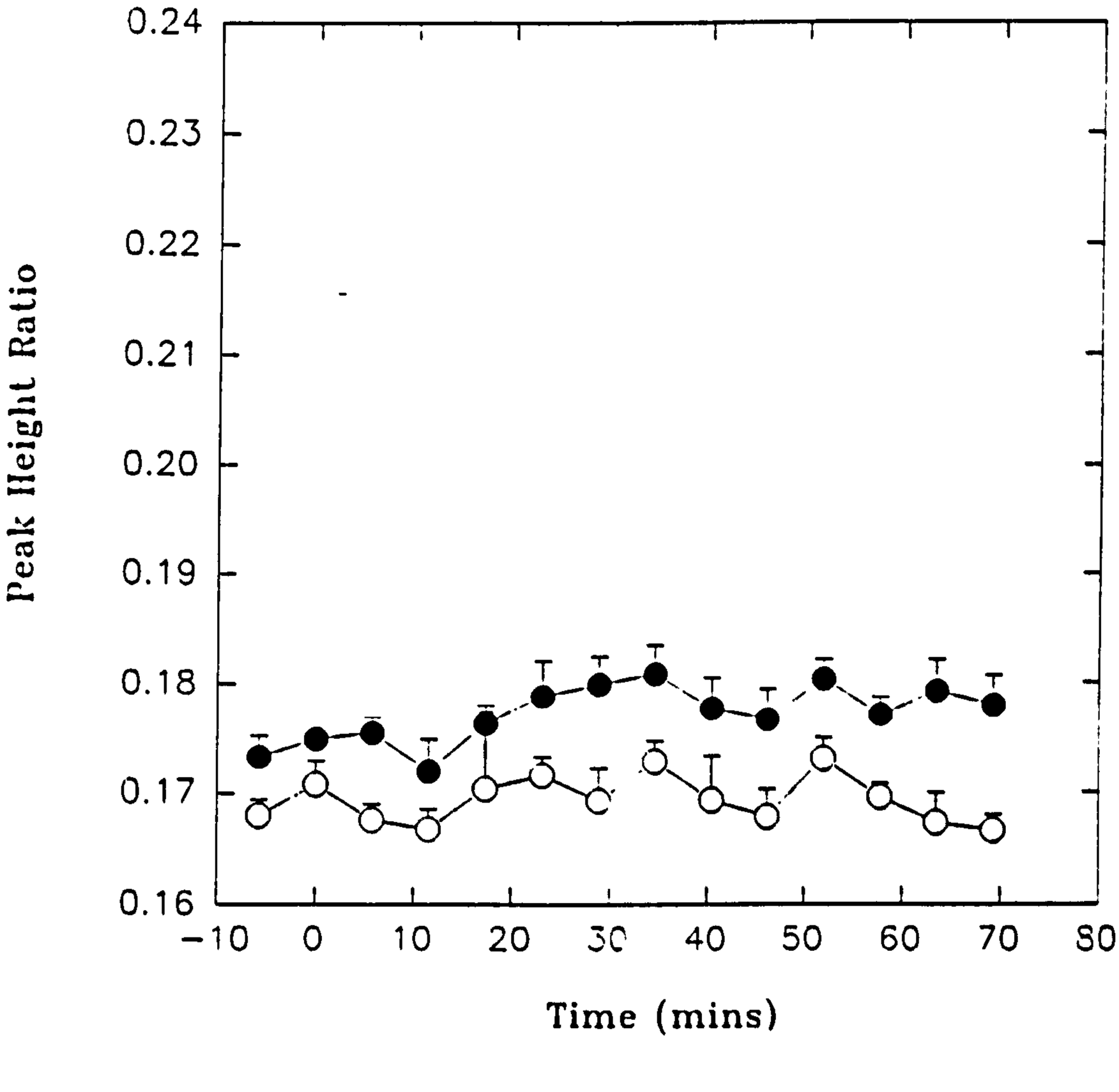

Figure 32.

Changes in Pi plus underlying phospholipid.

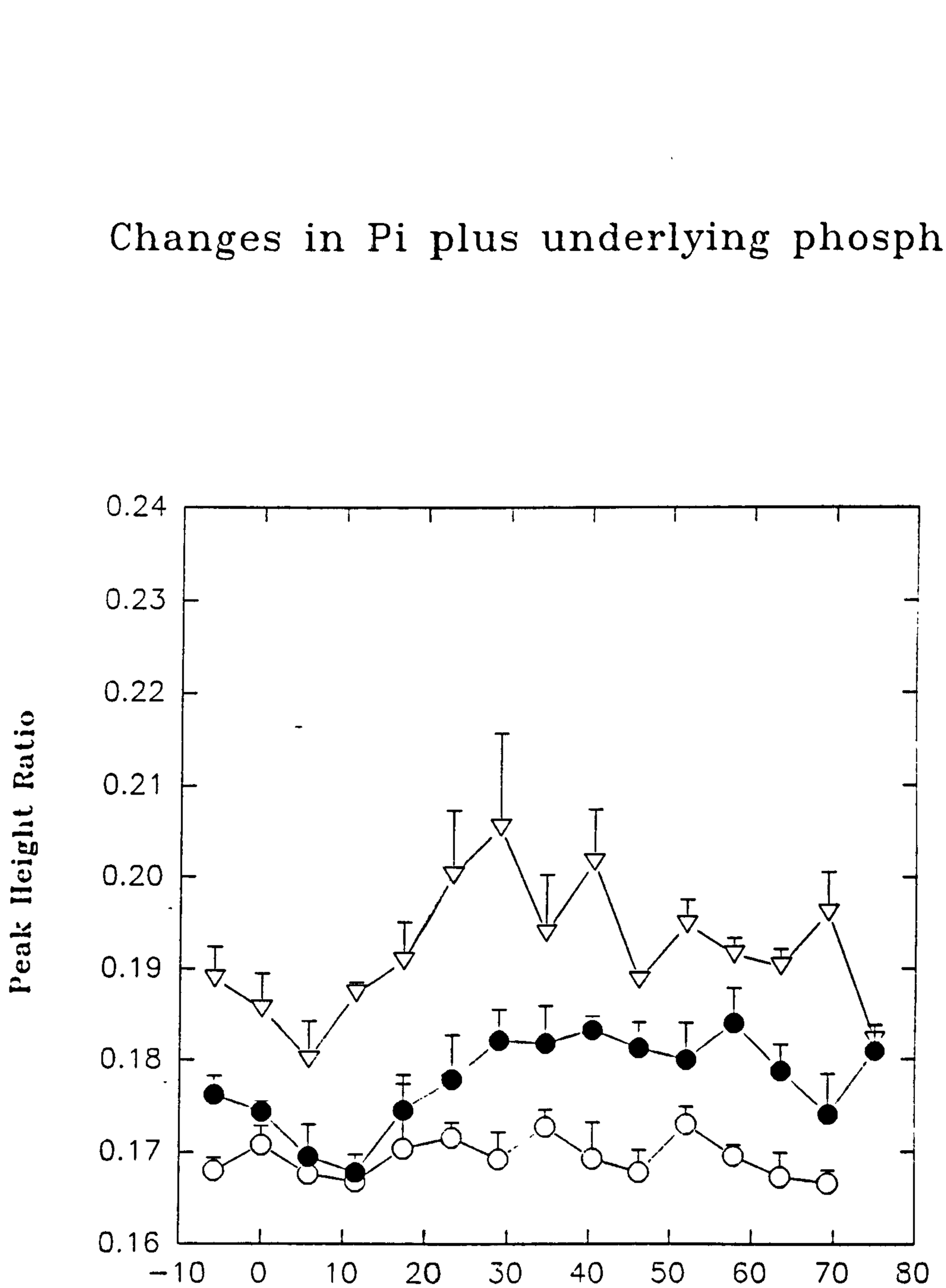

Figure 33.

Changes in Pi plus underlying phospholipid.

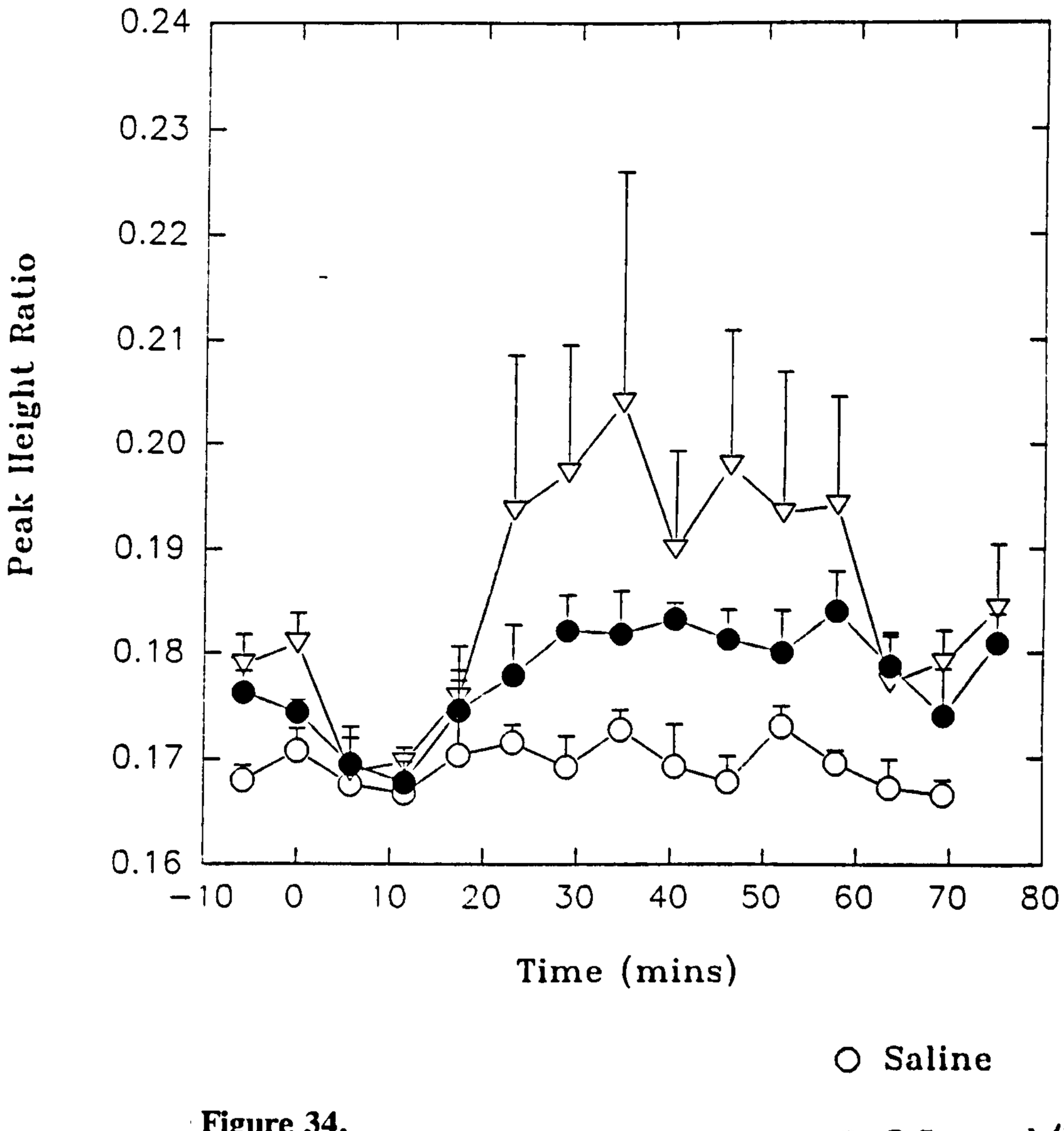

Figure 34.

Changes in Pi plus underlying phospholipid.

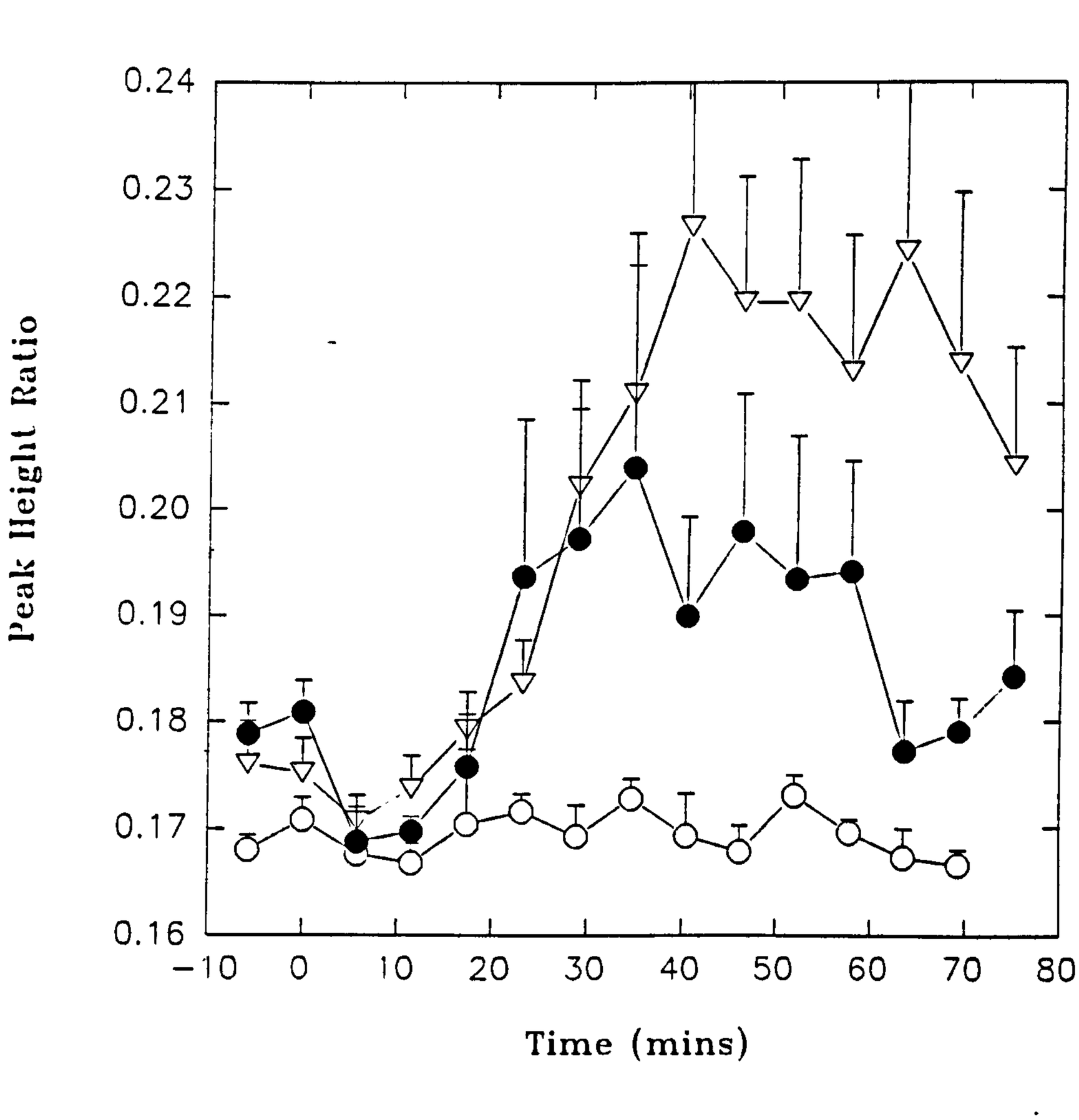

Figure 35.

Changes in Pi plus underlying phospholipid.

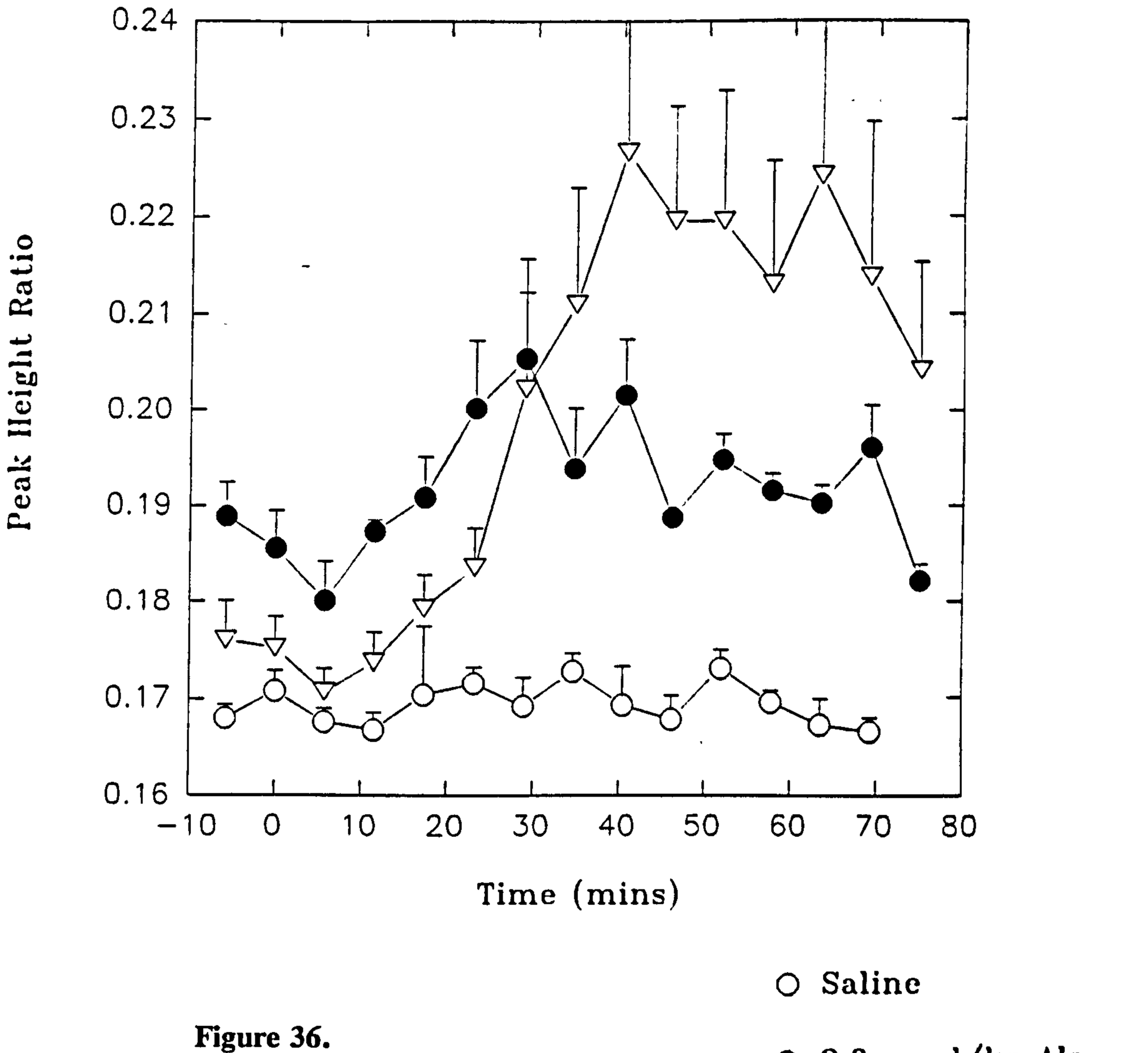

Figure 36.

6.6.4. Changes in hepatic ATP plus underlying phospholipid during alanine infusion in the rat.

Specific values have been tabulated in *tables 25*, *26* and *27*; comparisons have been made in *figures 37 - 41*. The tables show the changes in all three ATP_{PL} resonances following the various infusions of alanine. In general, all three phosphates show very similar responses to one another, however it must be remembered that the γ, α and ß-ATP resonances contain various contributions from other nucleotides. The γ-ATP resonance contain contributions from the terminal phosphate groups of γ-ATP and ß-ADP together with the respective phosphorylated nucleoside which, *in vivo*, are impossible to differentiate. The α-ATP resonance also contains contributions from both triphosphate and diphosphate nucleosides (see below), as the resonant form is the phosphate closest to the particular nucleoside, together with NADH. The closest approximation of ATP can only be gleaned from the ß-ATP which involves the resonance of the central phosphate of the nucleoside triphosphates (NTP), it is therefore impossible for nucleoside diphosphates (NDP) to co-resonate near this chemical shift. Even though ß-ATP is the closest approximation to the ATP levels in the tissue, it must be noted that included within this resonance will be contributions from GTP, UTP, CTP and ITP (guanine, uridine, cytosine and inosine triphosphates, respectively) at a concentration equivalent to one fifth of the total observed ATP.

From *graph 37* it can be seen that no significant changes were seen on infusion of either saline or glucagon. A small increase was shown by the glucagon group, however there was no significance with the pre-infusion values. Infusing the alanine

substrate at 2.8 mmol/kg, both with and without glucagon, also produced no dramatic changes in hepatic ß-ATP_{PL}. Most significant changes were observed when the alanine dose was increased to 5.6 mmol/kg, *see figure 39*. Decreases were seen from as early as 10 min post-infusion, with a maximal decrease of 14.4% ($P<0.02$) at 35 min post-infusion. Following this, the ß-ATP_{PL} level recovered to its original pre-infusion level at approximately 60 minutes post-infusion. Upon addition of glucagon to the 5.6 mmol/kg alanine infusate, *see graphs 40* and *41*, a very similar decline of 16.1% ($P<0.02$) was observed by the ß-ATP_{PL}. As can be seen from *graph 40* the rates of decline in levels of ß-ATP_{PL} were almost identical in the two groups ± glucagon, they both appear to reach a minimum value at 35 min and there-after, slowly recover. The recovery rate of these two groups however, are not quite as similar, since adding glucagon tended to slow the rate of recovery. Compared with pre-infusion values, the 5.6 mmol/kg + glucagon group showed the longest recovery rates with values 12.3% ($P<0.05$) lower at 70 min post-infusion.

When the changes seen in the 5.6 mmol/kg alanine (± glucagon) groups are compared to the same time points of hepatic Pi_{PL} fluctuations, important similarities are observed. As the ß-ATP_{PL} levels decrease there is a synchronous increase in Pi_{PL}, in fact, the maximal increases in Pi_{PL}, coincide directly with the maximum decrease in ß-ATP_{PL} in the two groups. Infusion of 5.6 mmol/kg alanine alone, results in the recovery to pre-infusion levels of the two metabolites over the same time scale. However when glucagon is present, both the Pi_{PL} and ß-ATP_{PL} remain at their respectively altered levels for a longer length of time when compared with just alanine infusion. These observations would seem to highly correlate these two effects.

Table 25. ***Changes in hepatic beta ATP plus underlying phospholipid levels during alanine infusions.***

Time (mins.)	Saline n=6	Glucagon n=5	2.8 mmol/kg Ala n=6	2.8mmol/kg Ala + Gln n=5	5.6mmol/kg Ala n=6	5.6mmol/kg Ala + Gln n=6
0.00	11.99 ± 0.15	11.46 ± 0.28	11.59 ± 0.19	12.10 ± 0.29	11.68 ± 0.28	11.69 ± 0.31
0.00	12.14 ± 0.41	11.40 ± 0.28	11.83 ± 0.30	12.51 ± 0.32	11.50 ± 0.13	12.12 ± 0.43
5.77	12.59 ± 0.35	11.73 ± 0.29	11.35 ± 0.14	12.33 ± 0.29	12.17 ± 0.12	11.62 ± 0.30
11.54	12.89 ± 0.33	11.90 ± 0.27	11.40 ± 0.31	12.04 ± 0.17	11.57 ± 0.19	11.47 ± 0.27
17.31	12.27 ± 0.21	11.86 ± 0.32	11.72 ± 0.31	12.37 ± 0.51	10.87 ± 0.39	11.09 ± 0.29
23.07	12.29 ± 0.22	11.21 ± 0.25	11.76 ± 0.14	11.61 ± 0.64	10.80 ± 0.30$^{\#}$	10.71 ± 0.29$^{\#\#}$
28.84	12.64 ± 0.34	11.60 ± 0.29	11.53 ± 0.26	11.58 ± 0.43	10.15 ± 0.56$^{\#\#}$	10.43 ± 0.44$^{\#\#}$
34.61	12.59 ± 0.41	11.71 ± 0.18	11.34 ± 0.25	12.11 ± 0.30	10.00 ± 0.47$^{\#\#\#}$	9.81 ± 0.58$^{\#\#\#}$
40.38	12.00 ± 0.27	12.08 ± 0.22	11.42 ± 0.30	11.01 ± 0.45	10.31 ± 0.34$^{\#\#\#}$	9.85 ± 0.62$^{\#\#\#}$
46.15	12.26 ± 0.09	11.84 ± 0.31	11.61 ± 0.31	12.47 ± 0.25	10.74 ± 0.44$^{\#}$	10.64 ± 0.63
51.92	12.23 ± 0.36	11.87 ± 0.27	11.35 ± 0.31	12.25 ± 0.27	10.74 ± 0.42$^{\#}$	10.28 ± 0.51$^{\#\#}$
57.69	12.42 ± 0.15	12.01 ± 0.19	11.43 ± 0.49	12.63 ± 0.16	10.98 ± 0.31	10.44 ± 0.48$^{\#\#}$
63.45	12.36 ± 0.21	12.12 ± 0.21	12.02 ± 0.52	12.18 ± 0.33	11.30 ± 0.30	10.57 ± 0.67
69.22	12.14 ± 0.36	12.32 ± 0.29	11.75 ± 0.53	12.41 ± 0.62	11.16 ± 0.17	10.25 ± 0.56$^{\#\#}$
74.99			11.67 ± 0.34	12.41 ± 0.20	10.82 ± 0.25$^{\#\#\#}$	10.23 ± 0.51$^{\#\#}$

Statistically significant differences to pre-infusion levels are indicated by $^{\#}P<0.1$; $^{\#\#}P<0.05$; $^{\#\#\#}P<0.02$. Infused during third time point. All values are arbitrary units relative to total ^{31}P signal. Abbreviations: Ala = alanine; Gln = 75 μg Glucagon.

Table 26. ***Changes in hepatic gamma ATP plus underlying phospholipid during alanine infusions.***

Time (mins.)	Saline n=6	Glucagon n=5	2.8 mmol/kg Ala n=6	2.8mmol/kg Ala + Gln n=5	5.6mmol/kg Ala n=6	5.6mmol/kg Ala + Gln n=6
0.00	19.30 ± 0.19	19.15 ± 0.15	19.27 ± 0.27	18.80 ± 0.32	18.63 ± 0.15	19.00 ± 0.36
0.00	19.52 ± 0.25	18.80 ± 0.15	19.67 ± 0.31	18.98 ± 0.21	18.77 ± 0.22	18.73 ± 0.22
5.77	19.49 ± 0.26	18.91 ± 0.30	19.23 ± 0.23	18.96 ± 0.15	18.87 ± 0.30	18.96 ± 0.32
11.54	19.71 ± 0.22	18.51 ± 0.46	18.78 ± 0.22	19.08 ± 0.15	17.96 ± 0.26$^{\#\#}$	18.75 ± 0.40
17.31	19.22 ± 0.21	17.98 ± 0.21$^{\#\#\#\#}$	18.57 ± 0.26$^{\#}$	18.52 ± 0.24	17.72 ± 0.27$^{\#\#\#}$	18.03 ± 0.43$^{\#}$
23.07	19.16 ± 0.33	18.18 ± 0.22$^{\#\#\#\#}$	18.78 ± 0.26	18.08 ± 0.34	17.84 ± 0.31$^{\#\#}$	17.94 ± 0.39$^{\#\#}$
28.84	19.24 ± 0.34	18.34 ± 0.27$^{\#\#}$	18.52 ± 0.13$^{\#\#}$	18.34 ± 0.20	16.96 ± 0.64$^{\#\#}$	17.51 ± 0.49$^{\#\#\#}$
34.61	19.01 ± 0.29	17.93 ± 0.41$^{\#\#}$	18.68 ± 0.31	17.72 ± 0.34$^{\#\#}$	17.37 ± 0.28$^{\#\#\#\#}$	16.86 ± 0.64$^{\#\#\#\#}$
40.38	19.58 ± 0.61	18.49 ± 0.15$^{\#\#\#}$	18.42 ± 0.35$^{\#}$	17.64 ± 0.42$^{\#}$	17.30 ± 0.33$^{\#\#\#\#}$	17.09 ± 0.73$^{\#\#}$
46.15	19.55 ± 0.52	18.64 ± 0.40	18.46 ± 2.89	18.43 ± 0.21	17.71 ± 0.38$^{\#\#}$	16.94 ± 0.78$^{\#\#}$
51.92	19.19 ± 0.22	18.54 ± 0.24$^{\#\#}$	18.66 ± 0.41	18.78 ± 0.18	17.85 ± 0.27$^{\#\#}$	17.54 ± 0.77$^{\#}$
57.69	19.08 ± 0.42	18.63 ± 0.26	18.40 ± 0.41	18.64 ± 0.34	18.13 ± 0.24	17.67 ± 0.85
63.45	19.00 ± 0.39	18.86 ± 0.17	18.76 ± 0.25	19.07 ± 0.19	18.35 ± 0.25	17.73 ± 0.80
69.22	19.26 ± 0.41	18.54 ± 0.37	19.09 ± 0.26	18.53 ± 0.40	17.92 ± 0.22$^{\#\#}$	17.73 ± 0.74
74.99			19.36 ± 0.52	19.02 ± 0.73	17.89 ± 0.41	17.67 ± 0.88

Statistically significant differences to pre-infusion levels are indicated by $^{\#}P<0.1$; $^{\#\#}P<0.05$; $^{\#\#\#}P<0.02$; $^{\#\#\#\#}P<0.01$. Infused during third time point. All values are arbitrary units relative to total ^{31}P signal. Abbreviations: Ala = alanine; Gln = 75 μg Glucagon.

Table 27. ***Changes in hepatic alpha ATP plus underlying phospholipid during alanine infusions.***

Time (mins.)	Saline n=6	Glucagon n=5	2.8 mmol/kg Ala n=6	2.8mmol/kg Ala + Gln n=5	5.6mmol/kg Ala n=6	5.6mmol/kg Ala + Gln n=6
0.00	20.03 ± 0.30	18.77 ± 0.43	20.35 ± 0.28	20.00 ± 0.33	20.08 ± 1.53	19.62 ± 0.38
0.00	19.99 ± 0.31	19.49 ± 0.48	20.42 ± 0.31	19.76 ± 0.24	19.85 ± 0.23	19.45 ± 0.32
5.77	19.86 ± 0.50	19.54 ± 0.32	20.38 ± 0.23	20.07 ± 0.33	20.06 ± 0.28	19.56 ± 0.41
11.54	19.88 ± 0.48	19.74 ± 0.46	20.75 ± 0.21	19.98 ± 0.22	20.30 ± 0.22	19.29 ± 0.39
17.31	19.92 ± 0.25	19.12 ± 0.46	20.20 ± 0.31	19.56 ± 0.21	20.09 ± 0.53	19.54 ± 0.33
23.07	20.27 ± 0.39	19.07 ± 0.49	20.17 ± 0.35	19.37 ± 0.37	19.48 ± 0.56	18.93 ± 0.45
28.84	20.18 ± 0.26	18.98 ± 0.62	19.89 ± 0.36	19.42 ± 0.37	18.54 ± 0.43$^{\#\#\#\#}$	18.70 ± 0.79
34.61	19.84 ± 0.18	19.08 ± 0.51	19.70 ± 0.30	19.67 ± 0.23	18.99 ± 0.29$^{\#\#\#\#}$	17.58 ± 0.82$^{\#\#}$
40.38	20.14 ± 0.30	19.20 ± 0.34	19.89 ± 0.36	19.47 ± 0.24	18.65 ± 0.56$^{\#\#}$	18.27 ± 0.89
46.15	20.04 ± 0.30	19.25 ± 0.39	19.82 ± 0.18	19.39 ± 0.22	18.99 ± 0.40$^{\#\#}$	18.06 ± 0.89
51.92	20.18 ± 0.21	18.92 ± 0.35	19.90 ± 0.23	19.74 ± 0.37	19.48 ± 0.27$^{\#}$	18.14 ± 0.84
57.69	20.37 ± 0.23	19.36 ± 0.43	19.87 ± 0.30	19.45 ± 0.35	19.18 ± 0.38$^{\#\#}$	18.53 ± 0.72
63.45	20.38 ± 0.32	19.33 ± 0.51	19.90 ± 0.40	19.42 ± 0.23	19.67 ± 0.47	18.77 ± 0.96
69.22	20.69 ± 0.25	19.64 ± 0.37	20.39 ± 0.41	19.61 ± 0.26	20.05 ± 0.35	18.51 ± 0.90
74.99			20.42 ± 0.55	19.81 ± 0.39	19.97 ± 0.27	18.36 ± 0.95

Statistically significant differences to pre-infusion levels are indicated by $^{\#}P<0.1$; $^{\#\#}P<0.05$; $^{\#\#\#}P<0.02$; $^{\#\#\#\#}P<0.01$. Infused during third time point. All values are arbitrary units relative to total ^{31}P signal. Abbreviations: Ala = alanine; Gln = 75 μg Glucagon.

Changes in β-ATP plus underlying phospholipid.

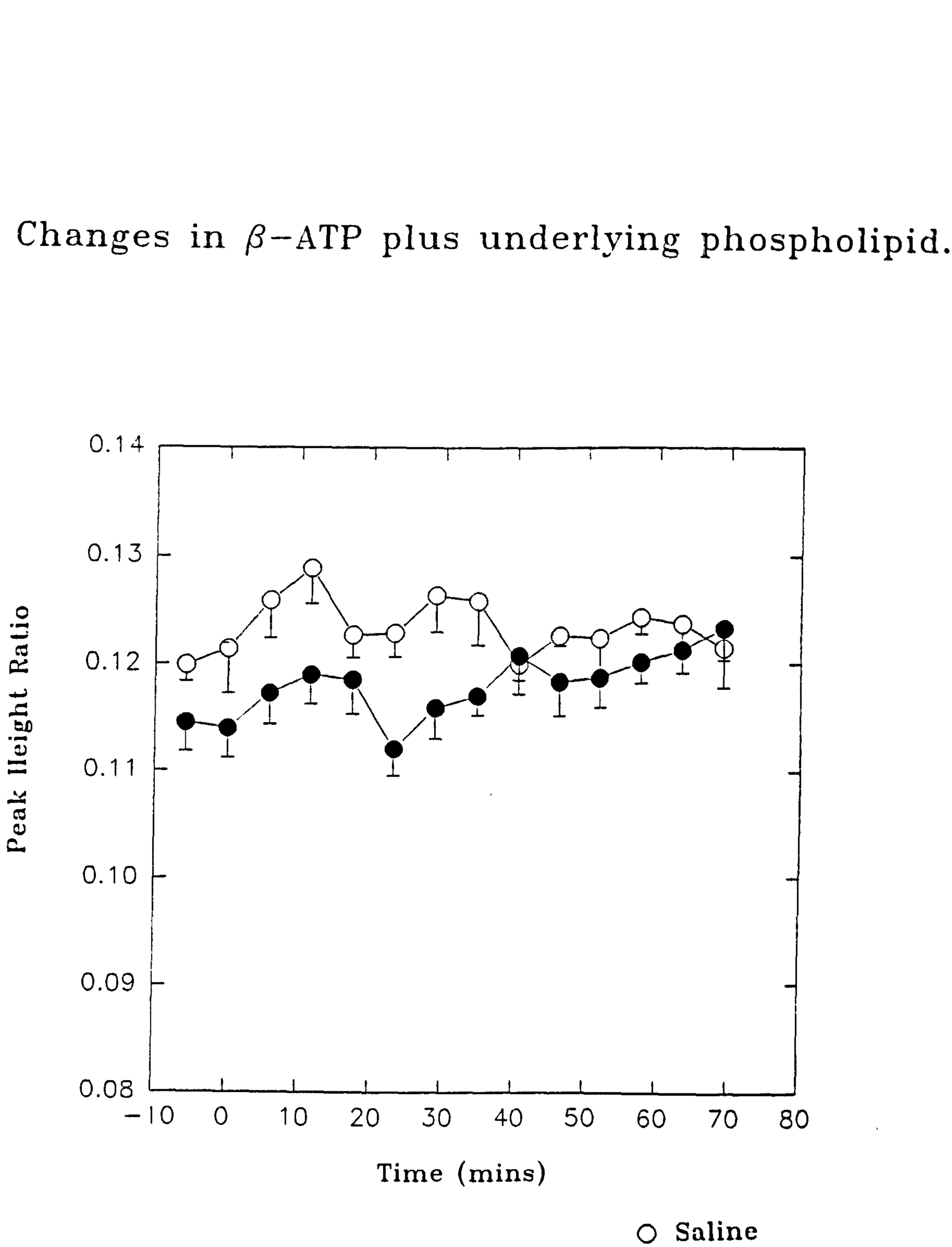

Figure 37.

Changes in β-ATP plus underlying phospholipid.

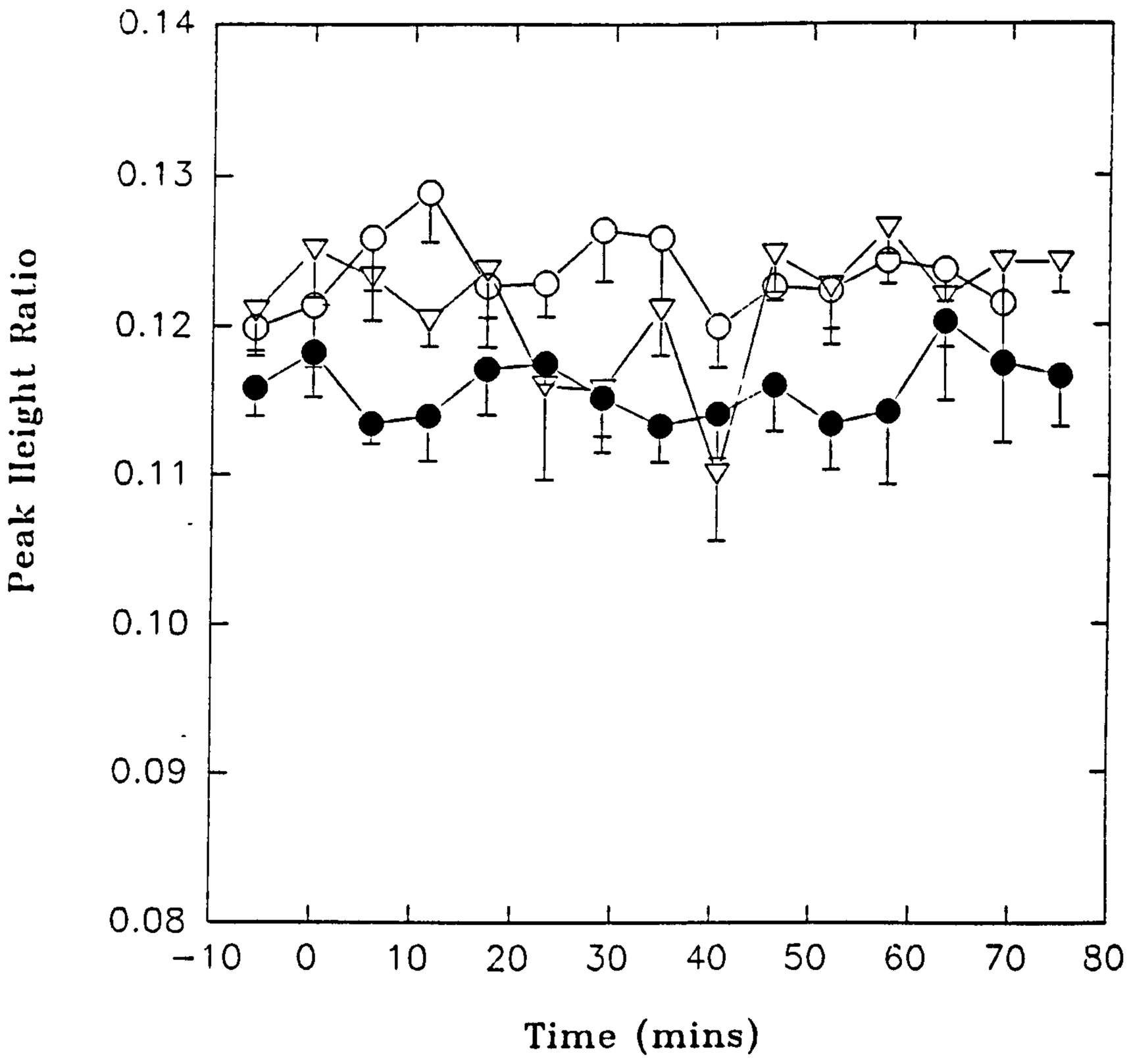

Figure 38.

Changes in β-ATP plus underlying phospholipid.

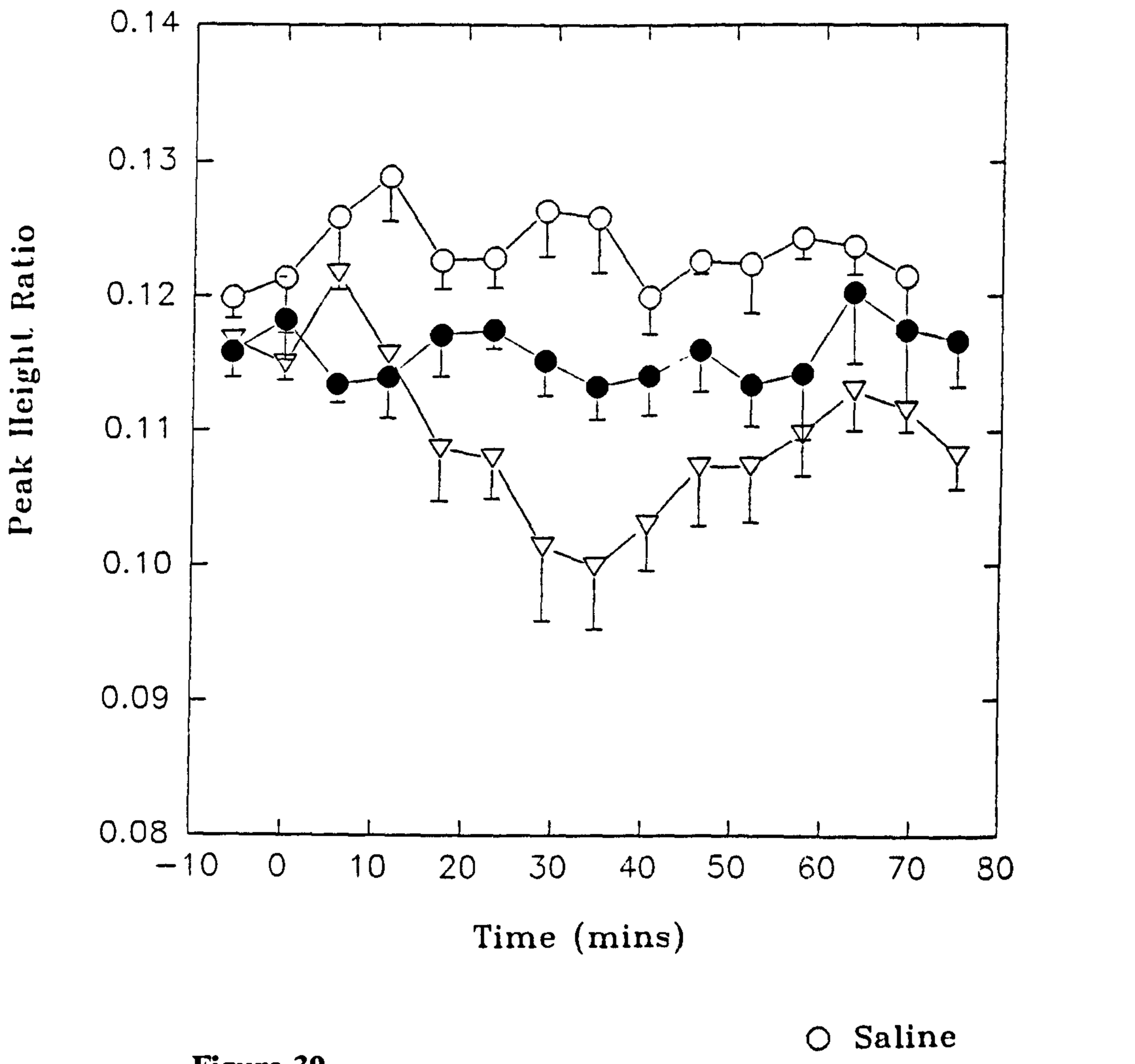

Figure 39.

Changes in β-ATP and underlying phospholipid.

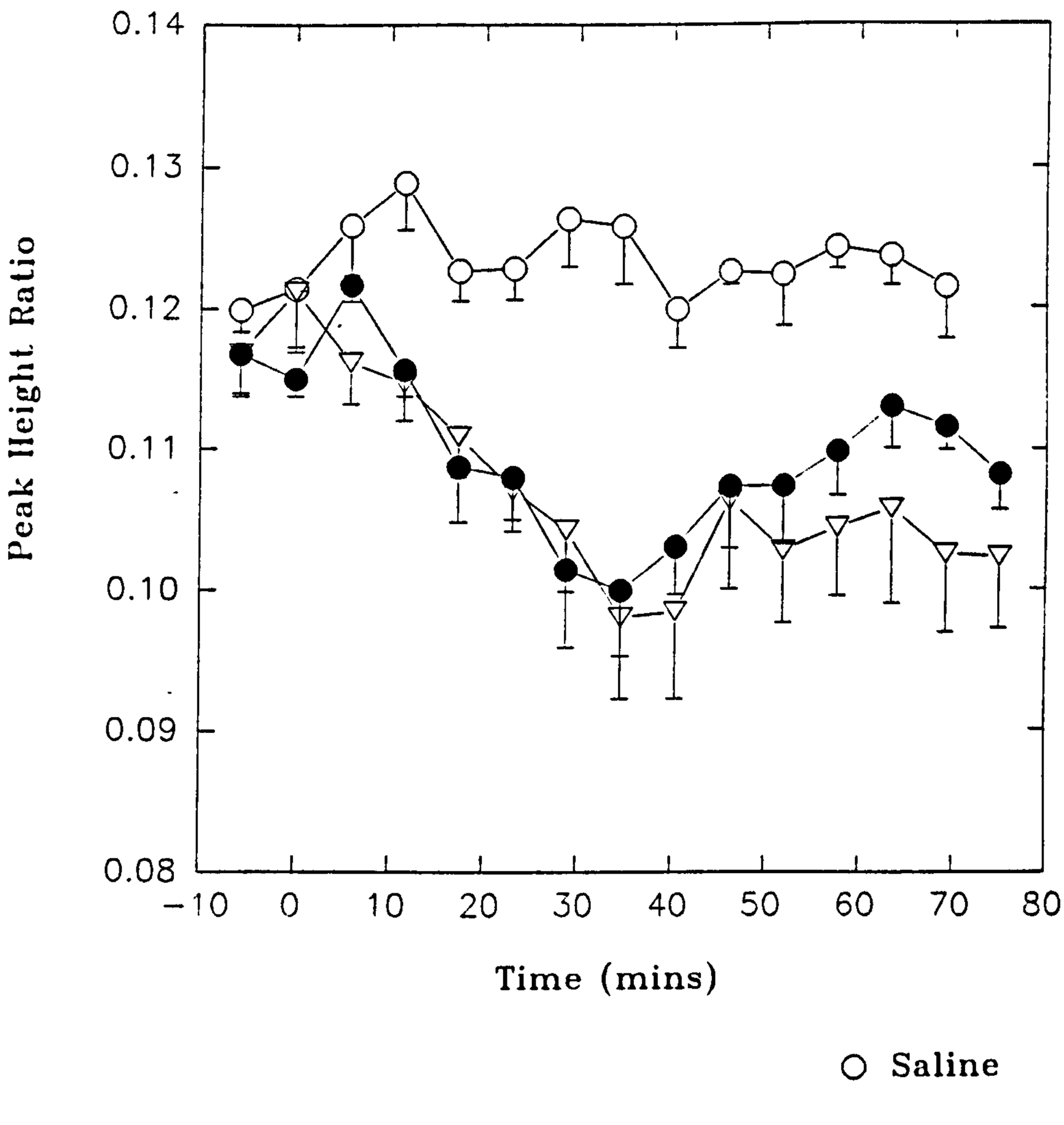

Figure 40.

Changes in β−ATP plus underlying phospholipid.

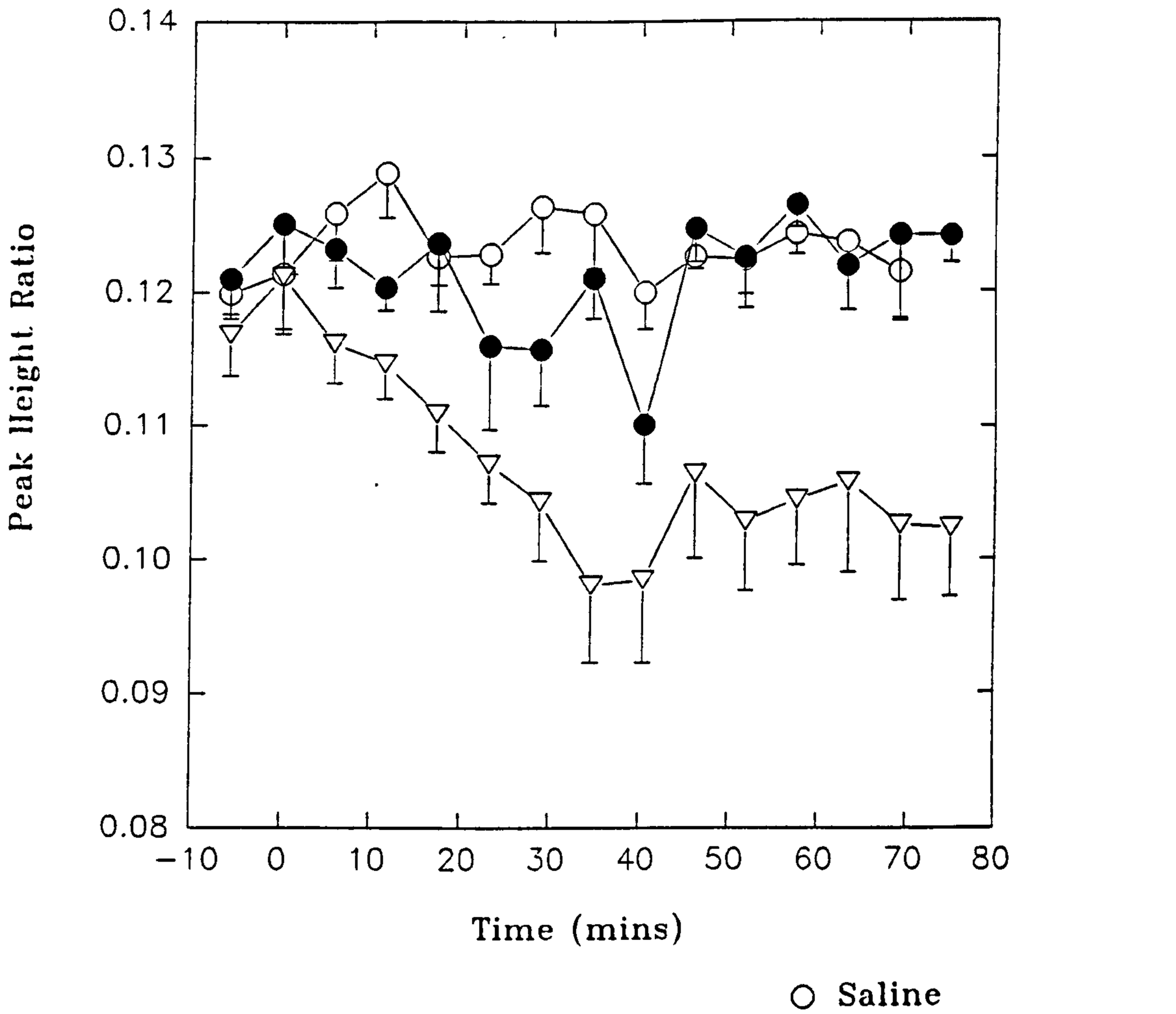

Figure 41.

6.6.5. Assessment of overall hepatic metabolism following the infusions of alanine.

Tables 28 and *29*, represent the overall response by calculating the incremental area under the curve (IAUC) for the saline and alanine (2.8 and 5.6 mmol/l) groups. Due to the incorporation into the results of all the standard errors of all time points, this representation does not depict the changes observed in the above results section. However, the changes seen *in vivo* can be represented in this fashion, and do show significant changes. On infusion of both 2.8 mmol/l and 5.6 mmol/l significant increases in PME_{PL} can be seen ($P<0.05$) when compared with saline controls. The Pi_{PL} also exhibits increases on addition of alanine, however they are not as well defined as in the *section 6.6.3.* due to the incorporation of all the errors from the means. With regard to ß-ATP_{PL} it can be seen from *table 28* that decreases are clearly observed from 0.17 ± 0.11 (IAUC units / 70 min) in the saline group to -0.16 ± 0.09 ($P<0.05$) and -0.43 ± 0.09 ($P<0.05$) in the 2.8 and 5.6 mmol/l alanine group, respectively.

Table 28.

Assessment of overall hepatic metabolite changes over a 70 min period post alanine infusion.

n=6	PME_{PL}	Pi_{PL}	γ-ATP_{PL}	α-ATP_{PL}	ß-ATP_{PL}
Saline	-0.13 ± 0.11	-0.04 ± 0.12	-0.06 ± 0.13	0.11 ± 0.07	0.17 ± 0.11
Alanine 2.8 mmol/kg	0.69 ± 0.19	0.18 ± 0.14	-0.57 ± 0.25	-0.23 ± 0.07	-0.16 ± 0.09
Alanine 5.6 mmol/kg	1.02 ± 0.27	0.03 ± 0.22	-0.57 ± 0.09	-0.39 ± 0.27	-0.43 ± 0.09

Table 29.

*Assessment of overall hepatic metabolite changes over a 70 min period *post alanine + glucagon infusion.*

n=6	PME_{PL}	Pi_{PL}	γ-ATP_{PL}	α-ATP_{PL}	ß-ATP_{PL}
Alanine 2.8 mmol/kg	0.69 ± 0.19	0.18 ± 0.14	-0.57 ± 0.25	-0.23 ± 0.07	-0.16 ± 0.09
Alanine 2.8 mmol/kg+ 75 µg Glucagon	0.99 ± 0.72	1.22 ± 1.19	-0.83 ± 0.74	-0.59 ± 0.60	-0.69 ± 0.6

All results represent the overall response over a 70 min. post alanine infusion. Results are expressed as incremental areas under the curve (IAUC). *Post alanine infusion = end of bolus infusion.

Table 30.

In vitro analysis of liver extracts from rats infused with alanine ± glucagon.

n=6	*3PG	**PEP	ß-ATP	ß-ATP:ADP
Saline	0.94 ± 0.20	0.05 ± 0.04	3.31 ± 0.34	1.82 ± 0.54
Alanine 5.6 mmol/kg	1.67 ± 0.42	0.77 ± 0.13	2.33 ± 0.30	1.67 ± 0.42
Alanine 5.6 mmol/kg + 75 μg Glucagon	1.40 ± 0.51	0.66 ± 0.05	1.75 ± 0.42	1.00 ± 0.31

Abbreviations: 3PG - 3-phosphoglycerate; PEP - phosphoenolpyruvate.

Glucagon concentrations infused = 250 μg/kg. Results are expressed as μmol/g liver wet weight.

Results obtained from separate bench experiments. *Assignment of 3PG = 7.18ppm (Bell *et al.* 1993). **Quantitation of PEP was by line height measurments compared with PCr standard (comparable line widths) due to a broad component associated with this resonance.

Figure 42. *In vitro* analysis of liver using high resolution NMR.

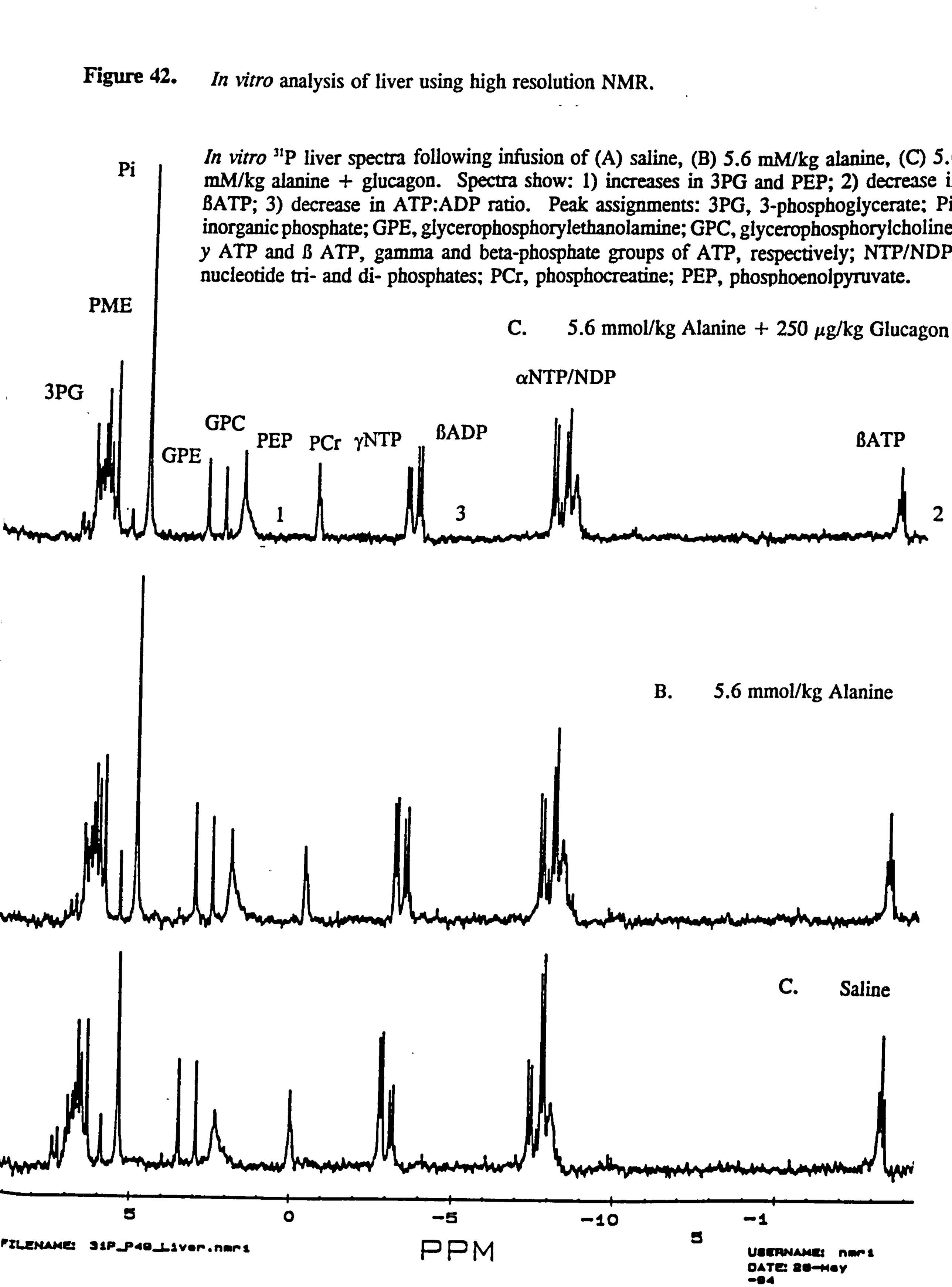

In vitro ^{31}P liver spectra following infusion of (A) saline, (B) 5.6 mM/kg alanine, (C) 5.6 mM/kg alanine + glucagon. Spectra show: 1) increases in 3PG and PEP; 2) decrease in ßATP; 3) decrease in ATP:ADP ratio. Peak assignments: 3PG, 3-phosphoglycerate; Pi inorganic phosphate; GPE, glycerophosphorylethanolamine; GPC, glycerophosphorylcholine; γ ATP and ß ATP, gamma and beta-phosphate groups of ATP, respectively; NTP/NDP nucleotide tri- and di- phosphates; PCr, phosphocreatine; PEP, phosphoenolpyruvate.

Figure 43. *In vitro* analysis of liver using high resolution NMR - expansion.

Expansions of the PME and PDE region of the *in vitro* liver spectra following infusion of (A) saline, (B) 5.6 mmol/kg alanine, (C) 5.6 mmol/kg + 250 μg/kg glucagon. Assignments: PE - phosphoethanolamine; PC - phosphocholine.

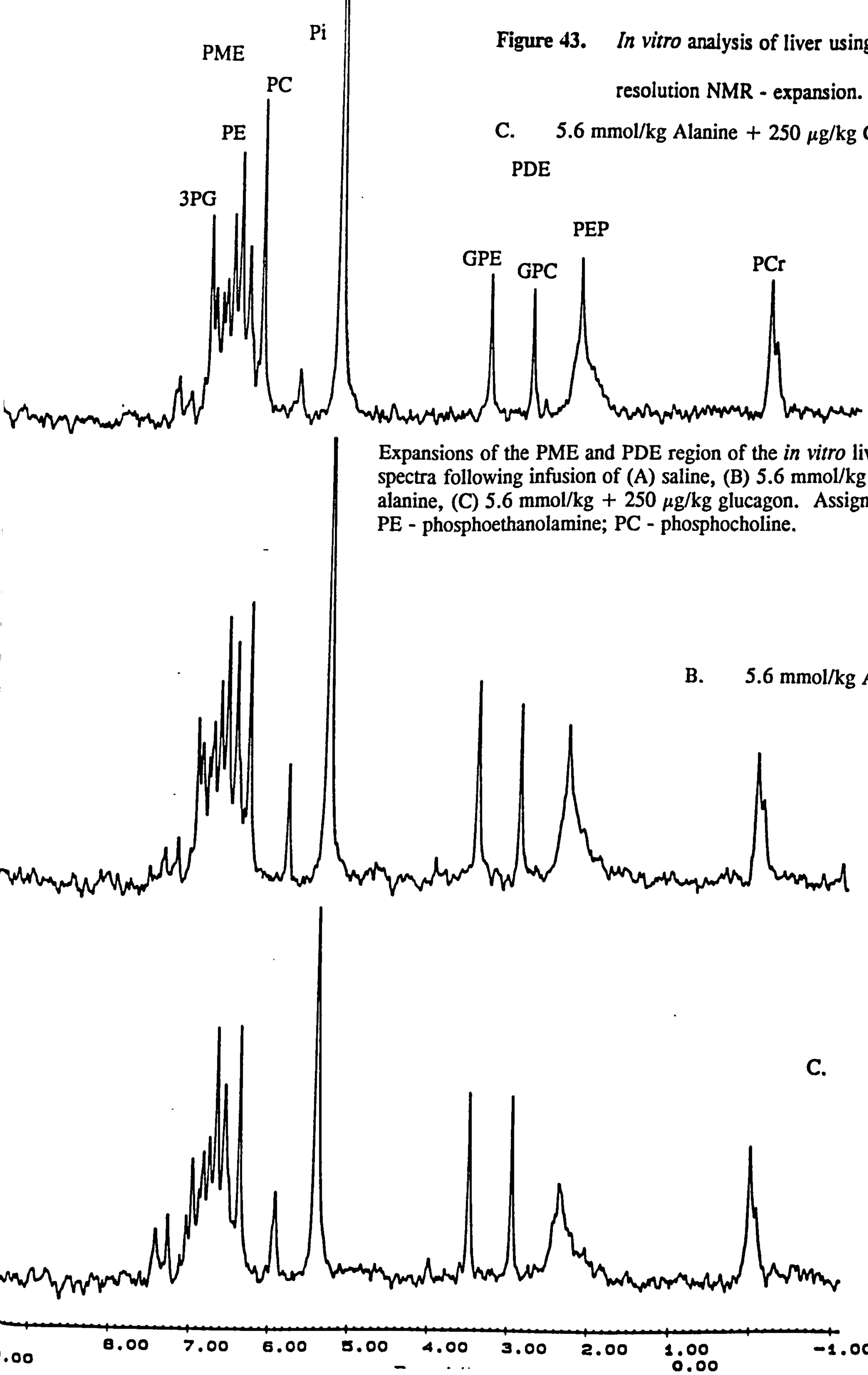

6.7. Discussion.

This study set out to evaluate the possibility of using ^{31}P-NMR as a technique for assessing changes seen during hepatic gluconeogenesis in disease states such as NIDDM, cancer cachexia and liver cirrhosis. In order to accomplish this it is essential to characterise the changes associated with the phosphorus spectrum upon infusion of the gluconeogenic precursors such as alanine. From the results it is apparent that changes associated with gluconeogenic flux, with respect to changes in sugar phosphates, C_3 intermediates, inorganic phosphate and ATP, are detectable by *in vivo* NMR. In order to assign the specific changes seen *in vivo* it was essential to perform *in vitro* tissue extracts, these studies accounted for some of the changes seen in the broad resonances of the *in vivo* spectrum.

Alanine is a major gluconeogenic precursor of the liver due to its structural similarity to pyruvate, the sole difference being the amine group attached to C_2. Alanine and glutamine make up 60% of the total release of amino acids from muscle which is surprising since the total content of these amino acids in contractile protein is only 10%. Prior to its entry into the gluconeogenic pathway the amine group is removed by a transamination reaction with α-ketoglutarate producing pyruvate and glutamate. Glutamate is then oxidatively deaminated releasing NH_4^+ for the urea cycle together with α-ketoglutarate, *see figure 44*. Pyruvate can then be oxidised to CO_2 (this is thought to be negligible [Felig, 1973]), synthesised to fatty acids or converted to glucose via oxaloacetate and phosphoenolpyruvate.

Figure 44. Reactions of the urea cycle.

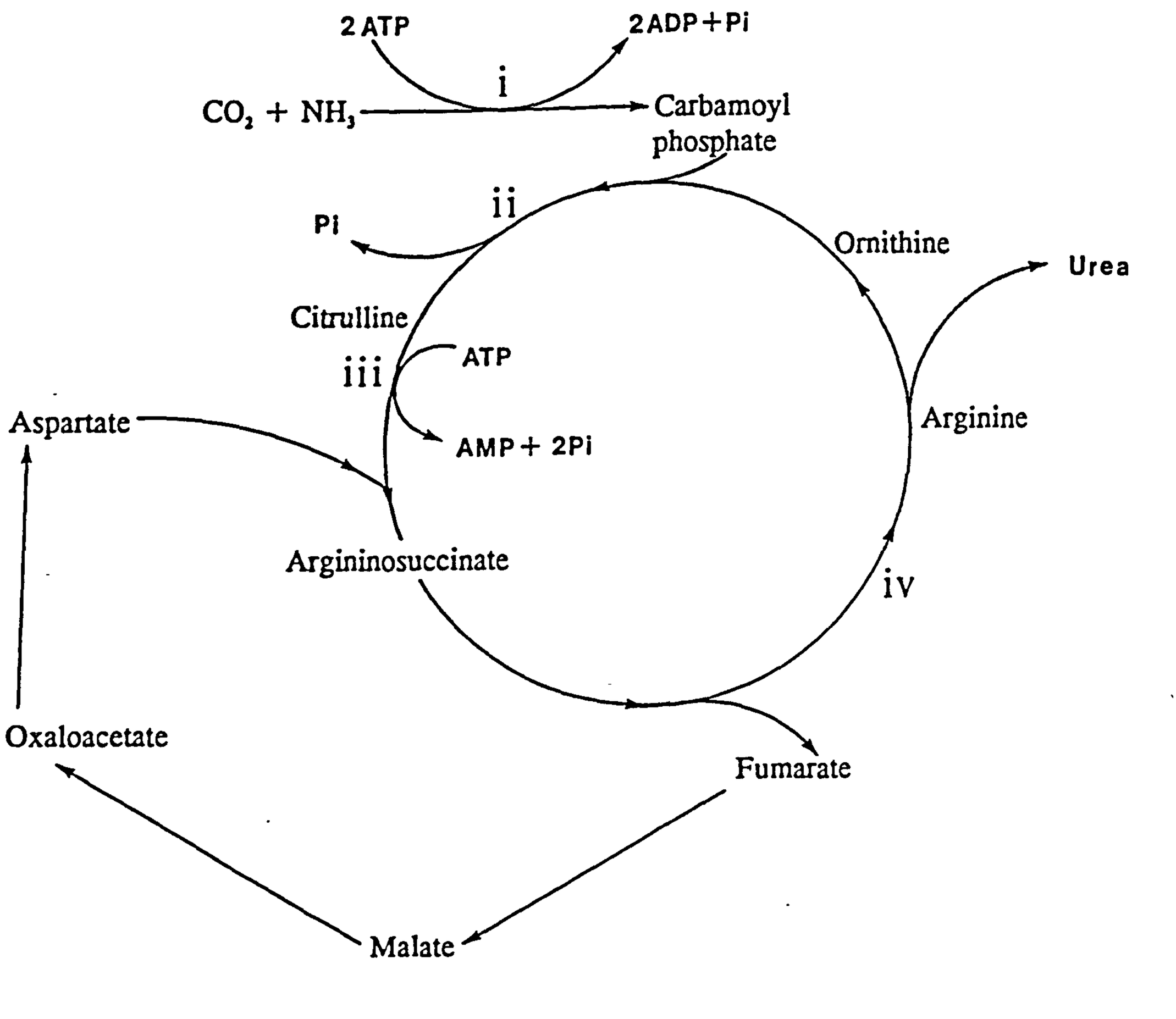

Key

i. Carbamoyl-phosphate synthetase [EC. 6.3.5.5.]
ii. Ornithine carbamoyltransferase [EC. 2.1.3.3.]
iii. Argininosuccinate synthetase [EC. 6.3.4.5.]
iv. Argininosuccinate lyase [EC. 4.3.2.1.]

It must be noted that if hepatic glycogen content is sufficient to maintain euglycaemic plasma levels then the contribution of alanine to hepatic glucose release is small. However, alanine has the direct effect of deactivating pyruvate kinase [EC. 2.7.1.40.] which indirectly inhibits 6-phosphofructokinase [EC. 2.7.1.11.], due to the build up of citrate.

The results of this study showed increases in the PME_{PL} region of the phosphorus spectrum which was consistent with the human studies (Dagnelie *et al.*, 1992). However, infusion of alanine at the lower dose of 2.8 mmol/kg produced only slight increases in both the PME_{PL} and Pi_{PL}, which was not true for the human study. The human study showed clear increases in PME at this concentration together with a concurrent decline in P_i. Significant increases in the PME_{PL} region were not achieved until a dose of 5.6 mmol/kg was administered in the rat. At this concentration dramatic increases were observed in both the PME_{PL} and Pi_{PL} region of the rat. The increases in PME_{PL} levels were secondary to increases in 3-phosphoglycerate and the sugar phosphates, which includes glucose-6-phosphate and fructose-6-phosphate, both of which are difficult to differentiate between following *in vitro* analysis, *see figures 42 & 43*. It is clear from *in vitro* analysis that increases seen in the PME_{PL} region of *in vivo* experiments are not due to increases in 3-phosphoglycerate alone but other gluconeogenic intermediates which are difficult to resolve even from *in vitro* extracts. Changes in the phosphodiesters were not evident during the *in vivo* protocol however, increases in the phosphoenolpyruvate moiety were seen from high resolution NMR. From *figure 43* it can be seen that upon administration of 5.6 mmol/kg alanine PEP concentrations substantially increased over and above administration of saline. The

failure to manifest *in vivo* changes associated with the PDE resonance is the result of the co-resonance of the broad phospholipid component of the spectrum. This resonance consists of various phospholipids associated with membrane structure and other less mobile phospholipids. There are four main ways in which removal of the broad hump can be achieved however, each method has its own inherent problem. The first would be to carry out the same experiments using a higher field magnet, the second would be to irradiate at some point on the spectrum, preferably at around 8 ppm or 1 ppm which would avoid irradiation of relevant metabolites. The third method is not really applicable to the protocol required for this study and that is *in vitro* liver perfusions performed at 6-10°C to "crystallise" cholesterol associated phospholipid membranes. Cholesterol in plasma membranes has the effect of allowing greater mobility of the phospholipid moiety and hence creating a "fluid" structure, at low temperatures the membrane becomes more rigid therefore, reducing the phospholipid component of the spectrum. This method has been used as a confirmation study for its viability and does suggest good preservation properties with respect to low P_i and high ATP levels (results not shown). However, for perfusions to be carried out at this temperature does reduce the physiological importance of the study. The fourth method is to use computer assisted processing packages which supposedly can remove this peak. Unfortunately, for this study the latter was the method of choice, however it became apparent that the computer program was not able to consistently remove the correct component associated with the phospholipid hump. Invariably large components associated with the ATP and PME resonances were removed along with the broad resonance. This produced spurious results not consistent with the observed changes.

From the *in vitro* results it is likely that dose dependent increases of the PME and PDE reflect the relative flux of alanine through the gluconeogenic pathway. The increases are directly attributed to increases in 3-phosphoglycerate and phosphoenolpyruvate. It is interesting to note that conversion of pyruvate to PEP is catalysed by non-equilibrium reactions however, conversion of PEP to 2-phosphoglycerate and 3-phosphoglycerate are controlled by near equilibrium reactions which is followed by an ATP dependent reaction to 3-phosphoglyceroyl phosphate, *see figure 45*. From the *in vitro* perfusion study glucose outputs confirmed the influence of alanine on the gluconeogenic pathway. Infusion of 5.6 mmol/l alanine produced an hepatic glucose output of 0.551 $\pm$ 0.024 μmol/min/100g rat whereas perfusion with the addition of just glucagon or saline produced a negligible output of 0.032 $\pm$ 0.004 μmol/min/100g rat at the time point corresponding to maximal spectral changes (30-40 min. post infusion). Infusion of glucagon plus alanine did not produce any significant changes in hepatic glucose output which is consistent with the findings of Ross *et al.* (1967) in 48 h starved perfused livers. An attempt was made to perform liver perfusions within the horizontal bore magnet system to obtain simultaneous hepatic glucose output measurements with real time changes in the phosphorus spectrum, however various problems arose from the inherent difficulties associated with a horizontal magnet. The first major problem was maintaining the temperature of the perfusate prior to liver entry due to a tubing length of 8 m being necessary between the perfusate box and the bore of the 4.7 T magnet. This distance was essential to prevent stray field lines affecting the perfusion apparatus (a stipulation enforced by the college). An elaborate heat transfer technique was applied involving water heated to 45°C running side by side with the perfusate tubing

maintaining the perfusate temperature at 37°C. However, a problem associated with prolonged heating caused denaturing of albumin which increased the pressure of the system due to liver blockage. A final problem also associated with distance required for the perfusate to flow which produced a general increase in the pressure of the system. The problems associated with the setup have now been rectified allowing NMR analysis and concurrent glucose output studies to be achieved in the 4.7 T horizontal bore magnet (but too late to use for this project).

An interesting observation with respect to changes seen from the NMR analysis was the time course of the changes. Alanine did not produce maximal changes until approximately 30 - 40 min. post infusion. These observations were very similar to the changes associated with human alanine studies. The study by Dagnelie *et al.* (1992) showed increases in the PME which attained maximal levels at 35 - 45 min. post infusion of alanine (2.8 mmol/kg). It does seem surprising that maximal increases in the PME region do not occur quicker in the rat compared with humans since metabolic rates are far quicker. It would be interesting, therefore, to evaluate the time course that lactate might have on gluconeogenic intermediates. If increases in the PME attain maximal levels quicker using lactate then it could be assumed that the deamination/transamination reactions are rate limiting for gluconeogenesis.

One of the major differences between the human and rat studies was the increase seen in the Pi_{PL} in this study. Dagnelie *et al.* (1992) suggested that the reduction in P_i levels following alanine infusion could be due to loss of P_i into the extracellular compartment or because of the extent of phosphorylation required for gluconeogenic

intermediates. Another possibility suggested was the movement of P_i into NMR invisible pools due to no apparent differences seen in their *in vitro* extractions of liver. The study presented in this thesis shows quite clear increases in intracellular Pi_{PL} together with concurrent declines in intracellular ATP_{PL} (together with decreases in ATP:ADP ratios) which was confirmed from *in vitro* analysis. These changes could be due to a number of factors. Firstly, it must be noted that upon administration of glucagon, P_i and ADP:ATP levels exceed those in rats not infused with this hormone. This could be due to the membrane signalling mechanism via the stimulation of adenylate cyclase converting ATP to cyclic AMP (cAMP) thus releasing $2P_i$, however this contribution is relatively small and not large enough to detect by NMR. Secondly, gluconeogenic flux requires both ATP and GTP, *see figure 45*, which upon glucose production will liberate P_i, adding to the intracellular pool. Thirdly, following deamination/transamination of alanine, ammonia and aspartate enter the urea cycle which has the effect of consuming 3 ATP and liberating four P_i molecules, however, in order for the cycle to complete, NADH is regenerated which should produce three molecules of ATP, therefore, producing a net ATP deficit of one. This would only be true once normal steady state had been achieved. However during gluconeogenesis, this pathway may be operating far quicker than the re-synthesis of ATP, hence producing an energy deficit. Another important area of consideration is the translocation of alanine into cells which can be achieved by a number of processes including carrier mechanisms (Guidotti *et al.*, 1978) and by the γ-glutamyl cycle (Meister *et al.*, 1981). The latter process converts the amino acid to γ-glutamyl-amino acid following the reaction with γ-glutamylcysteinylglycine. This compound can then enter the cytosolic compartment from where it is cleaved by

γ-glutamylcyclotransferase to release the amino acid and 5-oxoproline. The latter compound is then re-synthesised to glutathione to complete the cycle. The translocation of one amino acid requires three ATP molecules and hence can be regarded as an expensive utiliser of energy rich phosphate. The net effect would be to reduce ATP:ADP ratios and increase intracellular P_i. The dramatic changes associated with the P_i and ATP:ADP do appear to be clearly linked in this study. However, the discrepancy between this study and previous human studies with respect to P_i changes must be addressed. Even from the *in vitro* analysis of the livers it is apparent that P_i levels do increase which supports the observations seen *in vivo*. One variation between the pathways of gluconeogenesis seen in humans and rats must be considered when relating changes seen in experiments with rats to those seen in humans. All human gluconeogenic enzymes are located in the cytosol, except for pyruvate carboxylase [EC. 6.4.1.1.] which is found in the mitochondria. Phosphoenolpyruvate carboxykinase [EC. 4.1.1.31.] is found both in mitochondria and the cytosol. Conversion of oxaloacetate to PEP can be achieved within the mitochondria, after which PEP is transported to the cytosol presumably via the tricarboxylate mitochondrial carrier. This has consequences for the transfer of phosphate across the mitochondria and hence possible Pi "loss" in human gluconeogenic studies (Dagnelie *et al.*, 1992). In the rat however, phosphoenolpyruvate carboxykinase is found only in the cytosol. This then requires the transport of oxaloacetate into the cytosol via its conversion to malate or aspartate. Conversion of oxaloacetate to malate involves the reduction of NAD^+ to NADH, which is conveniently required for the conversion of 1,3 bis-phosphoglycerate to 3-phosphoglyceraldehyde during gluconeogenesis.

It appears, therefore, that increasing the alanine dose *in vivo* from 2.8 - 5.6 mmol/kg causes a fall in hepatic ATP_{PL} and increase in Pi_{PL} in rats whereas, at the maximum dose used in human studies (2.8 mmol/kg) P_i fell and ATP appeared to be unchanged (Dagnelie *et al.*, 1992). Assuming that increasing the alanine infusion dose provokes an increase in gluconeogenesis then a possible explanation for this phenomenon is the increased demand on supply of ATP. A lower hepatic ATP has been observed previously in the perfused rat liver after a rapid transition of perfusate lactate concentration from 1-10 mmol/l, whereas in the presence of acidosis, which inhibits gluconeogenesis, ATP was unaffected (Iles *et al.*, 1981). Complete disposal of alanine requires the urea cycle in addition to gluconeogenesis, since the nitrogen must be processed. Both of these pathways require ATP. Whatever the relative contributions of these pathways, under the conditions of these experiments, the normal balance between ATP synthesis and disposal is apparently altered. Further *in vitro* studies are required to determine whether the fall in ATP correlates with increases in gluconeogenic rate.

This study has demonstrated the potential for the alanine/^{31}P test in disease states which may show alterations in the gluconeogenic pathway. Further developments are required using ^{31}P NMR and concurrent liver perfusions, to directly assess the relative spectral changes to hepatic glucose output. It is quite clear from this study that spectral changes seen *in vivo* are secondary to the changes seen in 3-phosphoglycerate and PEP. A fundamental observation from this study was the decrease in ATP which directly relates the high demand on energy imposed by gluconeogenesis. Decreases in ATP levels however, may be species specific due to the high metabolic rate of rats

but are an important consideration if development to the human model are envisaged. If ATP decreases are present in humans then methods of absolute quantitation are required since using the ß-ATP resonance as an internal standard would produce values of gluconeogenic flux far higher than the true value. Using alanine and NMR as a test for gluconeogenic changes in pathophysiological conditions could identify the key changes associated with diseases such as NIDDM.

6.8. Future work.

An important aspect of this work was to evaluate the possibility of using alanine/^{31}P NMR as a test for gluconeogenic changes in disease states. A natural progression would therefore be to use a rat model of non insulin dependent diabetes which would be expected to give higher rates of gluconeogenesis than control rats. If these rats are then placed on therapy then the relative changes in the gluconeogenic flux could be monitored by ^{31}P NMR and correlated to the extent of treatment. The various treatments for NIDDM, such as the sulphonylurea drugs and metformin, can then be assessed which could provide an insight into producing new therapies. Other possibilities would be to use ^{13}C alanine as a precursor for the test, to assess the relative amount of ^{13}C glycogen repleted. If a phosphorus/carbon coil could be made then inter-leaved phosphorus and carbon spectra could be acquired one after the other. This would provide a wealth of information on gluconeogenic changes together with glycogen synthesis ability of the liver. Hepatic perfusions within the horizontal magnet could also be performed where spectral changes can directly be correlated

with hepatic glucose outputs. It would also be interesting to see the time course of changes using lactate as the gluconeogenic precursor. It was apparent in this study that maximal changes were not seen until approximately 30-40 min post alanine infusions. This could be due to slow intracellular transport of alanine or a rate limiting step at the level of transamination/deamination of the alanine prior to entry into the oxaloacetate pool. Since lactate can easily be converted to pyruvate, without the need of deamination, it is reasonable to assume an enhanced gluconeogenic rate.

Other important points which must be addressed include the method of absolute quantitation of the phosphorus spectrum which in most studies relies on the ß ATP resonance. However, in this study it is clear that ATP decreases upon alanine infusions in rats. If this is to be used on human patients then this problem must clearly be investigated.

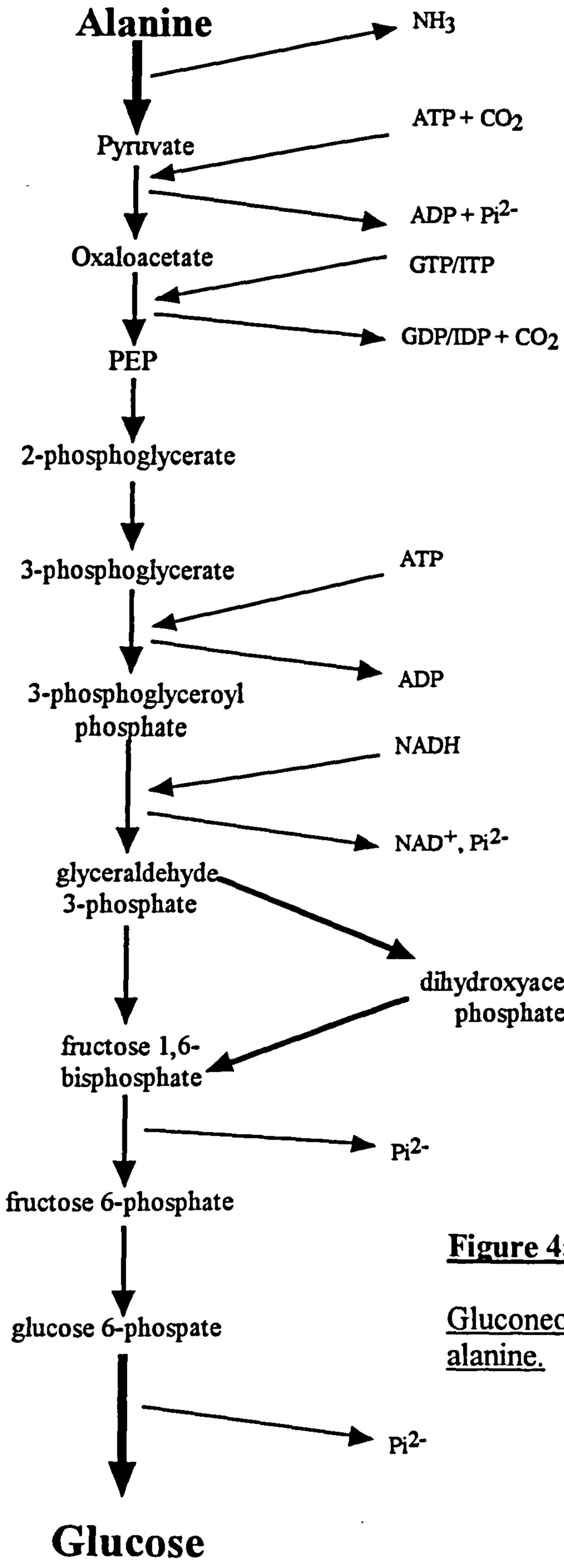

Figure 45.

Gluconeogenic pathway from alanine.

Publications arising from thesis.

Holness, M.J. Changani, K.K., Sugden, M.C. 1991 Biochem. J. 280 549-552.

Progressive suppression of muscle glucose utilisation during pregnancy.

Sugden, M.C. Changani, K.K., Bentley, J., Holness, M.J. 1992 Biochem. Soc. Trans. **20** 195S.

Cardiac glucose metabolism during pregnancy.

Barnard, M.L., Bell, J.D., Williams, S.C.R., Sanders, T.A.B., Parkes, H.G., Changani, K.K., Beech, J.S., Jackson, M.L. and Bloom, S.R. 1992 Soc. Mag. Res. Med. 11th annual meeting, Berlin. Works in progress 3339.

Dietary influence on tissue lipid composition measured by in vivo $^{13}C\{^{1}H\}$ N.M.R. spectrocopy.

Changani, K.K., Williams, S.C.R., Iles, R.A. 1993 Soc. Mag. Resonance in Medicine 12th Annual Meeting, New York, Oral Presentation, Vol. 1 pp90

In vivo hepatic glycogen synthesis during pregnancy.

Changani, K.K., Williams, S.C.R., Iles, R.A. 1993a Biochem. Soc. Trans. **21** 453S

In vivo hepatic glucose disposal during pregnancy.

Changani, K.K., Williams, S.C.R., Iles, R.A. 1994 Biochem Soc. Trans. 649th Meeting, **22** 126S.

In vivo hepatic glucose and glycogen metabolism in meal fed rats.

Changani, K.K., Williams, S.C.R. and Iles, R.A. 2nd Meeting of SMR, San Francisco 1994a. Vol 3 pp 1283.

^{13}C-Glycogen deposition during gestational undernutrition.

Changani, K.K. Barnard, M.L., Bell, J.D. Williams, S.C.R., Bloom, S.R. & Iles, R.A. 1994b Biochem. Soc. Trans. in press.

In vivo hepatic energy pertubations during alanine infusion using ^{31}P-NMR spectroscopy.

Changani, K.K. Williams, S.C.R., Bell, J.D. and Iles, R.A. 1994c Stable Isotopes in Nutrional and Metabolic Research 2nd World Conference, July 7-8, 1994 Rotterdam, The Netherlands. In press/oral presentation.

Hepatic ^{13}C-glucose and ^{13}C-glycogen perturbations during pregnancy.

References.

Alger, J.R., Sillerud, L.O., Behar, K.L., Gillies, R.J., Shulman, R.G., Gordon, R.E., Shaw, D., & Hanley, P.E.. 1981 Science **214** 660-662.

In vivo carbon-13 nuclear magnetic resonance studies of mammals.

Assali, N.S., Rauramo, L. and Peltonen, T. 1960 Am. J. Obstet. Gynecol. **79** 86-98.

Measurement of uterine blood flow and uterine metabolism.

Bailes, D.R., Bryant, D.J., Bydder, G.M., Case, H.E., Collins, A.G., Cox, I.J., Evans, P.R., Harman, R.R., Hall, A.S., Khenia, S., McArthur, P., Oliver, A., Rose, M.R., Ross, B.D. and Young, I.R. 1987 J. Mag. Reson. **74** 158-170.

Localised ^{31}P-NMR spectroscopy of normal and pathological human organs in vivo using phase encoding techniques.

Bailey, I.A., Gadian, D.G., Matthews, P.M., Radda, G.K. and Seeley, P.J. 1981 FEBS Lett. **123** (2) 315-318.

Studies of metabolism in the isolated, perfused rat heart using ^{13}C NMR.

Barnard, M.L., Bell, J.D., Williams, S.C.R., Sanders, T.A.B., Parkes, H.G., Changani, K.K., Beech, J.S., Jackson, M.L. and Bloom, S.R. 1992 Soc. Mag. Res. Med. 11th annual meeting, Berlin. Works in progress 3339.

Dietary influence on tissue lipid composition measured by in vivo $^{13}C\{^1H\}$ N.M.R. spectrocopy.

Barton, M.D., Killan, A.P. and Meschia, G. 1981 Proc. Soc. Exp. Biol. Med. **145** 996-1003.

Response of ovine uterine blood flow to epirephrine and norepirephrine.

Battaglia, F.C. and Meschia, G. 1978 Physiol. Rev. **58** 499-527.

Principle substrates of fetal metabolism.

Beckmann, N., Seelig, J. and Wick, H. 1990 Mag. Res. Med. **16** 150-160.

Analysis of glycogen storage disease by in vivo ^{13}C NMR. Comparison of normal volunteers with a patient.

Beckmann, N., Fried, R., Turkalj, I., Seelig, J., Keller, U. and Stalder, G. 1993 Mag. Reson. Med. **29** 583-590.

Non-invasive observation of hepatic glucogen formation in man by ^{13}C MRS after o ral and intravenous glucose adimistration.

Bell, J.D., Cox, I.J., Sargentoni, J., Peden, C.J., Menon, D.K., Foster, C.S., Watanapa, P., Iles, R.A. and Urenjak, J. 1993 Biochim. Biophys. Acta **1225** 71-77.

A ^{31}P and ^{1}H-NMR investigation in vitro of normal and abnormal human liver.

Berg, B.N. (1965) J. Nutr. **87** 344-348.

Dietary restriction and reproduction in the rat.

Blackledge, M.J., Rajagopalan, B., Oberhaensli, R.D., Bolas, N.M., Styles, P. and Radda, G.K. 1987 Proc. Natl. Acad. Sci. U.S.A 84 4283-4287.

Quantitative studies of human cardiac metabolism ^{31}P rotating frame NMR.

Bloch, F. 1946 Phys. Rev. 70 461-474.

Nuclear induction.

Bloch, F., Hansen, W.W. and Packard, M. 1946 Phys. Rev. 70 474-485.

The nuclear induction experiment.

Bottomley, P.A., Hart, H.R., Edelstein, W.A., Schenck, J.F., Smith, L.S., Leue, W.M., Mueller, O.M. and Redington, R.W. 1983 Lancet ii: 273-274.

NMR imaging/spectroscopy system to study both anatomy and metabolism.

Brown, F.F., Campbell, I.D., Henson, R., Hirst, C.W.J. and Richards, R.E. 1973 Eur. J. Biochem. 38 54-58.

A study of the interaction of manganese ions with ATP by ^{31}P fourier-transform nuclear-magnetic resonance

Burt, R.L. 1956 Obstet. Gynecol. (N.Y.) 2 658-664.

Peripheral utilization of glucose in pregnancy. III. Insulin tolerance.

Campbell, I.D. and Dobson, C.M., 1979 Methods Biochem. Anal. 25 1-133

The application of high resolution nuclear magnetic resonance to biological systems.

Canioni, P., Alger, J.R. and Shulman, R.G., 1983 Biochemistry 22 4974-4980.

Natural abundance carbon-13 nuclear magnetic resonance spectroscopy of liver an d adipose tissue of the living rat.

Cerdan, S., Künnecke, B. and Seelig, J., 1990 J. Biol. Chem. 265 (22) 12916-12926.

Cerebral metabolism of [1,2-^{13}C$_2$] acetate as detected by in vivo and in vitro ^{13}C-NMR.

Changani, K.K., Williams, S.C.R., Iles, R.A. 1993 Soc. Mag. Resonance in Medicine 12th Annual Meeting, New York, Oral Presentation, Vol. 1 pp90

In vivo hepatic glycogen synthesis during pregnancy.

Changani, K.K., Williams, S.C.R., Iles, R.A. 1993a Biochem. Soc. Trans. 21 453S

In vivo hepatic glucose disposal during pregnancy.

Changani, K.K., Williams, S.C.R., Iles, R.A. 1994 Biochem Soc. Trans. 649th Meeting, 22 126S.

In vivo hepatic glucose and glycogen metabolism in meal fed rats.

Changani, K.K., Williams, S.C.R. and Iles, R.A. 2nd Meeting of SMR, San Francisco 1994a. Vol 3 pp 1283.

^{13}C-Glycogen deposition during gestational undernutrition.

Changani, K.K. Barnard, M.L., Bell, J.D. Williams, S.C.R., Bloom, S.R. & Iles, R.A. 1994b Biochem. Soc. Trans. in press.

In vivo hepatic energy perturbations during alanine infusion using ^{31}P-NMR spectroscopy.

Changani, K.K. Williams, S.C.R., Bell, J.D. and Iles, R.A. 1994c Stable Isotopes in Nutrional and Metabolic Research 2nd World Conference, July 7-8, 1994 Rotterdam, The Netherlands. In press/oral presentation.

Hepatic ^{13}C-glucose and ^{13}C-glycogen perturbations during pregnancy.

Clapp, J.F. 1978 Am. J. Obstet. Gynecol. 130 419-423.

Cardiac output and uterine blood flow in the pregnant ewe.

Cohen, R.D., Iles, R.A. and Lloyd, M.H. 1973 In: *Isolated Organ Perfusion* 120-134, eds. H.D. Richie and J.D. Hardcastle Crosby, Lockwood and Staples, London.

Cohen, S.M., Ogawa, S., Rottenberg, H., Glynn, P., Yamane, T., Brown, T.R., Shulman, R.G., and Williamson, J.R. 1978 Nature (London) 273 554-556.

^{13}P nuclear magnetic resonance studies of isolated rat liver cells.

Cohen, S.M., Shulman, R.G. and McLaughlin, A.C. 1979 Proc. Natl. Acad. Sci. U.S.A. 76 4808-4812.

Effects of ethanol on alanine metabolism in perfused mouse liver studied by ^{13}C NMR.

Cohen, S.M., Ogawa, S. and Shulman, R.G. 1979a Proc. Natl. Acad. Sci. USA 76 1603-1607.

^{13}C NMR studies of gluconeogenesis in rat liver cells: Utilisation of labeled glycerol by cells from euthyroid and hyperthyroid rats.

Cohen, S.M. and Shulman, R.G. 1980 Philos. Trans. R. Soc. Lond. Biol. 289 407-411

^{13}C NMR studies of gluconeogenesis in rat liver suspensions and perfused mouse livers.

Cohen, S.M., Shulman, R.G., Williamson, J.R. and McLaughlin, A.C. In: *Alcohol and Aldehyde Metabolising Systems*

R.G. Thurman Ed. (Plenum, New York, 1980a) vol. 4, pp. 419-431.

Cohen, S.M., Rognstad, R., Shulman, R.G. and Katz, J., 1981 J. Biol. Chem. 256 (7) 3428-3432.

A comparison of ^{13}C nuclear magnetic resonance and ^{14}C tracer studies of hepatic metabolism.

Cohen, S.M., Glynn, P. and Shulman, R.G. 1981a Proc. Natl. Acad. Science 78 (1) 60-64.

^{13}C NMR study of gluconeogenesis from labelled alanine in hepatocytes from euthyroid and hyperthyroid rat.

Cohen, S.M., Biochemistry 1987 **26** 563-572.

^{13}C and ^{31}P NMR study of gluconeogenesis: Utilization of ^{13}C-labelled substrates by perfused liver from streptozotocin diabetic and untreated rats.

Cohen, S.M., Biochemistry 1987a **26** 573-580.

Effects of insulin on perfused liver from streptozotocin diabetic and untreated rats: ^{13}C NMR assay of pyruvate kinase flux.

Cohen, S.M., Biochemistry 1987b 581-589.

^{13}C NMR study of effects of fasting and diabetes on the metabolism of pyruvate in the TCA cycle and of the utilization of pyruvate and ethanol in lipogenesis in perfused rat liver.

Consoli, A., Nurjhan, N., Capani, F. and Gerich, J. 1989 Diabetes **38** 550-557.

Predominant role of gluconeogenesis in increased hepatic glucose production in NIDDM.

Cooley, J.W. and Tukey, J.W. 1965 Math. Comput. **19** 297-301.

An algorithm for the machine calculation of complex Fourier series.

Costrini, N.V. and Kalkhoff, R.K. 1971 J. Clin. Invest. **50** 992-999

Relative effects of pregnancy, estradiol, and progesterone on plasma insulin and pancreatic islet insulin secretion.

Cox, I.J., Sargentoni, J., Calam, D.J., Bryant, D.J. and Iles, R.A. 1988 NMR Biomed. **1** 56-60

Four dimensional phosphorus-31 chemical shift imaging of carcinoid metastases in the liver.

Cox, I.J., Menon, D.K., Sargentoni, J., Bryant, D.J., Collins, A.G., Coutts, G.A., Iles, R.A., Bell, J.D., Benjamin, I.S., Gilbey, S., Hodgson, H.J.F., Morgan, M.Y. 1992 J. Hepatol. **14** 265-275.

Phosphorus-31 magnetic resonance spectroscopy of the human liver using chemical shift imaging techniques.

Cunningham, C.C., Malloy, C.R. and Radda, G.K. 1986 Biochim. Biophys. Acta. **885** 12-22.

Effect of fasting and acute ethanol administration on the energy state of in vivo liver as measured by ^{31}P NMR spectroscopy.

Dagnelie, P.C., Menon, D.K., Cox, I.J., Bell, J.D., Sargentoni, J., Coutts, G.A., Urenjak, J. and Iles, R.A. 1992 Clinical Science **83** 183-190.

Effect of l-alanine infusion on ^{31}P nuclear magnetic resonance spectra of normal human liver: towards biochemical pathology in vivo.

Darmady, J.M. and Postle, A.D. 1982 Br. J. Obstet. and Gynaecology **89** 211-215.

Lipid metabolism in pregancy.

Davey, D.A., O'Sullivan, W.J. and Browne, J.C.M. 1961 Lancet **1** 519-523.

Total exchangeable sodium in normal pregnancy and pre-eclampsia.

Davidson, M.B. 1984 Metab. Clin. Exp. **33** 532-537.

Insulin resistance of late pregnancy does not include the liver.

Dawson, M.J., Gadian, D.G. and Wilkie, D.R. 1977 J. Physiol. (London) **267** 703-735.

Contraction and recovery of living muscles studied by ^{31}P nuclear resonance.

Dawson, M.J., Gadian, D.G. and Wilkie, D.R. 1978 Nature **274** 861-866.

Muscular fatigue investigated by phosphorus nuclear magnetic resonance.

Dickerson, V.C., Tepperman, J. and Long, C.N.H. 1943 Yale J. Biol. Med. **15** 875-892 cited Cruz and Williamson 1992.

Diezfalusy, E. 1969 Pecile, A. and Finzi, C. (eds.), Exerpta Medica Foundation, Amsterdam, pp. 65-77.

Steroid metabolism in the foeto-placental unit. In: The Foeto-placental Unit.

Edmond, J. 1974 J. Biol. Chem. **249** 72-80.

Ketone bodies as precursors of sterols and fatty acids in the developing rat.

Ehrlich, E.N. 1971 Am. J. Obstet. Gynecol. **109** (7) 963-970.

Heparinoid-induced inhibition of aldosterone secretion in pregnant women; the role of augmented aldosterone secretion in sodium conservation during normal pregnancy.

Ernst, R.R. and Anderson, W.A. 1966 Review Sci. Instrum. **37** 93-102.

Application of Fourier transform spectroscopy to magnetic resonance.

Ernst, R.R. 1966a Adv. Mag. Reson. **2** 1-5.

Sensitivity enhancement in magnetic resonance.

Everett, R.B., Worley, R.J., McDonald, P.C. and Gant, N.F. 1978 Am. J. Obstet. Gynecol. **131** 352-357.

Modification of vascular responsiveness to angiotensin II in pregnant women by intravenously infused 5-dihydroprogesterone.

Everett, R.B. and McDonald, P.C. 1979 Ann. Rev. Med. **30** 473-488.

Endocrinology of the placenta.

Fåhraeus, L., Larsson-Cohn, U. and Wallentin, L. 1985 Obstet. Gynecol. **66** 468-472.

Plasma lipoproteins including high density lipoprotein subfraction during normal pregancy.

Felig, P. and Lynch, V. 1970 Science **170** 990-992

Starvation in human pregnancy: hypoglycemia, hypoinsulinemia and hyperketonemia.

Felig, P., Kim, Y.J., Lynch, V. and Hendler, R. 1972 J. Clin. Invest. **51** 1195-1202.

Amino acid metabolism during starvation in human pregnancy.

Felig, P. 1973 Metabolism **22** 179-207.

The glucose-alanine cycle.

Felig, P. and Wahren, J. 1975 New. Engl. J. Med. **293** 1078-1084.

Fuel homeostasis in exercise.

Ferré, P., Leturque, A., Burnol, A.F., Penicaud, L. and Girard, J., 1985 Biochem. J. **228** 103-110.

A method to quantify glucose utilization in vivo in skeletal muscle and white adipose tissue of the anaesthetized rat.

Ferris, T.F., Stein, J.H. and Kauffman, J. 1972 J. Clin. Invest. **51** 2827-2833.

Uterine blood flow and uterine renin secretion.

Freinkel, N. and Goodner, C.J. 1960 J. Clin. Invest. **39** 116-131.

Carbohydrate metabolism in pregnancy. I. The metabolism of insulin by human placental tissue.

Freinkel, N., Metzger, B.E., Nitzan, M., Hane, J.W., Shambaugh, G.E., Marshall, R.T., Surmaczynska, B.Z. and Nagel, T.C. 1972 Isr. J. Med. Sci. **8** 426-439.

"Accelerated Starvation" and mechanisms for the conservation of maternal nitrogen during pregnancy.

Freinkel, N. 1980 Diabetes **29** 1023-1025.

Banting Lecture 1980. Of pregnancy and progeny.

Garlick , P.B., Radda, G.K. and Seeley, P.J. 1977 Biochem. J. **184** 547-554.

Studies of acidosis in the ischaemic heart by phosphorus nuclear magnetic resonance.

Gadian, D.G. *NMR and its applications to living systems*. Clarendon Press 1982.

Girard, J.R., Kervran, A., Soufflet, E. and Assan, R. 1974 Diabetes **23** 310-317.

Factors affecting the secretion of insulin and glucagon by the rat fetus.

Girard, J.R., Ferré, P., Gilbert, M., Kervran, A., Assan, R. and Marliss, E.B. 1977 Am. J. Physiol. **232** (5) E456-E463.

Fetal metabolic response to maternal fasting in the rat.

Goodner, C.J. and Freinkel, N. 1959 Endocrinology **65** 957-967.

Carbohydrate metabolism in pregnancy: the degradation of insulin by extracts of maternal and foetal structures in the pregnant rat.

Gordon, R.E., Hanley, P.E., Shaw, D., Gadian, D.G., Radda, G.K., Styles, P., Bore, P.J. and Chan, L. 1980 Nature (London) **287** 736-738.

Localisation of metabolites in animals using ^{31}P topical magnetic resonance.

Gordon, R.E., Hanley, P.E. and Shaw, D. 1982 Prog. Nucl. Magn. Reson. Spectr. **15** 1-47.

Topical magnetic resonance.

Gould, G.W. and Holman, G.D. 1993 Biochem. J. **295** 329-341.

The glucose transporter family: structure, function and tissue-specific expression.

Gray, M.J., Munro, A.B., Sims, E.A.H., Meeker, C.I., Salomon, S. and Watanabe, M. 1964 Am. J. Obstet. Gynecol. **89** 760-765.

Regulation of sodium and total body water metabolism in pregnancy.

Green, J.G. 1966 Am. J. Obstet. Gynecol. **95** 387-393.

Serum cholesterol changes in pregnancy.

Gresham, E.L., James, E.J., Raye, J.R.R., Battaglia, F.C., Makowski, E.L. and Meschia, G. 1972 Pediatrics **50** 372-379.

Production and excretion of urea by the fetal lamb.

Griffiths, J.R. and Iles, R.A. 1980 Clin. Sci. **59** 225-230.

Nuclear magnetic resonance - a 'magnetic eye' on metabolism.

Guidotti, G.G., Borghetti, A.F. and Gazzola, G.C. 1978 Biochim. Biophys. Acta. **515** 329-366.

The regulation of amino acid transport in animal cells.

Hanley, P.E. and Gordon, R.E 1981 J. Magn. Reson. **45** 520-524.

The use of high-order gradients to vary the spatial extent of B_0 homogeneity in a high resolution NMR experiment.

Hauguel, S. Gilbert, M. and Girard, J. 1987 Am J. Physiol. **252** E165-E169.

Pregnancy induced insulin resistance in liver and skeletal muscles of the conscious rabbit.

Holness, M.J. MacLennan, P.A., Palmer, T.N. and Sudgen, M.C. 1988 Biochem. J. **252** 325-330.

The deposition of carbohydrate between glycogenesis, lipogenesis and oxidation in liver during the starved to fed transition.

Holness, M.J. and Sugden, M.C. 1989 Biochem. J. **258** 529-533.

Pyruvate dehydrogenase activities during the fed to starved transition and on refeeding after acute or prolonged starvation.

Holness, M.J. and Sugden, M.C. 1989 Biochem. J. **262** 321-325.

Comparison of tissue pyruvate dehydrogenase activites on re-feeding rats fed ad libitum or meal fed rats with a chow diet meal.

Holness, M.J. and Sugden, M.C. 1990 Biochem. J. **268** 77-81.

Pyruvate dehydrogenase activites and rates of lipogenesis during the fed to starved transition in liver and BAT of rat.

Holness, M.J. and Sugden, M.C. 1990 Biochem. J. **270** 245-249.

Glucose utilization in heart, diaphragm and skeletal muscle during the fed to starved transition.

Holness, M.J. Changani, K.K., Sugden, M.C. 1991 Biochem. J. **280** 549-552.

Progressive suppression of muscle glucose utilisation during pregnancy.

Holness, M.J. and Sugden, M.C. 1993 Biochem. J. **292** 431-438.

Changes in rates of glucose utilization and regulation of glucose disposal by fast-twitch skeletal muscles in late pregnancy.

Holzman, I.R., Lemons, J.A., Meschia, G. and Battaglia, F.C. 1977 Proc. Soc. Exp. Biol. Med. **156** 27-30.

Ammonia production by the pregnant uterus.

Holzman, I.R., Lemons, J.A., Meschia, G. and Battaglia, F.C. 1979 J. Dev. Physiol. **1** (2) 137-149.

Uterine uptake of amino acids and placental glutamine-glutamate balance in the pregnant ewe.

Hönger, P.W. 1968 Scand. J. Clin. Lab. Invest. **21** 3-9.

Albumin metabolism in normal pregnancy.

Hoult, D.I., Busby, S.J.W., Gadian, D.G., Radda, G.K., Richards, R.E. and Seeley, P.J. 1974 Nature (Lond.) **252** (5481) 285-287.

Observation of tissue metabolites using ^{31}P nuclear magnetic resonance.

Hoult, D.I. 1978 Prog. Nucl. Magn. Reson. Spect. **12** 41-77

The NMR receiver: A description and analysis of design.

Hytten, F.E. and Leitch 1964 *The Physiology of Human Pregnancy*, Blackwell, Oxford.

Iles, R.A., Baron, P.G. and Cohen, R.D. 1979 Biochem. J. **184** 635-642.

The effect of reduction of perfusion rate on lactate and oxygen uptake, glucose output and energy supply in the isolated perfused liver of starved rats.

Iles, R.A. Griffiths, J.R., Stevens, A.N., Gadian, D.G. and Porteous, R. 1980 Biochem. J. **192** 191-202.

Effects of fructose on the energy metabolism and acid-base status of the perfused starved rat liver.

Iles, R.A., Cohen, R.D. and Baron, P.G. 1981 Clin. Sci. **60** 537-542.

The effect of combined ischaemia and acidosis on lactate uptake and gluconeogenesis in the perfused rat liver.

Iles, R.A., Stevens, A.N., Griffiths, J.R. and Morris, P.G. 1985 Biochem. J. **229** 141-151.

Phosphorylation status of liver by ^{31}P-n.m.r. spectroscopy, and its implications for metabolic control.

Iles, R.A., Cox, I.J., Bell, J.D., Dubowitz, L.M.S., Cowan, F. and Bryant, D.J. 1990 NMR Biomed. **3** (2) 90-94.

^{31}P Magnetic resonance spectroscopy of the human paediatric liver.

Jans, A.W.H. and Willem, R. 1989 Biochem. J. **263** 231-241.

A ^{13}C-NMR investigation of the metabolism of amino acids in renal proximal convoluted tubules of normal and streptozotocin treated rats and rabbits.

Jepson, J.H. 1968 Can. Med. Assoc. J. **98** 844-847.

Endocrine control of maternal and foetal erythropoiesis.

Jue, T., Rothman, D.L., Hanstock, C.C., Hughes, E. and Shulman, R.G. 1987 Proceedings of the Sixth Annual Meeting of the Soc. Magn. Res. Med. pp 607.

^{31}P NMR spectra of human liver and kidney using surface coil ISIS.

Jue, T., Rothman, D.L., Tavitian, B.A. and Shulman, R.G. 1989 Proc. Natl. Acad. Sci. USA. **86** 1439-1442.

Natural abundance ^{13}C NMR study of glycogen repletion in human liver and muscle.

Jue.,T., Rothman, D.L., Shulman, G.I., Tavitian, B.A., De Fronzo, R.A. and Shulman, R.G. 1989 Proc. Natl. Acad. Sci. USA. **86** 4489-4491.

Direct observation of glcogen synthesis in human muscle with ^{13}C NMR.

Kalderon, B., Gopher, A. and Lapidot, A. 1987 FEBS **213** (1) 209-214.

A quantitative analysis of the metabolism pathways of hepatic glucose synthesis in vivo with ^{13}C-labelled substrates.

Kalhan, S.C., D'Angelo, L.J., Savin, S.M. and Adam, P.A.J. 1979 J. Clin. Invest. **63** 388-394.

Glucose production in pregnant women at term gestation.

Kalkhoff, R.K., Schalch, D.D., Walker, L.J., Beck, P., Kipnis, D.M. and Daughaday, W.H. 1964 Trans. Assoc. Am. Physicians 77 270-280.

Diabetogenic factors associated with pregnancy.

Kalkhoff. R.K., Kissebach, A.H. and Kim, H.J. 1978 Semin. Perinatol. **2** 291-308.

Carbohydrate and lipid metabolism during normal pregnancy: relationship to gestational hormone action.

Kerbey, A.L., Radcliffe, P.M. and Randle, P. J. 1977 Biochem. J. **164** 509-579.

Diabetes and the control of PDH in rat heart mitochondria by concentration ratios of ATP/ADP, of red/ox NAD^+ and Acetyl CoA/CoA.

Kim, Y.J. and Felig, P. 1972 Metabolism **21** 507-512

Maternal and amniotic fluid substrate levels during caloric deprivation in human pregnancy.

Kim, H.J. and Kalkhoff, R.K. 1975 J. Clin. Invest. **56** 888-896.

Sex steroid influence on triglyceride metabolism.

Kipnis, D.M. and Cori, C.F. J. Biol. Chem. **234** 171-177.

Studies of tissue permeability. V. The penetration and phosphorylation of 2-deoxyglucose in the rat diaphragm.

Kissebah, A.H., Harrigan, P. and Wynn, V. 1973 Horm. Metab. Res. **5** 184-192.

Mechanisms of hypertriglyceridemia associated with contraceptive steroids.

Knopp, R.H., Ruder, H.J., Herrera, E., Freinkel, N. 1970 Acta. Endocrinol. **65** 352-360.

Carbohydrate metabolism in pregnancy. VII) Insulin tolerance during late pregnancy in the fed and fasted rat.

Knopp, R.H., Saudek. C.D., Arky R.A. and O'Sullivan J.B. 1973 Endocrinology (Baltimore) **92** 984-988.

Two phases of adipose tissue metabolism in pregnancy: Maternal adaptations for fetal growth.

Kraegen, E.W., Sowden, J.A., Halstead, M.B., Clark, P.W., Rodnick, K.J., Chisholm, D.J. and James, D.E. 1993 Biochem. J. **295** 287-293.

Glucose transporters and in vivo glucose uptake in skeletal and cardiac muscle: fasting, insulin stimulation and immunoisolation studies of GLUT1 and GLUT4.

Krebs,. H.A. and Henseleit, K. 1932 Hoppe Seyler's Z. Physiol. Chem. **210** 33-66.

Untersuchungen uber die harnstoffbildung im tierkorper.

Krishnaumurti, C.R. and Kitts, D.D. 1992 Growth **46** 209-219.

Kinetics of amino acid metabolism in the ovine fetus in utero.

Lackner, R., Chaliss, J., West, D. and Newsholme, E.A. 1984 Biochem. J. **218** 649-651.

A problem in the radiochemical assay of glucose-6-phosphatase in muscle.

Laughlin, M.R., Petit, W.A., Dizon, J.M., Shulman, R.G. and Barrett E.J. 1988 J. Biol. Chem. **263** (5) 2285-2291.

N.M.R. Measurements of in vivo myocardial glycogen metabolism.

Lawson, J.W.R. and Veech, R.L. 1979 J. Biol. Chem. **254** 6528-6537.

Effects of pH and free Mg^{2+} on the K_{eq} of the creatine kinase reaction and other phosphate hydrolyses and phosphate transfer reactions.

Leake, N.H. and Burt, R.L. 1969 Am. J. Obst. & Gynecol. **103** 39-43.

Effect of HPL and pregnancy in glucose uptake in rat adipose tissue.

Lemons, J.A. and Schreiner, R.L. 1983 Am. J. Physiol. **244** E549-566.

Amino acid metabolism in the ovine fetus.

Leturque, A. Ferré, P., Satabin, P., Kervran, A. and Girard, J. 1980 Diabetologia **19** 521-528.

In vivo insulin resistance during pregnancy in the rat.

Leturque, A. Gilbert, M. and Girard, J. 1981 Biochem. J. **196** 633-636.

Glucose turnover during pregnancy in anaesthetised post absorpitive rats.

Leturque, A. Satabin, P., Ferré, P and Girard, J. 1981a Biochem. J. **200** 181-184.

Evidence that stimulation of glucose metabolism by insulin is not altered in isolated soleus muscle of pregnant rats.

Leturque, A., Guerre-Millo, M., Lavav, M. and Girard, J. 1984 Biochem. J. **224** 685-688.

Effect of insulin on glucose metabolism in adipocytes from virgin and late pregant

rats.

Leturque, A., Burnol, A.F., Ferré, P and Girard, J. 1984a Am. J. Physiol **246** (Endocrinol Metab. 9) E25-E31.

Pregnancy induced insulin resistance in rat: assessment of glucose clamp technique.

Leturque, A., Ferré, P., Burnol, A-F., Kande, J., Maulard, P. and Girard, J. 1986 Diabetes **35** 172-177.

Glucose utilization rates and insulin sensitivty in vivo in tissues of virgin and pregant rats.

Leturque, A., Hauguel, S. Kande, J. and Girard, J. 1987a Pediatric Research **22** (4).

Glucose utilization by the placenta of anaesthetised rats: Effects of insulin, glucose, and ketone bodies.

Leturque, A., Hauguel, S., Revelli, J-P., Burnol, A-F., Kandé, J. and Girard, J. 1989 Am. J. Physiol. **256** E699-E703.

Fetal glucose utilization in response to maternal starvation and acute hyperketonemia.

Leturque, A. Revelli, J.P., Hauguel, S., Kande, J. and Girard, J. 1987 Am. J. Physiol. **253** E616-E620.

Hyperglycaemia and hyperinsulinaemia increase glucose utilization in foetal rat tissues.

Magnusson, I., Rothman, D.L., Katz, L.D., Shulman, R.G. and Shulman, G.I. 1992 J. Clin. Invest. **90** 1323-1327.

Increased rate of gluconeogenesis in type II diabetes mellitus.

Malloy, C.R., Sherry, A.D. and Jeffrey, M.H. 1990 Am. J. Physiol **259** (2) H987-995.

Analysis of tricarboxylic acid cycle of the heart using ^{13}C isotope isomers.

Malloy, C.R., Sherry, D. and Jeffrey. F.M.H. 1988 J. Biol. Chem. **263** (15) 6964-6971.

Evaluation of carbon flux and substrate selection through alternative pathways invloving the citric acid cycle of the heart by ^{13}C NMR spectroscopy.

Malloy, C.R., Sherry, A.D. and Jeffrey, F.M.H. FEBS. Lett. 1987 **212** (1) 58-62.

Carbon flux through citric acid cycle pathways in perfused heart by ^{13}C NMR spectroscopy.

Maris, J.M., Evans, A.E., McLaughlin, A.C., D'Angio, G.J., Bolinger, L., Manos, H. and Chance, B. N. 1985 Engl. J. Med. **312** 1500-1505.

^{31}P nuclear magnetic resonance spectroscopy investigation of human neuroblastoma in situ.

McDonald, I., Robinson, J.J., Fraser, C. and Smart, R.I. 1979 J. Agric. Sci. **92** 591-603.

Studies on the reproduction in prolific ewes. 5: The accretion of nutrients in the foetuses and adnexa.

McLaughlin, A.C., Takeda, H. and Chance, B. 1979 Proc. Natl. Acad. Sci. USA **76** 5445-5449.

Rapid ATP assays in perfused mouse liver by ^{13}P NMR.

McMurry, M.P. Connor, W.E. and Goplerud, C.P. 1981 Metabolism **30** (9) 869-879

The effects of dietary cholesterol upon the hypercholesterolemia of pregnancy.

Meister, A. 1981 Curr, Top. Cellul. Regul. **18** 21-58.

On the cycles of glutathione metabolism and transport.

Meschia, G. 1975 Marselli, P.L. , Garattini, S. and Sereni, F. (eds.). Raven Press, New York pp. 89-95.

Basic and Therapeutic Aspects of Perinatal Pharmacology.

Metcalfe, J. and Parer, J.T. 1966 Am. J. Physiol. **210** 821-825.

Cardiovascular changes during pregnancy in ewes.

Miodovnik, M., Lavin, J.P., Harrington, D.J., Leung, L.S., Seeds, A.E. and Clark, K.E. 1982 Am. J. Obstet. Gynecol. **144** 585-593.

Effect of maternal ketoacidemia and the pregnant ewe and the fetus.

Moir, A.M.B. amd Zammit, V.A. 1993 Biochem.J. **291** 241-246.

Rapid switch of hepatic fatty acid metabolism from oxidation to esterification during diurnal feeding of meal-fed rats correlates with changes in the properties of acetyl-CoA carboxylase, but not of carnitine palmitoyltransferase I.

Morris, F.H. Jr., Makowski, E.L., Meschia, G. and Battaglia, F.C. 1975 Biol. Neonate **25** 44-52.

The glucose/oxygen quotient of the term human fetus.

Morris, F.H., Rosenfeld, C.R., Crandell, S.S. and Adcock, E.W. 1980 J. Nutr. **110** 2433-2493.

Effects of fasting on uterine blood flow and substrate uptake in the sheep.

Morrow, P.G., Marshall, W.P., Kim, H-J., Kalkhoff, R. 1981 Metabolism **30** 268-273.

Metabolic response to starvation. I. Relative effects of pregnancy and sex steroid administration in the rat.

Narayana, P.A., Jackson, E.F., Hazle, J.D., Fotedar, L.K., Kulkarni, M.W. and Flamig, D.P. 1988 Magn. Reson. Med. **8** 151-159.

In vivo localised proton spectroscopic studies of human gastrocnemius muscle.

Navon, G., Ogawa, S., Shulman, R.G. and Yamane, T. 1977 Proc. Natl. Acad. Sci. USA **74** 888-891.

^{13}P nuclear magnetic resonance studies in Ehrlich ascites tumor cells.

Navon, G., Lyon, R.C., Kaplan, O. and Cohen, S. 1989 FEBS Lett. **247** (i) 86-90.

Monitoring the transport and phosphorylation of 2-deoxy-D-glucose in tumor cells in vivo and in vitro by ^{13}C NMR spectroscopy.

Neurohr, K.J., Barrett, E.J. and Shulman, R.G. 1983 Proc. Natl. Acad. Sci. USA. **80** 1603-1607.

In vivo carbon-13 nuclear resonance studies of heart metabolism.

Noble, R.C. and Shand, J.H. 1981 IRCS J. Med. Sci. **9** 174-176.

The placenta: its role in the relationship between the lipids of the mother and foetus.

Oberhaensli, R.D., Bore, P.J., Rampling, R.P., Hilton-Jones, D., Hands, L., Radda, G.K. 1986 Lancet **ii** 8-11.

Biochemical investigation of human tumours in vivo with phosphorus-31 magnetic resonance spectroscopy.

Oberhaensli, R.D., Galloway, G.J., Taylor, D.J., Bore, P.J. and Radda, G.K. 1986 Br. J. Radiol. **59** (703) 695-699.

Assessment of human liver metabolism by phosphorus-31 magnetic resonance spectroscopy.

O'Sullivan, J.B. (1988) Carbohydrate Metabolism in Pregnancy and the Newborn, Vol IV, pp287-294, Berlin: Springer-Verlag.

The Boston gestational diabetes studies: review and perspectives.

Page, E.W. 1969 Am. J. Obstet. Gynecol. **104** 378-387.

Human fetal nutrition and growth.

Pahl-Wostl, C. and Seelig, J. 1986 Biochemisrty **25** 6799-6807.

Metabolic pathways for ketone body production. ^{13}C NMR spectroscopy of rat liver in vivo using ^{13}C-multilabelled fatty acids.

Pallardo, F.V. and Williamson, D.H. 1989 Biochem. J. **257** 607-610.

Comparson of the flux of carbon to hepatic glycogen deposition and fatty acid and cholesterol synthesis on refeeding rats fed ad libitum or meal fed rats with a chow diet meal.

Pan, J.W. Hamm, J.R., Rothman, D.L. and Shulman, R.G. 1988 Proc. Natl. Acad. Sci. U.S.A. **85** 7836-7839.

Intracellular pH in human skeletal muscle by ^{1}H NMR.

Penicaud L,. Ferré, P., Kande, L., Leturque, A., Issad, T. and Girard, J. 1987 Am. Phys. Soc. E365.

Effect of anaesthesia on glucose production and utilisation in rats.

Posner, B.I. 1974 Diabetes **23** 209-214.

Insulin receptors in human and animal placental tissue.

Pritchard, J.A. 1965 Anesthesiolgy **26** 393-399.

Changes in blood volume during pregnancy and delivery.

Purcell, E.M., Torrey, H.C. and Pound, R.V. 1946 Phys. Rev. **69** 37-38.

Resonance absorption by nuclear magnetic moments in a solid.

Randle, P.J., Garland, P.B., Hales, C.N. and Newsholme, E.A. Saturday 13th April 1963 The Lancet 785-789.

The glucose fatty acid cycle - its role in insulin sensitivity and the metabolic disturbances of diabetes mellitis.

Randle, P.J., Newsholme, E.A. and Garland, P.B. 1964 Biochem. J. **93** 652-665.

Regulation of glucose uptake by muscle (effects of fatty acids, ketones and pyruvate and of Alloxan-diabetes and starvation on the uptake and metabolic fate of glucose in rat heart and diaphragm).

Rattray, P.J., Garrett, W.N., East, N.E. and Huiman, N. 1974 J. Anim. Sci. **38** 613-626.

Growth, development and composition of the ovine conceptus and mammary gland during pregnancy.

Robinson, A.M. and Williamson, M.D. 1980 Physiol. Rev. **60** 143-187.

Physiological roles of ketone bodies as substrates and signals in mammalian tissues.

Ross, B.D., Hems, R. and Krebs, H.A. 1967 Biochem. J. **102** 942-951.

The rate of gluconeogenesis from various precursors in the perfused rat liver.

Ross, B.D. and Barker, P. 1988 7th Annual Meeting of the Society of Magnetic Resonance in Medicine, Book of Abstracts pp 33.

An NMR-invisible P_i pool developed in human liver during alanine infusion.

Ross, B.D., Higgins, R.J., Boggan, J.E., Willis, J.A., Knittel, B. and Unger, S.W. 1988 NMR Biomedicine **1** (1) 20-26.

Carbohydrate metabolism of the rat C6 glioma. An in vivo ^{13}C and in vitro ^{1}H magnetic resonance spectroscopy study.

Rosso, P. and Lederman, S.A. 1984 Adv. Perinat. Med. **4** 1-61.

Nutrition and fetal growth.

Rushakoff, R.J. and Kalkhoff, R.K. 1981 Diabetes **30** 545-550.

Effects of pregnancy and sex steroid administration on skeletal muscle metabolism in the rat.

Salhany, J.M., Stoths, S.J. Reinke, L.A., Pieper, G.M. and Hassing, J.M. 1979 Biochemical and Biophysical Research Communications **86** 1077-1083.

^{13}P nuclear magnetic resonance of metabolic changes associated with cyanide intoxication in the perfused rat liver.

Samman, N., Yen, S.C.C., Gonzàlez, D. and Pearson, O.H. 1968 J. Clin. Endocrinol. Metab. **28** 485-491.

Metabolic effects of placental lactogen (HPL) in man.

Sauter, R., Mueller, S. and Weber, H. 1987 J. Mag. Reson. **75** 167-173.

Localisation in in vivo ^{31}P NMR spectroscopy by combining surface coils and slice-selective saturation.

Scow, R.O., Chernick, S.S., Brinley and M.S. 1964 Am. J. Phsiol. **206** 796-804.

Hyperlipemia and ketosis in the pregnant rat.

Segebarth, C., Luyten, P.R. and den Hollander, A. 1987 J. Mag. Reson. **75** 345-351.

Improved depth-selective single surface-coil ^{31}P NMR spectroscopy using a combination of B_1 and B_0 selection techniques.

Sehr, P.A., Radda, G.K., Bore, P.J. and Sells, R.A. 1977 Biochemical and Biophysical Research Communications **77** 195-202.

A model kidney transplant studied by phosphorus nuclear magnetic resonance.

Shalwitz, R.A., Reo, N.V., Becker, N.N., Hill, A.C., Coleen, S.W., Ackerman, J.J.H. 1989 J. Biol. Chem. **264**(7) 3930-3934.

Hepatic glycogen synthesis from duodenal glucose and alanine.

Sherry, A.D., Malloy, C.R., Roby, R.E., Rajagopal, A. and Jeffrey, M.H. 1988 Biochem. J. **254** 593-598.

Propionate metabolism in the rat heart by ^{13}C NMR spectrocopy.

Shiu, R.P.C., Kelly, P.A. and Friesen, H.G. 1973 Science **180** 968-971.

Radioreceptor assay for prolactin and other lactogenic hormones.

Shulman, G.I., Rossetti, L., Rothman, D.L., Blair, J.B. and Smith, D. 1987 J. Clin. Invest. **80** 387-393.

Quantitative analysis of glycogen repletion by nuclear magnetic resonance spectroscopy in the conscious rat.

Shulman, G.I., Rothman, D.L. and Shulman, R.G. 1990 Phil. Trans. R. Soc. Lond. A. **333** 525-529.

"C NMR. studies of glucose disposal in normal and non-insulin dependent diabetic humans.

Schumann, W.C., Magnusson, I., Chanramouli, V., Kumaran, K., Wahren, J. and Landau, B.R. 1991 J. Biol. Chem. **266** 6985-6990.

Metabolism of [2-^{14}C]acetate and its use in assessing hepatic Krebs cycle activity and

gluconeogenesis.

Scofield, R.F. Kosugi, K., Schumann, W.C. Kumaran, K. and Landau, B.R. 1985

J. Biol. Chem. **260** (15) 8777-8782.

Quantitative estimation of the pathways followed in the conversion to glycogen of glucose administered to the fasted rat.

Sillerud, L.O. and Shulman, R.G. 1983 Biochemistry **22** 1087-1094.

Structure and metabolism of mammalian liver glycogen monitored by carbon-13 nuclear magnetic resonance.

Sims, E.A.H. and Krantz, K.E. 1958 Obstet. Gynecol. **45** 481-487.

Serial studies of renal function during pregnancy and the puerperium in normal women.

Sokoloff, L. Reivich, M. Kennedy, C., Des Rossers, M.H., Patlak, C.S., Pettigrew, K.D., Sakurada, O. and Shinohara, M. 1977 J. Neurochem. **28** 897-916.

The [^{14}C] deoxyglucose method for the measurement of local cerebral glucose utilisation, theory procedure and normal values in the conscious and anaesthetised albino rat.

Soman, V. 1979 Diabetes **28** 393.

Heterogeneity of insulin receptor changes in pregnancy.

Somogyi, M. 1945 J. Biol. Chem. **160** 69-73.

Determination of blood sugar.

Sugden, M.C. and Holness M.J. 1989 Biochem. J. **262** 669-672.

Effects of re-feeding after prolonged starvation on pyruvate dehydrogenase activites in heart, diaphragm and selected muscles of the rat.

Sugden, M.C., Holness, M.J. and Palmer, N.T. 1989 Biochem. J. **263** 313-323.

Fuel selection and carbon flux during the starved to fed transition.

Sugden, M.C. Changani, K.K., Bentley, J., Holness, M.J. 1992 Biochem. Soc. Trans. **20** 195S.

Cardiac glucose metabolism during pregnancy.

Sugden, M.C., Howard, R.M. and Holness, M.J. 1993 Biochem. J. **296** 217-223.

The regulation of hepatic carbon flux by pyruvate dehydrogenase and pyruvate dehydrogenase kinase during long-term food restriction.

Sutter-Dub, M.T., Leclerq, R., Felix, J.M., Jacquot, R. and Sutter, B. Ch. J. 1973 Metabolism **5** 18-21.

Serum progesterone and immuno-reactive insulin levels in the pregnant rat.

Svanborg, A. and Vikrot, O. 1965 Acta Medica Scandinavica **178** 615-630.

Plasma lipid fractions, including individual phospholipids, at various stages of pregnancy.

Taylor, D.J., Bore, P.J., Styles, P., Gadian, D.G. and Radda, G.K. 1983 Mol. Biol. Med. **1** 77-94.

Bioenergetics of intact human muscle: a ^{31}P nuclear magnetic resonance study.

Tepperman, J. and Tepperman, H.M. 1958 Am. J. Physiol. **193** 55-64

Effects of antecedent food intake pattern on hepatic lipogenesis.

Testar, X., Lasuncion, M.A., Chieri, R., Herrera, E. 1985 Diabetologia **28** (10) 743-748.

Effects of exogenous insulin on placental transfer of maternal glucose to the rat fetus.

Tindall, V.R. 1975 Clin. Obstet. Gynecol. **2** 441-462.

The liver in pregnancy.

Tyson, J.E., Austin, K.L., Farinholt, J.W. 1971 Am. J. Obstet. Gynecol. **109** 1080-1082.

Prolonged nutritional deprivation in pregnancy: changes in human chorionic somatomammotropin and growth hormone secretion.

Wallenburg, H.C.S. (1981) Int. J. Biol. Res. Pregnancy **2** 15-22.

Prostaglandins and the maternal placental circulation: review and perspectives.

Warth, M.R., Arkey, R.A. and Knopp, R.H. 1975 J. Clin. Endocrinol. Metab. **41** 649-655.

Lipid metabolism in pregnancy, the altered lipid composition intermediate, very low, low and high density lipoprotein fraction.

Warth, M.R. and Knopp, R.H. 1977 Diabetes **26** 1056-1062.

Lipid metabolism in pregnancy. V. Interaction of diabetes, body weight, age and high carbohydrate diet.

Wigglesworth, J.S. 1964 J. Pathol. Bact. **88** 1-13.

Experimental growth retardation in fetal rat.

Younger, J.B., St. Pierre, R.L and Zmijewski, C. 1969 Am. J. Obstet. Gynecol. **105** 9-13.

Effect of human chorionic gonadotropin on antibody production.

Ziegler, E.E., O'Donnell, A.M., Nelson, S.E. and Fomon, S.J. 1976 Growth **40** 329-341.

Body composition of the reference fetus.